School of Applied Chemistry

IDENTIFICATION OF ORGANIC FOULING AGENTS ON ACTIVATED CARBON BY EVOLVED GAS ANALYSIS

Nicholas Grant Fisher

This thesis is presented as part of the requirements for
the award of the Degree of Doctor of Philosophy
of the
Curtin University of Technology

February 2000

ABSTRACT

Activated carbon is widely used in the gold processing industry as an adsorbent for the gold cyanide complex, $[Au(CN)_2]^-$. However, many other processing reagents are also adsorbed (termed fouling), which compete with the gold cyanide complex for active sites on the carbon. So far the only way of assessing the amount of fouling due to organic compounds that has adsorbed on the carbon is through the use of thermogravimetry (TG). Unfortunately, thermogravimetry only gives the percentage total of organic fouling agents adsorbed and no information can be obtained on the identity of the individual organic fouling agents. Thus this current work reports the development of analytical methods capable of identifying specific fouling agents.

In this thesis the identification of two types of common organic fouling agents adsorbed on activated carbon during gold processing has been established using three thermal analysis techniques, namely thermal desorption-pyrolysis-gas chromatography-mass spectrometry (TD-py-GC-MS), thermogravimetry-mass spectrometry (TG-MS), and thermogravimetry-Fourier transform infrared (TG-FTIR) spectroscopy. TD-py-GC-MS was used to identify the individual decomposition gases of each sample. TG-MS and TG-FTIR were used to obtain the decomposition temperatures of the fouling agents, and to identify/monitor the gases evolved as a function of temperature. All analyses were performed in an inert atmosphere.

The organic fouling agents studied were xanthates and frothing agents, which are used as flotation reagents. The xanthates studied were sodium ethyl xanthate (SEX), sodium isobutyl xanthate (SiBX), potassium ethyl xanthate (PEX), and potassium amyl xanthate (PAX). The frothing agents studied were polypropylene glycol (PPG), polypropylene glycol methyl ether (PPGME), α-terpineol, and methyl isobutyl carbinol (MiBC). The thermal decomposition of each pure reagent was studied, and then the reagents were individually adsorbed on an activated carbon (Haycarb, -45 μm) and their thermal decomposition reinvestigated. These pure systems were then compared to the thermal decomposition of activated carbon samples taken from two gold processing plants.

Between seven and sixteen gases were identified via TD-py-GC-MS for the decomposition of each xanthate. Common gases and types of gases identified included carbonyl sulfide, carbon disulfide, thiols, alcohols, carbonates, sulfides, disulfides, and carbonothioic acid, O,S, dialkyl esters. The thermogravimetric curve of each xanthate displayed two mass losses. The mass losses and their corresponding temperatures were dependent on the alkyl chain and alkali cation of the xanthate. TG-MS and TG-FTIR showed carbonyl sulfide and carbon disulfide were the most significant gases evolved from the decomposition of each xanthate.

Each xanthate was adsorbed on activated carbon, and its thermal decomposition characteristics reinvestigated. On heating, similar gases were evolved to those detected for the xanthate alone. However, the TG curves displayed three mass losses compared to two with the xanthates not adsorbed on activated carbon. The first mass loss of each sample was attributed to a hydrolysis reaction between water retained in the activated carbon and the xanthate. TG-MS and TG-FTIR analyses showed carbon disulfide and carbonyl sulfide were the most significant gases evolved during the first mass loss and second mass losses respectively, and consequently these gases could be used as indicators of xanthate fouling on plant samples.

The TD-py-GC-MS, TG-MS, and TG-FTIR analyses of the frothing agents showed these compounds mainly boiled with little indication of thermal decomposition. The thermogravimetric curve of each frother displayed one mass loss. Upon reinvestigation of the frothing agents individually adsorbed on activated carbon, a number of different gases were identified by the TD-py-GC-MS analyses. For all adsorbed frothing agents (except MiBC) these included propanal, 2-ethyl-4-methyl-1,3-dioxolane, 3,3-oxybis-2-butanol, and dioxanes. Each TG curve displayed one mass loss due to the decomposition of the frothing agent. The TG-MS and TG-FTIR analyses showed propanal was the most significant gas evolved for the PPG and PPGME. For α-terpineol, propene was also a significant gas, although this gas was not detected by TG-FTIR. The TD-py-GC-MS and TG-FTIR analyses of the MiBC showed it mainly boiled off the carbon without significant alteration.

Four activated carbon samples were obtained from different parts of the process circuit in the Three Mile Hill plant in Western Australia. Nine to twelve gases were

identified by TD-py-GC-MS analysis of each sample. Common gases included butene, 2-methyl-1-butene, and butanol. The TG curve of each sample displayed one mass loss due to the presence of fouling agents. TG-MS analyses showed butene was the most significant gas evolved for this mass loss. TG-FTIR analyses showed that carbonyl sulfide had also evolved during this mass loss. Thus it was concluded from the detection of carbonyl sulfide and its temperature of evolution, that fouling of the activated carbon by a xanthate had occurred.

Five activated carbon samples were obtained from the Salsigne plant in France. Nine to fourteen gases were identified by TD-py-GC-MS analysis of each sample. Common gases included cyclopropane, butene, propanal, isobutanol, isoamyl alcohol, and 2,5 and 2,6-dimethyl dioxene. The TG curve of each sample displayed one mass loss due to the decomposition of fouling agents, in the same temperature region as the Three Mile Hill samples. TG-MS analyses showed cyclopropane was the most significant gas evolved for this mass loss. TG-FTIR analyses showed that carbonyl sulfide had also evolved during this mass loss. Thus it was concluded from the detection of propanal, carbonyl sulfide, and their temperatures of evolution that fouling of the activated carbon by a xanthate and a frothing agent had occurred respectively.

A comparison of the techniques showed that TD-py-GC-MS analysis was essential for unambiguous identification of the complex gas mixture obtained from decomposition of organic fouling agents. Unfortunately TD-py-GC-MS provided no information on mass losses or temperatures of gas evolution. TG-MS permitted the monitoring of evolved gases versus temperature via their molecular ions. However the molecular ion signals were affected by overlapping fragment and/or isotope ion signals. The TG-FTIR was most useful when the evolved gases gave an infrared adsorption that was very characteristic of the molecule, as for the identification of carbonyl sulfide and carbon disulfide. This work was successful as a combination of the analytical techniques enabled identification of fouling agents adsorbed on plant samples.

ACKNOWLEDGEMENTS

I would like to thank my supervisor Professor J. G. Dunn for his invaluable advice, support and direction during the course of this project. The support of my associate supervisor, Dr Jim Avraamides, especially for the supply of industrial information and samples, is gratefully acknowledged.

I would like to thank the AJ Parker Cooperative Research Centre for Hydrometallurgy for the opportunity to be part of the centre, and for the provision of a supplementary scholarship along with maintenance money. I also gratefully appreciate the financial support received from the Australian Postgraduate Research Award scheme.

Also the expertise and helpfulness of the staff of the School of Applied Chemistry, in particular Mr Ian Sills of the Thermal Characterisation Laboratory and Mr Peter Chapman of the Vibrational Spectroscopy Facility, was much appreciated. I also would like to thank Dr Marc Lehmann for advice during the absence of my supervisor, Dr Mauro Mocerino for his invaluable advice on organic chemistry reactions, and Dr Steve Errington for the proof reading of this thesis.

Finally I would like to thank my parents for their support during my years of study.

TABLE OF CONTENTS

		page
ABSTRACT		i
ACKNOWLEDGMENTS		iv
TABLE OF CONTENTS		v
LIST OF SYMBOLS		viii
LIST OF FIGURES		ix
LIST OF TABLES		xvi
PUBLICATIONS		xix
CHAPTER 1	**INTRODUCTION**	
1.0	**Gold Production in Australia**	1
1.1	**Gold Deposits within Western Australia**	2
1.2	**Extraction of Gold from Sulfide Orebodies**	3
	1.2.1 Crushing/Grinding	5
	1.2.2 Flotation	5
	1.2.3 Gold Liberation	6
	1.2.4 Cyanide Leaching	8
	1.2.5 Adsorption of Gold on Activated Carbon and Recovery	8
1.3	**Activated carbon**	9
	1.3.1 Manufacture	9
	1.3.2 Structure	10
	1.3.3 Adsorptive Properties	12
	1.3.4 Fouling and Regeneration of Activated Carbon	13
	1.3.5 Gold Cyanide Adsorption	19
	1.3.6 Activated Carbon Surface Studies	19
1.4	**Current Test Methods for the Assessment of Activated Carbon**	20
1.5	**Thermal Analysis**	22
	1.5.1 Investigations of Fouling of Activated Carbon using Thermal Analysis	25
	1.5.2 Evolved Gas Analysis	26
1.6	**Proposed Research**	29

CHAPTER 2 EXPERIMENTAL

2.1	**Xanthates**	31
	2.1.1 Purification	31
	2.1.2 Characterisation	31
	i) Purity	31
	ii) Elemental analysis	32
	iii) NMR Analysis	32
2.2	**Frothing Agents**	33
2.3	**Industrial Activated Carbon Samples from Gold Plants**	34
2.4	**Adsorption of Xanthates and Frothing Agents on Activated Carbon**	34
	2.4.1 Adsorption of the Xanthates	34
	2.4.2 Adsorption of the Frothing Agents	36
2.5	**Thermal Analysis Techniques**	37
	2.5.1 TD-py-GC-MS	37
	2.5.2 TG-MS and TG-FTIR	38
	i) MS Analysis	39
	ii) FTIR Analysis	39

CHAPTER 3 THERMAL DECOMPOSITION OF XANTHATES

3.0	**Introduction**	40
3.1	**TD-py-GC-MS Analysis of Alkali Xanthates**	46
3.2	**Thermogravimetry - Evolved Gas Analysis of Alkali Xanthates**	57
	3.2.1 MS Analysis of the Evolved Gases	59
	3.2.2 FTIR Spectroscopy Analysis of the Evolved Gases	66
3.3	**TD-py-GC-MS Analysis of Alkali Xanthates Adsorbed on Activated Carbon**	74
3.4	**Thermogravimetry - Evolved Gas Analysis of Alkali Xanthates Adsorbed on Activated Carbon**	81
	3.4.1 MS Analysis of the Evolved Gases	83
	3.4.2 FTIR Analysis of the Evolved Gases	88
3.5	**Hydrolysis of Alkali Xanthates**	95
3.6	**Surface Analysis of SEX Adsorbed on Activated Carbon**	102
3.7	**Summary**	103

CHAPTER 4 THERMAL DECOMPOSITION OF FROTHING AGENTS

4.0 Introduction 107

4.1 TD-py-GC-MS Analysis of the Frothing Agents 110

4.2 Thermogravimetry - Evolved Gas Analysis of Frothing Agents 113
4.2.1 MS Analysis of the Evolved Gases 116
4.2.2 FTIR Spectroscopy Analysis of the Evolved Gases 116

4.3 TD-py-GC-MS Analysis of the Frothing Agents Adsorbed on Activated Carbon 121

4.4 Thermogravimetry - Evolved Gas Analysis of the Frothing Agents Adsorbed on Activated Carbon 126
4.4.1 MS Analysis of the Evolved Gases 129
4.4.2 FTIR Analysis of the Evolved Gases 131

4.5 Surface Analysis of Frothing Agents Adsorbed on Activated Carbon 132

4.6 Summary 132

CHAPTER 5 THERMAL DECOMPOSITION OF INDUSTRIAL SAMPLES

5.0 Introduction 137

5.1 Three Mile Hill 137
5.1.1 TD-py-GC-MS 137
5.1.2 TG-MS and TG-FTIR 141

5.2 Salsigne 150
5.2.1 TD-py-GC-MS 150
5.2.2 TG-MS and TG-FTIR 155

5.3 Summary 163

CHAPTER 6

6.0 Conclusion 167

REFERENCES 171

LIST OF SYMBOLS

t	ton
ppm	parts per million
g	grams
Myr	million years
μm	microns
°C	degrees Celsius
°C min^{-1}	degrees Celsius per minute
Å	angstrom
K	equilibrium constant
k	rate constant
ν	stretching vibration
δ	bending vibration
A	amp
w/w	weight-weight
eV	electron volts
cm^{-1}	wavenumber

LIST OF FIGURES

		page
Figure 1.1:	Simplified flowsheet of sulfide ore processing.	4
Figure 1.2:	Some functional groups found on the surface of activated carbon (a) carboxyl, (b) phenolic, (c) quinone, and (d) lactone.	11
Figure 1.3:	Effect of reactivation temperature on carbon activity.	18
Figure 1.4:	Schematic diagram of the temperatures used to define a thermal decomposition mass loss. Initial, final, extrapolated onset and offset temperatures are denoted T_i, T_f, T_e, and T_o respectively.	24
Figure 1.5:	TG and DTA curves of a plant carbon before and after acid washing.	25
Figure 2.1:	UV spectrum of an alkali xanthate.	35
Figure 3.1:	Chugaev (or Tschugaeff) reaction.	40
Figure 3.2:	Thermal rearrangement of xanthate esters.	40
Figure 3.3:	Proposed thermal decomposition mechanism for nickel alkyl xanthates (Cavell *et al* 1973).	43
Figure 3.4:	Thermal decomposition of potassium ethyl xanthate adsorbed on a sulfide mineral.	45
Figure 3.5:	TD-py-GC-MS total ion chromatogram of SEX heated at 25°C min^{-1} in an inert atmosphere.	48
Figure 3.6:	Proposed initial reaction sequence for the thermal decomposition of SEX.	50
Figure 3.7:	Proposed further reactions for the thermal decomposition of SEX.	51
Figure 3.8:	TD-py-GC-MS total ion chromatogram of SiBX heated at 25°C min^{-1}in an inert atmosphere.	54
Figure 3.9:	TD-py-GC-MS total ion chromatogram of PEX heated at 25°C min^{-1} in an inert atmosphere.	55

Figure 3.10: TD-py-GC-MS total ion chromatogram of PAX heated at 25°C min^{-1} in an inert atmosphere. 56

Figure 3.11: Typical TG curve with extrapolated onset/offset temperature tangents for the decomposition of SEX heated at 10°C min^{-1} in an argon atmosphere. 57

Figure 3.12: SM spectrum of SEX at 197°C. 60

Figure 3.13: amu 60 and 76 ion chromatograms of SEX heated at 10°C min^{-1} in an argon atmosphere. 62

Figure 3.14: amu 60 and 76 ion chromatograms of SiBX heated at 10°C min^{-1} in an argon atmosphere. 62

Figure 3.15: amu 60 and 76 ion chromatograms of PEX heated at 10°C min^{-1} in an argon atmosphere. 63

Figure 3.16: amu 60 and 76 ion chromatograms of PAX heated at 10°C min^{-1} in an argon atmosphere. 63

Figure 3.17: TG-GS curves of SEX heated at 10°C min^{-1} in an argon atmosphere. 67

Figure 3.18: Infrared spectra of the gases evolved from the two mass losses of SEX, (a) first mass loss, (b) second mass loss. 67

Figure 3.19: TG-GS curves of SiBX heated at 10°C min^{-1} in an argon atmosphere. 68

Figure 3.20: Infrared spectra of the gases evolved from the two mass losses of SiBX, (a) first mass loss, (b) second mass loss. 68

Figure 3.21: TG-GS curves of PEX heated at 10°C min^{-1} in an argon atmosphere. 69

Figure 3.22: Infrared spectra of the gases evolved from the two mass losses of PEX, (a) first mass loss, (b) second mass loss. 69

Figure 3.23: TG-GS curves of PAX heated at 10°C min^{-1} in an argon atmosphere. 70

Figure 3.24: Infrared spectra of the gases evolved from the two mass losses of PAX, (a) first mass loss, (b) second mass loss. 70

Figure 3.25: TD-py-GC-MS total ion chromatogram of SEX adsorbed on Haycarb, heated at 25°C min^{-1} in an inert atmosphere. 77

Figure 3.26: TD-py-GC-MS total ion chromatogram of SiBX adsorbed on Haycarb, heated at 25°C min^{-1} in an inert atmosphere. 78

Figure 3.27: TD-py-GC-MS total ion chromatogram of PEX adsorbed on Haycarb, heated at 25°C min^{-1} in an inert atmosphere. 79

Figure 3.28: TD-py-GC-MS total ion chromatogram of PAX adsorbed on Haycarb, heated at 25°C min^{-1} in an inert atmosphere. 80

Figure 3.29: Measurement of the mass loss temperatures for the SEX adsorbed on Haycarb -45 μm. 82

Figure 3.30: amu 60, 62, and 76 ion chromatograms of SEX adsorbed on Haycarb and heated at 10°C min^{-1} in an argon atmosphere. 84

Figure 3.31: amu 57, 60, and 76 ion chromatograms of SiBX adsorbed on Haycarb and heated at 10°C min^{-1} in an argon atmosphere. 85

Figure 3.32: amu 60, 62, and 76 ion chromatograms of PEX adsorbed on Haycarb and heated at 10°C min^{-1} in an argon atmosphere. 86

Figure 3.33: amu 60, 70, and 76 ion chromatograms of PAX adsorbed on Haycarb and heated at 10°C min^{-1} in an argon atmosphere. 87

Figure 3.34: TG-GS curves of the xanthates adsorbed onto Haycarb, -45 μm heated at 10°C min^{-1} in argon atmospheres, (a) SEX, (b) SiBX, PEX, (d) PAX. 89

Figure 3.35: Infrared spectra of the gases evolved from SEX adsorbed on Haycarb, (a) first mass loss, (b) second mass loss, (c) third mass loss. 90

Figure 3.36: Infrared spectra of the gases evolved from SiBX adsorbed on Haycarb, (a) first mass loss, (b) second mass loss, (c) third mass loss. 91

Figure 3.37: Infrared spectra of the gases evolved from PEX adsorbed on Haycarb, (a) first mass loss, (b) second mass loss, (c) third mass loss. 92

Figure 3.38: Infrared spectra of the gases evolved from PAX adsorbed on Haycarb,(a) first mass loss, (b) second mass loss, (c) third mass loss. 93

Figure 3.39: TG curves of, (a) water, (b) SEX, (c) ratio 1:1, (d) ratio 16:1, and (e) ratio 1:16 (SEX:water). Heated at 10 °C min^{-1} in argon. 97

Figure 3.40: FTIR spectra of the gases evolved from the mass losses of the 1:1 SEX:water mixture displayed in Figure 3.39. (a) first mass loss, (b) second mass loss, (c) third mass loss, and (d) fourth mass loss. 98

Figure 3.41: Mass loss curves of 1:1 w/w ratios of (a) SiBX, (b) PEX and (c) PAX to water. 100

Figure 4.1: Molecular structures of some common frothing agents, (a) PPG, (b) PPGME, (c) α-terpineol, and (d) MiBC. 107

Figure 4.2: Thermal degradation mechanism of PEG. 109

Figure 4.3: TD-py-GC-MS total ion chromatogram of PPG heated at 25°C min^{-1} in an inert atmosphere. 111

Figure 4.4: TD-py-GC-MS total ion chromatogram of PPGME heated at 25°C min^{-1} in an inert atmosphere. 111

Figure 4.5: TD-py-GC-MS total ion chromatogram of α-terpineol heated at 25°C min^{-1} in an inert atmosphere. 112

Figure 4.6: TG-GS-MS curves for PPG heated from ambient to 500°C at 10°C min^{-1} in an argon atmosphere. 114

Figure 4.7: TG-GS-MS curves for PPGME heated from ambient to 500°C at 10°C min^{-1} in an argon atmosphere. 114

Figure 4.8: TG-GS curves for α-terpineol heated from ambient to 500°C at 10°C min^{-1} in an argon atmosphere. 115

Figure 4.9: TG-GS curves for MiBC heated from ambient to 200°C at 10°C min^{-1} in an argon atmosphere. 115

Figure 4.10: Infrared spectrum of the gases evolved from the PPG mass loss at 315°C. 117

Figure 4.11: Infrared spectrum of the gases evolved from the PPGME mass loss at 226°C. 117

Figure 4.12: Infrared spectrum of the gases evolved from the α-terpineol mass loss at 171°C. 118

Figure 4.13: Infrared spectrum of the gases evolved from the MiBC mass loss. 119

Figure 4.14: TD-py-GC-MS total ion chromatogram of PPG adsorbed on Haycarb, heated at 25°C min^{-1} in an inert atmosphere. 122

Figure 4.15: TD-py-GC-MS total ion chromatogram of PPGME adsorbed on Haycarb, heated at 25°C min^{-1} in an inert atmosphere. 123

Figure 4.16: TD-py-GC-MS total ion chromatogram of α-terpineol adsorbed on Haycarb, heated at 25°C min^{-1} in an inert atmosphere. 124

Figure 4.17: TD-py-GC-MS total ion chromatogram of MiBC adsorbed on Haycarb, heated at 25°C min^{-1} in an inert atmosphere. 125

Figure 4.18: TG-GS-MS curves for PPG adsorbed on Haycarb, heated from ambient to 1000°C at 10°C min^{-1} in an argon atmosphere. 127

Figure 4.19: TG-GS-MS curves for PPGME adsorbed on Haycarb, heated from ambient to 1000°C at 10°C min^{-1} in an argon atmosphere. 127

Figure 4.20: TG-GS-MS curves for α-terpineol adsorbed on Haycarb, heated from ambient to 1000°C at 10°C min^{-1} in an argon atmosphere. 128

Figure 4.21: TG-GS-MS curves for MiBC adsorbed on Haycarb, heated from ambient to 1000°C at 10°C min^{-1} in an argon atmosphere. 128

Figure 4.22: Infrared spectrum of the gases evolved from the mass loss of PPG adsorbed on Haycarb, at 308°C. 132

Figure 4.23: Possible formation of propanal from the thermal decomposition of PPG adsorbed on activated carbon. 134

Figure 5.1: TD-py-GC-MS total ion chromatogram of (a) loaded, and (b) barren samples from Three Mile Hill heated at 25°C min^{-1} in an inert atmosphere. 139

Figure 5.2: TD-py-GC-MS total ion chromatogram of (a) acid washed, and (b) regenerated samples from Three Mile Hill heated at 25°C min^{-1} in an inert atmosphere. 140

Figure 5.3: Ion chromatograms of the gases evolved from the decomposition of the Three Mile Hill loaded sample heated at 10°C min^{-1} in an argon atmosphere. 143

Figure 5.4: TG-GS curves of Three Mile Hill samples heated from ambient to 1000°C at 10°C min^{-1} in an argon atmosphere; (a) loaded, (b) barren, (c) acid washed, and (d) regenerated. 145

Figure 5.5: Typical infrared spectrum of the gases evolved from the first mass loss of a Three Mile Hill sample. 146

Figure 5.6: Infrared spectra of the second mass loss gases of the Three Mile Hill industrial samples; (a) loaded, (b) barren, (c) acid washed, and (d) regenerated. 147

Figure 5.7: Typical infrared spectrum of the third mass loss gases of Three Mile Hill industrial samples. 149

Figure 5.8: Typical infrared spectrum of the suspected fourth mass loss gases of Three Mile Hill industrial samples. 149

Figure 5.9: TD-py-GC-MS total ion chromatogram of (a) cloaded, and (b) cbarren samples from Salsigne heated heated at 25°C min^{-1} in an inert atmosphere. 151

Figure 5.10: TD-py-GC-MS total ion chromatogram of (a) tloaded, and(b) tbarren samples from Salsigne heated at 25°C min^{-1} in an inert atmosphere. 152

Figure 5.11: TD-py-GC-MS total ion chromatogram of the regenerated sample from Salsigne heated at 25°C min^{-1} in an inert atmosphere. 153

Figure 5.12a: Ion chromatograms of the evolved gases for the decomposition of the cloaded sample from Salsigne heated at 10°C min^{-1} in an argon atmosphere. 157

Figure 5.12b: Ion chromatograms of the evolved gases for the decomposition of the cloaded sample from Salsigne heated at 10°C min^{-1} in an argon atmosphere. 158

Figure 5.13a: TG-GS curves of Salsigne samples heated from ambient to 1000°C at 10°C min^{-1} argon atmospheres; (a) cloaded, (b) cbarren, (c) tloaded, and (d) tbarren. 160

Figure 5.13b: TG-GS curves of Salsigne regenerated sample heated from ambient to 1000°C at 10°C min^{-1} in an argon atmosphere. 161

Figure 5.14a: Infrared spectra of the second mass loss evolved gases from the Salsigne concentrate and tailing samples (a) cloaded, (b) cbarren, (c) tloaded, and (d) tbarren. 162

Figure 5.14b: Infrared spectra of the second mass loss evolved gases from the Salsigne regenerated sample. 163

LIST OF TABLES

		page
Table 1.1:	Mineralogy of WA Archaean ores.	2
Table 1.2:	Sulfide ore treatment plants.	5
Table 1.3:	Pore diameters in activated carbon.	11
Table 1.4:	Rate constants for fouled activated carbon from La Brooy *et al* (1986).	16
Table 1.5:	Analyses used to characterise activated carbon in CIP or CIL circuits.	20
Table 1.6:	Advantages and disadvantages of MS and FTIR detectors (Raemaekers and Bart 1997).	29
Table 2.1:	Elemental analysis of SEX, SiBX, PEX, and PAX.	32
Table 2.2:	Conditions used for thermogravimetric analyses.	38
Table 3.1:	A comparison of the decomposition temperatures of postassium xanthate obtained from the literature.	42
Table 3.2:	Gases evolved from the pyrolysis of SEX, SiBX, PEX, and PAX.	49
Table 3.3:	Mass losses and corresponding temperatures of SEX, SiBX, PEX, and PAX heated at 10°C min^{-1} in an argon atmosphere.	57
Table 3.4:	Relative peak areas of the evolved gases from SEX, SiBX, PEX, and PAX heated at 10 °C min^{-1} in argon atmospheres.	65
Table 3.5(a):	Peak wavelength assignments of the gases evolved from the first mass loss. Abbreviations: ν (stretch); ν_s, ν_{as} (symmetric, asymmetric stretch); δ (bending).	73
Table 3.5(b):	Peak wavelength assignments of the gases evolved from the second mass loss. Abbreviations: ν_s, ν_{as} (symmetric, asymmetric stretch).	73
Table 3.6:	Gases evolved from the pyrolysis of Haycarb activated carbon.	74
Table 3.7:	Gases evolved from the pyrolysis of SEX, SiBX, PEX, and PAX adsorbed on activated carbon.	76

Table 3.8: Mass losses and their corresponding temperatures for SEX, SiBX, PEX, and PAX adsorbed on Haycarb, -45 μm. 81

Table 3.9: Experimental versus theoretical mass losses for SEX, SiBX, PEX, and PAX adsorbed onto Haycarb. 83

Table 3.10: Relative peak areas of the decomposition gases from SEX, SiBX, PEX, and PAX adsorbed on Haycarb and heated at 10°C min^{-1} in an argon atmosphere. 88

Table 3.11: Mass losses of the TG curves in Figure 3.39. 99

Table 3.12: A comparison of each 1:1 w/w ratio xanthate:water TG curve mass losses. 100

Table 3.13: Comparison of the relative peak area (%) of gases evolved from the thermal decomposition of the xanthates by TD-py-GC-MS and TG-MS. 105

Table 4.1: Gases evolved from the pyrolysis of α-terpineol heated from 150 to 500°C at 25°C min^{-1} in an inert atmosphere. 113

Table 4.2: Mass losses and their corresponding temperatures of PPG, PPGME, α-terpineol, and MiBC heated at 10 °C min^{-1} in argon atmospheres. 113

Table 4.3: Gases evolved from the pyrolysis of PPG, PPGME, α-terpineol, and MiBC adsorbed on activated carbon. 120

Table 4.4: Mass losses and their corresponding temperatures for PPG, PPGME, α-terpineol, and MiBC adsorbed on Haycarb. 126

Table 4.5: Experimental versus theoretical mass losses for PPG, PPGME, α-terpineol, and MiBC adsorbed onto Haycarb. 129

Table 4.6: Relative peak area of the evolved gases from PPG, PPGME, α-terpineol, and MiBC adsorbed on Haycarb and heated at 10 °C min^{-1} in an argon atmosphere. 130

Table 4.7: Comparison of the relative peak area (%) of gases evolved from the thermal decomposition of the frothing agents adsorbed on Haycarb by TD-py-GC-MS and TG-MS (ND = not detected). 135

Table 5.1: Gases evolved from the pyrolysis of Three Mile Hill samples. 138

Table 5.2: Mass losses and their corresponding temperature ranges for loaded, barren, acid washed, and regenerated activated carbon samples from Three Mile Hill. 142

Table 5.3: Relative peak areas of the evolved gases from the Three Mile Hill samples heated at 10°C min^{-1} in argon atmospheres. 144

Table 5.4: Gases evolved from the pyrolysis of the Salsigne samples. 154

Table 5.5: Mass losses and their corresponding temperatures for cloaded, cbarren, tloaded, tbarren, and regenerated activated carbon samples from Salsigne. 155

Table 5.6: Relative peak areas of the evolved gases from the Salsigne samples heated at 10°C min^{-1} in argon atmospheres (A = cloaded, B = cbarren, C = tloaded, D = tbarren, E = regenerated). 156

Table 5.7: Maximum and minimum temperatures of carbonyl sulfide evolution during the second mass loss of each Salsigne activated carbon sample. 161

Table 6.1: Advantages and limitations of TD-py-GC-MS, TG-MS, and TG-FTIR techniques for thermal analysis of organic fouling agents on activated carbon. 169

PUBLICATIONS

Dunn JG, Avraamides J, Chamberlain AC and Fisher N (1996) 'The Thermal Decomposition of Sodium Ethyl Xanthate Adsorbed on Activated Carbon', The AusIMM Annual Conference, Perth 24-28 March.

Dunn JG, Chamberlain AC, Fisher NG and Avraamides J (1997) 'The Influence of Activated Carbon on the Thermal Decomposition of Sodium Ethyl Xanthate', Journal of Thermal Analysis, 49:1399-1408.

Fisher NG and Dunn JG (1999) 'Analysis of a Complex Gaseous Mixture by TG-MS and TG-FTIR', Journal of Thermal Analysis and Calorimetry, 56:43-49.

CHAPTER 1

INTRODUCTION

1.0 Gold Production in Australia

Since the first discovery of gold in Australia at the 1850s, there have been four boom periods of gold production. The latest occurred during the 1980s and as a result Australia is now the world's third largest gold producer, behind South Africa and the USA (Crowson 1994; Kelly 1992; Morgan 1993; Woodall 1990). This position has been achieved because of an eleven-fold increase in Australian gold production during the 1980s. Total gold production for the decade was 730.4 t, and the export revenue increased from A$75 million in 1980 to A$2.65 billion in 1989. This extraordinary increase has been attributed to a number of factors, although one of the main contributors was a dramatic increase in gold prices during this period, which unfortunately is no longer the case. The gold price has declined from a high of A$800 an ounce to the current level of $400. Hence most research in recent times has been focussed on the refinement of processes with a concomitant reduction in processing costs.

The other major contributor to the most recent gold boom was the application of the rediscovered activated carbon technology to gold processing. Some 100 years ago it was found that carbon (in the form of charcoal) was a good adsorbent for gold complexes such as the dicyanogold(I) ion and the gold was recovered by burning the carbon and smelting the ash. In the 1970s this approach was developed into a cost-effective technology using activated carbon for the recovery of gold from gold bearing cyanide solutions. The key feature of activated carbon (rather than charcoal) is that it rapidly strips gold cyanide from the leached pulp, containing typically 1-2 ppm soluble gold, to give an exit gold tail solution containing less than 0.05 ppm gold, a previously unattainable efficiency of recovery. This enabled previously uneconomic gold bearing ores, with values of less than 1 g of gold per tonne, to be profitably treated. This greatly increased the available ore reserves. In addition this technology permitted the retreatment of tailings dumps.

In this introductory chapter, a description of a typical gold processing plant will be given, indicating the various reagents used in the process. The role and function of

activated carbon used for gold adsorption will be discussed, including the undesirable interaction between processing reagents and the carbon. This will lead into the objectives for the research reported in this thesis.

1.1 Gold Deposits within Western Australia

Australia's most important gold province is located within the Yilgarn and Pilbara Cratons of Western Australia (Vaughan and Dunne 1987). The Cratons are portions of continental crust, the Yilgarn being the largest in terms of area, which includes the Kalgoorlie Golden Mile as well as the Boddington deposit. The Pilbara Craton includes the Telfer deposit. Gold formed within these Cratons during the Archean period, when approximately half of Australia's gold endowment occurred, 2700-2600 Myr ago (Myers and Hickman 1990; Woodall 1990).

The Archaean ores within Western Australia are subdivided on the basis of their gold and associated mineralogies as presented in Table 1.1. The mineralogical associations of the gold determine the most efficient processing route for maximum gold extraction (Vaughan and Dunne 1987).

Ores in the weathered profile	**Primary ores**

• alluvial deposits (including deep leads)
• lateritic ores
• supergene ores
	• gold associated with sulfides
	  • pyrite-associated
	  • arsenopyrite-associated
	  • associated with other sulfides
	• gold/silver telluride ores
	• gold in siliceous and/or carbonate gangue

Table 1.1: Mineralogy of WA Archaean ores.

Ores within the weathered profile are deep and are located 60-100 m above most primary orebodies. These ores are very similar in composition and are usually processed in the same way. Processing of oxide ores is relatively easy as the gold is contained within a soft gangue. Liberation of the gold generally consists of gravity

separation of free gold, followed by milling of the ore and dissolution of the gold by leaching in cyanide solution. The gold cyanide complex is adsorbed onto activated carbon, and then the gold recovered by dissolution from the carbon pellets by cyanide leaching in alkaline solution (Vaughan and Dunne 1987).

However a diverse mineralogy exists within the primary ores, which is dominated by pyrite, arsenopyrite, and telluride-associated ores, the first type being the most common. Within sulfide ores, gold is contained as inclusions, along grain boundaries or microfractures, or in solid solution. Extraction of the gold from the primary ore bodies is difficult and such ores are described as refractory. That is, refractory ores do not provide economic gold recovery with conventional cyanidation. Processing depends on how the gold is contained within the sulfide matrix, requiring several pre-concentration steps so the gold is accessible to cyanidation (Vaughan and Dunne 1987).

Gold can be contained within sulfide matrix in a number of ways. It may be physically encapsulated in minerals such as in sulfides, oxides, and silicates; as gold alloys or compounds, such as electrum and gold tellurides; or gold substituted as a solid solution in the sulfide lattice. Finally, a chemical layer may cause surface passivation of the gold (LaBrooy, Linge and Walker 1994).

1.2 Extraction of Gold from Sulfide Orebodies

The choice of a production route to extract gold from primary orebodies depends primarily on the refractoriness of the ore to be processed. A simplified production route for the processing of a refractory sulfide ore is presented in Figure 1.1. The flotation step and the other pretreatment step (highlighted by a thicker edged box) are the main additional steps required for refractory ore processing.

Several plants both within Australia and overseas (see Table 1.2) use the same type of processing route as shown in Figure 1.1.

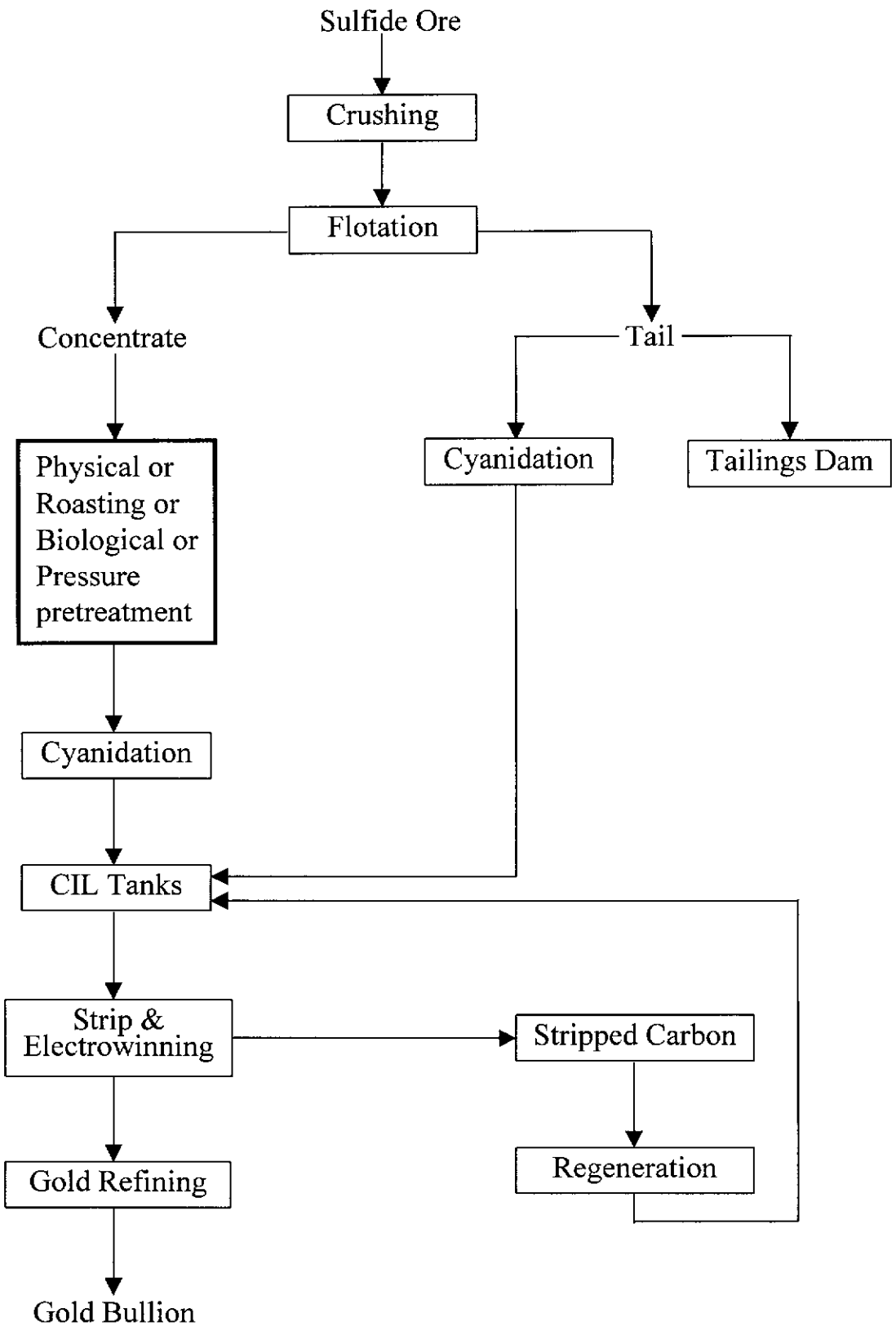

Figure 1.1: Simplified flowsheet of sulfide ore processing.

Australia	Overseas
• Queensland • Red Dome • New South Wales • Peak • Western Australia • Fimiston • Three Mile Hill • Wiluna Gold Mines	• Papua New Guinea • Porgera • New Zealand • Macraes Flat • France • Salsigne

Table 1.2: Sulfide ore treatment plants.

1.2.1 Crushing/Grinding

Crushing and grinding circuits are required to separate the mineral and the gangue into relatively clean particles of a size suitable for flotation (Wills 1997). Crushing circuits usually consist of 3 stages reducing the ore particle size to 10-15 millimetres. The grinding circuit usually consists of a ball mill reducing the particle size to less than 100 microns (Cutifani 1993).

1.2.2 Flotation

Flotation, patented in 1906, is considered as the most important and versatile mineral processing technique available. The flotation circuit concentrates the ore by removing the sulfide minerals from the gangue (extraneous rocky material). In the flotation circuit the hydrophilic ore particles are coated with a reagent known as a collector, such as the xanthates in the flotation of sulfide ores. Xanthate molecules consist of an anion containing a non-polar radical and a connected polar group, and a monovalent cation such as sodium or potassium (Wills 1997). It has been suggested that the xanthate molecule attaches to the sulfide mineral by replacement of the monovalent cation by a metal ion in the mineral (Bodsworth 1994). However, there is some dispute over this comment, as Crozier (1992) has reported it is not a metal-sulfur bond but a sulfur-sulfur bond between the mineral and xanthate molecule. A more recent paper by Vreugdenhil (1997) states it is a metal-sulfur bond.

Air is passed through the pulp and the non-polar ends of the xanthate coated ore particles attach to bubbles ascending to the gas-liquid surface. At the surface a frothing agent is present to prevent the bubbles collapsing, retaining the ore in the surface froth which is periodically skimmed off. Frothing agents consist of a non-polar group and a polar end such as hydroxyl, carboxyl, carbonyl, amino, and sulfo groups. The reactions of these groups with air and water mean frothing agents will adsorb at the air-water interface, reducing surface tension, and thus stabilising the air bubbles. Common frothing agents include pine oil (active chemical is α-terpineol), methyl isobutyl carbinol (MiBC), polyglycol ethers, and polyglycols. Other reagents such as modifiers, activators, and depressants are present in the circuit to provide optimum conditions for the flotation of the ore (Wills 1997).

1.2.3 Gold Liberation

After flotation, liberation of the gold encapsulated in the sulfide matrix, or from solid solution in arsenopyrite, is required to achieve good recoveries. There are several ways of liberating the gold, which are categorised into physical, roasting, biological, and pressure treatment.

Fine grinding is the only physical way of pretreatment, and is used if the gold is contained in the matrix primarily as included particles. Fine grinding the concentrate to 100 %, -38 μm will tend to produce good gold recoveries. This process, which is the cheapest pretreatment method, can even be used on arsenopyrite concentrates providing that the gold is not in solid solution (Bax and Bax 1993). Also ultrafine grinding may reduce the ore size to 1-20 μm (LaBrooy, Linge and Walker 1994).

Roasting is performed by heating the concentrate in the presence of oxygen to convert the sulfide to a calcine of haematite (Fe_2O_3) (Cutifani 1993). For example, in the roasting of pyrite (at 650-700°C), the following reaction occurs.

$$4FeS_2 + 11O_2 \rightarrow 2Fe_2O_3 + 8SO_2$$

The hematite formed is porous, and the gold is liberated for dissolution by leaching. Any gold telluride compounds present in pyrite ores will be decomposed according to the following equation.

$$AuTe + O_2 \rightarrow Au + TeO_2$$

Gold recoveries from roasted products usually are in excess of 95%. Although roasting is considered as one of the most cost effective pretreatment methods the control of sulfur dioxide emission can increase costs significantly (LaBrooy, Linge and Walker 1994).

Biological pretreatment refers to bacterial attack of sulfide ore (known as biooxidation). The process is performed with the use of bacteria such as *Thiobacillus ferrooxidans* and *Sulpholobus*. The conditions employed with bacteria are aerated, acidic solutions at ambient temperature and pressure. For example arsenopyrite is exothermically oxidised at a pH of 1.0-1.5 according to the equation (LaBrooy, Linge and Walker 1994; Odd and Hardy 1993).

$$FeAsS + 2.5H_2O + 3.5O_2 \rightarrow 0.5Fe_2O_3 + H_2SO_4 + H_3AsO_4$$

The solid product of hematite and an arsenic/iron compound contains the liberated gold.

Pressure oxidation pretreatment using an autoclave can be divided up into acid or alkaline conditions, and is most suited to ores that require complete sulfide destruction such as those which contain solid solution gold. Acid pressure oxidation of pyrite and arsenopyrite forms iron(III) sulfate and arsenate ions, which are then hydrolysed to form compounds such as haematite and iron sulfates. Alkaline conditions are used for high carbonate and low sulfur content ores; pyrite is thus dissolved to form iron oxides/hydroxides and sulfuric acid (LaBrooy, Linge and Walker 1994).

1.2.4 Cyanide Leaching

Gold is dissolved from the ore or concentrate by leaching with a cyanide solution in the presence of air or oxygen. Leaching involves oxidising the gold to the gold(I) ion by oxygen, and the gold(I) is stabilised by complexation with the cyanide in solution.

$$4Au_{(s)} + 8CN^-_{(aq)} + O_{2(g)} + 2H_2O_{(l)} \rightarrow 4Au(CN)_2^-{}_{(aq)} + 4OH^-_{(aq)}$$

Unfortunately gold is not the only metal leached by cyanide in leach circuits. Other metals from the ore such as copper, iron, zinc, nickel, and cobalt also react with cyanide to form soluble or insoluble cyano-metal complexes (Wang and Forssberg 1990).

1.2.5 Adsorption of Gold on Activated Carbon and Recovery

Gold cyanide is adsorbed on activated carbon in a carbon-in-pulp (CIP) or carbon-in-leach (CIL) circuit. A CIP adsorption circuit involves counter current contact between activated carbon and the discharge pulp from cyanide leaching in a series of agitated adsorption vessels. Leached pulp is added to the first tank, and then passes down the series of tanks where it meets increasingly fresh carbon travelling in the other direction. Thus the least concentrated solution in the final tank meets fresh activated carbon, thus ensuring that the exit solution has been stripped as efficiently as possible of its gold cyanide complex. This sequence ensures that minimal gold loss occurs during adsorption. CIL is a variation of CIP technology where dissolution of gold and adsorption of gold cyanide by carbon are carried out at the same time. It is postulated that CIL improves the rate of dissolution, and mitigates the loss of gold to other gold adsorbing substances found in the ore (Dahya and King 1983). CIL is also used where gold leaching is fast.

The gold-loaded carbon granules or pellets are separated from the barren pulp by sieving through a screen of suitable mesh size (usually around 0.85-1.0 mm). The loaded carbon is then treated with hot alkaline cyanide solution to desorb the gold

cyanide, to produce a relatively concentrated solution containing about 100-300 ppm of gold. Gold recovery can be achieved by electrowinning or zinc precipitation. Electrowinning is the preferred process in most cases and consists of electrolytic deposition of the gold on a steel wool cathode. The loaded cathode is treated with HCl to remove the iron followed by smelting of the gold. The zinc precipitation process is rarely used today as it is more complicated and labour intensive (Dahya and King 1983).

1.3 Activated carbon

Activated carbon is a generic term for a family of highly porous carbonaceous materials, none of which can be characterised by a structural formula or by chemical analysis (McDougall 1991, p109).

Approximately 3,500 t of activated carbon is imported into Australia each year for the CIP/CIL process. Total imports of activated carbon are valued at $10 million per year, and the market value is estimated at A$2,600 to $4,000 per ton (A.C.T.E.D. Pty Ltd 1998). The types of activated carbon used in the gold industry are usually derived from either coconut shell or peat, which is extruded to form cylindrical pellets of about 5 mm in length by 1 mm in diameter. These particular raw materials are preferred because of their hardness, low attrition and high loading capacity (McDougall 1991).

1.3.1 Manufacture

Activated carbon can be manufactured from many different carbonaceous materials such as coal, coconut shells, peach stones, peat, nut shells and sawdust (Bansel, Donnet and Stoecli 1988, Hassler 1974, McDougall 1991).

For the production of activated carbon for gold recovery, a two step process is used. The first step is carbonisation, in which the raw material is converted to a char by heating in the absence of oxygen below 700-800°C. During this step rudimentary

pores are formed. The second step involves activation, and consists of heating the char at 800 to 1100°C in the presence of air, enhancing the pore structure and creating new porosity (Bansel, Donnet and Stoecli 1988, McDougall 1991), as well as forming new surface oxides. The manufacturing process influences the resultant surface oxides and surface area, while the raw product determines the pore size distribution (McDougall 1991).

1.3.2 Structure

The basic structure of activated carbon is closely approximated by ideal graphite. Ideal graphite consists of fused hexagon layers held approximately 3.35 Å apart by weak van der Waals forces. Activated carbon is believed to consist of disordered fused hexagonal rings, that is the layers (only a few carbon atoms thick and 20-100 Å in diameter) contain rings many of which have been cleaved and are randomly orientated. The edges of the layers therefore change the electron density in the carbon skeleton and unpaired electrons appear. Also located at the edges of the layers are organic functional groups, referred to as surface oxides. Under the conditions used to produce the carbon for gold recovery, the surface groups are predominantly acidic in nature, which provide a negative surface potential. Although their structures are not known with certainty, a number of propositions as to the nature of these groups has been made, which include carboxyl, phenolic hydroxyl, quinones, and lactones to name a few. Some examples are given in Figure 1.2 (Cookson 1978; Bansel, Donnet and Stoecli 1988; McDougall 1991).

The fused disordered ring layers make up the walls of the pores of the activated carbon. The pore system has been classified into three different size ranges, macropores, transitional pores (or mesopores), and micropores. Their diameters are presented in Table 1.3.

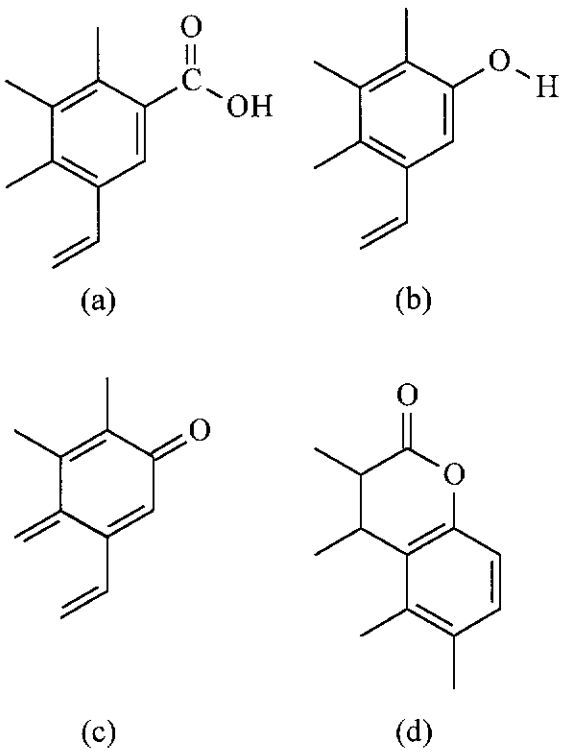

Figure 1.2: Some functional groups found on the surface of activated carbon (a) carboxyl, (b) phenolic, (c) quinone, and (d) lactone.

Pore	Pore Diameter (Å)
macropore	500-20,000
mesopore	100-500
micropore	8-100

Table 1.3: Pore diameters in activated carbon.

The function of the macropores is to serve as transport arteries to the meso and micropores. The micropores account for 95 %, and the mesopores 5 %, of the internal surface area. The macropores contribute very little to the internal surface area (Cookson 1978; McDougall 1991). Typical surface areas of activated carbon used for gold adsorption are around 1000 m^2 per gram.

1.3.3 Adsorptive Properties

The adsorptive properties of carbon are usually determined experimentally by constructing an adsorption isotherm for a series of similar compounds, altering the surface of the activated carbon by increasing or decreasing the concentration of acidic sites, and repeating the isotherm. The data usually fit a Langmuir isotherm. The tendency of compounds to adsorb is quantitatively expressed by use of an equilibrium constant, K, which is the concentration of the adsorbed species divided by the concentration remaining in solution. Hence K values greater than 1 indicate a preference to adsorb (Cookson 1978).

Activated carbon owes its adsorptive properties to its large internal surface area, and pore-size distribution. The external surface area is considered to play only a minor role. Although they are only a relatively minor component of the carbon, the surface oxides play a major role in its chemical behaviour providing acid-base, redox and catalytic oxidative properties as well as imparting a hydrophilic character to hydrophobic carbon (McDougall 1991). In addition, the surface groups affect the capacity and rate of adsorption. Adsorption occurs via physical (Van der Waals, hydrogen bonding, dipole-dipole interactions) or chemical means (ionic, covalent bonding), the latter being generally irreversible. The absorptive properties of aqueous solutions on activated carbon are influenced by temperature, pH, chemical nature of the species present and their relative concentration, the nature of the activated carbon, and its particle size distribution (Cookson 1978; McDougall 1991). The adsorption of inorganic and organic compounds may occur via several different mechanisms.

Adsorption of organic compounds usually occurs by simple mechanisms which are primarily a balance between hydrogen bonding in solution and Van der Waals attraction between the surface of the carbon and the organic species (McDougall 1991). However, with aromatic organic compounds, there is the possibility of an electron donor/acceptor interaction between the aromatic ring and surface carbonyl groups such as quinones and hydroquinones (Cookson, 1978, p 267). This can be

quite a strong interaction, at least as suggested by the relatively large K values exhibited by some aromatic compounds.

In general, an increase in the oxygen content of the carbon, which corresponds to an increase in the number of acidic groups present, has been found to decrease the adsorption of most species in solution. This is true for organic compounds as well as inorganic complexes such as the dicyanoaurate(I) ion. Since gold solutions are at pH values of around 10, most of the acidic groups will be significantly ionised. This suggests that the negative potential on the surface of the carbon will tend to repel any negatively charged species in solution, unless other attractive forces are powerful enough to overcome this repulsion. Evidence for this effect comes from measurement of K values at different pH values, when the surface charge bias changes. In acidic solutions of pH 1-4 the dicyanoaurate(I) ions adsorbs more strongly than in basic solutions. This may be due to non-ionisation of the acidic groups as well as the formation of ion pairs such as $H[Au(CN)_2]$. Thermal decomposition of the acidic groups tends to restore the full adsorptive capacity.

The presence of metal ions within the structure of the carbon increases the adsorption for negatively charged ions. For example, the presence of calcium and sodium ions increases the amount of silver cyanide adsorbed, and the presence of sodium, potassium and calcium increases the rate of gold loading (Yapu *et al* 1994).

1.3.4 Fouling and Regeneration of Activated Carbon

One of the disadvantages of activated carbon when used for gold recovery is its lack of selectivity. The carbon will adsorb, with various degrees of efficiency, most of the dissolved inorganic or organic compounds present in the leach solution. Thus some of the active sites are occupied by unwanted compounds, and the quantity of gold that can be adsorbed is diminished. Even when the gold has been dissolved from the carbon by alkaline cyanide solution, the other adsorbents remain on the carbon, and its activity towards gold is diminished. Such carbons are said to be fouled. Recycling of the activated carbon is required due to its high cost. There are two

stages to the regeneration step, acid washing to remove inorganic contaminants, and thermal reactivation to remove volatile or unstable organic impurities.

Inorganic fouling agents, such as adsorbed base metal complexes present in the leach solution, are usually removed by acid washing. This also prevents build up of calcium carbonate, silica, etc, which block pores and/or coat gold cyanide particles (La Brooy and Bax 1985; La Brooy *et al* 1986; La Brooy 1988).

It is the organic fouling agents that are of a greater concern in plant circuits. Organic compounds (oils, greases, process chemicals) are present in most CIP/CIL circuits as a result of their addition or spillage during mining, milling, flotation, and equipment maintenance operations. Also the ore or process water often contains organic products derived from mine timbers, vegetation and sewage (La Brooy and Bax 1985; La Brooy *et al* 1986; La Brooy 1988).

The relative deactivation of activated carbon by circuit organic compounds has been comprehensively assessed by La Brooy *et al* (1986, 1988). Both papers reported on the effects of various organic fouling agents on the kinetic activity of gold adsorption. The experimental program consisted of ageing the activated carbon in a solution containing various fouling agents, and then placing the carbon in a gold solution. That is, 10-100 ppm of fouling agents plus 200 ppm NaCN was added to activated carbon samples for 24 hours before adding 10 ppm Au as $Au(CN)_2^-$. Thus competition between the gold and fouling agents for adsorption was neglected.

The kinetic activity of gold adsorption is used in determining plant efficiency. Kinetic activity can be determined using a rate constant, k. La Brooy *et al* (1986) used the following rate equation to determine the rate constant for activated carbon, and it is linear up to 4 hours.

$$\Delta[Au]_c^t = k[Au]_s^t \, t^n$$

where $\Delta[Au]_c^t$ = change in gold adsorption from time t = 0 to t = t (grams/tonne),

$[Au]_s^t$ = gold concentration in solution (ppm) at time t,

k = rate constant (h^{-1}),

c = nitial gold concentration (ppm),

n = empirical constant dependent on the carbon,

t = time of adsorption (h).

Fouling agents studied included a grinding aid, viscosity modifiers, flocculants, collectors (xanthates), frothing agents, oils, vegetation products, and organic solvents. These were compared to a control sample. The rate constants calculated for the control sample, collectors, frothing agents, oils, and vegetation products are reproduced in Table 1.4.

As seen in Table 1.4 the rate constant for activated carbon that hasn't undergone ageing is 1200 h^{-1}, but this falls to 640 h^{-1} with ageing in distilled water. Comparison of these control rate constants to the fouled carbon rate constants shows the lower the value, the greater the deactivating effect of the fouling agent.

The grinding aid, viscosity modifiers, and flocculants had little effect on carbon activity and their rate constant values are not presented in Table 1.4. It was suspected these larger molecules were unable to enter the carbon micropores, and so did not impede access of hydrated $Au(CN)_2^-$ ions due to their hydrophilic nature. Organic solvents such as acetonitrile, ethanol, and methanol also had little effect on carbon activity and their k values are not presented in Table 1.4 (La Brooy *et al* 1986, La Brooy 1988).

The rate constants for the xanthate-fouled carbon samples show that xanthates have a serious effect on the kinetic activity of gold adsorption. Also the longer alkyl chain xanthates have a more serious effect on the kinetic activity (from 280 h^{-1} for ethyl to 40 h^{-1} for amyl). This agrees with Traube's rule which predicts that the longer the chain in a homologous series, the stronger is the adsorption. It was suggested that

the hydrophobic anionic nature of xanthates inhibit solution diffusion, competing with gold cyanide for surface-active carbon sites.

Fouling agent (10-100 ppm)	**k (h^{-1})**
Control	
• no ageing	1200
• distilled water	640
Collectors	
• Sodium ethyl xanthate	280
• Sodium isobutyl xanthate	140
• Potassium amyl xanthate	40
• Aerofloat 208	270
Frothing Agents	
• Teric 401	110
• Teric 402	140
• Dowfroth 200	130
• MIBC	270
Oils	
• Mobil ALMO 527	200
• Diesel	190
• Multigrade	390
Vegetation Products	
• swamp water	120

Table 1.4: Rate constants for fouled activated carbon from La Brooy *et al* (1986).

The frothing agents studied were of the polyoxyethylene/propylene glycol ether type (Teric frothing agents) and MIBC (methyl isobutyl carbinol). The effect of the polyoxyethylene/propylene glycol ether frothing agents on carbon activity was serious (140-110 h^{-1}) and second to that of potassium amyl xanthate (40 h^{-1}). Frothing agents are thought to render the carbon surface more hydrophobic, impeding access of gold cyanide. As seen in Table 1.4 MiBC does not deactivate carbon as seriously (270 h^{-1}) as the glycol ether frothing agents. This is possibly due to the lower molecular weight of MIBC (La Brooy *et al* 1986, La Brooy 1988).

Oils had a moderate effect (390-190 h^{-1}), possibly clogging pores rendering the carbon hydrophobic.

Of the vegetation decomposition products, only the swamp water rate constant was reported which showed serious deactivation (120 h^{-1}). Further tests were performed using humic and fulvic acids but no rate constants were reported. However, it was reported that the humic acid fraction was considered to be responsible for the most serious deactivation. Humic acids are complex polymeric molecules based on phenols. It is suspected humic acids are adsorbed strongly on activated carbon via surface carbonyl groups (La Brooy and Bax 1985; La Brooy *et al* 1986; La Brooy 1988).

Examination of Figure 1.1 shows flotation reagent fouling of activated carbon in a CIL circuit may occur via two routes. The first is through the concentrate stream from the flotation circuit. The fouling agents may possibly pass through the gold liberation process if regrinding or biooxidation is used as a means of liberating the gold. If roasting was used, the fouling agents are most likely oxidatively decomposed to gaseous products, and in fact roasting is also used to remove carbonaceous species. However it is most likely that the majority of flotation reagents come from the tailings stream (see Figure 1.1). The tailings do not undergo any pretreatment at all and is recombined with the treated concentrate in the CIL circuit, thus fouling of the carbon occurs. Oils such as diesel, air compressor and multigrade engine lubricants could enter the CIP/CIL circuit via a number of routes. Humates produced from natural vegetation could enter the CIP/CIL circuit via the process water or from timber, etc in the ore.

Thermal regeneration is required to remove the various organic fouling agents which are adsorbed onto the activated carbon before recycling back to the CIP/CIL circuit. Thermal reactivation involves heating the fouled activated carbon to approximately 650°C for up to 30 minutes in the absence of air. The most common method uses an externally heated rotary kiln. The process consists of introducing the activated carbon into the kiln in a wet state. The feed end of the kiln is sealed so that steam generated from the moisture in the carbon passes over the carbon bed and is exhausted from a flue pipe at the discharge end, preventing air from entering the kiln. This results in partial burn-off of the carbon.

$$C + H_2O \rightarrow CO \quad (\text{or } CO_2) + H_2$$

The reaction is thermodynamically favourable at temperatures greater than 650°C. It has been found, however, that some degree of burn-off is actually beneficial increasing the activity of the carbon (Dahya and King 1983).

The efficiency of thermal regeneration has been studied by La Brooy *et al* (1984), using rate constants for 6 different West Australian CIP plants. Some of their results are reproduced in Figure 1.3, and shows the effect of regeneration temperature on the carbon activity for one of the plants after stripping, and for plant and laboratory regenerated samples.

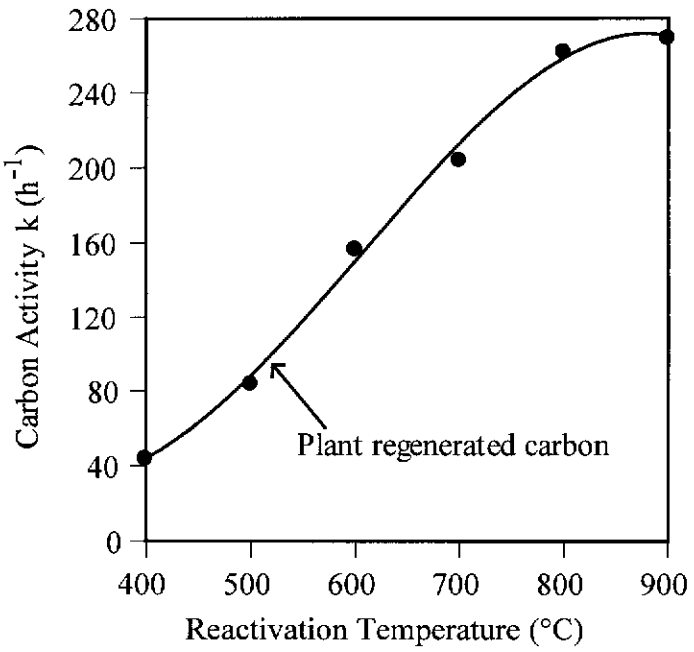

Figure 1.3: Effect of reactivation temperature on carbon activity.

Figure 1.3 shows carbon activity starts to increase at 500°C, rising sharply at 600-800°C, and then plateaus at 800-900°C. Also the plant regenerated sample at approximately 500°C only improved the activity to 90 h^{-1}. Although increasing the kiln temperature will increase the carbon activity, the problem of increased carbon burn off occurs. The authors note thermal regeneration of up to 750°C is usually required to obtain an operation kinetic activity of 50-150 h^{-1}.

1.3.5 Gold Cyanide Adsorption

Numerous investigators have attempted to determine the mechanism of gold cyanide on activated carbon. There are currently two most widely accepted theories, adsorption involving ion pairs, and adsorption of unpaired ions. The ion pair theory is based on an ion pair $M^{n+}Au(CN)_2^-$, where M^{n+} is most likely potassium, sodium, or calcium. Several investigators have also proposed a single water molecule may exist between the pairs. The wide acceptance of this theory is that it explains how a negatively charged complex can adsorb on a negatively charged surface. However, it has been pointed out that adsorption will occur between two negatively charged species if the electrostatic repulsion is exceeded by a very strong adsorbate-adsorbent interaction (Ibrado and Fuerstenau 1995).

1.3.6 Activated Carbon Surface Studies

The main technique used in the literature to study the surface groups and interaction of adsorbed compounds on activated carbon is diffuse reflectance infrared spectroscopy (DRIFT). Other infrared techniques which have been used include attenuated total reflection, internal reflection, and KBr disc (Boehm 1994; Friedel and Hofer 1970; Mattson, Mark, and Weber 1969).

The spectrum of a compound studied by KBr disc is due to infrared absorption of that compound. DRIFT differs from the KBr technique in that it is the diffuse reflection that produces the infrared spectrum. Diffuse reflection results from incident radiation striking the surface of many compound particles and scattering in all directions as reflection and refraction radiation (Nishikida, Nishio, and Hannah 1995). Thus DRIFT is a surface infrared technique.

Although DRIFT appears to be the preferred method for surface characterisation, the resulting spectra have been difficult to interpret due to the strong infrared absorption of activated carbon (Boehm 1994). A DRIFT study on the formation of surface groups on carbon black (a substance similar to activated carbon but with a very low

surface area) has been reported by Fanning and Vennice (1993). From their studies they concluded that although difficult, it was possible to use DRIFT as a means of detecting and monitoring surface groups. The authors also constructed a table of principle functional groups found on the surface of carbon and their infrared assignments from a review of the literature.

DRIFT was also used by Park *et al* (1997) to study the interaction of copper, zinc, and molybdenum on activated carbon. The authors also produced a table of functional group assignments found on activated carbon. However as the authors used a high resolution infrared spectrometer (up to 0.125 cm^{-1}), a sensitive mercury-cadmium-telluride detector and long scans they were used to observe previously unreported functional groups. Unfortunately it was difficult to compare the metal-impregnated activated carbon infrared spectra with that of just activated carbon, so it was not possible to determine which groups, if any, had interacted with the metals.

1.4 Current Test Methods for the Assessment of Activated Carbon

There are numerous tests used to determine the effectiveness of activated carbon in a gold plant. Samples taken during various stages in a CIP or CIL circuit can be analysed for properties shown in Table 1.5.

Physical Properties	Fouling
• kinetic activity	• ash content
• K-value	• extractable calcium
• total gold	• total silica
• gas adsorption	• apparent density
• apparent density	• lab scale regeneration
• wet attrition	• thermogravimetric analysis (TG)
• abrasion index	
• particle size distribution	
• visual inspection	

Table 1.5: Analyses used to characterise activated carbon in CIP or CIL circuits.

Kinetic activity is an important factor in determining plant efficiency and it was discussed in detail in section 1.3.4. The K-value is calculated using a Freundlich isotherm and can be used to determine if sufficient reactivation has occurred. Gas adsorption of butane, benzene, and carbon tetrachloride is used to obtain information on pore structure. The total gold content gives the loading and hence the plant profitability.

Apparent density is used to determine how much carbon can be placed in a vessel under well packed conditions (reported as g/L of dry carbon). As seen in Table 1.5, apparent density can also be used for a rapid indication of fouling. For example, if virgin carbon density is 500 g/L and that of a used carbon is 600 g/L (without the presence of other solids), severe inorganic fouling has occurred.

Wet attrition is as the name suggests a measure of the physical degradation of the carbon in a circuit, and gives some idea of how much replacement carbon is needed to maintain the correct quantity in the circuit. The abrasion index is a faster method for determination of carbon degradation. The particle size distribution is important as much of the carbon handling within a plant uses screens.

Visual inspection is a fast/cheap method of determining the condition of both virgin and used carbon. Factors used in inspecting a carbon sample include the shape, colour, and the presence of wood chips. If the shape of virgin carbon particles exist mainly as thin platelets, a high carbon loss may occur. Light grey colours indicate the presence of inorganic fouling. If any wood chips in a thermally regenerated carbon have not carbonised (appear brown) the kiln temperature is much lower than it should be.

Determination of inorganic fouling is performed using ash content and extractable calcium methods. Thus the efficiency of the acid washing step can be evaluated. The total silica is a measure of the amount of blockage that might be found in the pores of the carbon. Laboratory scale regeneration is a good method of determining if the plant kiln is performing properly.

Although there are many tests used to assess the condition of activated carbon from industrial plants, thermal methods of analysis are the only methods that are available so far for the direct determination of fouling by organic compounds.

1.5 Thermal Analysis

Thermal analysis is a term used to describe a family of techniques that involve monitoring either a physical or chemical property of a material in a specified atmosphere versus programmed temperature (Haines 1995). Two of the major thermal analysis techniques are thermogravimetry (TG) and differential thermal analysis (DTA).

The property measured in TG is mass loss or gain, and so typically the data is presented as mass loss or gain on one axis and temperature on the other axis. The first derivative of the mass loss (dm/dT) can be plotted as an alternative mode of presentation against temperature, and gives rise to the DTG curve. Since the sample is usually heated or cooled at some constant rate, such as 10°C min^{-1}, the temperature axis can also be presented in units of time. The apparatus typically consists of a microbalance with the sample suspended from one arm of the balance or on a sample carrier sitting on a microbalance into a furnace. A temperature programmer enables the furnace to be heated or cooled at set rates, usually in the range 1-100°C min^{-1}, or held at some fixed temperature for a period of time. The whole system is enclosed in a glass or ceramic vessel, which permits control of the atmosphere.

In DTA, it is the energy of reaction that is measured as a function of time or temperature. The energy of the reaction is determined by measurement of the temperature difference between the sample and an inert reference material, using thermocouples, one placed under the sample and the another under a blank sample. The sample and reference are enclosed in a furnace, which can be programmed in the same manner as described for TG. The two thermocouples are set in opposition, so that when no reaction takes place the differential output voltage of the thermocouples is zero, and a flat baseline is observed. When an endothermic reaction takes place,

the sample is cooled relative to the furnace temperature, and so a difference voltage signal is generated which is recorded as a peak. Once the reaction is complete, the sample and sample pan are reheated to the furnace temperature and the peak returns to the baseline. By convention, peaks resulting from an endothermic reaction are presented as a negative or downward peak, and exothermic reactions are presented as a positive peak or upward direction.

One of the major applications of thermal methods of analysis is in the study of decomposition reactions. Substances can be heated under a variety of conditions, and the temperature range over which the reaction takes place can be determined. The interpretation of the data needs some consideration. The temperature at which a material starts to decompose can be defined thermodynamically as the temperature at which the free energy of the reaction is zero. Hence in thermodynamic terms there is one specific and constant decomposition temperature (Dunn and Sharp, 1993, p 173). In thermal analysis experiments, however, there is a temperature range over which a thermal decomposition reaction takes place. Furthermore, this temperature range is dependent on the experimental conditions chosen for the experiment. That is, the temperature range is dependent on the sample preparation, sample mass, sample container, heating rate, and the atmosphere.

Generally, increasing the particle size of a solid, increasing the sample mass and increasing the heating rate will bring about two changes. Firstly, the temperature interval between the start and finish of the TG curve and/or DTA peak will increase. Secondly, the TG curve and DTA peak will shift to higher temperatures. The geometry and type of a sample container also effects the TG curve in decomposition reactions. Since a decomposition reaction involves the mass transfer of evolved gases, any container configuration that inhibits gas diffusion away from the sample will also produce the same two effects discussed above. Finally, the atmosphere used will influence the type of decomposition that takes place. Inert atmospheres will produce pyrolysis reactions, whereas air will produce oxidation reactions. There may be no similarity between the TG curves and/or DTA peaks obtained from the reaction of a material under these two different gases (Dunn and Sharp 1993).

TG does have some distinct advantages over DTA when used to study decomposition reactions. Firstly, with TG, the temperature range does accurately reflect the beginning and end of the reaction. With DTA, however, whilst the temperature at which the peak commences reflects the start of the reaction, the temperature at which the peak returns to the baseline does not. The reaction has probably been completed somewhere between the temperature of the peak maximum and the return of the peak to the baseline. The remainder of the peak is simply the time that it takes for the sample and sample pan to be either reheated (for an endothermic reaction) or cooled (for an exothermic reaction) back to the temperature of the furnace. Hence the temperature interval of a DTA curve does not reflect the beginning and end of the reaction. Secondly, if just a single reaction is taking place, and provided the microbalance has been correctly calibrated for mass change, then the mass loss is a quantitative measure of the amount of material decomposed. The area of the DTA peak is proportional to the amount of material decomposed, but calibration of the DTA apparatus with a suitable standard energy calibrant is not a trivial task.

For the analysis of TG decomposition curves, the best method of identifying the temperature at which a reaction starts and finishes is using the extrapolated onset (T_e) and offset temperatures (T_o). This method is considered as the most reproducible. The method for determining these values is shown in Figure 1.4.

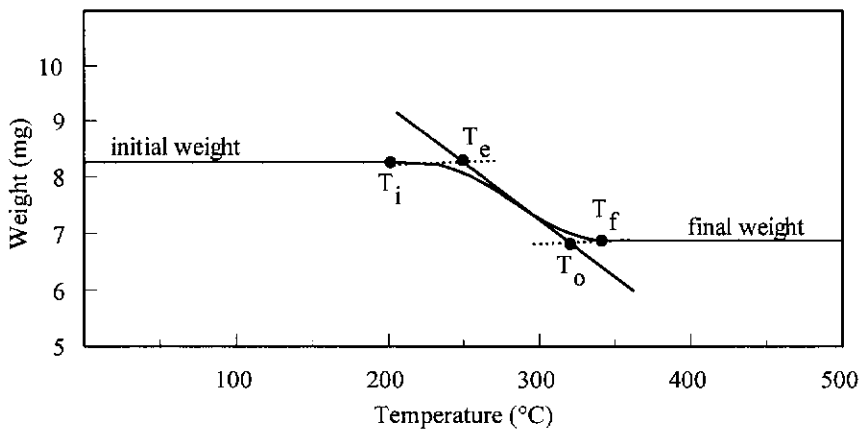

Figure 1.4: Schematic diagram of the temperatures used to define a thermal decomposition mass loss. Initial, final, extrapolated onset and offset temperatures are denoted T_i, T_f, T_e, and T_o respectively.

Figure 1.4 also shows the determination of the initial (T_i) and final temperatures (T_f). These values are less reproducible, and are dependent on procedural variables such as the sensitivity of the microbalance, sample size etc (Dunn and Sharp 1993).

1.5.1 Investigations of Fouling of Activated Carbon using Thermal Analysis

Researchers investigating organic fouling to date have only been able to predict classes of organic compounds from the mass losses observed at various temperature ranges. For example, it has been reported by La Brooy and Bax (1985) that a TG curve of fouled carbon consists of two main weight loss regions after water has evaporated (see Figure 1.5). The first mass loss commenced at around 300°C and the second at around 650°C. Work by Suzuki *et al* (1978) suggested that the first mass loss is due to simple long chain organic compounds such as collectors and frothing agents. The second mass loss was believed most likely due to more stable complex organic compounds like humates.

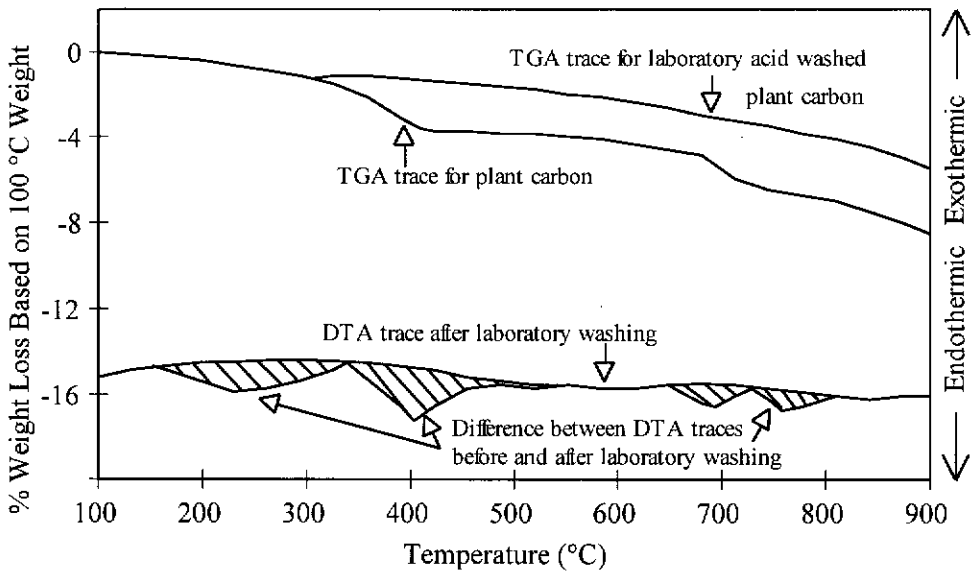

Figure 1.5: TG and DTA curves of a plant carbon before and after acid washing.

DTA curves were also recorded. The broad endothermic peak from 150-350°C could be due to the evolution of water, which takes a considerable time to diffuse out of the micropores of the activated carbon. This corresponds to the gradual mass loss up to

350°C. The next endothermic peak corresponds to the second mass loss, but the third mass loss has two associated endothermic events, indicating that there are probably two reactions taking place in this temperature range. The first DTA peak may be due to the decomposition of humate compounds as suggested by Suzuki *et al* (1978), but the second endothermic peak could be due to the decomposition of calcium carbonate, which takes place at approximately 700°C with the evolution of carbon dioxide.

Once the carbon has been reactivated in the plant, a TG curve can be used as a diagnostic test for the effectiveness of reactivation by comparing the mass losses in the untreated plant carbon, and the regenerated material. Ideally, the TG curve for the regenerated carbon should be the same as the fresh activated carbon. If some mass losses are still evident in the regenerated form, then the plant regeneration equipment may not be operating at optimum conditions.

However, TG can only be used to determine the total organic fouling, and not individual fouling agents such as collectors, frothing agents, oils, humates, etc. Thus it cannot be determined which organic compounds are responsible for causing the most serious problems of deactivation of carbon in a CIP or CIL circuit.

Advances in thermal analysis technology have provided researchers with new methods for the identification of gases evolved from thermal decompositions/ desorptions.

1.5.2 Evolved Gas Analysis

Evolved gas analysis (EGA) is defined as a technique that monitors the nature and/or amount of volatile products evolved by a sample when subjected to a controlled temperature program. EGA can be used in tandem with thermal analysis when the identification of volatile products is required. Common combinations are DTA-EGA and TG-EGA. There are numerous techniques for detecting and identifying volatile products, the two most common being mass spectrometry (MS) and Fourier

transform infrared (FTIR) spectroscopy. Both techniques are able to monitor the volatile products continuously over a controlled temperature program (Haines 1995; Hatakeyama and Quinn 1994).

MS and FTIR instruments are generally connected to thermal analysis instruments via heated transfer lines, usually at 200-250°C. For most systems it takes approximately one second from the time of gas evolution to the time of detection. Thus secondary gas phase reactions and condensation can be avoided. Connection of a FTIR is relatively easy, but is more difficult with MS due to the low pressures required to prevent secondary reactions. This is achieved by using a capillary tube to transfer the gases and an orifice or jet separator to reduce the pressure (Haines 1995).

Mass spectrometry is considered by many as the most powerful identification technique available. In thermal analysis, quadrupole mass spectrometers are generally employed as they are smaller and easier to use. Essentially the technique involves bombardment of a volatile product entering the mass spectrometer by electrons. This removes an outer shell electron from the volatile product producing a molecular ion. Due to the high energy imparted by the process the molecular ion may fragment into a lower mass fragment ion and a neutral fragment and so on. The degree and type of fragmentation is dependent on the ionisation potential of the volatile product. Thus a fragmentation pattern results which is characteristic to that volatile product, and is known as a mass spectrum.

Separation of the fragment ions for detection is achieved by the quadrupole. The quadrupole essentially consists of four rods, which are continuously subjected to varying radio frequency and direct current fields with opposite polarities on pairs of opposing rods. The ions oscillate between the rods. Some will pass through if they are of the correct mass, and others will not, hitting the rods and being pumped away by a vacuum pump. Once through the quadrupole the ion signals are generally amplified by an electron multiplier, and then pass onto a collector giving a current which is then detected (McLafferty 1980).

FTIR spectroscopy is considered to be more selective than MS, as molecules have their own characteristic infrared fingerprints. However it can only be used for molecules possessing a dipole moment. Infrared spectroscopy consists of subjecting a molecule to an infrared beam of continuously changing frequency. The molecule absorbs certain frequencies as energy is consumed via stretching and bending of different bonds. Absorption of energy weakens the infrared beam and a curve will be constructed for the absorption versus wavenumber, producing an infrared spectrum (Nakanishi and Solomon 1977). It is worthwhile to note that for gaseous samples complex ro-vibrational spectra such as the multitude of fine peaks in a water vapour spectrum can occur. Also gaseous spectra can and often do appear very different to condensed phase spectra of the same material (Haines 1995).

Although MS detectors are considered as the best for sensitivity and versatility, FTIR detectors are also very popular. Both can be used for qualitative and quantitative analysis, although the error for FTIR quantitative analysis is in the order of ±10 % (Raemaekers and Bart 1997). Table 1.6 illustrates the advantages/disadvantages of each detector. It can be seen that the strengths of each technique complement one another.

The main disadvantage displayed in Table 1.6 is that if these EGA techniques are used to study a material that decomposes into multiple gases, a number of problems arise (Raemaekers and Bart 1997). Of these, the most significant problem is the overlap of signals from different gases, preventing identification as well as quantification. For complex gas mixtures, a separation step must be used if identification of specific evolved gases is required. The most popular separation system is gas chromatography-mass spectrometry (GC-MS). Such methods can be either off-line, in which the evolved gases are bubbled through a solvent or into an absorbent and then injected onto a GC-MS; or on-line where the TG apparatus is coupled directly to a GC-MS (Reggers *et al* 1997). Another technique that could be used is pyrolysis-gas chromatography-mass spectrometry (py-GC-MS). Most pyrolysis units operate by heating the sample rapidly from ambient to a set temperature, although some pyrolysis units are temperature programmable. In the

later mode the py-GC-MS system is closest to the experimental conditions used in TG-GC-MS.

	Mass Spectrometry Detectors	Fourier Transform Infrared Detectors
Advantages	• detection levels in the order of pico-grams, • identification of individual compounds, • structure elucidation of very large molecular weight compounds is possible.	• functional group identification and specific compound analysis, • scanning of effluent from direct thermal processing, • simultaneous spectral information on many species.
Disadvantages	• limited due to low resolution, • cannot be used directly for quantitative gas determination, • cannot distinguish between ions of equal molecular weight, • careful choice of purge gas, its ions should not interfere with any expected reaction products, • a high vacuum and more stringent operating conditions are required, • results can be misleading because of secondary products from ion fragmentation.	• relative low sensitivity, • difficult to analyse mixtures of compounds with similar functional groups, • difficult to analyse mixtures of weak IR absorbers in the Presence of strong IR absorbers, • cannot detect compounds without a dipole, • does not readily distinguish between hydrocarbons above propane.

Table 1.6: Advantages and disadvantages of MS and FTIR detectors (Raemaekers and Bart 1997).

1.6 Proposed Research

Only one technique exists for the determination of organic fouling agents on activated carbon, that is thermogravimetry. Used alone this technique is insufficient to identify individual organic fouling agents. However, the use of coupled techniques in which the gaseous products from the decomposition of the adsorbed species can be identified is likely to enable identification of the original adsorbed compound. Consequently as part of this research program three techniques, namely thermal desorption-pyrolysis-gas chromatography-mass spectrometry (TD-py-GC-

MS), TG-MS, and TG-FTIR are investigated for their ability to identify individual fouling agents adsorbed on activated carbon from operating gold processing plants.

In this thesis, the thermal decomposition of the two groups of organic fouling agents that cause the most severe deactivation of activated carbon was investigated. That is, xanthates and frothing agents. In Chapter 3 the thermal decomposition of four alkali metal xanthates of differing chain length and cation are discussed, and in Chapter 4 the thermal decomposition of four common frothing agents are discussed.

In Chapters 3 and 4 the thermal decomposition properties of each pure fouling agent were determined first. Of specific interest were the temperature(s) of decomposition, the corresponding mass loss or losses, and the identification of any decomposition gases. The thermal decomposition properties of the each fouling agent individually adsorbed on activated carbon were then studied. The thermal decomposition properties of the non-adsorbed and adsorbed fouling agents were then compared. Finally, attempts were made to explain any differences that exist between the gaseous decomposition products of the non-adsorbed and adsorbed fouling agents.

The last chapter (Chapter 5) in this thesis focuses on the thermal decomposition of fouling agents adsorbed on activated carbon samples from two different gold processing plants. A suite of carbon samples were analysed, taken after the final tank in the gold loading train, the stripping tank, after the gold has been dissolved from the carbon with alkaline cyanide solution, the acid washing tank and the thermal regeneration furnace. There were two aims of this chapter. First, to compare the thermal decomposition properties of industrial activated carbons to pure systems of known fouling agents and concentration. Second, to see what differences exist between each processing stage of the activated carbon, and to determine how efficient the thermal regeneration process is for each industrial plant.

CHAPTER 2

EXPERIMENTAL

2.0 Experimental

2.1 Xanthates

The xanthates, sodium ethyl xanthate (SEX), sodium isobutyl xanthate (SiBX), potassium ethyl xanthate (PEX), and potassium amyl xanthate (PAX) were obtained from Hoechst Chemicals as industrial grade.

2.1.1 Purification

The industrial grade xanthates were recrystallised using a method based on that described by Rao (1971). Each xanthate (10 g) was dissolved by stirring in 40°C acetone (100 ml), the resulting solutions filtered through a hot funnel to prevent crystallisation, and the impurities discarded. Toluene (400 ml) was added slowly to the cold filtrate and stirred until the xanthate precipitated. This was vacuum filtered and washed with toluene. The purified xanthates were stored under vacuum in a desiccator containing silica gel.

2.1.2 Characterisation

i) Purity

The purity of each recrystallised xanthate was determined via the so-called acetone method (Hoechst). Each xanthate was crushed into a fine powder, weighed out into a 100 ml stoppered measuring cylinder, mixed with 40 ml of acetone and shaken for 5 minutes to dissolve. The resultant solution was made up to the 50 ml mark, mixed and filtered into a 500 ml conical flask. To each flask, 100 ml of water, 100 ml of acetone, and 50 ml of HCl (0.100 M) was added. Each solution was mixed well and left to stand for 30 minutes. After standing, 3 drops of methyl red indicator was added to each flask and the solution titrated with NaOH (0.1 M) until a colour change was observed.

Each analysis was performed in duplicate. The purity of the SEX, SiBX, PEX, and PAX based on this method were 100, 88, 100, and 100 percent respectively.

ii) Elemental analysis

The carbon, hydrogen, oxygen, and sulfur contents of each xanthate was determined by Chemical and Micro Analytical Services (CMAS). The alkali content of each xanthate was determined by Atomic Adsorption Spectrometry (AAS). Table 1 shows the experimental results versus the theoretical values for the elemental analysis.

	SEX		SiBX		PEX		PAX	
	Theo.	Expt.	Theo.	Expt.	Theo.	Expt.	Theo.	Expt.
C	24.97	24.11	34.84	31.65	22.46	22.63	35.59	33.23
H	3.50	3.58	5.27	6.03	3.14	3.18	5.48	5.01
O	11.09	14.76	9.29	14.58	9.98	11.85	7.91	9.93
S	44.52	42.12	37.28	36.92	40.05	39.94	31.74	31.99
Na	15.94	15.87	13.35	13.35	-	-	-	-
K	-	-	-	-	24.39	21.94	19.33	18.41
Total	100	100.44	100	102.53	100	99.54	100	98.57

Table 2.1: Elemental analysis of SEX, SiBX, PEX, and PAX.

As seen in Table 2.1 the theoretical and experimental values for each element of each xanthate matched tolerably well, and the sum totals were within experimental error of 100% for each xanthate. The total values also agreed with the titration method for all except SiBX.

iii) NMR Analysis

Each xanthate was also characterised by Nuclear Magnetic Resonance (NMR), a technique which can give information about the alkyl chain. A ^{1}H analysis was performed on each xanthate using D_2O as the solvent and *tertiary* butanol for the reference peak in each spectrum (at 1.3 ppm). No reference NMR spectra were found for any of the xanthates. Each spectrum contained a singlet at 4.8 ppm which was due to water from the D_2O.

The ^{1}H spectrum of SEX exhibited a triplet at 1.4 ppm and a quartet at 4.5 ppm due to the methyl and methylene groups respectively. Analysis of the molecular structure of SEX indicated the ^{1}H spectrum was in fact that of SEX. The ^{1}H spectrum of PEX was exactly the same as that of the SEX.

The ^{1}H spectrum of SiBX exhibited a doublet at 1.0 ppm, a septet at 2.1 ppm and a doublet at 4.3 ppm due to the methyl and methine and methylene groups respectively. Analysis of the molecular structure of SiBX indicated the ^{1}H spectrum was in fact that of SiBX.

The ^{1}H spectrum of PAX exhibited a doublet of a doublet of a doublet at 1.0 ppm (which looked like a triplet and was attributed to the methylene groups in the middle of the pentyl chain), a multiplet at 1.6-2.2 ppm (due to slow rotation of the methylene group), and another multiplet at 4.25-4.6 ppm due to the methylene group attached to the oxygen group. Although the spectrum of the PAX which more complex than the other xanthates, analysis of the molecular structure of PAX indicated the ^{1}H spectrum was consistent with that expected for PAX.

2.2 Frothing Agents

Frothing agents were originally obtained from Hoechst chemicals. FTIR analyses were performed on these samples to determine their chief constituent, which was confirmed by literature data. Once the chief constituents were identified, AR grade reagents of these constituents were obtained (except for polypropylene glycol methyl ether, PPGME, as no AR grade could be found).

All AR grade reagents were obtained from Acros. These reagents were polypropylene glycol (PPG, average molecular weight 425, catalog number 19215-5000), α-terpineol (98%, catalogue number 42005-5000), and 4-methyl-2-pentanol (that is methyl isobutyl carbinol , MiBC) (99+%, GC, catalogue number 14938-0025). The reagents were characterised by FTIR analysis, which showed agreement with the published spectra.

2.3 Industrial Activated Carbon Samples from Gold Plants

Industrial samples were obtained from two different gold plants, Salsigne in France and Three Mile Hill in Western Australia. Both these plants obviously have a flotation circuit. Treatment of the samples before thermal analysis consisted of removing any particles by hand which did not resemble activated carbon, and then grinding to -45 μm.

2.4 Adsorption of Xanthates and Frothing Agents on Activated Carbon

The coconut activated carbon Haycarb was obtained from the Chemistry Centre of Western Australia. The Haycarb was conditioned before use, using the method described by Ruane et al (1983). Briefly this consisted of soaking 100 g of activated carbon in HCl (200 ml, 5 %) for 30 minutes in a wide mouth plastic bottle, bottle rolling for 24 hours, decanting any fine carbon, and washing twice with deionised (DI) water. The carbon was then soaked twice for 1 hour each in DI water (200 ml). Finally the carbon was filtered and dried for 16 hours at 120°C. The conditioning procedure approximates plant treatment of activated carbon and ensures no fouling agents were present on the Haycarb.

2.4.1 Adsorption of the Xanthates

To ensure maximum xanthate adsorption, the pretreated Haycarb was ground by hand and sieved through a -45 μm sieve. The -45 μm fraction was retained. The adsorption was performed in 600 ml beakers containing three baffles approximately 120° apart. For each adsorption approximately 0.5 g of the ground Haycarb was contacted with 400 ml of xanthate solution (approximately 1.25 gL^{-1}). The beakers were placed in a water bath set at 20°C and the solutions stirred for 24 hours using overhead stirrers (Heidolph RZR 2021) set at 400 rpm. To minimise evaporation the top of the beakers were covered. The baffled beakers and stirring blades ensured uniform adsorption of each xanthate on the Haycarb particles. After 24 hours the Haycarb was separated by filtration and stored under vacuum in a desiccator containing silica gel until required for analysis.

To determine the amount of xanthate adsorbed on the activated carbon UV spectrophotometry was used. The liquor obtained after adsorption and the initial xanthate solutions were diluted 10 times. The concentrations were determined using a Hewlett Packard 8452A Diode Array Spectrometer. A wavelength of 301 nm and a quartz sample cell of path length 2 mm were used. At these settings and concentrations the Lambert-Beer law is followed ($A = \varepsilon cl$). The concentrations were determined by using the molar absorptivity coefficient of 1.75×10^4 L mol^{-1} cm^{-1} (Harris 1984). The UV spectrum of a xanthate is presented in Figure 2.1.

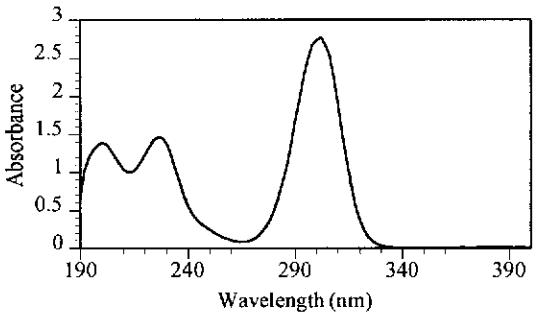

Figure 2.1: UV spectrum of an alkali xanthate.

The peak at 206 nm is due to carbon disulfide, which forms in neutral or alkaline xanthate solutions (Rao 1971).

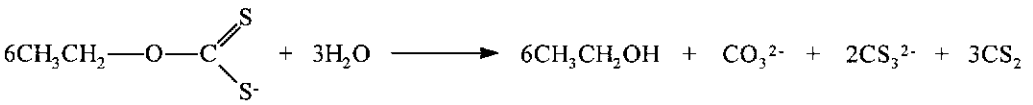

Because carbon disulfide is a hydrolysis product of xanthates, the amount of carbon disulfide present in solution was determined. This was done by constructing a carbon disulfide calibration curve. From the calibration curve it was found that the amount of carbon disulfide present in any given SEX solution was approximately 70 times less than the concentration of SEX. Therefore the formation of carbon disulfide was minimal, and did not have any significant effect on the SEX loading capacity.

The peaks at 226 and 301 nm are due to transitions of the ethyl xanthate ion. The peak at 226 nm is due to the $\pi \rightarrow \pi^*$ transition and the peak at 301 nm is due to the $\pi \rightarrow \sigma^*$ transition (Rao 1971).

2.4.2 Adsorption of the Frothing Agents

The frothing agents were adsorbed on activated carbon using the same method as for the xanthate adsorption except different amounts were used, and different methods were used to calculate the amount of frothing agent remaining in the liquor after adsorption.

Polypropylene glycol and polypropylene glycol methyl ether (100 ml of approximately 80 gL^{-1}) were individually adsorbed on approximately 10 g of Haycarb, -45 μm. The high quantities were required so the remaining liquors could be quantitatively analysed by horizontal attenuated total reflectance (HATR) spectroscopy, using a Bruker IFS 66 FTIR spectrometer. A series of standards were made and the spectra recorded along with the liquor spectra on the HATR. A calibration curve was constructed using the 1380 cm^{-1} peak and the liquor concentrations for both frothing agents determined.

The α-terpineol had to be dissolved in a 1:1 ethanol:water mixture as it did not fully dissolve in deionised water. This solution (100 ml of approximately 50 gL^{-1} α-terpineol) was adsorbed on approximately 0.5 g of Haycarb, -45 μm. To determine the amount of α-terpineol adsorbed the remaining liquor was diluted 50 times and analysed by a Hewlett Packard 8452A Diode Array Spectrometer. A wavelength of 202 nm and a quartz sample cell of path length 1 cm were used. A series of standards were made and a calibration curve constructed to determine the amount of α-terpineol in the liquor.

The MiBC was adsorbed onto the Haycarb, -45 μm in the same manner and concentrations used for the adsorption of the xanthates. The amount adsorbed was determined by analysing the liquor using a Hewlett Packard 5890A GC gas chromatograph. Specifically a series of standards (90 ml of 0.01 to 0.05 gL^{-1}) were

made containing butanol (10 ml of 0.35 gL^{-1}) as an internal standard. An aliquot of the liquor (90 ml) was taken and the butanol was added to it. A calibration curve was constructed using the ratio of the MiBC peak area to its internal standard peak area versus concentration. This technique was used as the amount of sample injected onto the GC does not have to be accurate (Robards, Haddad and Jackson 1994, p 480-481).

2.5 Thermal Analysis Techniques

Three techniques were used to characterise the thermal decomposition properties of the xanthates, frothing agents, and the industrial activated carbon samples.

2.5.1 TD-py-GC-MS

Thermal desorption-pyrolysis-gas chromatography-mass spectrometry (TD-py-GC-MS) of the samples was performed using a Geofina Hydrocarbon Meter (GHM) furnace. The xanthates (each diluted ten times its weight in quartz), frothing agents (coated onto sodium sulfate, approximately 10 % w/w), and the xanthates/frothing agents individually adsorbed on Haycarb (-45 μm), were heated from 150 to 500°C at 25°C min^{-1}, with a final hold time of 5 minutes at 500°C. The industrial samples were heated from 150°C to the maximum temperature of 800°C at 25°C min^{-1}.

The volatiles from the thermal desorption pyrolyser were cryogenically focussed onto a capillary column by immersing a loop (approximately 10 cm long) into liquid nitrogen. Separation of the volatiles was achieved by removing the liquid nitrogen trap and injecting onto a Hewlett Packard 5809 (series I) gas chromatograph fitted with a Hewlett Packard, HP-5ms, 30 m × 0.25 mm ID × 0.25 μm phase thickness. Helium was used as both pyrolysis and carrier gas (linear velocity 60 cm s^{-1}), and injections were split approximately 90:1.

The oven was programmed from 40 to 280°C at 6°C min^{-1} where it was held isothermally for 15 minutes. Eluting compounds were monitored by a Hewlett Packard 5970 mass selective detector in the electron impact (EI) mode, full scan

mode from 20 to 500 amu. Typical mass spectrometer operating conditions were: electron multiplier voltage 2350 V, emission current 220 μA, electron energy 70 eV, source temperature 220°C. Thermal desorption pyrolysis products were identified by direct compound identification using a mass spectra database.

2.5.2 TG-MS and TG-FTIR

Thermogravimetric analysis was performed using a Netzsch STA-409 simultaneous TG-DTA (thermogravimetry-differential thermal analysis). The conditions employed for TG analysis are presented in Table 2.2.

	Xanthates and Frothing Agents	**Adsorbed on Haycarb, -45 μm**	**Industrial Samples**
Sample mass	~ 10 mg	~ 30 mg	~ 1000 mg
Container	alumina crucible	alumina crucible	large alumina cup
Heating rate	10°C min^{-1}	10°C min^{-1}	10°C min^{-1}
Atmosphere	argon	argon	argon
Flow rate	60 ml min^{-1}	60 ml min^{-1}	60 ml min^{-1}

Table 2.2: Conditions used for thermogravimetric analyses.

The dimensions of the alumina crucible were 6 mm internal diameter and 4 mm in depth; and the dimensions for the large alumina cup were 16 mm internal diameter and 20 mm in depth.

The Netzsch STA-409 was checked on a regular basis for temperature error using the DTA carrier with tin and zinc standards (ICTA Certified Reference Material). It was found for up to 500°C, the error in temperature was less than ± 5°C. The mass error was checked using calcium oxalate (Kanto Chemical Co. Inc., extra pure reagent, purity minimum 98.5 %). It was found the mass error up to 1000 °C was less than ± 0.5 %.

i) MS Analysis

The Netzsch STA-409 apparatus was interfaced via a heated transfer line (at 200°C) to a Balzers Thermostar quadrupole mass spectrometer. Operation of the system involved evacuation of the Netzsch STA-409 with a roughing pump, purging with argon gas, and allowing steady state conditions to establish before heating from ambient temperature. The evolved gases were passed through the heated transfer line containing a capillary column (SGE SVSD-150 ID deactivated tubing), through an orifice (to reduce the pressure to approximately 4×10^{-6} mbar), and into the ion source of the MS. A typical ion source electron energy of 70 eV was used. The ions produced at the ion source were separated by a quadrupole and before detection using a secondary electron multiplier. The Balzers software was set to operate by either scanning from 10-300 attenuated mass units or monitoring selected ions.

ii) FTIR Analysis

The Netzsch STA-409 was interfaced by the same method described in **i)** to a Bruker IFS 55 FTIR spectrometer fitted with a MCT (Hg-Cd-Te) detector. The instrumentation was optimised using SEX adsorbed onto activated carbon.

Operation of the instrumentation involved evacuation of the Netzsch STA-409 with a roughing pump, purging with argon gas, and allowing steady state conditions to establish before heating from ambient temperature. The evolved gases were passed through the transfer line, through a heated light pipe fitted with outer (KBr) and inner (ZnSe) windows, where an infrared beam passed through and the infrared spectrum acquired. The number of scans was set to produce an infrared spectrum between 4000-650 cm^{-1} for every 5°C increase in temperature. The Gram Schmidt (GS) chromatogram showed infrared activity between 4000-650 cm^{-1} as a function of time. Infrared spectra could be extracted from any point within the chromatogram.

CHAPTER 3

THERMAL DECOMPOSITION OF XANTHATES

3.0 Introduction

Several reports have appeared concerning the thermal decomposition of alkyl xanthates, alkali salts of xanthates, and transition metal complexes of xanthates.

The thermal decomposition of methyl xanthate (a xanthate ester) was first reported in the literature in 1899. The mechanism proposed is presented in Figure 3.1, and it is known as the Chugaev (or Tschugaeff) reaction, after the discoverer.

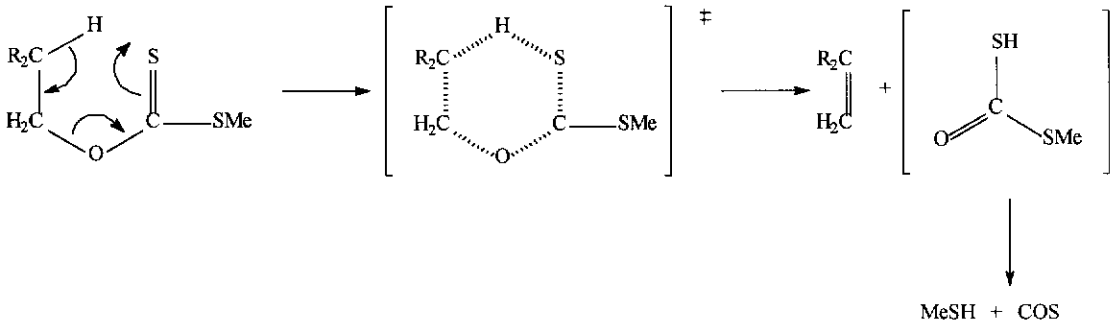

Figure 3.1: Chugaev (or Tschugaeff) reaction.

Decomposition occurs between 100-250°C, dependent on the alkyl group. There are three major products of the reaction, an alkene, a thiol, and carbonyl sulfide (March 1992, p1014; Finar 1973, p95). The Chugaev reaction is valuable in the synthesis of alkenes from sensitive alcohols without carbon skeleton rearrangement. Xanthate esters also undergo O-alkyl to S-alkyl rearrangements with heat to obtain S,S-dialkyldithiocarbonates. This reaction is shown in Figure 3.2 (Dunn and Rudorf 1989).

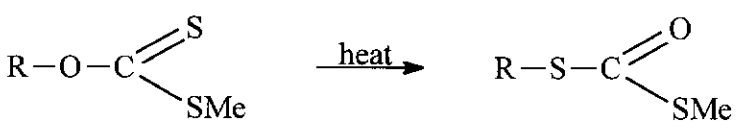

Figure 3.2: Thermal rearrangement of xanthate esters.

In 1911 Hebert reported dixanthogens, alcohols, elemental sulfur, dialkyl xanthates,

thiols, and metallic sulfides as the products of xanthate thermal decomposition (Rao 1971).

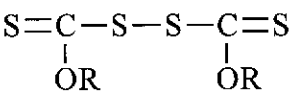

dixanthogen

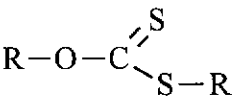

dialkyl xanthate

(R represents an alkyl chain)

In 1966 Tyden reported the thermal decomposition of potassium xanthates. Samples were placed on a gauze which could be heated rapidly under an inert atmosphere to various set temperatures, thus pyrolysing the sample. The gaseous products were separated by gas chromatography, using silica gel and dinonyl phthalate columns. The potassium xanthates with alkyl chains (ethyl, isopropyl, butyl, and amyl) were pyrolysed at 225, 675, 1000 and 1225°C, and the products from each temperature collected onto the silica gel column. Gaseous compounds and carbon disulfide were separated for each pyrolysis, while liquid products were retained on the column. Peaks were identified by comparison to known substances under the same experimental conditions as used for the potassium xanthates. Hydrogen sulfide was detected in some experiments, but not in repeat experiments on the same compound, and so the detection of this gas was not reproducible. Methyl, ethyl, propyl, isopropyl, butyl, isobutyl, and *sec*-butyl potassium xanthates were pyrolysed between 200 and 1075°C onto the dinonyl phthalate column. It was established that all the potassium xanthates produced carbonyl sulfide, carbon disulfide, thiols, alcohols, and probably aldehydes, sulfides and disulfides. However, aldehydes were only identified for the butyl and *sec*-butyl potassium xanthates. The sulfides could only be identified for the methyl, ethyl and butyl potassium xanthates.

Differential thermal analysis (DTA) was used as an independent check on the decomposition temperatures of the potassium xanthates (Tyden 1966). These decomposition temperatures are shown in Table 3.1. The temperature range was taken from the initial and final temperatures of the endothermic peak associated with the decomposition reaction. Also displayed in Table 3.1 are literature values

reported in the same paper, although the method of making these measurements was not indicated.

K xanthate	Temperature (°C)	
	DTA	Literature
methyl	165-185	182-186
ethyl	210-225	225-226
propyl	220-240	233-239
isopropyl	230-275	278-282
butyl	235-255	255-256
isobutyl	250-265	260-270
sec-butyl	220-260	-

Table 3.1: A comparison of the decomposition temperatures of potassium xanthate obtained from the literature.

It is obvious from Table 3.1 that the decomposition temperature increases with the alkyl chain length and the presence of branching.

The difference in the decomposition temperature range between the two different sets of results shown in Figure 3.1 was most likely due to the misinterpretation of the temperature range of the endothermic peak in the DTA curve as being the temperature range of decomposition. Whilst the initial temperature of the peak is probably close to the actual decomposition temperature, the temperature at which the peak returns to the baseline will be much higher than the actual final temperature of decomposition. There are two reasons for this. Firstly, the chemical reaction is complete somewhere near the maximum in the DTA curve. The return of the peak to the baseline on the high temperature side is the result of the sample pan and sample being reheated to the furnace temperature after being cooled down during the endothermic reaction. Secondly, as indicated in section 1.6, thermal methods are not equilibrium techniques, and the position of the DTA peak along the temperature axis is dependent on a number of experimental variables. Hence the choice of DTA as a means of estimating decomposition temperature ranges is not a good one.

Although data exists on the decomposition products of alkali xanthates, no decomposition mechanisms have been proposed in the literature so far. However, several mechanisms have been proposed for the thermal decomposition of some

transition metal xanthates. These transition metal xanthates consist of nickel (II), palladium (II), arsenic (III), antimony (III), bismuth (III), and zirconium (IV) with various alkyl chain lengths (Hill and Magee 1981; Pandey, Sengupta and Tripathi 1985).

Among the earliest work reported was on the decomposition of eleven nickel(II) complexes of different alkyl chain length, which were heated in a TG apparatus in air and nitrogen. The major mass loss occurred between 140-180°C, forming nickel sulfide. There appeared to be little difference between the TG curves obtained in air and nitrogen atmospheres. Gaseous products were collected in a cold trap and analysed by mass spectrometry. It was found that the thermal stability increased as the alkyl chain decreased and with the introduction of branched alkyl chains. The mechanism of decomposition was proposed on the basis that one C-S bond within a molecule is longer (and therefore weaker) due to the interaction with a neighboring molecule, causing a breakup of the molecule. The gases evolved were carbonyl sulfide, and S-ethyl O-ethyl xanthate (Cavell *et al* 1973). This mechanism is shown in Figure 3.3.

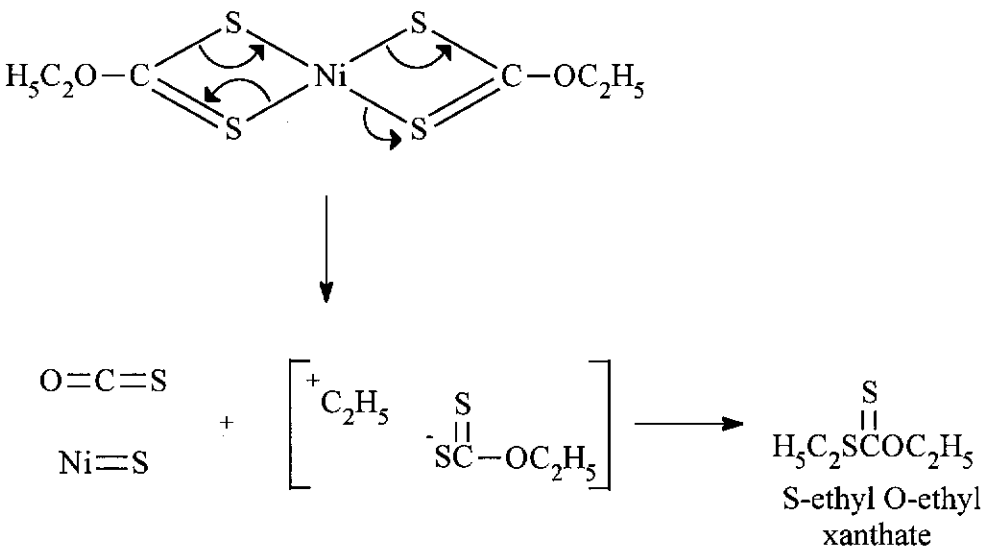

Figure 3.3: Proposed thermal decomposition mechanism for nickel alkyl xanthates (Cavell *et al* 1973).

The thermal decomposition of eleven palladium (II) complexes was studied in air and nitrogen. The thermogravimetric curves consisted of two mass losses; the first mass loss was the most rapid and largest, while the second mass loss was slower and consisted of two stages. The decomposition temperature was dependent on the alkyl chain. It was found the thermal stability increased as the chain length increased (except for the n-propyl derivative, which was the most stable complex) and the degree of branching decreased. The mechanism of decomposition proposed for the palladium xanthates was similar to that of the nickel xanthates proposed by Cavell *et al* (1973). The first step was the initiation of the reaction, which occurred by the breaking of a long C-S bond producing carbonyl sulfide and S-alkyl O-alkyl xanthate. After this step, the mechanism differs to that of Cavell *et al* (1973), with two more long C-S bonds breaking to give two additional molecules of carbonyl sulfide and a solid intermediate $Pd_2C_2H_6S_3$. The intermediate then decomposed to palladium sulfide and methyl sulfide. The palladium sulfide finally decomposed to palladium metal (Sceney, Hill and Magee 1973).

A series of arsenic, antimony and bismuth xanthate complexes were studied via thermogravimetry in air. All complexes decomposed to produce two mass losses, the first of which was rapid and the largest, while the second mass loss was gradual. It was found the thermal stability increased as the alkyl chain length increased. Two possible mechanisms were proposed. The first involved the rupture of C-S single bonds to produce the metal sulfide, carbonyl sulfide, and S-alkyl O-alkyl xanthate. This mechanism is the same as that proposed by Cavell *et al* (1973) and to some extent by Sceney, Hill and Magee (1973). The S-alkyl O-alkyl xanthate could then decompose in a variety of ways to produce carbonyl sulfide, carbon disulfide, alkenes, etc. The second mechanism proposed was that S-alkyl O-alkyl xanthate was not formed, but the metal sulfide, carbonyl sulfide, carbon disulfide, and alkenes were produced. This was because no evidence of the existence of S-alkyl O-alkyl xanthate was found by mass spectrometry. The equation for this mechanism is presented below (M and R represent a metal and alkyl chain respectively, and (R-H) an alkene) (Khwaja, Cardwell and Magee 1973).

$$2(ROCS_2)_3M \rightarrow M_2S_3 + 3COS + CS_2 + 3H_2O + 6(R\text{-}H)$$

More recently the thermal decomposition of some zirconium xanthate complexes in air and nitrogen were investigated. The first mass loss was due to the loss of water, and a second mass loss due to the decomposition of the complex into zirconium sulfide, carbonyl sulfide, S-alkyl O-alkyl xanthate, and oxygen. It was found that the thermal stability increased as the alkyl chain length increased (Pandey 1988).

Although many transition metal xanthates have been studied no straightforward relation has been established between the thermal decomposition and the transition metal type. Also the effect of the alkyl group varies between the different types of transition metal xanthates. However the decomposition products of most transition metal xanthates are carbonyl sulfide and S-alkyl, O-alkyl xanthates, with metal sulfides as end products. Also arsenic, antimony, and bismuth xanthates have been reported to form alkenes and carbon disulfide (Hill and Magee 1981; Pandey, Sengupta and Tripathi 1985).

There does exist in the literature one reference on the thermal decomposition of potassium ethyl xanthate adsorbed on sulfide minerals. Using headspace analysis gas-phase infrared spectroscopy, and ^{2}H- and ^{13}C- labeling experiments, Vreugdenhil *et al* (1997) proposed decomposition pathways for the production of carbon disulfide and carbonyl sulfide. The proposed reactions are presented in Figure 3.4.

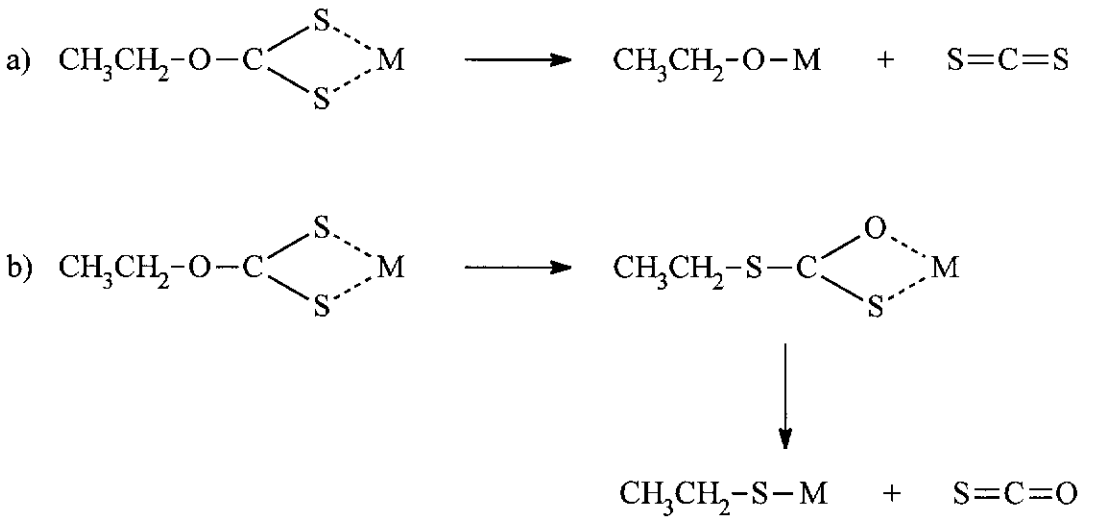

Figure 3.4: Thermal decomposition of potassium ethyl xanthate adsorbed on a sulfide mineral.

The first reaction (a) of Figure 3.4 involves elimination of the CS_2 group from the xanthate to produce carbon disulfide. The second reaction (b) involves a thermal rearrangement (alkyl migration from oxygen to sulfur) and elimination of the COS group to produce carbonyl sulfide.

In this chapter the results of the thermal decomposition-evolved gas analysis (EGA) of alkali xanthates are reported. The alkali xanthates studied were sodium ethyl xanthate (SEX), sodium isobutyl xanthate (SiBX), potassium ethyl xanthate (PEX), and potassium amyl xanthate (PAX).

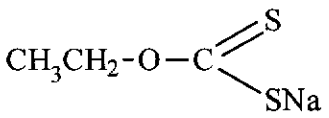

SEX

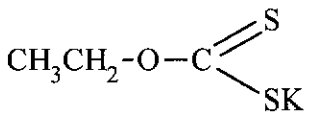

PEX

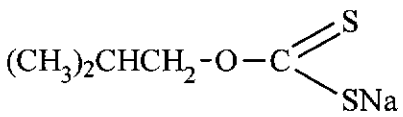

SiBX

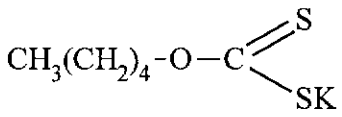

PAX

Thermal decomposition-EGA was achieved using the techniques of thermal desorption pyrolysis-gas chromatography-mass spectrometry (TD-py-GC-MS), thermogravimetry-mass spectrometry (TG-MS), and thermogravimetry-Fourier transform infrared (TG-FTIR) spectroscopy. The results of the thermal decomposition-EGA of each xanthate adsorbed on activated carbon are also reported.

3.1 TD-py-GC-MS Analysis of Alkali Xanthates

TD-py-GC-MS was used to identify the gases evolved from each xanthate when heated at 25°C min^{-1} in an inert atmosphere from ambient to 500°C. A typical total ion chromatogram for SEX is shown in Figure 3.5. Including carbon dioxide and sulfur dioxide, at least 16 peaks were observed, indicating that at least 16 gases were evolved from the decomposition of SEX. This is nine more than previously reported

for potassium ethyl xanthate (Tyden 1966). Carbon dioxide and sulfur dioxide are combustion products due to the small amount of oxygen present during analysis. Although good resolution was achieved for most of the evolved gases, those that eluted in the first 1.5 minutes were not well resolved. In order to check these unresolved peaks, mass spectral scans were obtained at several points across a broad peak. Thus the peak between retention times of 1.04-1.48 minutes was found to contain at least three gases. For simplicity, gases with a peak area less than 10 % of the largest peak were excluded from the study. This left nine significant peaks. The gases which produced these peaks were identified using a mass spectra database and manual interpretation, and are tabulated, along with their retention time (RT), in Table 3.2. For comparison purposes, the peak areas of the nine significant peaks were divided by the sum of peak areas and expressed as percent relative peak area.

The largest peak in the chromatogram was due to the presence of carbon disulfide, followed by diethyl carbonate, and then ethanol. Of the nine identified gases, seven have been previously reported, but diethyl carbonate and carbonothioic, O,S,-diethyl ester have not been previously reported.

Unfortunately, because of differences in the efficiency of formation of the molecular ions, the peak areas of the gases in the chromatogram do not directly give the concentration of the individual gases. However the peak areas give at least a semi-quantitative indication of the concentration of each gas.

Based on the information in the literature, the Chugaev reaction could be used to predict the formation of carbonyl sulfide and ethanethiol. However this reaction is unlikely as no alkene formation was observed. Also, although COS formation occurs for transition metal xanthates by breaking a C-S bond, the authors of those papers did not report the formation of a thiol.

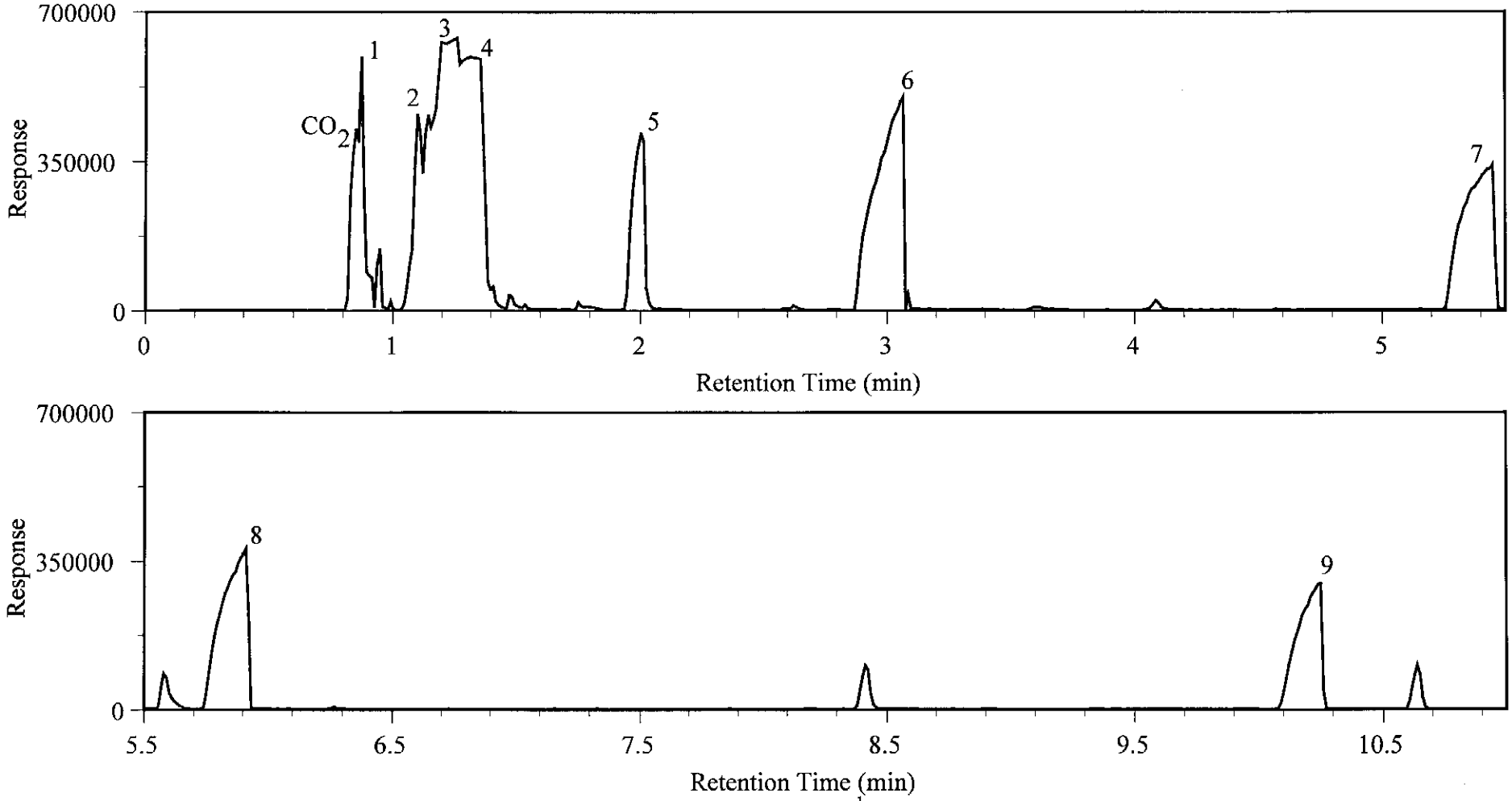

Figure 3.5: TD-py-GC-MS total ion chromatogram of SEX heated at 25°C min^{-1} in an inert atmosphere.

	Peak	RT (min)	Relative Peak Area (%)	Gas Evolved	Previously Reported
SEX	1	0.87	3.0	carbonyl sulfide	a, b, d, f, g, h , i
	2	1.10	3.9	ethanethiol	b, h, i
	3	1.23	19.1	carbon disulfide	c, d, e, h, i
	4	1.34	16.2	ethanol	h, i
	5	2.00	6.0	diethyl sulfide	h
	6	3.07	18.4	diethyl carbonate	not previously reported
	7	5.45	13.0	diethyl disulfide	h
	8	5.91	12.1	carbonothioic acid, O,S, diethyl ester	not previously reported
	9	10.3	8.7	carbonodithioic acid O,S, diethyl ester	a, d, f, g
SiBX	1	0.85	1.5	carbonyl sulfide	a, b, d, f, g, h , i
	2	1.18	8.0	carbon disulfide	c, d, e, h, i
	3	1.75	17.1	isobutanol	h, i
	4	1.84	1.7	butanethiol	h
	5	9.44	14.1	di-isobutyl carbonate	not previously reported
	6	13.1	51.5	carbonothioic acid, O,S, dibutyl ester	not previously reported
	7	16.8	6.2	dibutyl disulfide	h
PEX	1	0.91	6.7	carbonyl sulfide	a, b, d, f, g, h , i
	2	1.16	5.1	ethanethiol	b, h, i
	3	1.26	9.4	carbon disulfide	c, d, e, h, i
	4	2.37	35.5	diethyl sulfide	h
	5	2.83	1.4	ethyl isopropyl sulfide	h
	6	6.12	26.6	diethyl disulfide	h
	7	6.31	6.8	carbonothioic acid, O,S, diethyl ester	not previously reported
	8	11.3	8.6	carbonodithioic acid O,S, diethyl ester	a, d, f, g
PAX	1	0.92	1.3	carbonyl sulfide	a, b, d, f, g, h , i
	2	1.30	3.4	carbon disulfide	c, d, e, h, i
	3	1.89	9.4	isobutanol	h, i
	4	2.81	9.3	isoamyl alcohol	h, i
	5	6.22	3.5	unidentified (132 g mol^{-1})	-
	6	7.19	2.7	di-isobutyl sulfide	h
	7	8.56	2.8	3-methyl butyl propyl sulfide	h
	8	9.79	6.4	di-isobutyl carbonate	h
	9	10.1	11.1	unidentified (160 g mol^{-1})	-
	10	13.0	26.2	di-isopentyl sulfide	h
	11	13.2	3.00	carbonothioic acid, O,S, dibutyl ester	h
	12	14.9	6.0	di-isopentyl carbonate	h
	13	15.3	3.3	isobutyl 3-methyl butyl disulfide	not previously reported
	14	15.7	4.1	unidentified (204 g mol^{-1})	-
	15	17.7	4.5	di-isopentyl disulfide	h
	16	22.6	3.0	unidentified (260 g mol^{-1})	-

(a) Cavell *et al* 1973, (b) March 1992, (c) Hill and Magee 1981, (d) Khwaja, Cardwell and Magee 1973, (e) Pandey, Sengupta and Tripathi 1985, (f) Pandey 1988, (g) Sceney, Hill and Magee1973, (h) Tyden 1966, (i) Vreugdenhil *et al* (1997)

Table 3.2: Gases evolved from the pyrolysis of SEX, SiBX, PEX, and PAX.

Based on the paper by Vreugdenhil *et al* (1997), there are two fundamental reactions proposed for the thermal decomposition of SEX. The first is elimination of the CS_2

group from the SEX to form carbon disulfide and ethanol. The second is thermal rearrangement of the SEX via alkyl migration from oxygen to sulfur and its subsequent decomposition to carbonyl sulfide and ethanethiol. These reactions are shown in Figure 3.6.

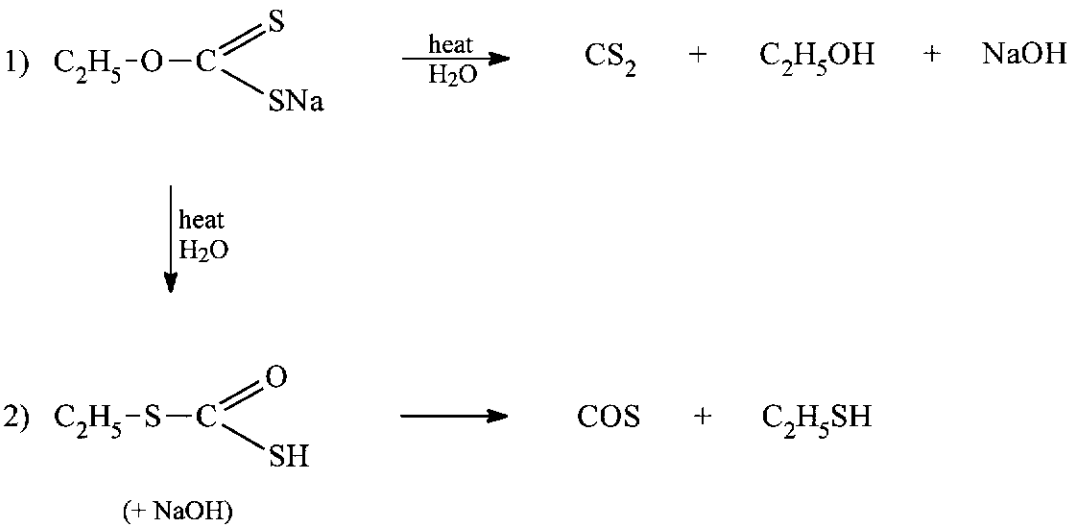

Figure 3.6: Proposed initial reaction sequence for the thermal decomposition of SEX.

The reaction sequence of Figure 3.6 is complicated by the presence of the sodium. For the formation of ethanol and ethanethiol to occur, the reactions require the replacement of sodium with hydrogen. How, when and where this occurs during the reaction sequence is unknown. The most likely way for this to occur would be via the addition of water absorbed from moisture in the atmosphere. Also the amount of water present was not able to be determined.

Reactions for the formation of diethyl sulfide, diethyl carbonate, diethyl disulfide, and carbonothioic acid, O,S, diethyl ester have not been proposed in the literature. However, it is most likely these compounds are formed from reactions of carbon disulfide, carbonyl sulfide, ethanol and ethanethiol, which can take place when these compounds coexist in the cold trap prior to injection into the GC. Compounds such as carbon disulfide are highly susceptible to attack by nucleophilic reagents (Dunn

and Rudorf 1989) such as the ethoxide ion ($CH_3CH_2O^-$). Some suggested reactions for the formation of these gases are shown in Figure 3.7.

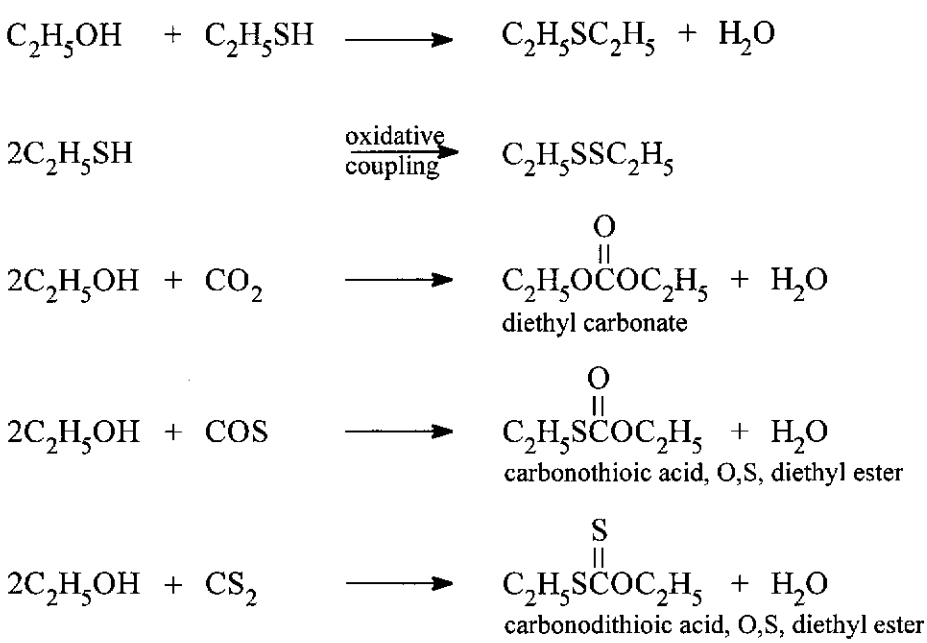

Figure 3.7: Proposed further reactions for the thermal decomposition of SEX.

Of course there are many different ways in which the decomposition gases of SEX could form. The prediction of a reaction sequence is not easy and many facts are required. Identification of reaction products is only one step in the process and many other studies such as isotopic labelling are required (March 1992). However this is not the main purpose of this thesis and thus detailed studies have not been done.

Similarly, complex chromatograms were observed from the thermal decomposition of the other three xanthates. The total ion chromatograms for SiBX, PEX, and PAX are presented in Figures 3.8, 3.9, and 3.10 respectively. The data from SiBX, PEX, and PAX pyrolyses were processed in the same manner as for data from the decomposition of SEX.

A typical total ion chromatogram of SiBX is shown in Figure 3.8, which displays at least 23 peaks (including CO_2/SO_2). This is 16 more than previously reported for a potassium isobutyl xanthate (Tyden 1966). After excluding peaks with areas less

than 10 % of the largest peak, seven significant peaks were identified (for their identity, RT, and percent relative peak area see Table 3.2). The largest peak in the chromatogram was due to the presence of carbonothioic acid, O,S, dibutyl ester, followed by isobutanol, and then di-isobutyl carbonate. Five of the seven identified gases have been previously reported, but carbonothioic acid, O,S, dibutyl ester and di-isobutyl carbonate have not been previously reported.

A typical total ion chromatogram of PEX is shown in Figure 3.9, which displays at least 18 peaks (including CO_2/SO_2). This is 11 more than previously reported by Tyden (1966). After excluding peaks with areas less than 10 % of the largest peak, eight significant peaks were identified (for their identity, RT, and percent relative peak area see Table 3.2). The largest peak in the chromatogram was due to the presence of diethyl sulfide, followed by diethyl disulfide, and then carbon disulfide. Seven of the eight identified gases have been previously reported, but carbonothioic acid, O,S, diethyl ester has not been previously reported.

A typical total ion chromatogram of PAX is shown in Figure 3.10, which displays at least 96 peaks (including CO_2/SO_2), although many are very small. This is 89 more than previously reported by Tyden (1966). After excluding peaks with areas less than 10 % of the largest peak, twelve significant peaks were identified and four significant peaks were not identified (for their identity, RT, and percent relative peak area see Table 3.2). The largest peak in the chromatogram was due to the presence of di-isopentyl sulfide, followed by isobutanol, and then isoamyl alcohol.

The decomposition gases of SiBX, PEX, and PAX are very similar to those of SEX, and the types of reactions that were proposed for SEX decomposition are also likely to be very similar (see Figures 3.6 and 3.7).

One gas for which a reaction cannot be proposed is for the formation of ethyl isopropyl sulfide from the decomposition of PEX. This gas is unusual in that it has a propyl group, which cannot be explained. However, the match to the mass spectra database was 91 %. Some other differences in product distribution and type of products were noted between SEX and PEX, indicating that the alkali cation does

play a role in the thermal decomposition.

In the decomposition of PAX, a number of gases evolved with an isobutyl group. These are isobutanol, di-isobutyl sulfide, di-isobutyl carbonate, carbonothioic acid, O,S, dibutyl ester, and isobutyl 3-methyl butyl disulfide. Additionally, 3-methyl butyl propyl sulfide was formed. No reaction scheme could be proposed for either the formation of the isobutyl or propyl group.

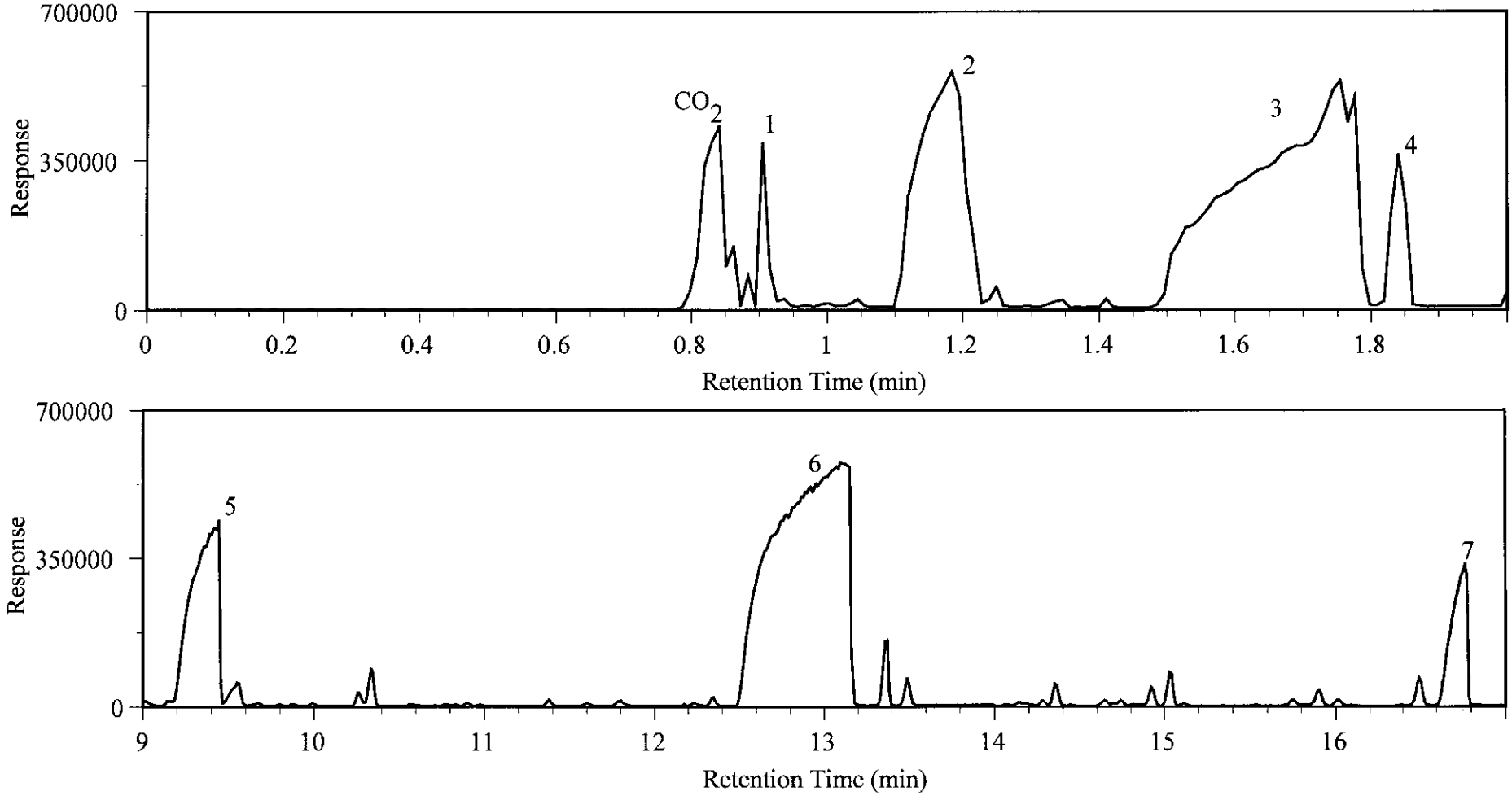

Figure 3.8: TD-py-GC-MS total ion chromatogram of SiBX heated at 25°C min^{-1} in an inert atmosphere.

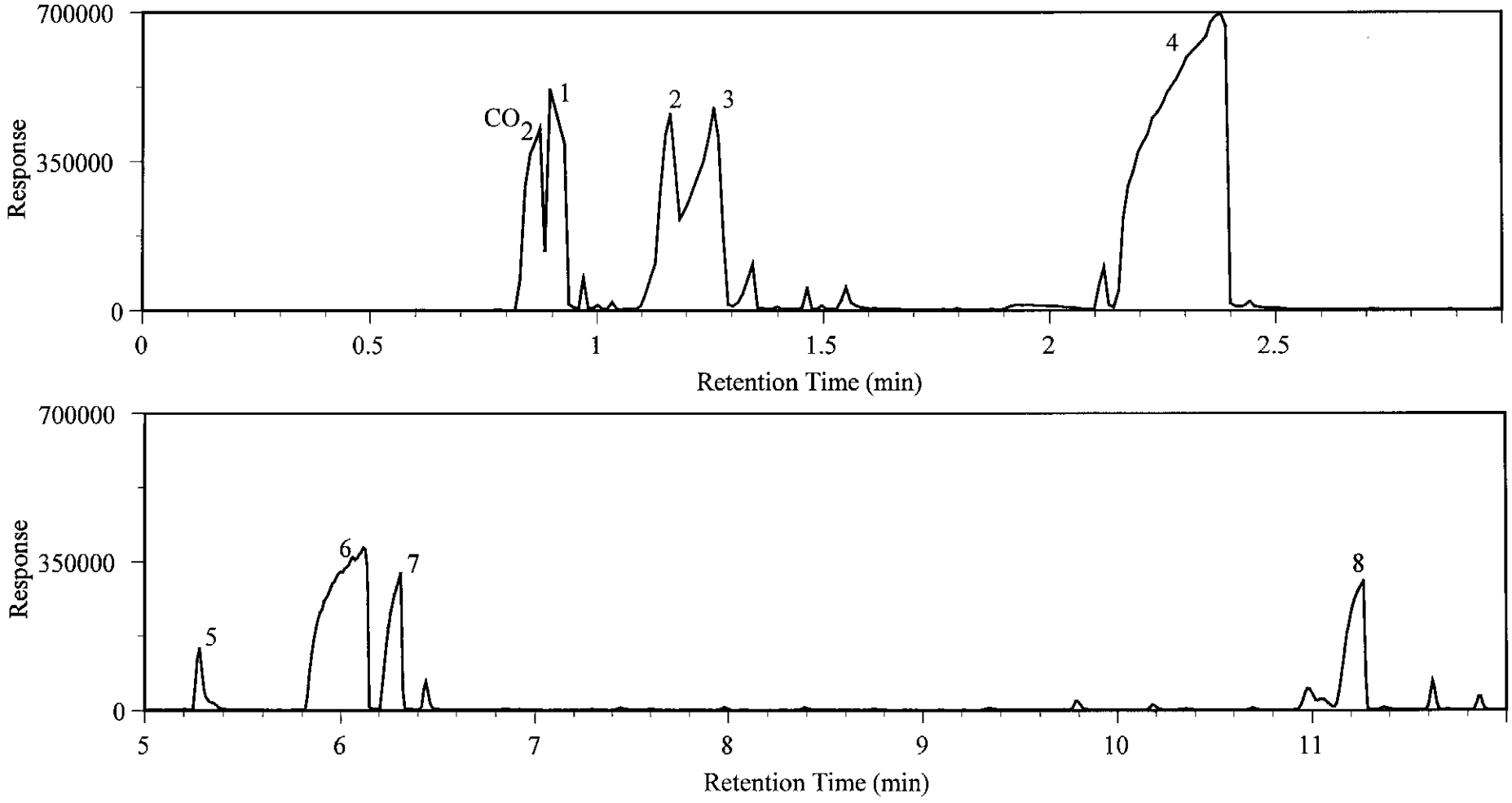

Figure 3.9: TD-py-GC-MS total ion chromatogram of PEX heated at 25°C min^{-1} in an inert atmosphere.

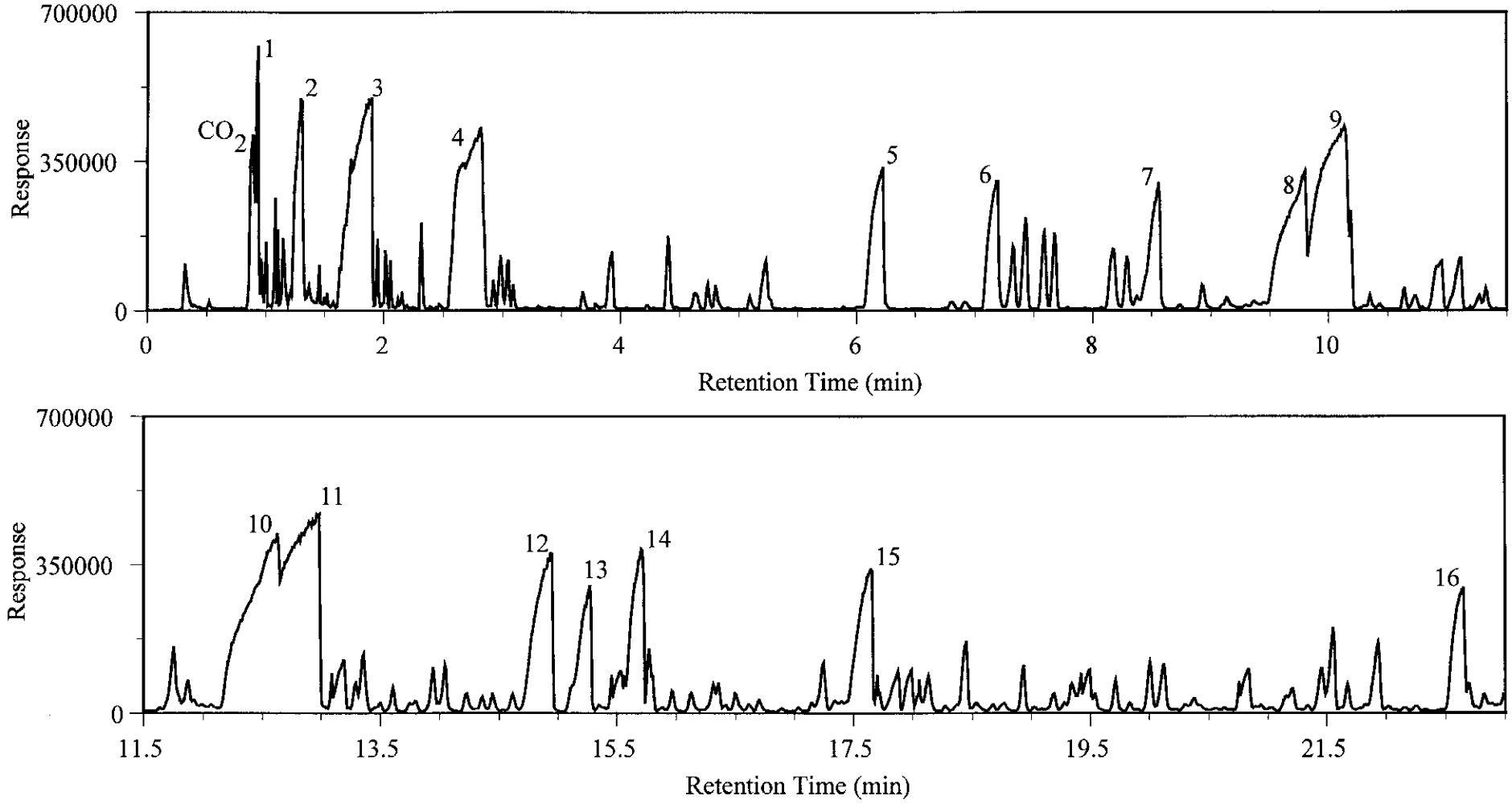

Figure 3.10: TD-py-GC-MS total ion chromatogram of PAX heated at 25°C min^{-1} in an inert atmosphere.

3.2 Thermogravimetry - Evolved Gas Analysis of Alkali Xanthates

The thermal decomposition of the four xanthate compounds were each studied by TG-EGA, at a heating rate of 10°C min^{-1} under an argon atmosphere. The evolved gases were analysed by MS and FTIR spectroscopy. The TG curve of each xanthate consisted of two mass losses. In each case the first mass loss was rapid, and the second mass loss was gradual and took place over a wide temperature range. The mass losses and their extrapolated onset/offset temperatures are presented in Table 3.3. A typical TG curve for the decomposition of SEX showing the extrapolated onset/offset temperature tangents is presented in Figure 3.11.

	Xanthate			
Mass Loss	**SEX**	**SiBX**	**PEX**	**PAX**
First	189-200°C (42.3 %)	189-213°C (52.6 %)	213-217°C (45.9 %)	245-255°C (53.3 %)
Second	287-321°C (20.8 %)	274-325°C (20.4 %)	294-483°C (6.5 %)	332-494°C (5.9 %)

Table 3.3: Mass losses and corresponding temperatures of SEX, SiBX, PEX, and PAX heated at 10°C min^{-1} in an argon atmosphere.

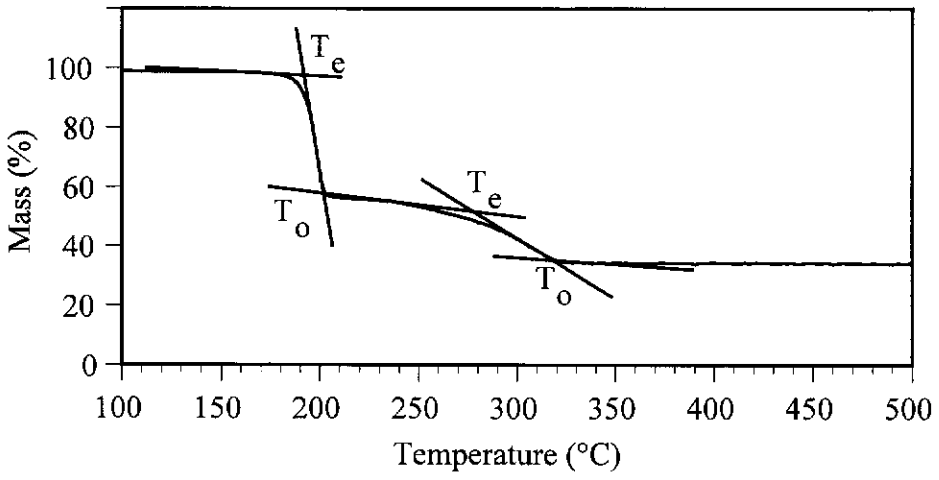

Figure 3.11: Typical TG curve with extrapolated onset/offset temperature tangents for the decomposition of SEX heated at 10°C min^{-1} in an argon atmosphere.

For the first mass loss, the maximum rate of mass loss (corresponding to the DTG peak temperature) occurred at 197°C for SEX, at 201°C for SiBX, at 215°C for PEX, and at 248°C for PAX. An inspection of the mass losses indicates that for the sodium compounds, the second mass losses were still significant relative to the first mass loss. However, for the potassium compounds the second mass loss was minor relative to the first mass loss.

Tyden (1996) has previously reported that the thermal decomposition of PEX occurs between 210-225°C, although in the same paper he also quotes 225-226°C. These values compare well to the values in Table 3.3, as well as to the DTG peak temperature of 215°C. Any difference is probably due to the purity of xanthate used.

Comparison of the SEX and PEX decomposition temperatures indicates the potassium xanthates are more thermally stable than the sodium xanthates, decomposing at a higher temperature. This was expected as the potassium xanthates have a slightly higher molecular weight.

From the reactions proposed in section 3.1, the residue left after the decomposition of a xanthate should be the salt of a thiol and a hydroxide. Thus for the decomposition of SEX it would be expected that the residue was sodium hydrogen sulfide (NaSH) and sodium hydroxide (NaOH).

To further evaluate the decomposition of SEX, a sample was quenched at 325°C and the residue analysed by FTIR. From the previous reaction schemes, the products would be expected to be a combination of NaSH and NaOH. Because the quenched sample was exposed to the moisture in the atmosphere, however, NaSH would react according to the following reversible equations (Kolthoff 1969, p335).

$$NaSH_{(s)} + H_2O_{(l)} \rightarrow H_2S_{(g)} + NaOH_{(s)}$$

$$NaOH_{(s)} + NaSH_{(s)} \rightarrow Na_2S_{(s)}$$

Thus the infrared spectrum of the quenched product was compared with the infrared spectra of analytical grade NaOH and Na_2S. Comparison of the spectra showed

peaks at 1456 and 866 cm^{-1} in the quenched sample also occurred in the NaOH spectrum; and peaks at 1456, 1129, 1000 and 662 cm^{-1} that occurred in the Na_2S spectrum.

Analysis of the quenched sample produced a sulfur value of 39.9 %. This value compared well to the theoretical value of 41.1 % expected for Na_2S. Thus this information combined with infrared analysis of the quenched sample indicated the solid decomposition products of SEX are sodium hydrogen sulfide and sodium hydroxide.

Comparison of the xanthate mass losses also shows the decomposition temperature is dependent on the alkyl chain length, and the presence of branching. The longer the alkyl chain, the more thermally stable the molecule, hence it decomposes at a higher temperature. However, branching in the alkyl chain destabilises the molecule influencing the temperature of decomposition more so than the alkali cation. That is, SiBX has a slightly higher molecular weight than PEX, but it decomposes at a lower temperature.

3.2.1 MS Analysis of the Evolved Gases

The gases evolved from each xanthate were studied by two different TG-MS techniques. The first technique consisted of recording a mass spectrum (10-300 amu, attenuated mass unit) for every 10°C increase, from ambient to 500°C (this will be referred to as scan mode or SM). The second technique, known as selected ion monitoring (SIM), was used to monitor selected ions from ambient to 500°C.

The SM analysis produced spectra with many peaks. An example of this is shown in Figure 3.12 for the gases evolved during the first mass loss of SEX. Although no spectra are shown in this report for the other xanthates, their spectra were just as, if not more, complex. The lack of a separation step meant that all the gases and their fragments were presented to the mass spectrometer at the same time. Thus identification of individual gases was difficult due to the overlapping of molecular, fragment, and/or isotope ion signals from the mixture of gases. Identification of the molecular ions and thus the gases evolved was only made possible by a comparison

to the TD-py-GC-MS analyses. All other peaks were attributed to fragment or isotope ions. Therefore the mass spectra could not be used to determine if any different gases had evolved when the xanthates were decomposed in the TG apparatus compared to the TD-py-GC-MS analyses.

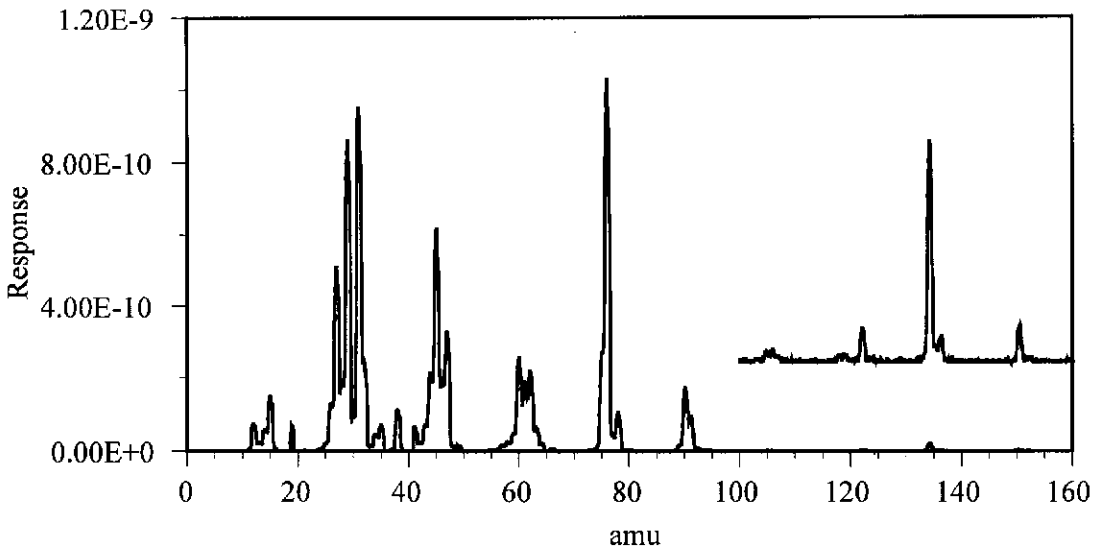

Figure 3.12: SM spectrum of SEX at 197°C.

Selected ion monitoring (SIM) was used to monitor the molecular ions (as determined by the TD-py-GC-MS analyses) of the evolved gases versus temperature. An ion chromatogram was produced for each evolved gas, and typical examples are presented in Figures 3.13 to 3.16 along with their mass loss curves. The relative percent peak areas for each of the gases for each xanthate analysis are presented in Table 3.4.

In discussing the ion chromatograms the interference due to fragment ion and/or isotope ions has been ignored for simplicity. Correction of the ion chromatograms for fragment ion and/or isotope ion contributions could be performed using reference spectra. However, the reference spectra must be collected on the same mass spectrometer for accurate and reliable correction. This was not practical for the mass spectrometer used in this study. It is worthwhile to note that the fragment/isotope error associated with each molecular ion increases with decreasing amu.

Also, the efficiency of formation of the molecular ions is not known for each gas, a problem alluded to in the TD-py-GC-MS analyses discussion. Therefore only a semi-quantitative indication of the concentration of each gas can be given.

Inspection of the SIM spectra for a number of gases indicated that during the first mass loss all the gases were evolved more or less simultaneously, and so the peaks occurred in the same temperature range. During the second mass loss, the gases were evolved at different temperatures, and so shifted relatively along the x axis in the SIM spectra.

Figure 3.13 shows the ion chromatograms for carbon disulfide (amu 76) and carbonyl sulfide (amu 60) evolution from the decomposition of SEX. Both these gases had the largest relative peak areas. Several other gases such as ethanol (amu 46) and ethanethiol (amu 62) produced very similar temperature profiles, and are not reproduced here. These two gases had the next largest relative peak areas. All other monitored gases (amu 90, 118, 122, 136, and 150) are omitted from Figure 3.13 as they were minor in quantity and produced sharp peaks during the first mass loss (similar to the carbon disulfide).

All of the nine gases detected by TD-py-GC-MS for SEX decomposition were detected during the first mass loss, but only ethanol, carbonyl sulfide, ethanethiol, and carbon disulfide were detected during the second mass loss. These gases also evolved over a wider temperature range, so that the rate of evolution for carbonyl sulfide peaked at 260°C, while for ethanol, ethanethiol, and carbon disulfide the rate of evolution peaked at 315°C.

Figure 3.14 shows the ion chromatograms for carbon disulfide (amu 76) and carbonyl sulfide (amu 60) evolution from the decomposition of SiBX. Both these gases had the largest relative peak areas. All other monitored gases (amu 86, 88, 174, and 190) are omitted from Figure 3.14 as they were minor in quantity and produced very small peaks during the first mass loss. Only amu 178 was not detected. During the second mass loss the largest peak was due to carbon disulfide, which accounted for approximately half of all decomposition products observed. Carbonyl sulfide was the only other gas detected during the second mass loss.

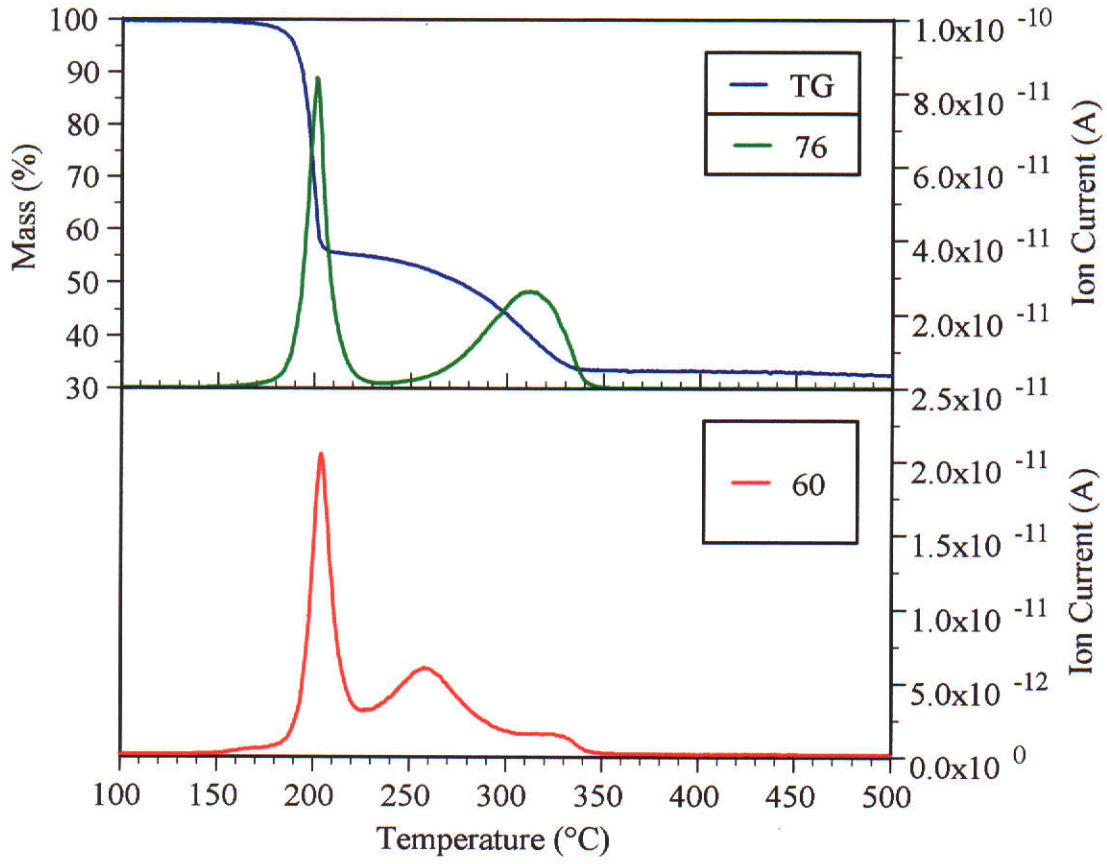

Figure 3.13: amu 60 and 76 ion chromatograms of SEX heated at 10°C min^{-1} in an argon atmosphere.

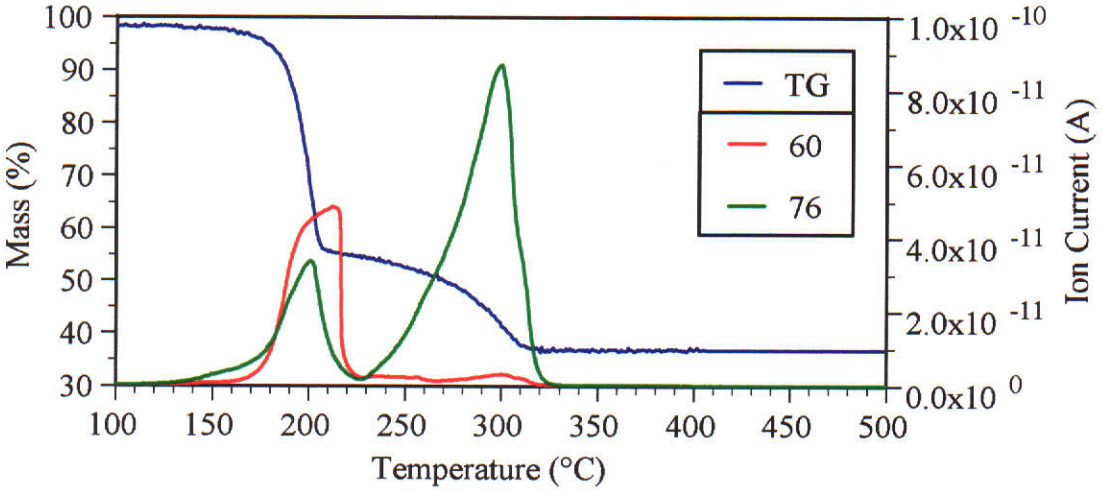

Figure 3.14: amu 60 and 76 ion chromatograms of the decomposition products of SiBX heated at 10°C min^{-1} in an argon atmosphere.

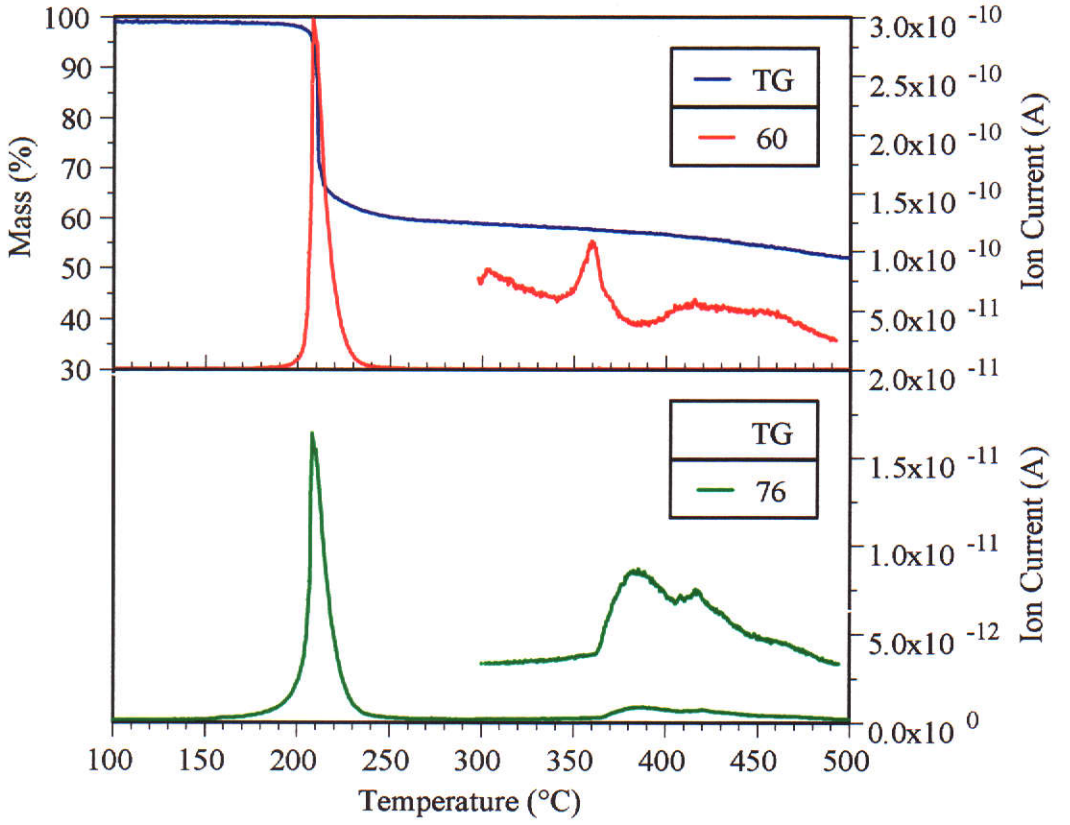

Figure 3.15: amu 60 and 76 ion chromatograms of PEX heated at 10°C min^{-1} in an argon atmosphere.

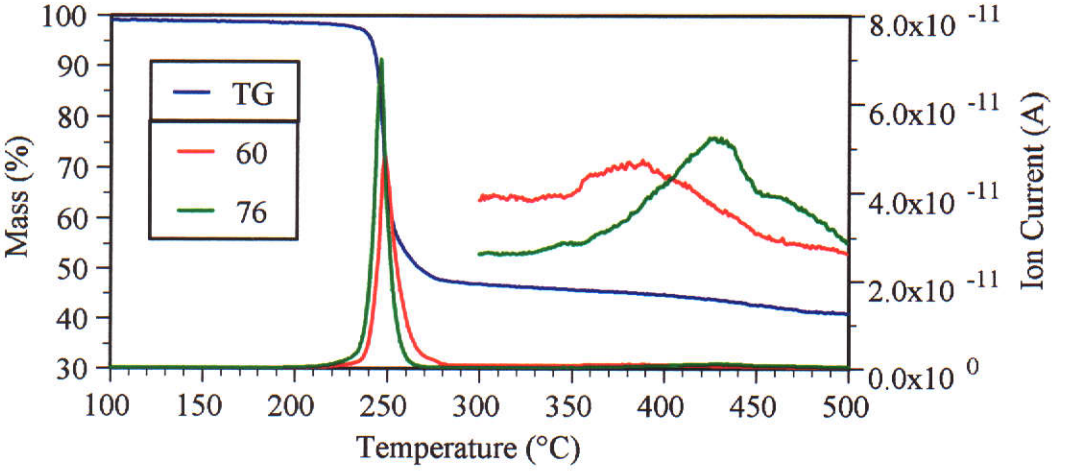

Figure 3.16: amu 60 and 76 ion chromatograms of PAX heated at 10°C min^{-1} in an argon atmosphere.

Figure 3.15 shows the ion chromatograms for carbonyl sulfide (amu 60) and carbon disulfide (amu 76) evolution for the decomposition of PEX. Both these gases had the largest relative peak areas. Ethanethiol (amu 62) had the next largest relative peak area, followed by diethyl sulfide (amu 90). These gases were only detected during the first mass loss as sharp peaks and are not displayed in Figure 3.15. All other monitored gases (amu 104, 122, 136, and 150) are omitted from Figure 3.15 as they were minor in quantity and produced sharp peaks during the first mass loss (similar to carbonyl sulfide and carbon disulfide).

Figure 3.16 shows the ion chromatograms for carbon disulfide (amu 76) and carbonyl sulfide (amu 60) evolution from the decomposition of PAX. Both these gases had the largest relative peak areas. The other monitored gases (amu 74, 88, 132, 146, 160, 174, 190, and 260) are omitted from Figure 3.16 as they were minor in quantity and produced sharp peaks during the first mass loss (similar to carbonyl sulfide and carbon disulfide). Also gases of amu 192, 202, 204, and 206 were not detected.

Only carbonyl sulfide and carbon disulfide were detected during the second mass losses for PEX and PAX decomposition. The ion chromatograms for these gases have been enlarged in Figures 3.15 and 3.16 as only very small amounts were detected. This was not unexpected given that the majority of reaction had taken place in the first mass loss, and the second mass loss was relatively minor.

Table 3.4 shows the relative peak areas of gases evolved for each xanthate. The relative peak area of each gas evolved has been expressed as a percentage. That is the ion abundance (in amps per degree Celsius) of each gas was divided by the sum of the ion abundances for both mass losses. Therefore a semi-quantitative comparison between each gas can be made.

	amu	Relative Peak Area (%) First Mass Loss	Relative Peak Area (%) Second Mass Loss	Gas
SEX	46	6.23	0.97	ethanol
	60	9.11	9.07	carbonyl sulfide
	62	3.89	0.99	ethanethiol
	76	30.0	36.4	carbon disulfide
	90	2.03	0	diethyl sulfide
	118	0.29	0	diethyl carbonate
	122	0.31	0	diethyl disulfide
	136	0.41	0	carbonothioic acid, O,S, diethyl ester
	150	0.28	0	carbonodithioic acid O,S, diethyl ester
SiBX	60	23.5	3.41	carbonyl sulfide
	74	1.10	0	isobutanol
	76	15.3	55.9	carbon disulfide
	88	0.23	0	butanethiol
	174	0.19	0	di-isobutyl carbonate
	178	0	0	dibutyl disulfide
	190	0.37	0	carbonothioic acid, O,S, dibutyl ester
PEX	60	56.4	1.99	carbonyl sulfide
	62	20.3	0	ethanethiol
	76	4.25	2.16	carbon disulfide
	90	13.4	0	diethyl sulfide
	104	0.33	0	ethyl isopropyl sulfide
	122	0.67	0	diethyl disulfide
	136	0.25	0	carbonothioic acid, O,S, diethyl ester
	150	0.24	0	carbonodithioic acid O,S, diethyl ester
PAX	60	35.4	8.14	carbonyl sulfide
	74	2.32	0	isobutanol
	76	38.7	7.37	carbon disulfide
	88	1.91	0	isoamyl alcohol
	132	1.07	0	unidentified
	146	0.94	0	di-isobutyl sulfide 3-methyl butyl propyl sulfide
	160	1.10	0	unidentified
	174	1.00	0	di-isobutyl carbonate di-isopentyl sulfide
	190	1.25	0	carbonothioic acid, O,S, dibutyl ester
	192	0	0	isobutyl 3-methyl butyl disulfide
	202	0	0	di-isopentyl carbonate
	204	0	0	unidentified
	206	0	0	di-isopentyl disulfide
	260	0.72	0	unidentified

Table 3.4: Relative peak areas of the evolved gases from SEX, SiBX, PEX, and PAX heated at 10°C min^{-1} in argon atmospheres.

A comparison of all four xanthates (except PEX) shows that the largest peak in the SIM spectra was carbon disulfide followed by carbonyl sulfide. In the PEX analysis carbonyl sulfide produced the largest peak, and a minor peak for carbon disulfide was evident.

Temperature/concentration profiles for carbonyl sulfide and carbon disulfide obtained from the decomposition of potassium xanthate compounds have been previously reported (Tyden 1966). As written earlier in section 3.0, Tyden pyrolysed a range of potassium xanthates with differing alkyl chains at 225, 675, 1000, and 1225°C onto a silica gel column. The carbonyl sulfide and carbon disulfide were identified by comparison of their retention times to known substances under the same conditions. For each pyrolysis temperature Tyden found the amount of carbonyl sulfide and carbon disulfide evolved was relatively similar for each xanthate studied. Tyden found that at a pyrolysis temperature of 675°C the evolution of carbonyl sulfide was at its maximum for each xanthate. At 1000°C Tyden found the evolution of carbon disulfide was at its maximum for each xanthate. These results do not compare at all to this current work where it has been established the maximum evolution of carbonyl sulfide and carbon disulfide occurs below 500°C and the amount produced was dependent on the alkyl chain. This discrepancy is most likely due to the non-linear temperature calibration of the pyrolysis unit used by Tyden and that the equipment used was rather primitive.

3.2.2 FTIR Spectroscopy Analysis of the Evolved Gases

Typical Thermogravimetric-Gram-Schmidt (TG-GS) curves of SEX, SiBX, PEX, and PAX heated at 10°C min^{-1} in argon atmospheres are presented in Figures 3.17, 3.19, 3.21, and 3.23. The infrared spectra resulting from the gases evolved during the mass losses of each xanthate are presented in Figures 3.18, 3.20, 3.22, and 3.24 for SEX, SiBX, PEX, and PAX respectively. All the TG curves coincided with their respective GS curves.

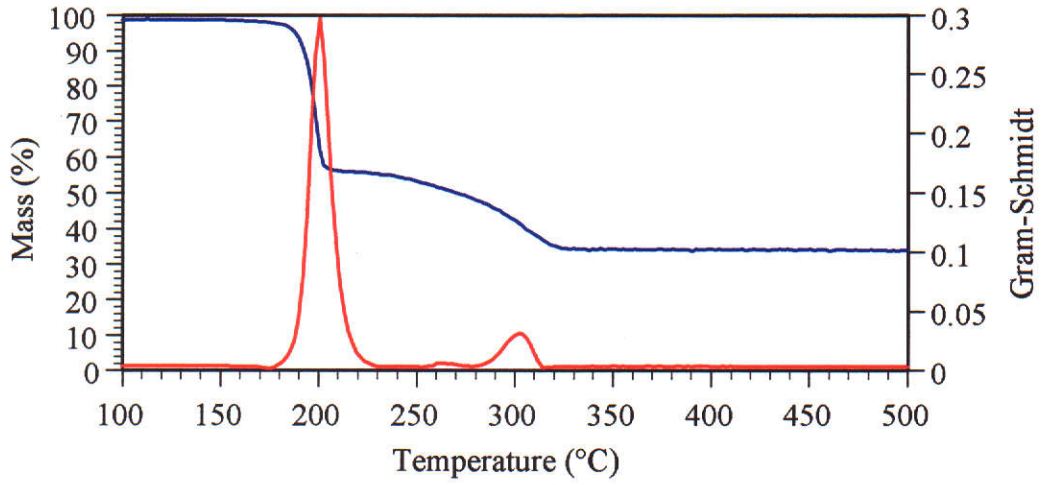

Figure 3.17: TG-GS curves of SEX heated at 10°C min^{-1} in an argon atmosphere.

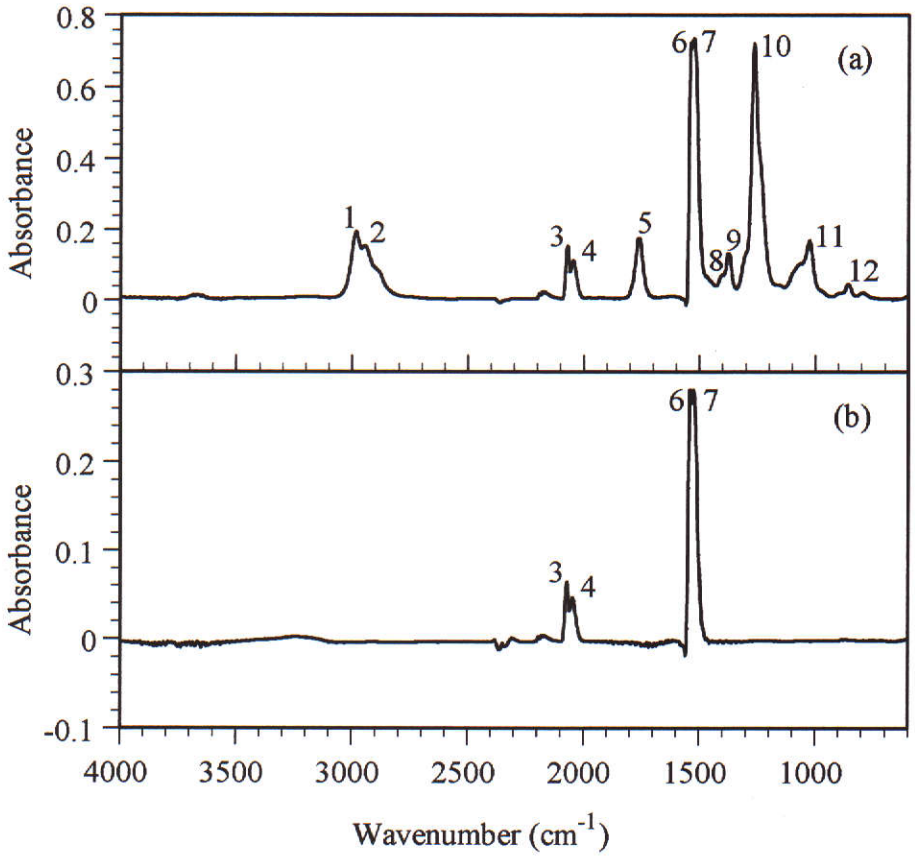

Figure 3.18: Infrared spectra of the gases evolved from the two mass losses of SEX, (a) first mass loss, (b) second mass loss.

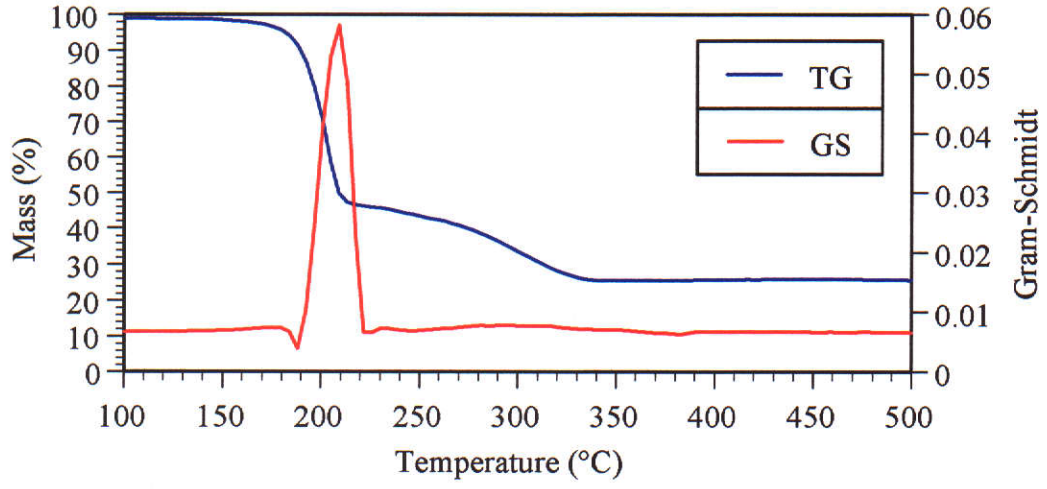

Figure 3.19: TG-GS curves of SiBX heated at 10°C min^{-1} in an argon atmosphere.

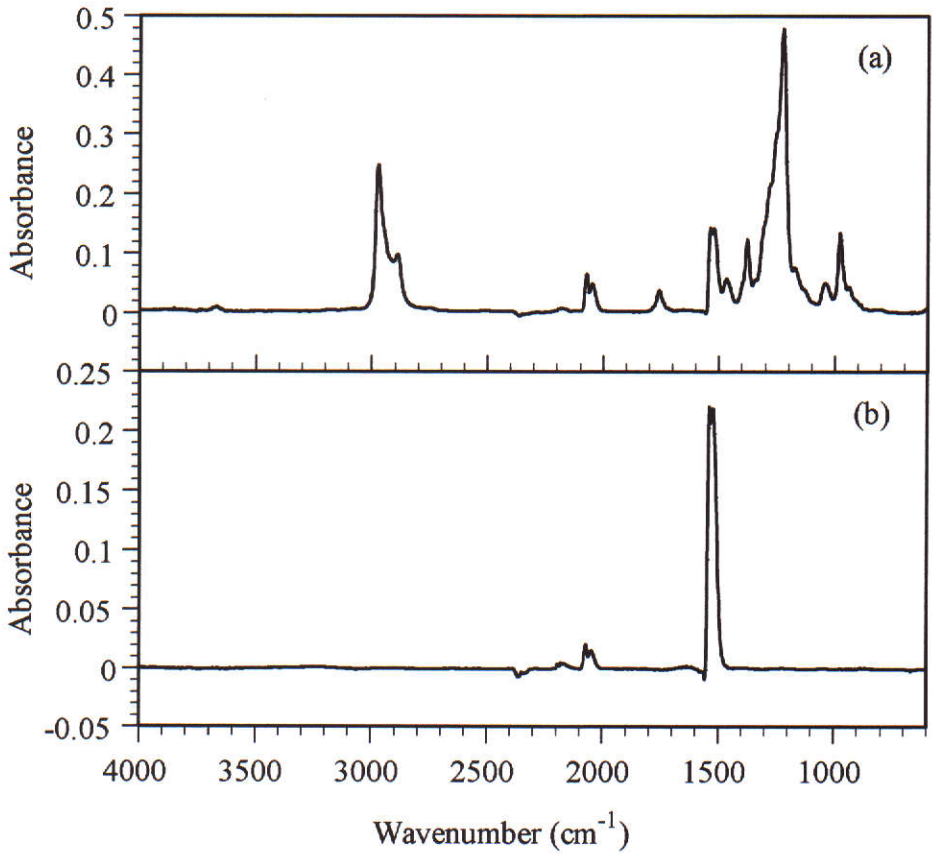

Figure 3.20: Infrared spectra of the gases evolved from the two mass losses of SiBX, (a) first mass loss, (b) second mass loss.

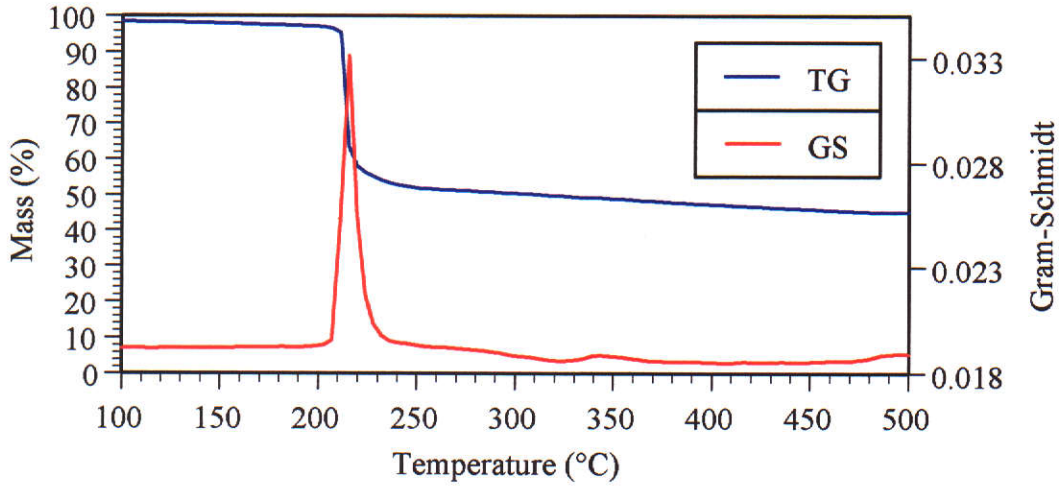

Figure 3.21: TG-GS curves of PEX heated at 10°C min^{-1} in an argon atmosphere.

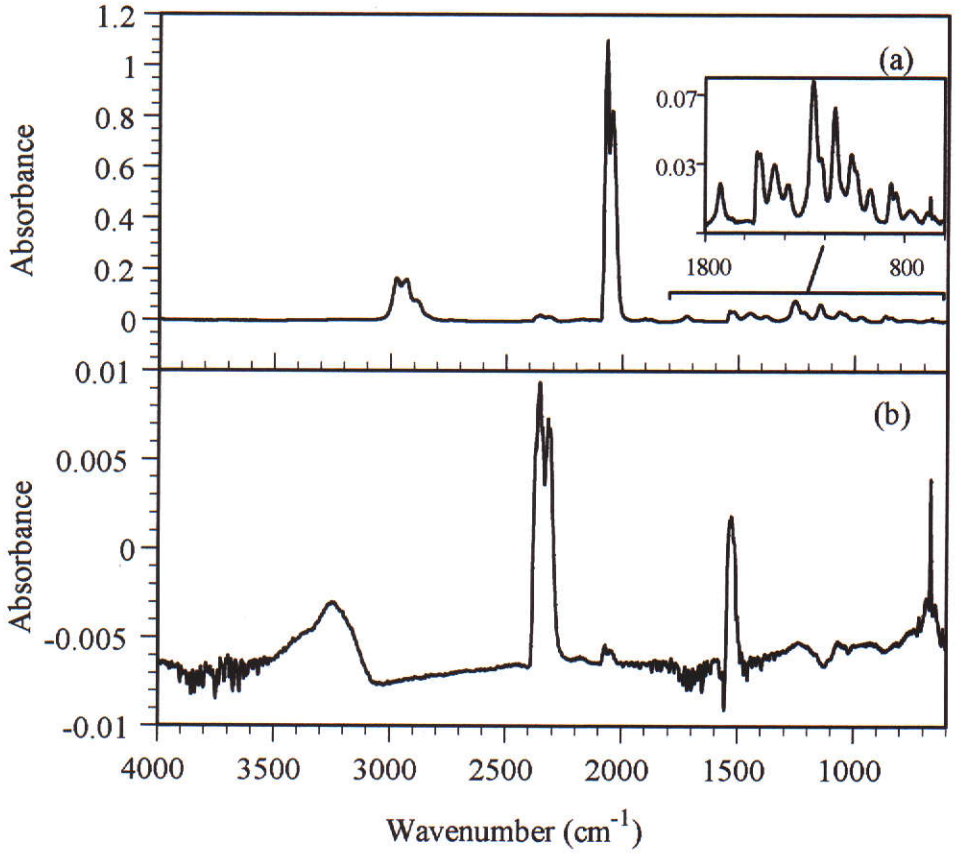

Figure 3.22: Infrared spectra of the gases evolved from the two mass losses of PEX, (a) first mass loss, (b) second mass loss.

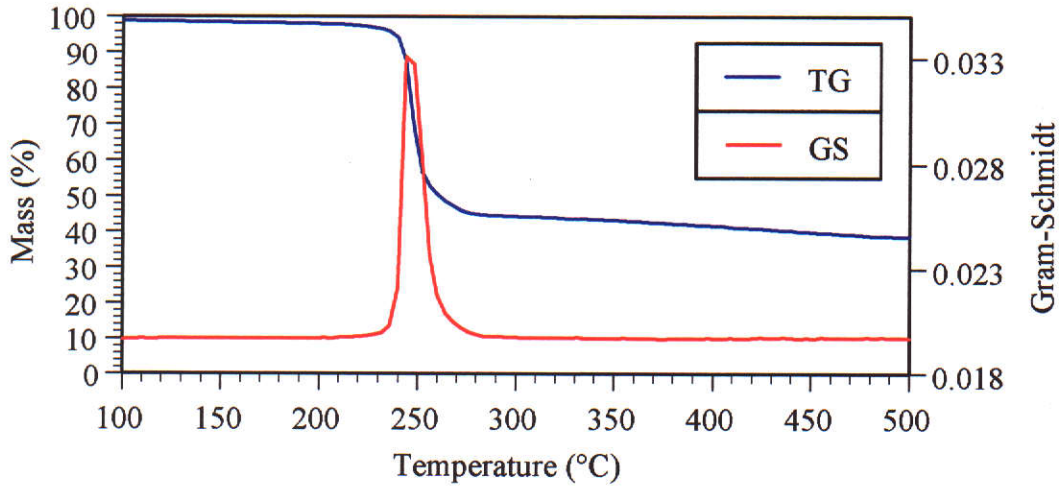

Figure 3.23: TG-GS curves of PAX heated at 10°C min^{-1} in an argon atmosphere.

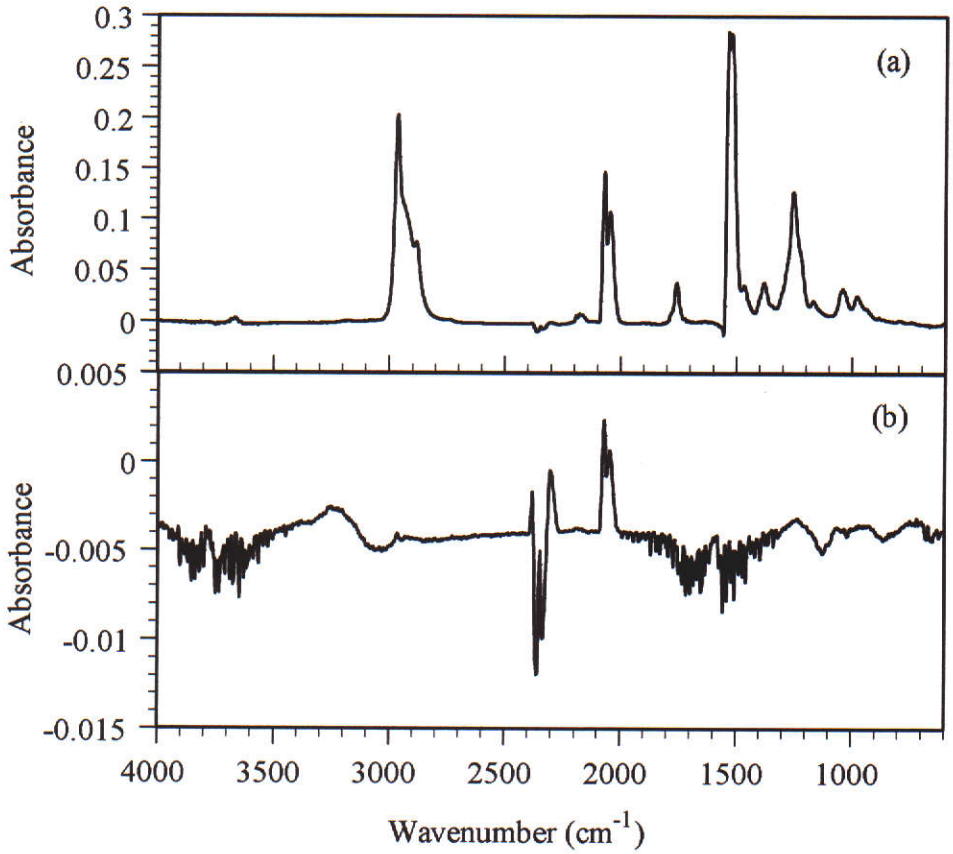

Figure 3.24: Infrared spectra of the gases evolved from the two mass losses of PAX, (a) first mass loss, (b) second mass loss.

The infrared spectra of the gases evolved from the first mass loss of Figures 3.18, 3.20, 3.22, and 3.24 are all reasonably complex due to the numerous absorption bands. A comparison of the spectra shows that they are all very similar, with only slight deviations in the wavelengths detected and intensity of the peaks. Identification of the absorption bands in each infrared spectrum was performed using characteristic infrared absorption wavelengths.

In the first mass loss evolved gas spectra of Figures 3.18(a), 3.20(a), and 3.24(a) there is a very small absorption band at 3670 cm^{-1}, which is characteristic of a free hydroxyl group. This band indicates the presence of an alcohol (Nakanishi 1977, Socrates 1994). Figure 3.22(a) did not contain this band indicating no alcohol was detected in the PEX decomposition.

An absorption band at 3000-2800 cm^{-1} was associated with symmetric and asymmetric stretching of the C-H bond in methyl and methylene groups (Nakanishi 1977; Socrates 1994). This region indicates the presence of alkyl compounds.

Absorption bands were also evident 2100-2000 cm^{-1}, 1760 cm^{-1}, and at 1540-1520 cm^{-1}. Within the 2100-2000 cm^{-1} absorption band there are two peaks. These peaks are due to the asymmetric and symmetric stretching of the carbonyl group contained in carbonyl sulfide (Kagann 1982; Herzberg 1945; Locker, Burkholder and Bair 1983). The single 1760 cm^{-1} absorption band is in a region which is characteristic for compounds containing a carbonyl group. There are also two peaks within the 1540-1520 cm^{-1} absorption band. These peaks are due to the asymmetric and symmetric stretching of C=S contained in carbon disulfide (Bellamy 1975; Herzberg 1945).

Below the 1520 cm^{-1} region there are numerous peaks. Identification of these peaks is difficult and it is most probable that these peaks are due to vibrations associated with alkyl and carbonyl groups. Also the peak at approximately 859 cm^{-1} has been attributed to stretching of the carbon-sulfur double bond in carbonyl sulfide (Kagann 1982; Herzberg 1945; Locker, Burkholder and Bair 1983).

The second mass loss evolved gas spectra of Figures 3.18(b), 3.20(b), 3.22(b), and 3.24(b) were less complex than the first mass loss evolved gas spectra. The spectra

were all similar, containing vibrations due to carbonyl sulfide and carbon disulfide. However the PAX second mass loss spectrum did not contain vibrations associated with carbon disulfide.

It was not possible to identify thiols, sulfides, and disulfides via their carbon-sulfur, sulfur-hydrogen, and sulfur-sulfur (for disulfides) stretching bands. Carbon-sulfur stretching is very weak and occurs in the region 660-630 cm^{-1}; sulfur-hydrogen stretching occurs in the region 2590-2560 cm^{-1}, but it is variable and usually weak; and sulfur-sulfur stretching occurs as a weak band in the region 500-400 cm^{-1} (Bellamy 1975).

Using the TD-py-GC-MS data it was possible to construct tables of the decomposition products, their absorption wavelength, and the type of absorption at that wavelength. This has been demonstrated in Table 3.5 for the thermal decomposition of SEX. The peak numbers shown in Table 3.5 are also shown in the infrared spectra of Figure 3.18. Tables for SiBX, PEX and PAX have not been presented here, as they are similar to the SEX thermal decomposition data.

Peak	Wavenumber	Assignment	Gas	References
1 2	2983.5 cm^{-1} 2948.0 cm^{-1}	ν_{as} CH_3, ν_{as} CH_2 ν_s CH_3, ν_s CH_2	ethanol ethanethiol diethyl sulfide diethyl carbonate diethyl disulfide carbonothioic acid, O,S, - diethyl ester carbonodithioic acid, O,S, - diethyl ester	Nakanishi (1977).
3 4	2071.5 cm^{-1} 2047.2 cm^{-1}	ν_{as} C=O ν_s C=O	carbonyl sulfide	Kagann (1982), Herzberg (1945), Locker, Burkholder and Bair (1983).
5	1758.9 cm^{-1}	ν C=O	diethyl carbonate carbonothioic acid, O,S, - diethyl ester carbonodithioic acid, O,S - diethyl ester	Morrison and Boyd (1992).
6 7	1531.3 cm^{-1} 1524.2 cm^{-1}	ν_{as} C=S ν_s C=S	carbon disulfide	Bellamy (1975), Herzberg (1945).
8	1404.8 cm^{-1}	δ C-H of CH_2, CH_3	same as peaks 1 and 2	Morrison and Boyd (1992).
9	1376.2 cm^{-1}	δ C-H of CH_3	same as peaks 1 and 2	Morrison and Boyd (1992).
10	1265.7 cm^{-1}	ν C–O	same as peak 5	Morrison and Boyd (1992).
11	1026.1 cm^{-1}	ν C-O	same as peak 5	Morrison and Boyd (1992).
12	859.4 cm^{-1}	ν C=S	carbonyl sulfide	Kagann (1982), Herzberg (1945), Locker, Burkholder and Bair (1983).

Table 3.5(a): Peak wavelength assignments of the gases evolved from the first mass loss. Abbreviations: ν (stretch); ν_s, ν_{as} (symmetric, asymmetric stretch); δ (bending).

Peak	Wavenumber	Assignment	Gas	References
3 4	2071.5 cm^{-1} 2047.2 cm^{-1}	ν_{as} C=O ν_s C=O	carbonyl sulfide	Kagann (1982), Herzberg (1945), Locker, Burkholder and Bair (1983).
5 6	1540.2 cm^{-1} 1524.4 cm^{-1}	ν_{as} C=S ν_s C=S	carbon disulfide	Bellamy (1975), Herzberg (1945).

Table 3.5(b): Peak wavelength assignments of the gases evolved from the second mass loss. Abbreviations: ν_s, ν_{as} (symmetric, asymmetric stretch).

3.3 TD-py-GC-MS Analysis of Alkali Xanthates Adsorbed on Activated Carbon

SEX, SiBX, PEX, and PAX were individually adsorbed onto the Haycarb (-45 μm) and the quantities adsorbed were 41.9, 39.7, 42.6, and 42.7 % w/w respectively (all ± 0.7 % w/w).

A blank experiment was first conducted on the commercial activated carbon Haycarb, of particle size -45 μm, by heating it in an inert atmosphere from ambient to 1000°C. The retention time (RT), percentage relative peak area (calculated the same way as for Table 3.2), and gases evolved are presented in Table 3.6.

RT	Relative Peak Area (%)	Gas Evolved
0.72	56.7	carbon dioxide
0.75	1.14	unidentified
0.79	2.95	sulfur dioxide
0.81	2.26	unidentified
0.83	2.00	ethanal
0.88	1.39	chloroethene
0.93	5.01	ethanol
0.97	1.87	unidentified
1.04	5.24	dichloromethane
1.21	0.31	hexene
1.24	0.49	unidentified
1.53	3.34	unidentified
1.56	1.82	benzene
1.82	3.48	acetic acid
2.46	1.07	toluene
4.39	1.35	styrene
11.4	1.30	phthalic anhydride
15.2	1.35	tolylene
25.4	1.29	2-dimethylamino-5,6-dimethylpyrimidine-4-yl-dimethyl carbonate
27.1	1.36	hexadecanoic acid
30.3	0.75	octadecanoic acid
35.8	3.52	1,2-benzenedicarboxylic acid, bis-(2-ethylhexyl) ester

Table 3.6: Gases evolved from the pyrolysis of Haycarb activated carbon.

The most abundant gas evolved from the pyrolysis of the activated carbon was carbon dioxide, probably resulting from adsorbed oxygen reacting with the carbon, and/or the thermal decomposition of carboxylic acid groups on the structure of the carbon. The other gases evolved are also most likely due to the surface group bonds breaking from the carbon hexagonal rings and/or the bonds within the surface groups breaking.

TD-py-GC-MS was used to identify the gases evolved from each xanthate adsorbed on activated carbon when heated in an inert atmosphere from ambient to 1000°C. Each pyrolysis produced numerous gases. The total ion chromatograms of the samples are presented in Figures, 3.25, 3.26, 3.27, and 3.28 respectively.

For simplicity, gases with a peak area less than 10 % of the largest peak were excluded from the study, as well as those gases identified from the blank experiment. The remaining gases were identified using a mass spectra database and manual interpretation. The gases produced for each pyrolysis, along with their retention time and relative peak area are presented in Table 3.7.

A typical total ion chromatogram of SEX is shown in Figure 3.25. After excluding gases as indicated above, seven significant peaks were identified. Carbonothioic acid, O,S, diethyl ester had the largest relative peak area, followed by carbon disulfide, and ethanethiol. Eight significant peaks were identified from the decomposition of SiBX, of which isobutanol had the largest relative peak area, followed by carbonothioic acid, O,S, dibutyl ester, and carbon disulfide. The decomposition of PEX produced nine significant peaks, of which carbonothioic acid, O,S, diethyl ester had the largest relative peak area, followed by carbonodithioic acid, O,S, diethyl ester and carbon disulfide. Finally, the decomposition of PAX produced eleven significant peaks, of which butanol had the largest relative peak area, followed by 3-methyl-l-butanethiol, and carbon disulfide.

	Peak	RT (min)	Relative Peak Area (%)	Gas Evolved
SEX-AC	1	0.89	7.05	carbonyl sulfide
	2	1.12	16.8	ethanethiol
	3	1.22	18.2	carbon disulfide
	4	2.98	9.47	diethyl carbonate
	5	5.49	8.80	diethyl disulfide
	6	6.19	35.6	carbonothioic acid, O,S, diethyl ester
	7	11.1	4.12	carbonodithioic acid O,S, diethyl ester
SiBX-AC	1	0.90	3.85	carbonyl sulfide
	2	0.98	5.59	2-methyl-1-propene
	3	1.25	12.8	carbon disulfide
	4	2.02	46.5	isobutanol
	5	9.48	4.29	di-isobutyl carbonate
	6	10.2	4.15	carbonodithioic acid O,S, diethyl ester
	7	12.9	17.5	carbonothioic acid, O,S, dibutyl ester
	8	13.7	5.37	methyl propanoate
PEX-AC	1	0.93	5.62	carbonyl sulfide
	2	1.15	4.99	ethanethiol
	3	1.25	14.0	carbon disulfide
	4	2.96	3.84	diethyl carbonate
	5	5.26	4.16	diethyl disulfide
	6	5.56	11.5	unidentified (134 g mol^{-1})
	7	6.02	36.8	carbonothioic acid, O,S, diethyl ester
	8	7.66	4.66	diethyl sulfate
	9	10.4	14.4	carbonodithioic acid O,S, diethyl ester
PAX-AC	1	0.86	6.38	carbonyl sulfide
	2	1.01	5.86	3-methyl-1-butene
	3	1.23	9.88	carbon disulfide
	4	1.90	28.6	butanol
	5	2.83	5.61	isoamyl alcohol
	6	2.91	15.9	3-methyl-1-butanethiol
	7	10.2	4.13	carbonodithioic acid O,S, diethyl ester
	8	12.8	4.45	unidentified (135 g mol^{-1})
	9	15.4	6.72	unidentified (204 g mol^{-1})
	10	19.3	6.28	unidentified (220 g mol^{-1})
	11	21.5	6.23	unidentified (234 g mol^{-1})

Table 3.7: Gases evolved from the pyrolysis of SEX, SiBX, PEX, and PAX adsorbed on activated carbon.

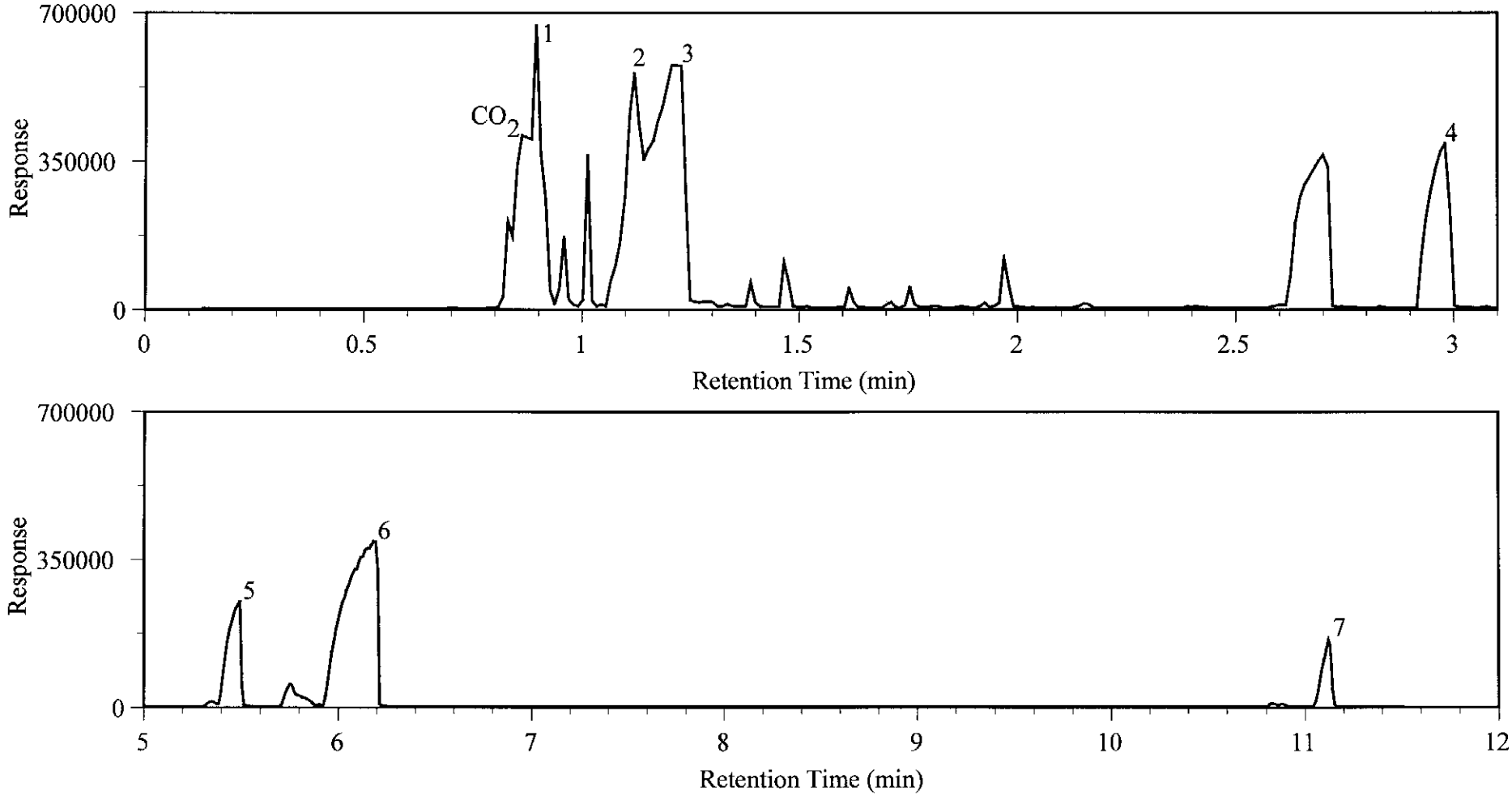

Figure 3.25: TD-py-GC-MS total ion chromatogram of SEX adsorbed on Haycarb, heated at 25°C min^{-1} in an inert atmosphere.

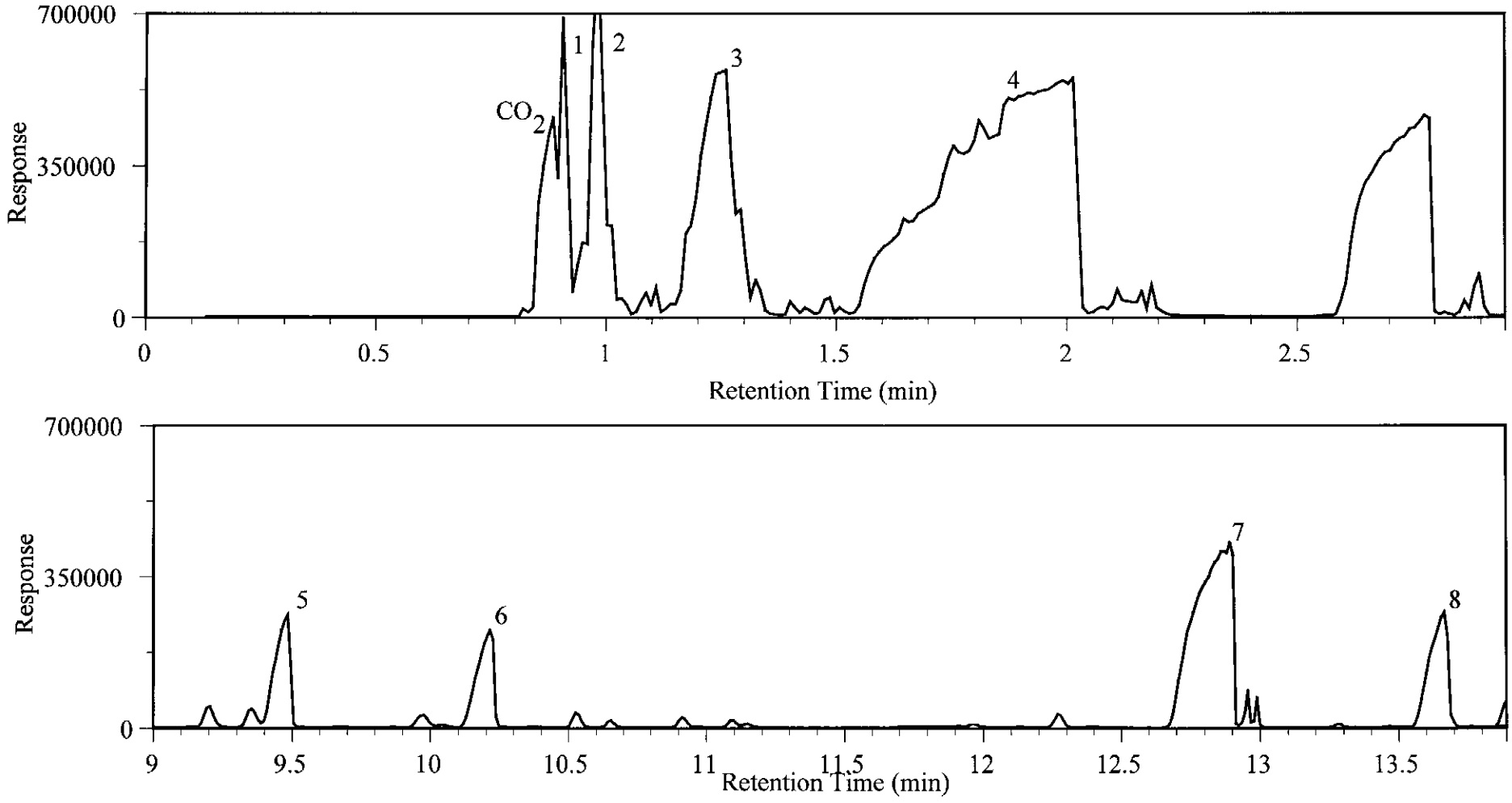

Figure 3.26: TD-py-GC-MS total ion chromatogram of SiBX adsorbed on Haycarb, heated at 25°C min^{-1} in an inert atmosphere.

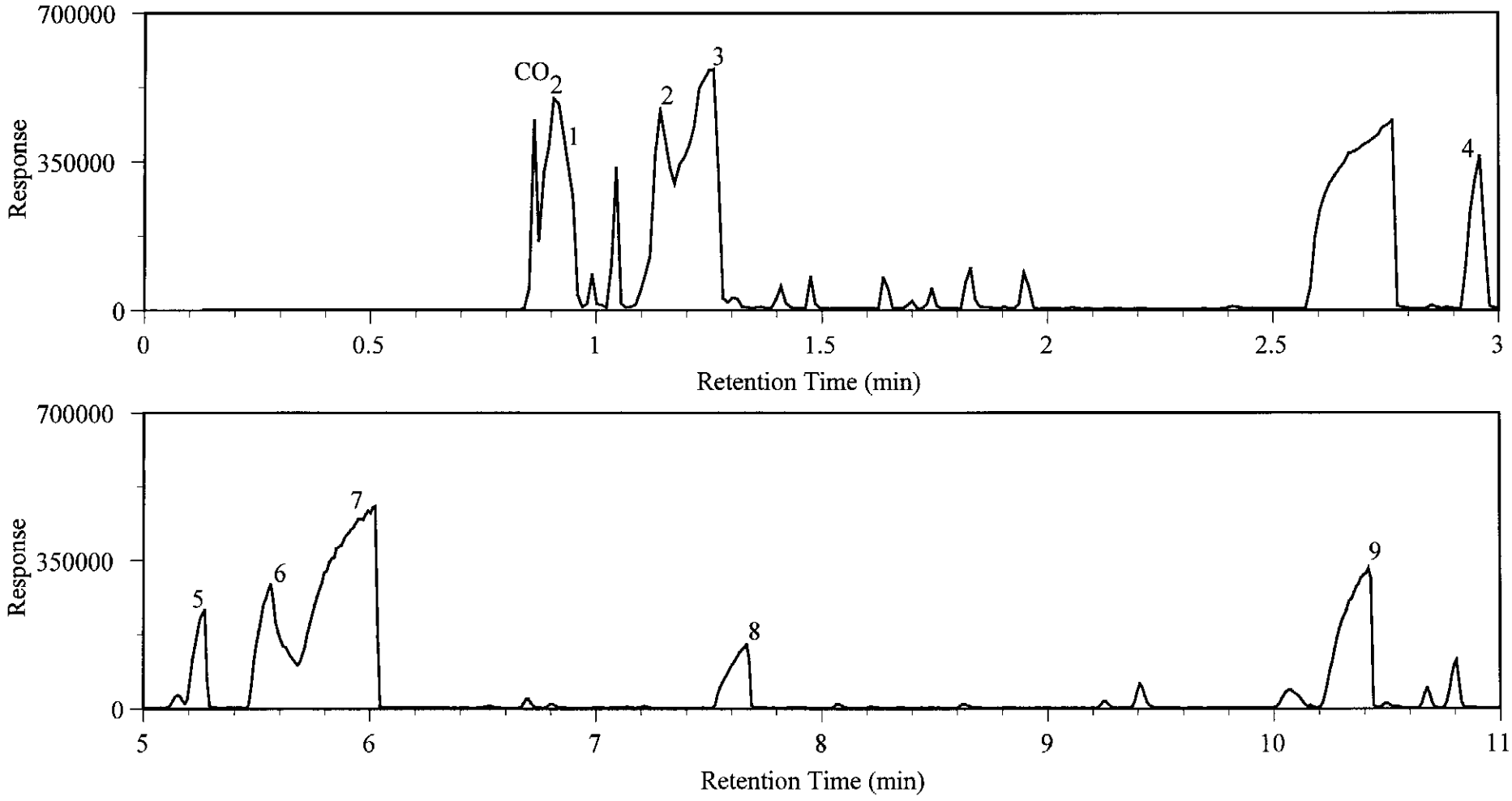

Figure 3.27: TD-py-GC-MS total ion chromatogram of PEX adsorbed on Haycarb, heated at 25°C min^{-1} in an inert atmosphere.

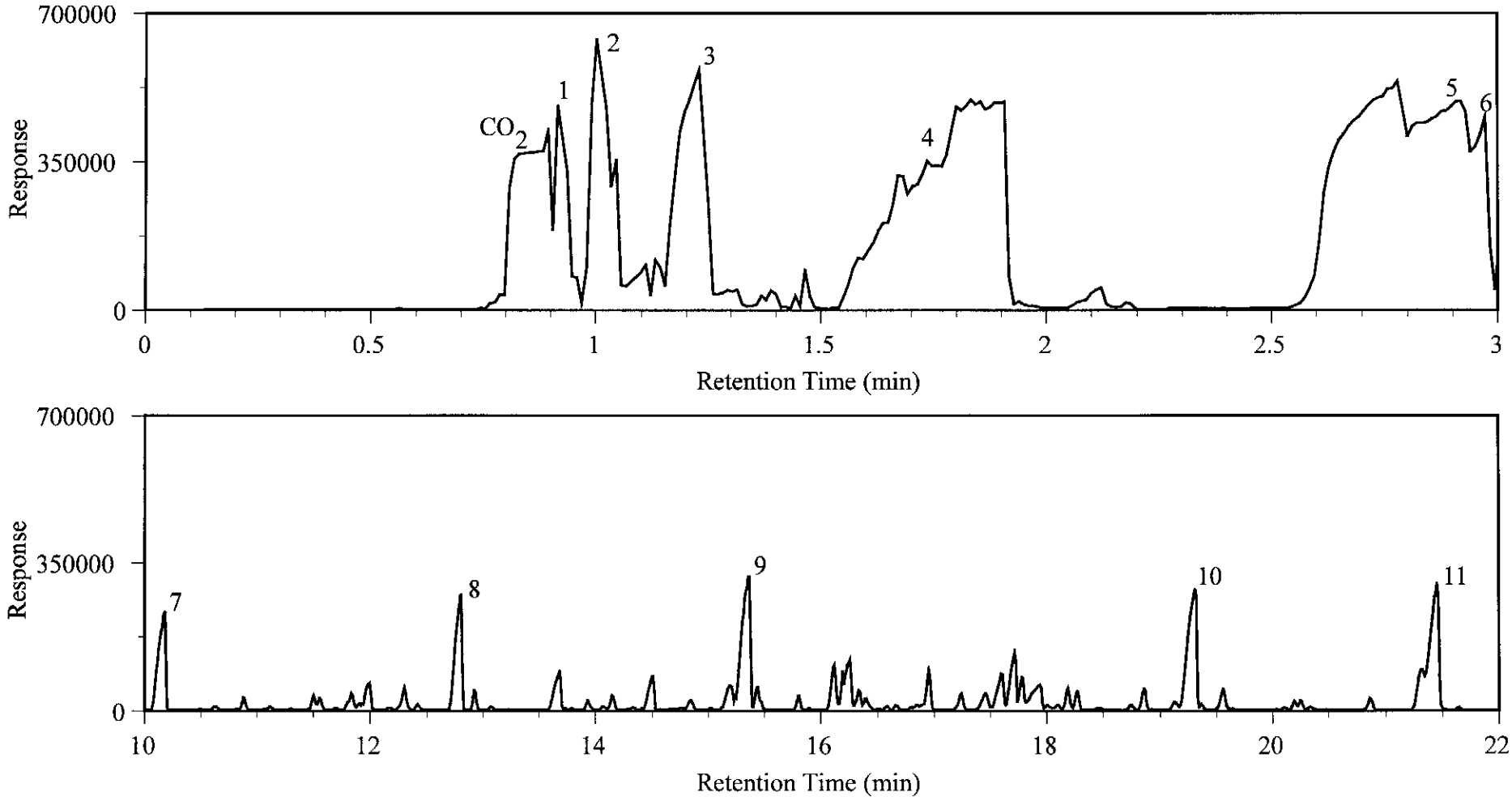

Figure 3.28: TD-py-GC-MS total ion chromatogram of PAX adsorbed on Haycarb, heated at 25°C min^{-1} in an inert atmosphere.

3.4 Thermogravimetry - Evolved Gas Analysis of Alkali Xanthates Adsorbed on Activated Carbon

Before the analysis of the xanthates adsorbed on activated carbon was performed, the thermal decomposition of the Haycarb, -45 μm, was studied in an argon atmosphere. TG-MS and TG-FTIR analyses showed two distinct mass losses, the first from ambient to 520°C (1.4 %), which was attributed to the evolution of water, carbon monoxide and carbon dioxide. The second, larger mass loss (4.5 %) occurred above 550°C, which was attributed to the decomposition of the Haycarb into carbon monoxide and carbon dioxide, according to the reaction:

$$C + H_2O \rightarrow CO \text{ or } (CO_2) + H_2$$

Above 650°C the reaction is thermodynamically favorable (Dahya and King 1983).

These samples were studied by thermogravimetric analysis and the evolved gases were analysed by MS and FTIR spectroscopy. Each sample exhibited three mass losses. The mass losses and their extrapolated onset/offset temperatures for each sample are presented in Table 3.8. The temperatures quoted between the first and second mass losses are not extrapolated onset/offset values, as these were difficult to assess accurately, but they are quoted as the temperature in the middle of those mass losses.

	Adsorbed Xanthate			
Mass Loss	**SEX**	**SiBX**	**PEX**	**PAX**
First	173-230°C (17.47 %)	169-220°C (14.88 %)	146-207°C (15.88 %)	138-209°C (12.53 %)
Second	230-288°C (14.81 %)	220-255°C (13.23 %)	207-271°C (15.32 %)	209-263°C (14.90 %)
Third	288-431°C (1.13 %)	255-373°C (3.98 %)	271-389°C (0.967 %)	263-367°C (4.27 %)
Total	33.41 %	32.09 %	32.17 %	31.70 %

Table 3.8: Mass losses and their corresponding temperatures for SEX, SiBX, PEX, and PAX adsorbed on Haycarb, -45 μm.

An example of how the temperatures were obtained for each xanthate adsorbed on the activated carbon is shown in Figure 3.29 for SEX. Figure 3.29 shows the extrapolated onset temperature (T_e) for the first mass loss, the extrapolated offset temperature (T_o) for the second mass loss, and the temperature in the middle of those two mass losses (T_m). Also shown in Figure 3.29 is the derivative of the TG curve (the DTG curve). It was the DTG curve that was used to obtain T_m, that is where the curve is at its minimum between each mass loss.

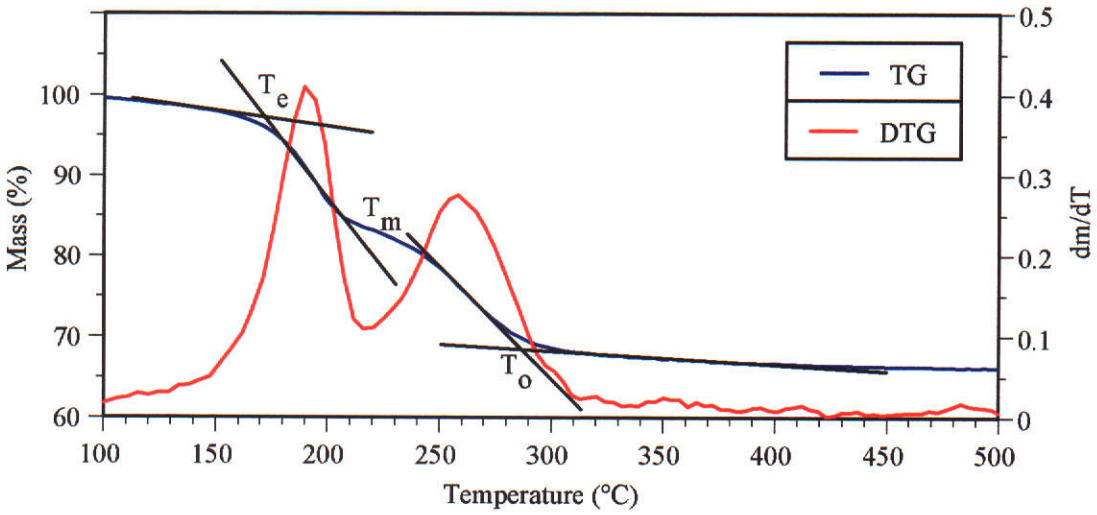

Figure 3.29: Measurement of the mass loss temperatures for the SEX adsorbed on Haycarb -45 μm.

There was little difference between the mass loss temperatures for each adsorbed xanthate and no trend was evident. The amount of mass loss for each adsorbed xanthate was also similar and again no clear trend was evident. The only clear difference was the first mass loss of each adsorbed xanthate was the largest except for PAX. Also the SEX and PEX displayed similar trends in mass loss, and so did the SiBX and PAX.

For each xanthate adsorbed onto the activated carbon it was possible to calculate a theoretical mass loss. To do this the amount of each xanthate adsorbed (%) was multiplied by the total mass loss for each xanthate when not adsorbed on activated carbon. To correct for the mass loss due to the decomposition of activated carbon, 1.4 % was subtracted from each experimental mass loss. This number was obtained

from the activated carbon TG curve with no xanthates or other compounds adsorbed. The theoretical and experimental mass losses for each xanthate are presented in Table 3.9.

	SEX	SiBX	PEX	PAX
Experimental (%)	32.01	30.69	30.77	30.30
Theoretical (%)	26.44	28.98	22.32	25.27

Table 3.9: Experimental versus theoretical mass losses for SEX, SiBX, PEX, and PAX adsorbed onto Haycarb.

The experimental mass loss values for all the xanthates were larger than that of the theoretical values. This indicated that besides the mass loss attributed to the decomposition of the xanthates, another mass loss occurred as the result of another adsorbed compound. This other adsorbed compound was most likely water, as it was used as the solvent during the adsorption process, and no other compounds were present. This of course assumes that for each xanthate the same amount decomposes regardless of its adsorption on activated carbon.

3.4.1 MS Analysis of the Evolved Gases

The gases evolved from each xanthate adsorbed on activated carbon were studied by SIM from ambient to 1000°C in argon atmospheres. The gases evolved were monitored via their molecular ions, which were identified by the TD-py-GC-MS analyses. Qualitative analysis was only possible due to interfering fragment ions and/or isotope ion signals. Presented in Figures 3.30 to 3.33 are some of the ion chromatograms for each evolved gas along with their corresponding mass loss curves. Discussion of these ion chromatograms assumes that the contribution of fragment or isotope ion signals is very small and insignificant.

Figure 3.30 shows the ion chromatograms for carbon disulfide (amu 76), carbonyl sulfide (amu 60), and ethanethiol (amu 62) for the decomposition of SEX adsorbed on Haycarb, -45 um. The gas evolved with the largest relative peak area during the

first mass loss of the adsorbed SEX was carbon disulfide followed by carbonyl sulfide. All other gases evolved in small quantities. During the second mass loss carbonyl sulfide had the largest relative peak area, followed by ethanethiol, and carbon disulfide. During the second mass loss the rate of evolution of carbonyl sulfide peaked at 255°C, while the rates of evolution of carbon disulfide and ethanethiol peaked at 280°C. During the third mass loss only minor quantities of gases evolved. Ion chromatograms (amu 122 and 136) are not displayed in Figure 3.30 because they were severely affected by background noise. Also ion chromatograms (amu 118 and 150) have been omitted from Figure 3.30, as these gases were not detected.

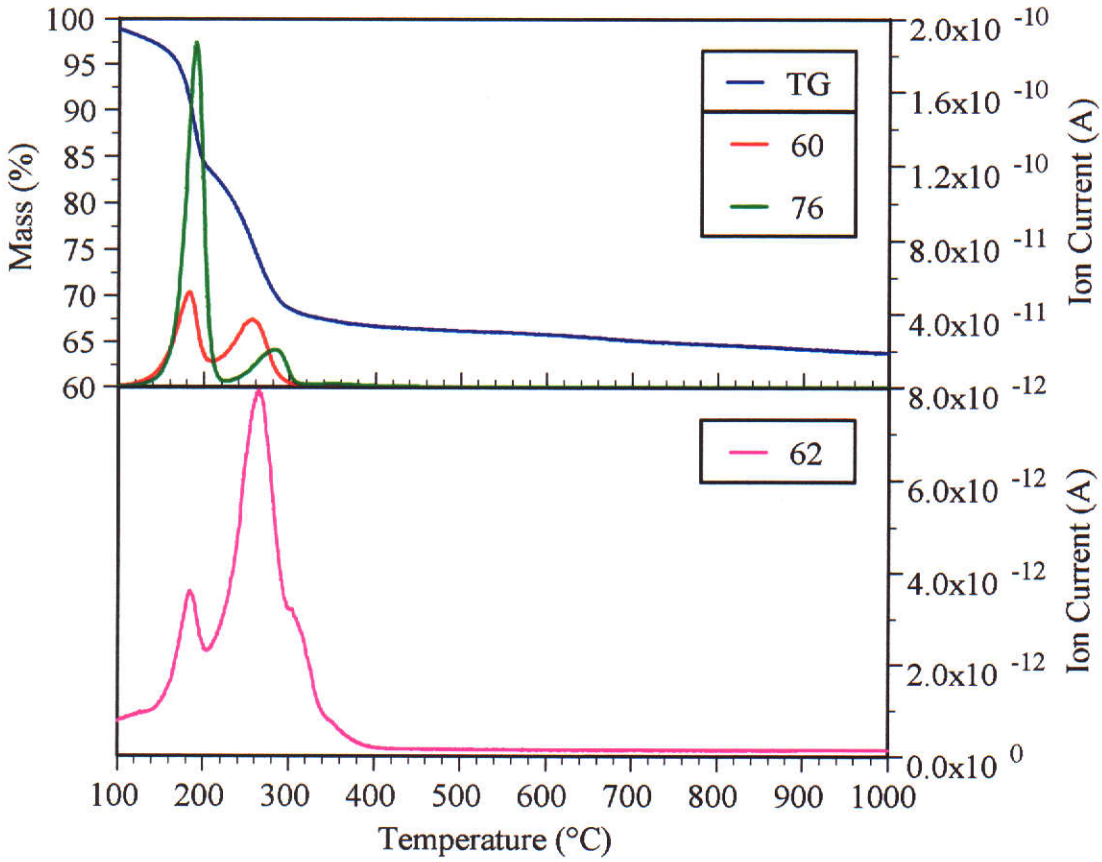

Figure 3.30: amu 60, 62, and 76 ion chromatograms of SEX adsorbed on Haycarb and heated at 10°C min^{-1} in an argon atmosphere.

Figure 3.31 shows the ion chromatograms for carbon disulfide (amu 76), carbonyl sulfide (amu 60), and 2-methyl-1-propene (amu 57) for the decomposition of SiBX adsorbed on Haycarb, -45 um. The gas evolved with the largest relative peak area

during the first mass loss of the adsorbed SiBX was carbon disulfide followed by carbonyl sulfide. All other gases evolved in small quantities. During the second mass loss carbonyl sulfide has the largest relative peak area, followed by 2-methyl-1-propene, and carbon disulfide. During the third mass loss only minor quantities of gases evolved. An ion chromatogram for amu 74 is not displayed in Figure 3.31 because it had a small relative peak area and evolved similarly to amu 57. Also ion chromatograms (amu 123, 134, 150, 174, and 190) have been omitted from Figure 3.31, as these gases were not detected.

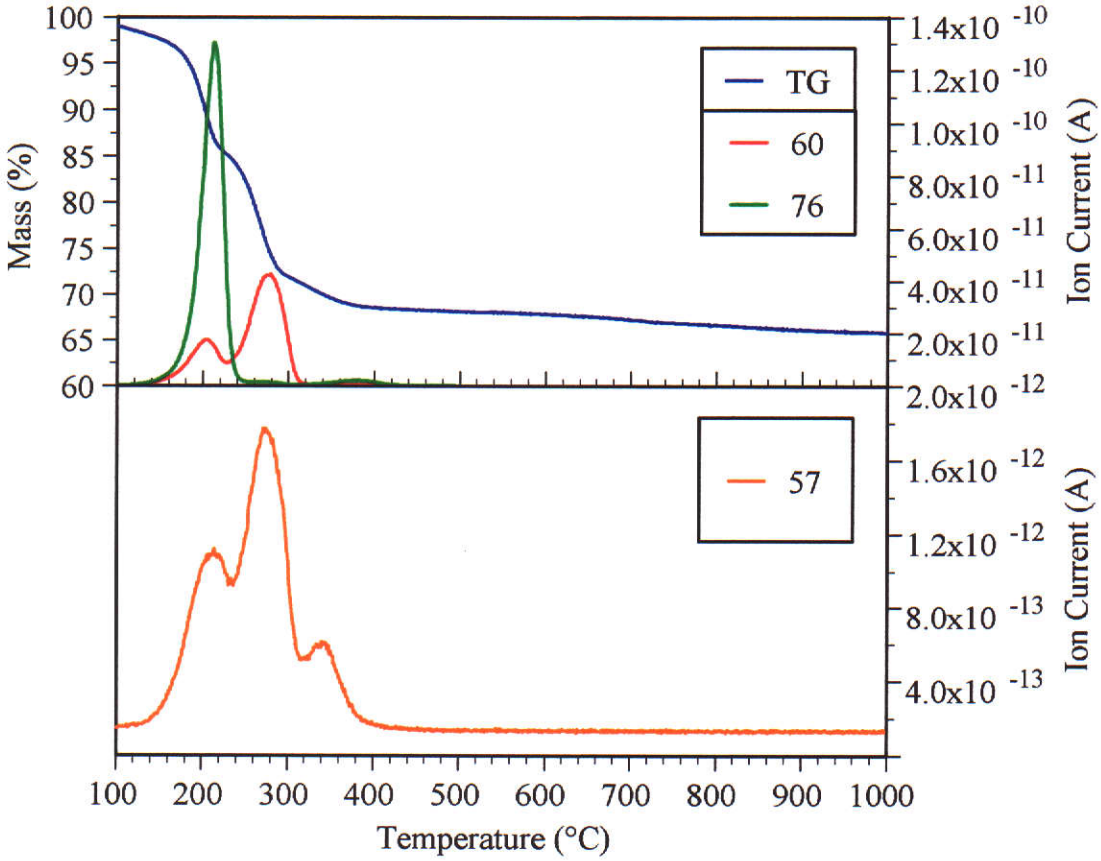

Figure 3.31: amu 57, 60, and 76 ion chromatograms of SiBX adsorbed on Haycarb and heated at 10°C min^{-1} in an argon atmosphere.

The ion chromatograms for the decomposition of PEX adsorbed on Haycarb, -45 µm are shown in Figure 3.32. These ion chromatograms are almost identical to that of ion chromatograms produced from the decomposition of SEX adsorbed on Haycarb, -45 µm. The amounts of each evolved gas are also similar. This indicated that the

alkali cation did not play a role in the thermal decomposition of the xanthates adsorbed on activated carbon.

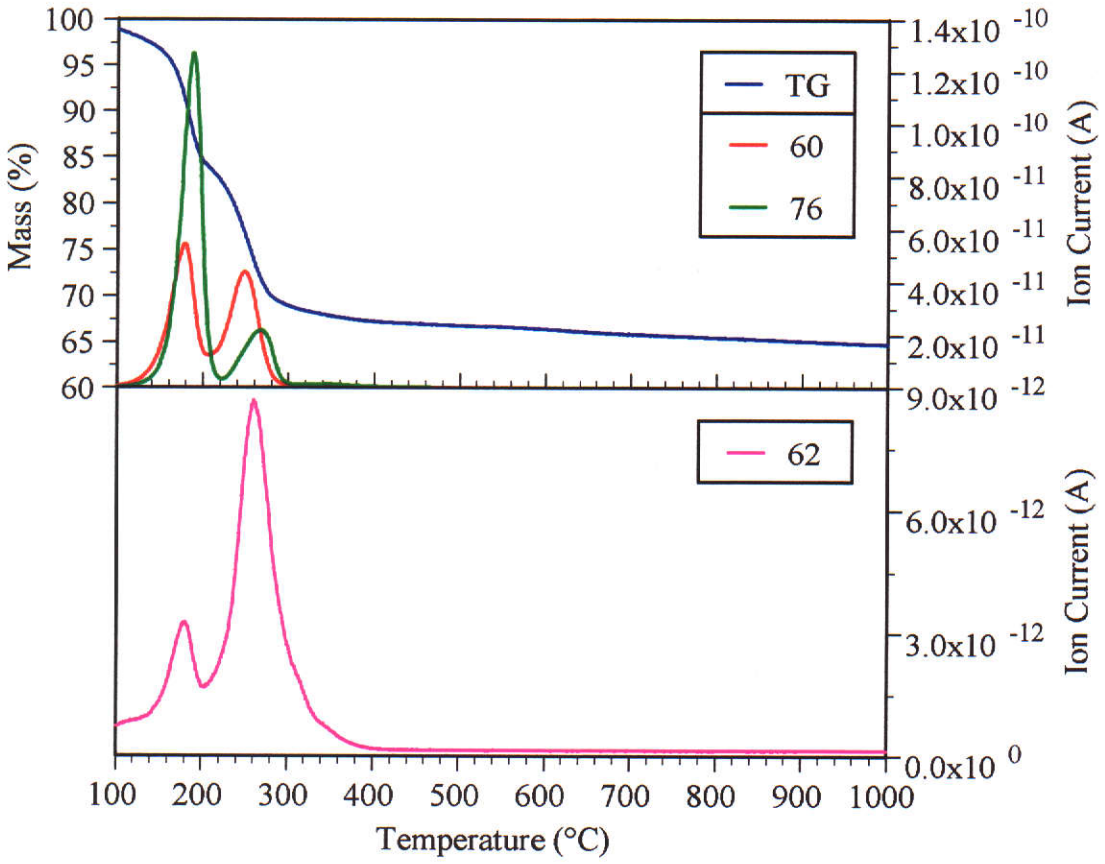

Figure 3.32: amu 60, 62, and 76 ion chromatograms of PEX adsorbed on Haycarb and heated at 10°C min^{-1} in an argon atmosphere.

Figure 3.33 shows the ion chromatograms for carbon disulfide (amu 76), carbonyl sulfide (amu 60), and 2-methyl-1-butene (amu 70) for the decomposition of PAX adsorbed on Haycarb, -45 um. The gas evolved with the largest relative peak area during the first mass loss of the adsorbed PAX was carbon disulfide followed by carbonyl sulfide. All other gases evolved in small quantities. During the second mass loss carbonyl sulfide had the largest relative peak area. During the third mass loss only minor quantities of gases evolved. Ion chromatograms (amu 74, 88, and 104) are not displayed in Figure 3.33 because they were had a minor relative peak area and evolved similarly to amu 70. Also ion chromatograms (amu 135, 149, 150, 165) have been omitted from Figure 3.33, as these gases were not detected.

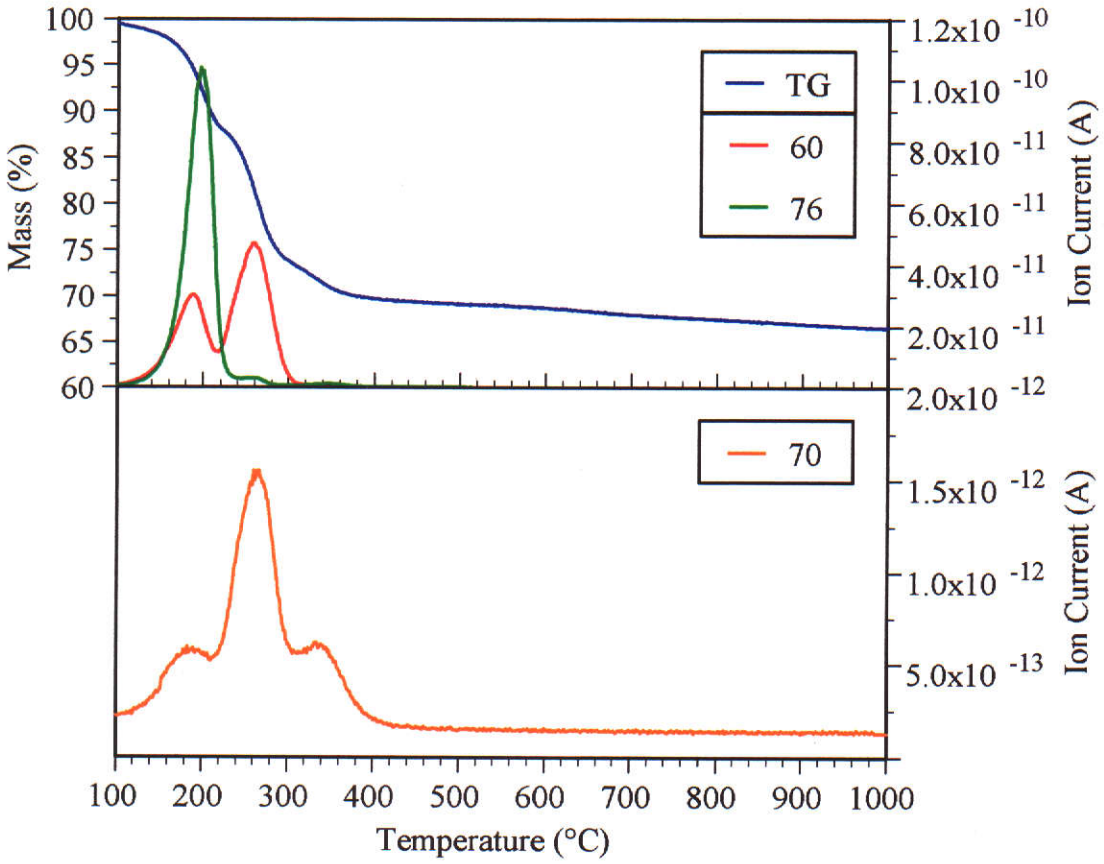

Figure 3.33: amu 60, 70, and 76 ion chromatograms of PAX adsorbed on Haycarb and heated at 10°C min^{-1} in an argon atmosphere.

Table 3.10 shows the relative peak area of the major gases evolved for each xanthate adsorbed on activated carbon. The relative peak area of each gas has been expressed as a percentage (similar to Table 3.4).

A comparison of all four xanthates adsorbed on activated carbon shows that carbon disulfide and then carbonyl sulfide evolved during the first mass losses with the largest relative peak areas. During the second mass losses carbonyl sulfide had the largest relative peak area and in the third mass losses only minor amounts of each gas were detected. Overall carbon disulfide had the largest relative peak area. All other gases evolved appear insignificant in comparison to carbonyl sulfide and carbon disulfide evolution.

	amu	Relative Peak Area (%) First Mass Loss	Second Mass Loss	Third Mass Loss	Gas Evolved
SEX	60	16.5	18.4	0.48	carbonyl sulfide
	62	1.61	4.54	1.32	ethanethiol
	76	44.0	10.4	1.41	carbon disulfide
SiBX	57	0.89	1.40	0.59	2-methyl-1-propene
	60	10.3	27.9	0.89	carbonyl sulfide
	76	53.5	0.97	2.31	carbon disulfide
PEX	60	18.1	29.0	0	carbonyl sulfide
	62	1.60	5.32	0	ethanethiol
	76	34.2	9.18	1.12	carbon disulfide
PAX	60	16.9	29.2	0.71	carbonyl sulfide
	70	0.64	1.21	0.59	3-methyl-1-butene
	76	46.1	1.43	1.00	carbon disulfide

Table 3.10: Relative peak areas of the decomposition gases from SEX, SiBX, PEX, and PAX adsorbed on Haycarb and heated at 10°C min^{-1} in an argon atmosphere.

3.4.2 FTIR Analysis of the Evolved Gases

Typical TG-GS curves of SEX, SiBX, PEX, and PAX adsorbed onto Haycarb, -45 μm heated at 10°C min^{-1} in argon atmospheres are presented in Figure 3.34. The infrared spectra of the gases evolved from each mass loss for each xanthate from Figure 3.34 are presented in Figures 3.35 to 3.38.

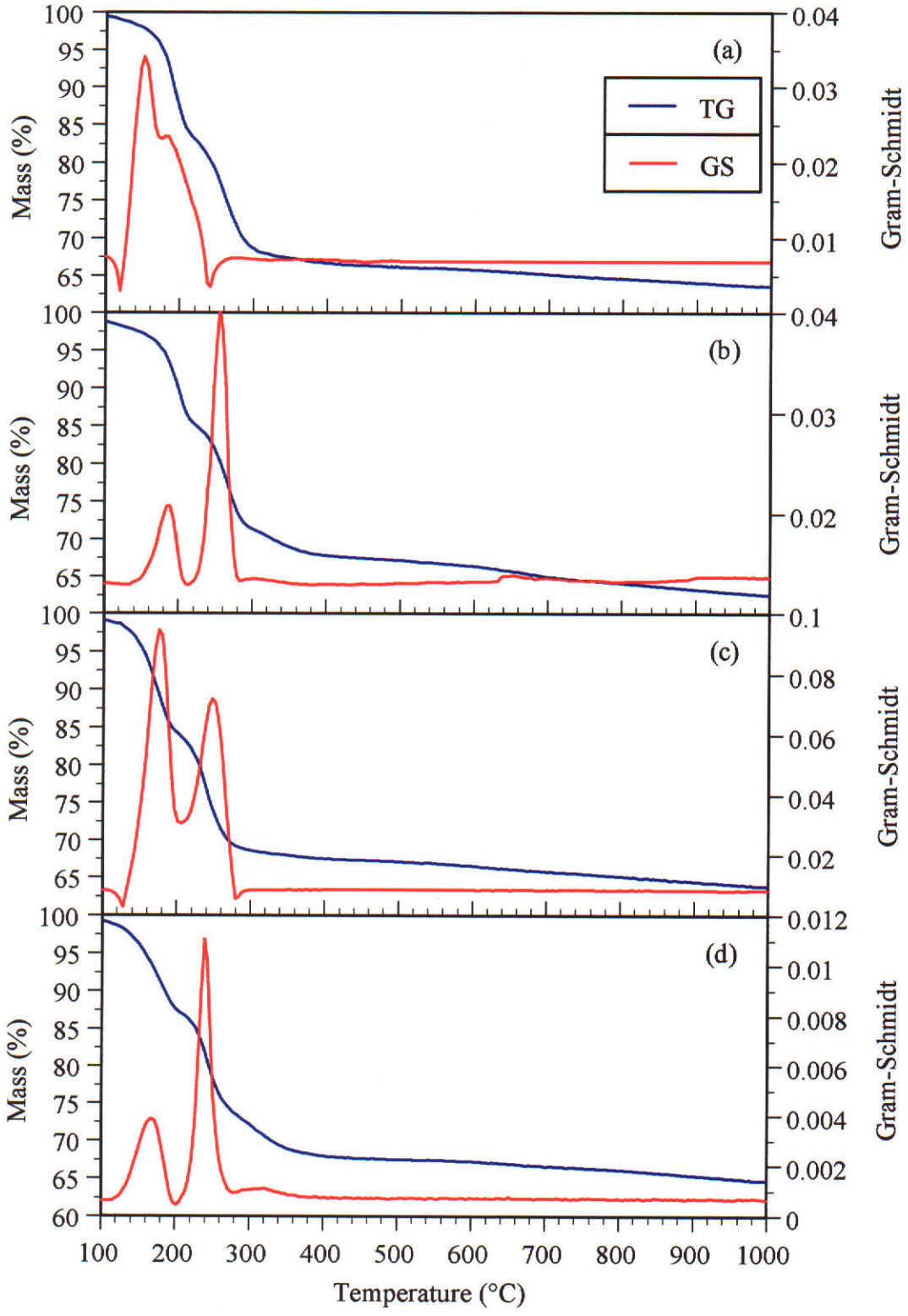

Figure 3.34: TG-GS curves of the xanthates adsorbed onto Haycarb, -45 µm heated at 10°C min^{-1} in argon atmospheres, (a) SEX, (b) SiBX, (c) PEX, (d) PAX.

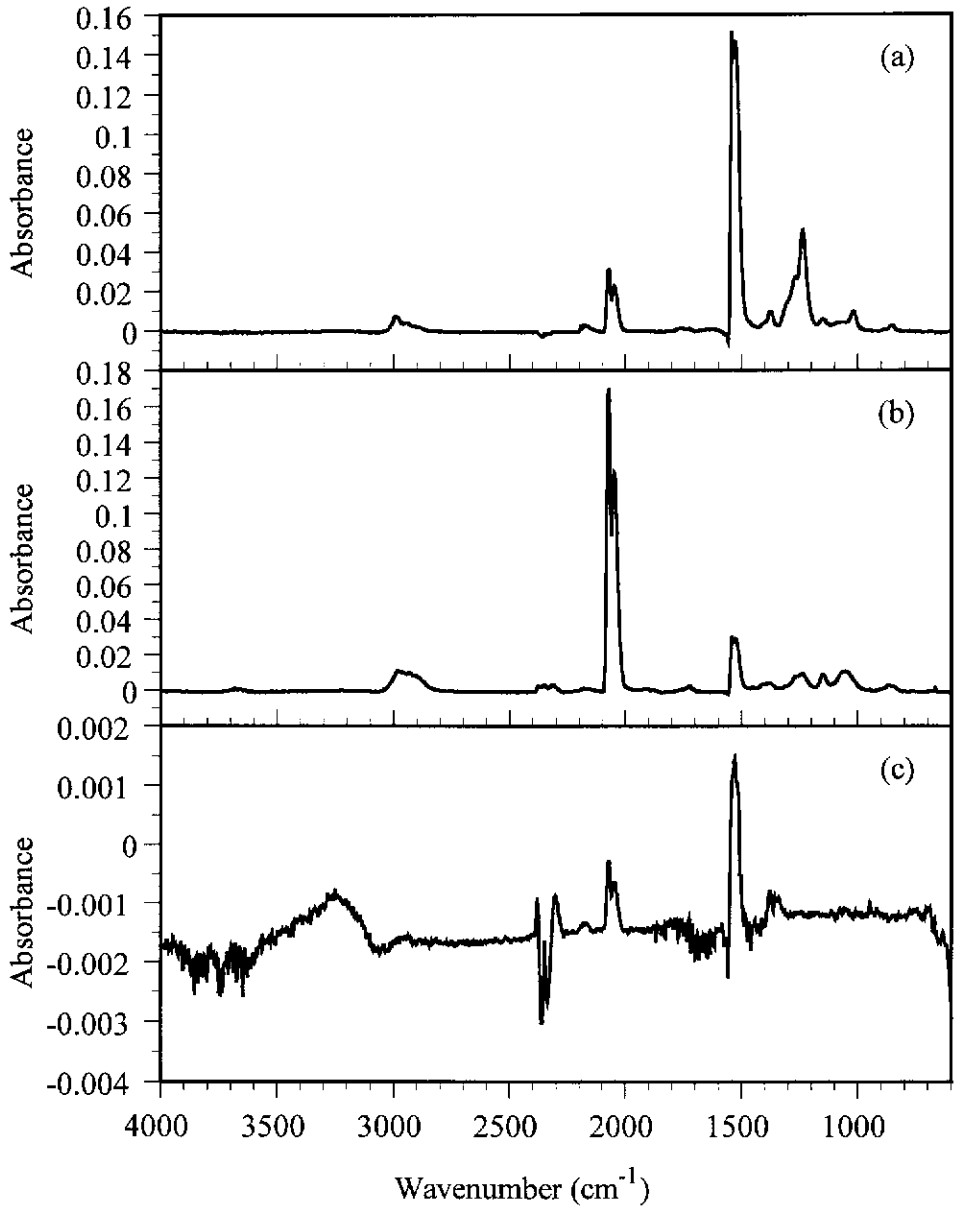

Figure 3.35: Infrared spectra of the gases evolved from SEX adsorbed on Haycarb, (a) first mass loss, (b) second mass loss, (c) third mass loss.

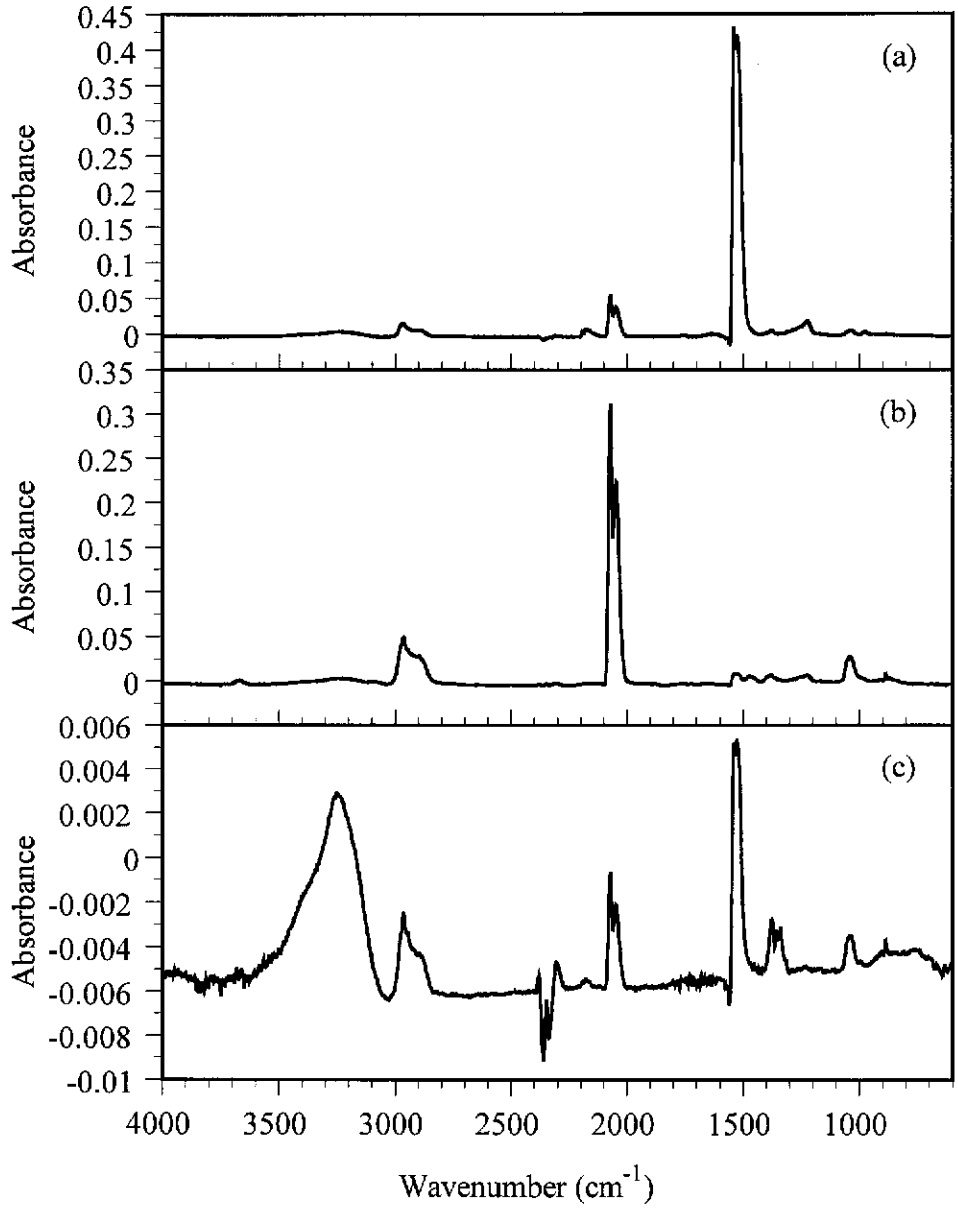

Figure 3.36: Infrared spectra of the gases evolved from SiBX adsorbed on Haycarb, (a) first mass loss, (b) second mass loss, (c) third mass loss.

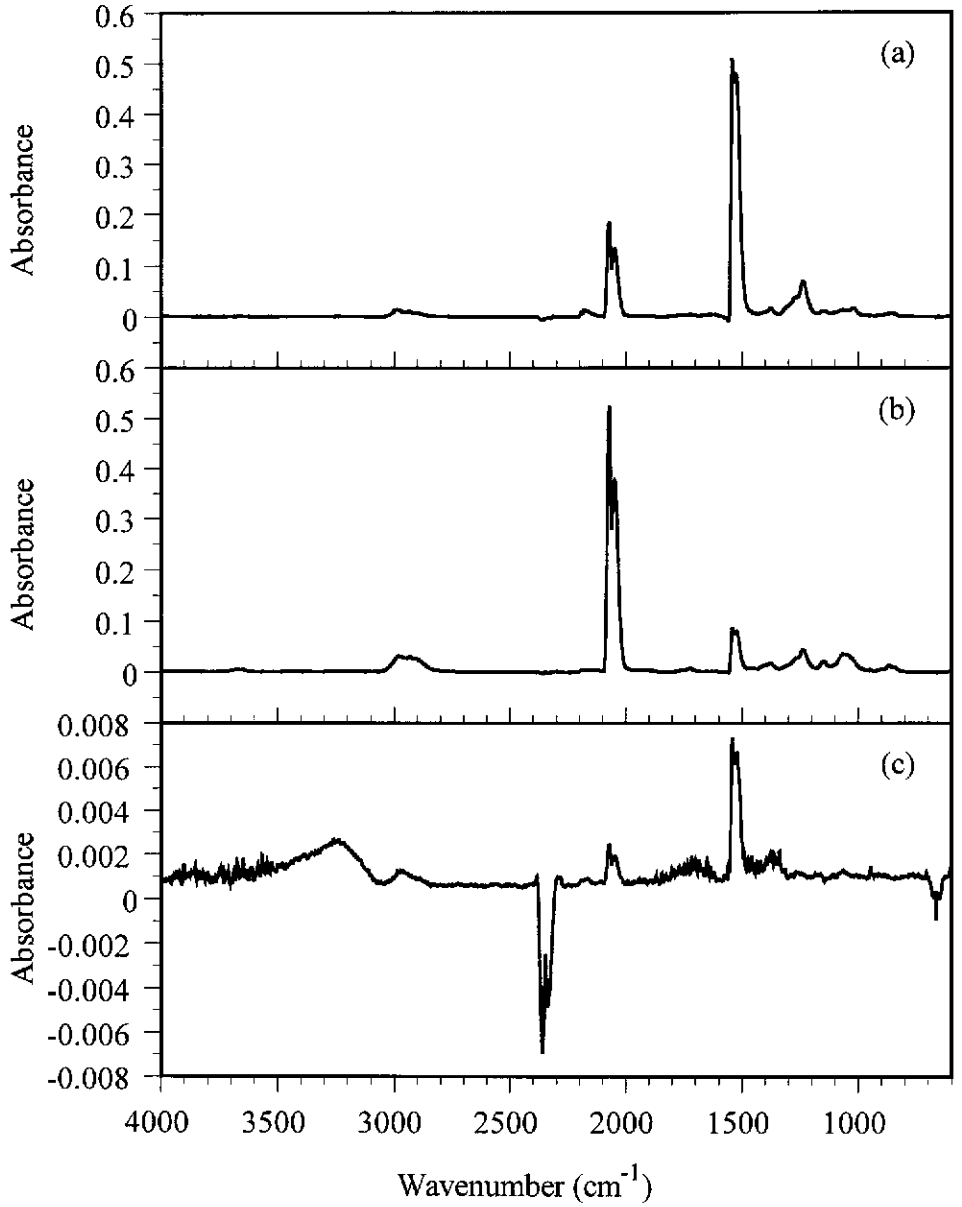

Figure 3.37: Infrared spectra of the gases evolved from PEX adsorbed on Haycarb, (a) first mass loss, (b) second mass loss, (c) third mass loss.

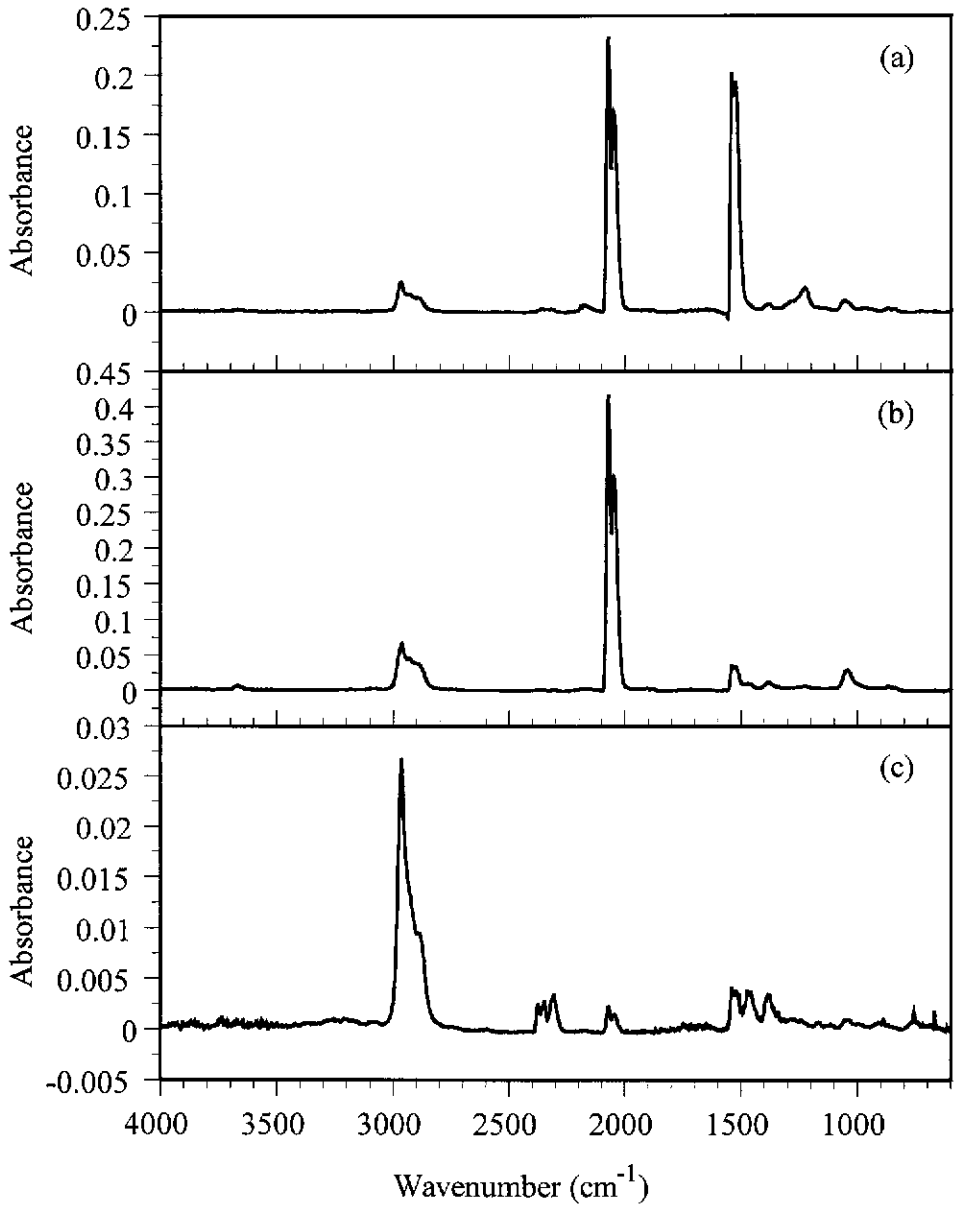

Figure 3.38: Infrared spectra of the gases evolved from PAX adsorbed on Haycarb, (a) first mass loss, (b) second mass loss, (c) third mass loss.

The most significant aspect of the first mass loss of the adsorbed SEX is the high carbon disulfide absorbance, which decreases to a moderate absorbance in the second mass loss, and to a minor absorbance in the third mass loss. The absorption band indicating alkyl compounds are present (3000-2800 cm^{-1}) is minor in the first mass loss, increases to a maximum in the second mass loss, and then disappears in the third mass loss. Carbonyl sulfide has a moderate absorption band in the first mass loss, this increased to become the highest absorption in the second mass loss, and decreased to a minor absorbance during the third mass loss. There was no carbonyl peak during the first mass loss, although it appeared as a very small peak during the second mass loss and there was no absorption in the third mass loss. In the first mass loss the spectra show that below 1400 cm^{-1} (due to various vibrations of alkyl and C-O containing compounds) most peaks are relatively strong and these decrease over the next two mass losses.

The absorption band due to carbon disulfide is also very high in the first mass loss of adsorbed SiBX, this decreases to almost nothing during the second mass loss, and further in the third mass loss. The 3000-2800 cm^{-1} absorption band is small during the first mass loss, this increases to a maximum during the second mass loss, and then decreases in the third mass loss. Carbonyl sulfide has a moderate absorbance in the first mass loss, increases to become the maximum absorption in the second mass loss, and then decreases in the third mass loss. No carbonyl peak was seen in any mass loss spectra. The peaks below 1400 cm^{-1} were very small in the first mass loss and these only increased slightly in the second mass loss, all but one peak disappeared in the third mass loss.

The mass loss spectra of the PEX displayed the same results as for the SEX analysis.

The absorbance of carbonyl sulfide and carbon disulfide were the highest in the first mass loss of PAX and they were approximately the same height. Carbonyl sulfide increased during the second mass loss while the carbon disulfide displayed a minor absorption band. Both were seen in the third mass loss as minor peaks. The alkyl 3000-2800 cm^{-1} band had a minor abundance in the first mass loss, this increased to a maximum in the second mass loss, and in the third mass loss it was the highest

absorption band within that spectrum. The absorption bands below 1400 cm^{-1} were minor for all three mass losses.

A comparison of Figures 3.35 to 3.38 shows that the spectra for each mass loss of each xanthate adsorbed on activated carbon are very similar. The spectra of the first mass losses showed high amounts of carbon disulfide and moderate amounts of carbonyl sulfide. During the second mass loss the spectra show the carbonyl sulfide is the dominant gas evolved while carbon disulfide has been reduced to a minor amount. The third mass loss spectra contained a diminished abundance of carbon disulfide and carbonyl sulfide as indicated by the low absorbance and that water bands from the background could be seen. The absorption bands of various other compounds were relatively low for each mass loss in comparison to the carbon disulfide and carbonyl sulfide absorption bands.

3.5 Hydrolysis of Alkali Xanthates

High amounts of carbon disulfide were observed during the first mass loss of the xanthates adsorbed on activated carbon and it was suspected that water had evolved as well. Thus it was proposed that hydrolysis of the xanthates could have had occurred. Under neutral to mildly alkaline conditions the following reaction occurs (Rao 1971; Crozier 1992).

$$6C_2H_5OCS_2^- + 3H_2O \rightarrow 6C_2H_5OH + 2CS_3^{2-} + 3CS_{2(g)} + CO_3^{2-}$$

The thiocarbonate may split up into sulfide and carbon disulfide. Although the reaction is slow at ambient temperatures, at elevated temperatures the rate of reaction is increased considerably (Rao 1971).

Activated carbon adsorbs water from aqueous solution. This was demonstrated by mixing a sample of activated carbon with water, air drying it, and analysing the sample by TG-MS and TG-FTIR. The thermal analysis data showed water was evolved at 20-130°C, with the majority boiling off at 100°C. Water continued to be evolved, together with carbon monoxide and carbon dioxide, although at a lesser

rate, above 130°C. Hence during adsorption of each xanthate onto the activated carbon, water was also adsorbed. As the sample was heated, water reacted with the xanthate according to previous equation. Previous investigators reported similar observations when adsorbing an organic from aqueous solution on activated carbon and analysing the sample by thermal analysis (Amicarelli, Baldassarre and Liberti 1979).

To demonstrate that water did hydrolyse the xanthates when adsorbed on activated carbon, they were mixed with varying amounts of water without the presence of activated carbon. SEX was mixed with water in w/w ratios of 16:1, 1:1, and 1:16. The TG curves for the various water/SEX mixtures are presented in Figure 3.39 and the spectra from each mass loss in Figure 3.40. The 16:1 w/w ratio is the stoichiometric ratio for the reaction indicated above. The other xanthates, SiBX, PEX, and PAX were only mixed with water in 1:1 w/w ratios. The experiments were performed using platinum crucibles and a lid with a pinhole, which provided a self-generated atmosphere of water vapor to react with the xanthates.

All the TG curves for the SEX-water ratios, except the 1:16 ratio, had four mass losses. A comparison of the SEX-water TG curves to the water TG curve indicates the first mass loss was due to water. A comparison with the TG curve for the SEX indicates the third and fourth mass losses were due to the two thermal decomposition reactions of the SEX. These observations are supported by the spectra of the gases shown in Figure 3.40. However, the second mass loss product(s) could only be determined by observing the infrared spectrum of Figure 3.40(b), which shows carbon disulfide was formed, which was attributed to the hydrolysis of SEX. From these experiments it is evident that the presence of water will cause carbon disulfide to evolve before the thermal decomposition of the SEX.

Figure 3.40(b) also shows an alkyl band at 3000-2800 cm^{-1} and a carbonyl band at approximately 1050 cm^{-1}. This can be attributed to ethanol, which was formed during the hydrolysis of SEX.

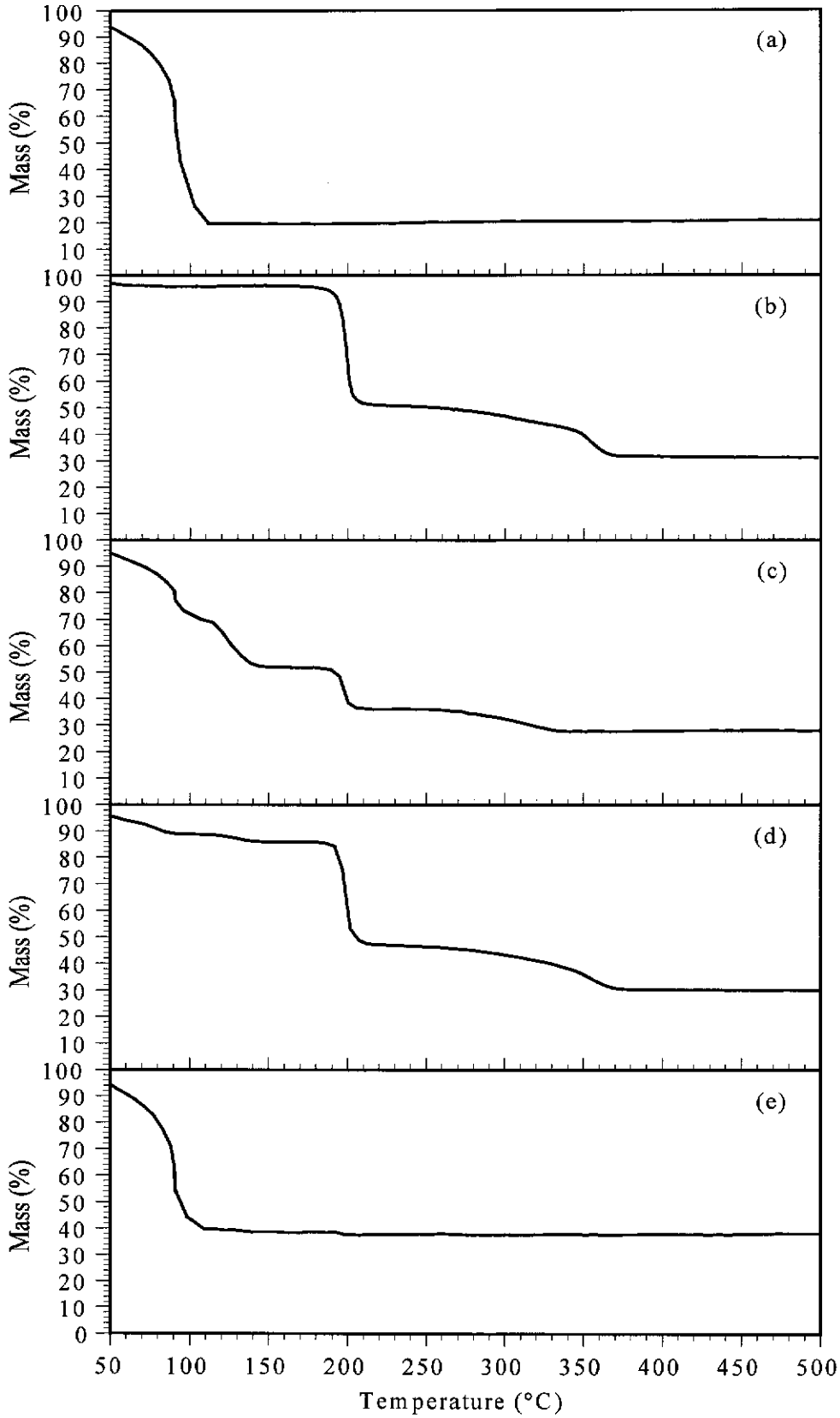

Figure 3.39: TG curves of, (a) water, (b) SEX, (c) ratio 1:1, (d) ratio 16:1, and (e) ratio 1:16 (SEX:water). Heated at 10°C min^{-1} in argon.

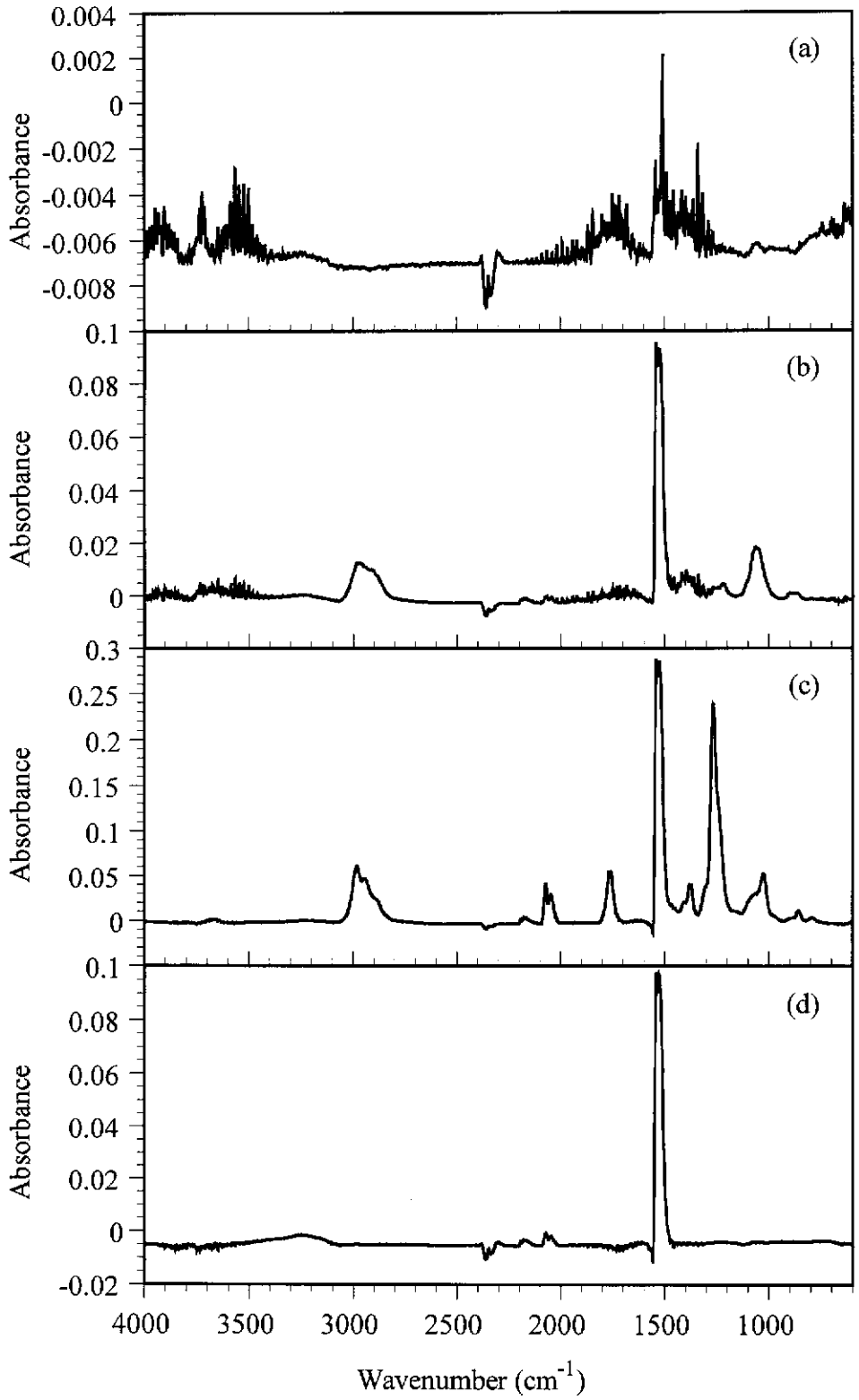

Figure 3.40: FTIR spectra of the gases evolved from the mass losses of the 1:1 SEX:water mixture displayed in Figure 3.39. (a) first mass loss, (b) second mass loss, (c) third mass loss, and (d) fourth mass loss.

Table 3.11 shows the temperature ranges at which mass losses occurred for the various TG curves of Figure 3.39. It is apparent that as the ratio of water to SEX increases, the SEX is increasingly hydrolysed and the total mass loss above 200°C decreases from 65.2 % to 1.4 %. This data supports the suggestion that when SEX is adsorbed onto activated carbon, the first reaction is mostly due to the hydrolysis of SEX, followed by the thermal decomposition of any unreacted SEX.

	Mass Loss (%)			
	50-104°C	**104-136°C**	**200°C**	**225-368°C**
Water	72.0	No mass loss	No mass loss	No mass loss
SEX	No mass loss	No mass loss	42.9	22.3
16:1 SEX-Water	4.3	2.6	37.9	17.2
1:1 SEX-Water	23.0	18.0	16.0	7.8
1:16 SEX-Water	55.1	0.9	1.4	No mass loss detected

Table 3.11: Mass losses of the TG curves in Figure 3.39.

The TG curves of the 1:1 xanthate-water ratios of SiBX, PEX, and PAX are presented in Figure 3.41. The spectra from the mass losses are not presented, as they are similar to that of Figure 3.39, except the last two mass losses of each system, which are due to the thermal decomposition of each xanthate. A comparison of each 1:1 xanthate:water system is presented in Table 3.12.

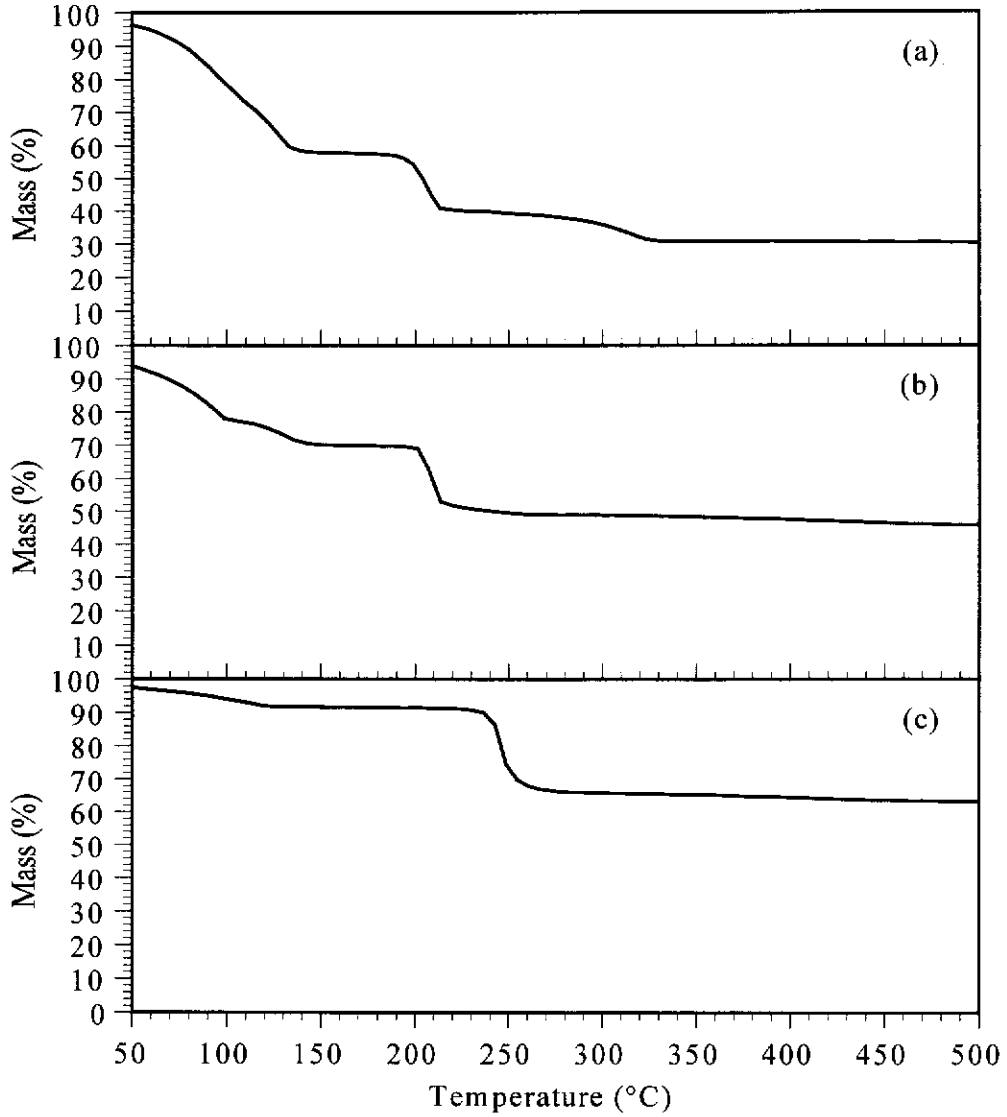

Figure 3.41: Mass loss curves of 1:1 w/w ratios of (a) SiBX, (b) PEX and (c) PAX to water.

	Mass Loss (%)			
	Water	**CS_2**	**1st Thermal Decomposition**	**2nd Thermal Decomposition**
SEX	23.0	18.0	16.0	7.8
SiBX	23.2	16.3	17.6	9.0
PEX	17.6	7.5	20.8	3.1
PAX	3.8	2.2	25.6	2.5

Table 3.12: A comparison of each 1:1 w/w ratio xanthate:water TG curve mass losses.

From examination of Table 3.12 it is evident that hydrolysis of the xanthates is dependent on the cation type and the chain length. The sodium xanthates had a far higher mass loss attributed to hydrolysis than the potassium xanthates. The hydrolysis mass losses also decreased as the chain length of the xanthate increased.

Unfortunately the experiments performed by mixing the xanthates with water did not prove that hydrolysis was a reaction that occurred when xanthates are adsorbed on activated carbon. The most obvious way to prove, without doubt, that hydrolysis did occur was to analyse SEX adsorbed onto activated carbon without the presence of water. To do this several different experiments were performed.

The first set of experiments involved adsorbing SEX onto activated carbon in the presence of dried aprotic solvents. The purpose of these experiments was to adsorb SEX without water adsorption. The solvents used were dimethylformamide (DMF), acetonitrile and nitromethane. In all systems very little SEX was adsorbed unless saturated solutions were used. However, all the solvents adsorbed in greater amounts, thus competing with the SEX molecules for adsorption sites and in far greater amounts than the water molecules. The thermal analysis data showed that the solvents decomposed or boiled off in the same temperature range as SEX adsorbed on activated carbon. This obscured the adsorbed xanthate reaction temperature region.

The second set of experiments consisted of adsorbing the SEX and PEX onto known adsorbents using water as a solvent. The purpose of these experiments was to determine if the mechanisms of adsorption (no matter what the absorbent) altered the thermal decomposition of xanthates (without water present). Attapulgite (a compound used for adsorbing chemical spills) and activated silica were used. Very little SEX was adsorbed on the attapulgite, but activated silica was a good adsorbent for PEX. The TG-FTIR of the PEX-activated silica system contained a high abundance of carbon disulfide indicating hydrolysis was occurring (very little carbon disulfide is present in the thermal decomposition of pure PEX). PEX was also adsorbed onto charred coconut shell and graphite. Both thermal analysis infrared spectra showed large amounts of carbon disulfide evolving.

The third set of experiments involved mixing SEX separately with activated silica, attapulgite, and activated carbon. In the case of the silica and attapulgite no difference in the decomposition was observed compared to that of the pure SEX. However a difference was observed when the SEX was mixed with activated carbon. The SEX was mixed with wet and dry activated carbon. The wet sample was made by mixing activated carbon with water and left to air dry. The dry sample was made by drying activated carbon for 24 hours at 150°C. The thermal analysis data from the mixture of SEX and wet carbon was similar to that observed when SEX is adsorbed on the activated carbon. The mixture of SEX with the dry carbon showed minor evidence of hydrolysis, but now the thermal decomposition was the major reaction.

Although none of these experiments proved the hydrolysis theory alone, when combined they suggest that the carbon disulfide evolved in the first mass loss of each xanthate adsorbed on activated carbon must be due to xanthate hydrolysis.

3.6 Surface Analysis of SEX Adsorbed on Activated Carbon

A study of the surface of the activated carbon with and without adsorbed SEX was performed in an attempt to determine the bonding interactions between the carbon and xanthate. Most surface studies of activated carbon and similar compounds have been performed using diffuse reflectance infrared Fourier transform (DRIFT) spectroscopy (Boehm 1994).

There are a number of ways in which xanthate molecule may chemically adsorb on the activated carbon surface. The adsorption is mainly dependent on the amount of acidic surface oxides (such as carboxyl groups) and the presence of metal ions on the surface. Adsorption of the non-polar end of the xanthate molecule would be preferential if there are very few acidic surface oxides. Preferential adsorption of the polar end of the molecule would occur if there was an abundance of acidic surface oxides. The presence of metal ions would attract the areas on the molecule with excess localized electrons, such as the lone pairs of electrons on the oxygen and double bonded sulfur atoms (Cookson 1978).

DRIFT spectra were obtained for SEX, activated carbon, SEX adsorbed on activated carbon (ground and unground), and SEX mixed with activated carbon. The SEX-activated carbon sample was ground so that the internal surface area could be exposed (Hyun Park et al 1997). The SEX was mixed with activated carbon in the same ratio as the adsorbed SEX.

While the DRIFT spectra of the SEX and the SEX mixed with activated carbon were featureless with many peaks, the spectra of the other samples were not. The results were inconclusive and could not be used to determine if the SEX was physically or chemically adsorbed, and how the molecule was oriented on the surface.

3.7 Summary

The thermal decomposition of a xanthate occurred in two steps, with mass losses in the temperature range 190-500°C. Two of the major gases evolved were carbon disulfide and carbonyl sulfide. When xanthates were absorbed on activated carbon, the thermal decomposition showed both two major and one minor mass losses, but these occurred in the temperature ranges 140-230°C and 210-290°C. The first mass loss was not due to the effect of the absorption process, however, but rather to the hydrolysis reaction between water absorbed in the carbon and the xanthate. This reaction accounted for the new low temperature mass loss, and carbon disulfide was the major gaseous product.

After the initial mass loss due to the hydrolysis reaction for the xanthates adsorbed on activated carbon, another mass loss of similar size occurred. During this mass loss the evolution of carbonyl sulfide dominated. This could only be due to the thermal decomposition of any remaining xanthate.

The third mass loss due to the xanthates adsorbed on activated carbon was minor and as the FTIR spectra show, minor amounts of carbonyl sulfide and carbon disulfide evolved. This mass loss is in approximately the same temperature range as the second mass loss for the non-adsorbed xanthates and the same gases evolve. Therefore it is proposed the third mass loss of the xanthates adsorbed on activated

carbon is due to decomposition of any residual xanthate (similar to that of the non-adsorbed xanthates).

Comparison of the TD-py-GC-MS results (see Tables 3.2 and 3.7) of the xanthates and adsorbed xanthates showed that whilst not many different gases were detected between the two systems, the distribution of gases was significantly different. For example in the analysis of SEX, carbon disulfide was the most abundant gas; while in the analysis of the SEX-AC sample, carbonothioic acid, O,S, diethyl ester was the most abundant gas. There is no clear reason for the differences except that the adsorption on activated carbon does play some role in the relative abundance of products from the pyrolysis of absorbed xanthates.

Two of the most significant gases evolved from all reactions were carbon disulfide and carbonyl sulfide. Therefore the evolution of these two gases from industrial plant samples of activated carbon at these temperatures would indicate the presence of xanthate fouling.

Analysis of the xanthates absorbed and not absorbed on activated carbon by the various techniques showed there were some differences between the type and amount of decomposition products for the same sample. Comparison of the relative peak areas (%) of gases evolved from the thermal decomposition of the xanthates by TD-py-GC-MS and TG-MS are presented in Table 3.13. The data for each gas is only semi-quantitative for both techniques due to the differences in efficiencies of ionisation of the gases. However, it is possible to compare the quantity of gases detected for the same compound between the two techniques, since clearly the ionisation efficiencies are the same (ignoring overlapping of fragment and isotope ion signals). Unfortunately it was not possible to determine if different gases evolved between the techniques, as the TG-MS data collection was dependent on the results of the TD-py-GC-MS analyses. Also it is not possible to compare the data from TD-py-GC-MS and TG-MS to the TG-FTIR data, as the FTIR method was qualitative only.

	Relative Peak Areas (%)		Gas
	TD-py-GC-MS	TG-MS	
SEX	3.0	7.21	carbonyl sulfide
	3.9	18.2	ethanethiol
	19.1	66.4	carbon disulfide
	16.2	4.88	ethanol
	6.0	2.03	diethyl sulfide
	18.4	0.29	diethyl carbonate
	13.0	0.31	diethyl disulfide
	12.1	0.41	carbonothioic acid, O,S, diethyl ester
	8.7	0.28	carbonodithioic acid O,S, diethyl ester
SiBX	1.5	26.9	carbonyl sulfide
	8.0	71.2	carbon disulfide
	17.1	1.10	isobutanol
	1.7	0.23	butanethiol
	14.1	0.19	di-isobutyl carbonate
	51.5	0.37	carbonothioic acid, O,S, dibutyl ester
	6.2	0	dibutyl disulfide
PEX	6.7	58.4	carbonyl sulfide
	5.1	20.3	ethanethiol
	9.4	6.41	carbon disulfide
	35.5	13.4	diethyl sulfide
	1.4	0.33	ethyl isopropyl sulfide
	26.6	0.67	diethyl disulfide
	6.8	0.25	carbonothioic acid, O,S, diethyl ester
	8.6	0.24	carbonodithioic acid O,S, diethyl ester
PAX	1.3	43.5	carbonyl sulfide
	3.4	46.1	carbon disulfide
	9.4	2.32	isobutanol
	9.3	1.91	isoamyl alcohol
	3.5	1.07	unidentified (132 g mol^{-1})
	2.7	0.94	di-isobutyl sulfide
	2.8		3-methyl butyl propyl sulfide
	6.4	1.00	di-isobutyl carbonate
	26.2		di-isopentyl sulfide
	11.1	1.10	unidentified (160 g mol^{-1})
	3.00	1.25	carbonothioic acid, O,S, dibutyl ester
	6.0	0	di-isopentyl carbonate
	3.3	0	isobutyl 3-methyl butyl disulfide
	4.1	0	unidentified (204 g mol^{-1})
	4.5	0	di-isopentyl disulfide
	3.0	0.72	unidentified (260 g mol^{-1})

Table 3.13: Comparison of the relative peak area (%) of gases evolved from the thermal decomposition of the xanthates by TD-py-GC-MS and TG-MS.

The main difference between the relative peak areas of the gases is that a greater amount of higher molecular weight gases is observed in the TD-py-GC-MS analyses than in the TG-MS. For example, in the TD-py-GC-MS analysis of SEX, the higher molecular weight gases diethyl sulfide, diethyl carbonate, and diethyl disulfide contribute 43.5 % of all the gases evolved; while in the TG-MS analysis these gases only contribute to 1.01 %. Also in the TD-py-GC-MS analysis of SEX the lower molecular weight gases carbonyl sulfide, ethanethiol, carbon disulfide, and ethanol contribute to 42.2 % of all gases evolved; while in the TG-MS analysis these gases contribute to 96.69 %.

The abundance of higher molecular weight gases in the TD-py-GC-MS analyses can be explained by the cold trapping of the gases evolved after pyrolysis and before heating for separation by the GC and then detection by the MS. That is, there is a stage where all the evolved gases are mixed together in the liquid state, and have sufficient time to react with one another. In the TG-MS, there is very little time for the higher molecular weight gases to form as they are flushed straight onto the MS from the TG without condensation.

These statements are also backed up by the proposed formation of the higher molecular weight gases as presented in Figure 3.6. That is, the higher molecular weight gases are most likely formed from the reactions of carbonyl sulfide, ethanethiol, carbon disulfide, and ethanol.

Similar observations for the comparison of the evolved gas relative peak areas for the analysis of the xanthates adsorbed on activated carbon by TD-py-GC-MS and TG-MS were made.

CHAPTER 4

THERMAL DECOMPOSITION OF FROTHING AGENTS

4.0 Introduction

Frothing agents are divided into two categories, those that are completely soluble in water and those that are partially soluble. Completely soluble frothing agents include polyglycol ethers and polyglycol glycerol ethers. Those frothing agents which are partially soluble include aliphatic alcohols (C_6 to C_8), natural oils, cresylic acids, and alkoxy paraffins (Crozier 1992).

Polyglycol ethers are also referred to as polyglycols, polyoxyalkylene glycols, and polyalkylene glycol ethers (of which the last is the most accurate term). First developed for use as frothing agents between 1952 to 1954 (Crozier 1992), polyalkylene glycol ethers are also used as heavy duty lubricants, and in the manufacture of paper, leather, and emulsifiers (Snell and Ettre 1971).

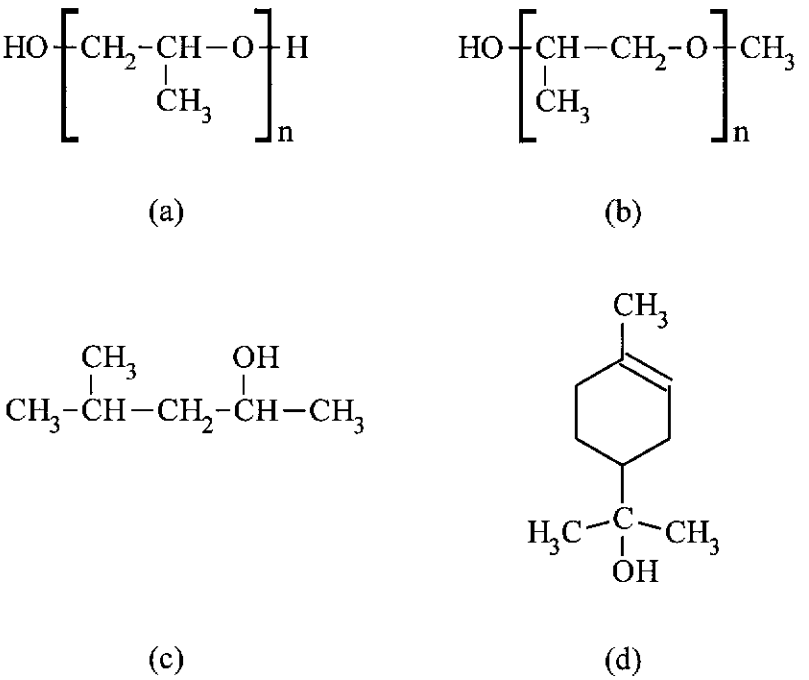

Figure 4.1: Molecular structures of some common frothing agents, (a) PPG, (b) PPGME, (c) α-terpineol, and (d) MiBC.

Polypropylene glycol (PPG) is the most common polyalkylene glycol ether, and is available in a wide range of molecular weights (Crozier 1992). Shown in Figure 4.1(a) is the molecular structure of PPG. PPG is produced by the addition of

propylene oxide to water and propylene glycol in the presence of a caustic catalyst (Snell and Ettre 1971). Another common frothing agent that is similar to PPG is polypropylene glycol methyl ether (PPGME), and its molecular structure is also presented in Figure 4.1(b). There appears to be very little information on this compound in the literature.

The PPG used in this work has an average molecular weight of 425 g mol^{-1}. The thermal decomposition of PPG has been studied by Vo Van, Malhotra and Blanchard (1974a) using differential scanning calorimetry in a nitrogen atmosphere. From this work the maximum rate of thermal decomposition occurs at approximately 300°C. In another paper (Vo Van, Malhotra and Blanchard 1974b), the rate of thermal decomposition of a range of different molecular weight PPG's was studied, and two pathways of decomposition were proposed based on the results. It was suggested that for one pathway, the molecular chains dissociate then this is followed by decomposition of the dissociated fragments to produce volatile substances associated with a rapid mass loss. For the pathway, it was suggested that reactants in the liquid state decompose into lower molecular weight liquids plus gases, followed by another stage producing even lower molecular weight liquids plus greater quantities of gases, until all the PPG was volatised. This is known as stepwise depolymerisation. Although these reaction pathways were proposed, there was no detailed mechanism given indicating the points in the polymer chain where dissociation was initiated.

In general, polymers like PPG and PPGME degrade by one or by a combination of three primary mechanisms. These primary mechanisms are random scission, depolymerisation (also known as unzipping), and degradation of weak links (thermally labile defects). There are also other mechanisms that may occur such as intramolecular cyclisations and eliminations, side group scission, intermolecular cross-linking, and radical chain transfer reactions (Chartoff 1997).

Random scission, as the name suggests, is where all bonds within a polymer have an equal chance of being broken at any stage of degradation. Examples of this type include the degradation of polyethylene and polyethylene terephthalate. Depolymerisation is the process of a polymer breaking down into its monomeric units. This commences at a chain end and successive monomer units are produced.

This type of degradation is characteristic of many hydrocarbon chain and heterochain polymers. When a polymer has weak links (such as C-O bonds), the weak links are usually the place where thermal degradation is initiated (Chartoff 1997).

A polymer similar to PPG is polyethylene glycol (PEG), which has been studied by pyrolysis-gas chromatography-mass spectrometry (py-GC-MS) for molecular weights 8000, 16000, and 20000 (Voorhees, Baugh and Stevenson 1994). The pyrolysis products reported included PEG of various chain lengths, dichloromethane, furan, dioxolanes, dioxane, aldehydes, and ethers. From the pyrolysis products a mechanism was proposed which is shown in Figure 4.2. The mechanism indicates that decomposition starts by homolytic cleavage of C-C or C-O bonds, followed via disproportionation and hydrogen abstraction reactions (Voorhees, Baugh and Stevenson 1994).

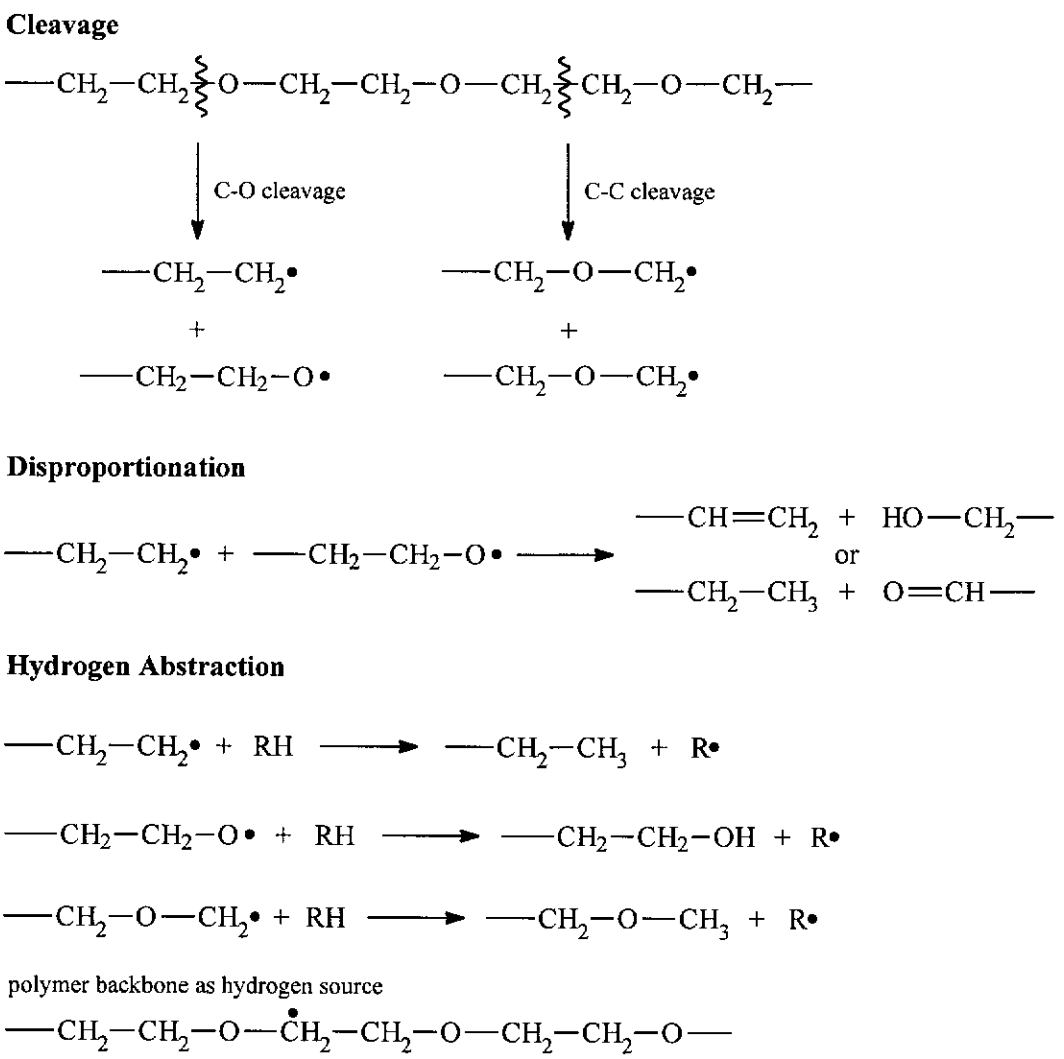

Figure 4.2: Thermal degradation mechanism of PEG.

Pine oil is the most common natural oil used as a frothing agent. The chief ingredient of pine oil is α-terpineol. The molecular structure of α-terpineol is presented in Figure 4.1(c) and it has a boiling point of 219°C (Crozier 1992).

Of all the frothing agents available, the aliphatic alcohol methyl isobutyl carbinol (MiBC), is used in the greatest quantity. MiBC is also referred to as 4-methyl-2-pentanol (IUPAC name) and methyl amyl alcohol. Its molecular structure is presented in Figure 4.1(d). From the literature MiBC boils at 132°C (Crozier 1992).

In this chapter the results of the thermal decomposition of the four frothing agents described above are reported. The thermal decomposition of each frothing agent adsorbed on activated carbon is also reported. Studies were performed using the same techniques described in Chapter 3.

4.1 TD-py-GC-MS Analysis of the Frothing Agents

Because the frothing agents are liquids they were adsorbed on sodium sulfate (approximately 10 % w/w) prior to analysis in order to facilitate sample handling in the pyrolysis unit. Samples were heated from 150-500°C at 25°C min^{-1}.

Presented in Figures 4.3 and 4.4 are the total ion chromatograms for the pyrolysis of PPG and PPGME. The ion chromatograms show similar characteristics, with the initial carbon dioxide peak followed by a series of peaks that differ by a constant molecular weight. Hence the interpretation of the ion chromatograms is that the peaks are due to PPG or PPGME of differing chain length (where n equals the number of repeating monomer units) boiling off from the mixture. The peaks within each group are due to the various isomers of that particular PPG or PPGME. The molecular weights of PPG detected were 134, 192, 250, 308, 366, 424, 482, 540, and 598 g mol^{-1} for n equal to 2 through to 10 respectively; and for PPGME 148, 206, 264, 322, 380, 438, and 496 g mol^{-1} for n equal to 2 through to 8 respectively.

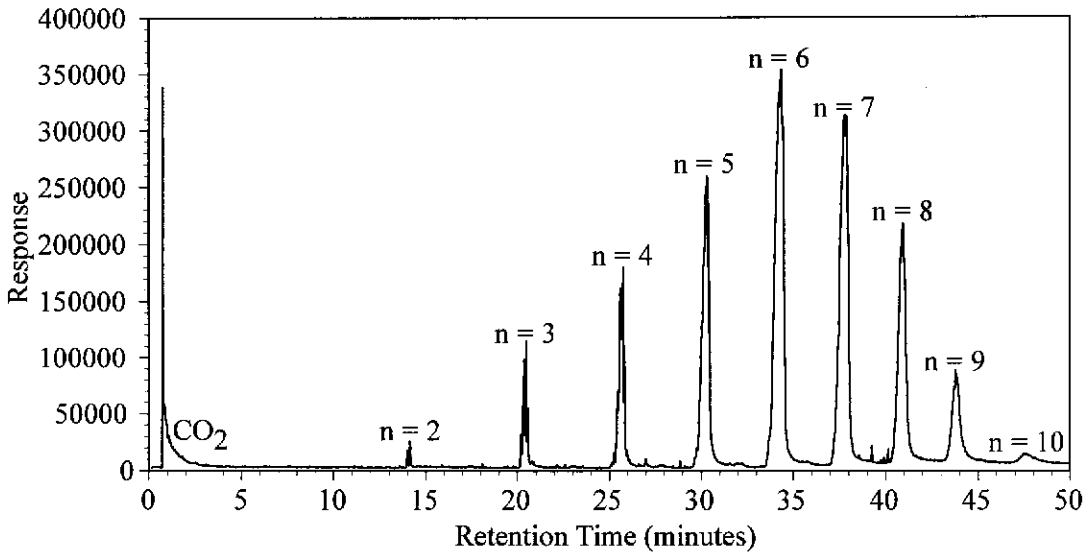

Figure 4.3: TD-py-GC-MS total ion chromatogram of PPG heated at 25°C min^{-1} in an inert atmosphere.

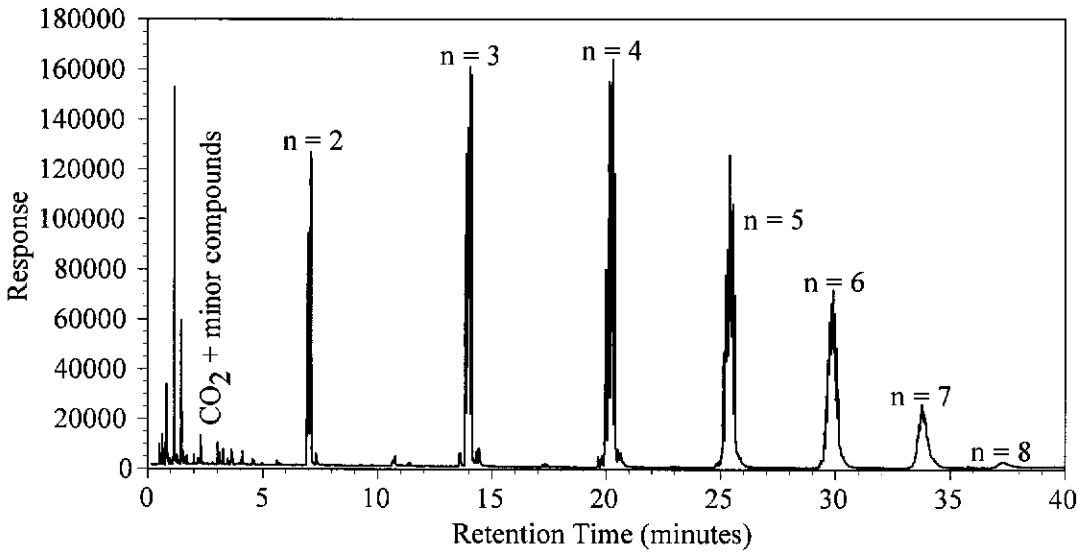

Figure 4.4: TD-py-GC-MS total ion chromatogram of PPGME heated at 25°C min^{-1} in an inert atmosphere.

It is difficult to determine if thermal degradation of any higher molecular weight PPG/PPGME compounds to lower molecular weight polymers occurred during the pyrolysis. The relative peak area (%) of each peak was multiplied by its molecular weight, and then this sum was averaged for all the peaks. An average molecular weight of 390 g mol^{-1} was calculated for PPG, and 292 g mol^{-1} PPGME. Although

the result for PPG is close to the expected value of 425 g mol^{-1}, it is slightly lower indicating that some minor thermal degradation of the PPG may have occurred. This is supported by Vo Van et al (1974), who proposed PPG might decompose into lower molecular weight liquids plus some gases, followed by further decomposition into lower molecular weight liquids plus gases, and so on. The manufacturers given value for PPGME is 250 g mol^{-1}, which is lower than the experimentally determined value. Degradation is thus unlikely to have taken place.

Presented in Figure 4.5 is the total ion chromatogram of the α-terpineol pyrolysis. Apart from background peaks, there were 7 peaks detected. The identity, retention time, and relative peak area of the gases evolved is presented in Table 4.1.

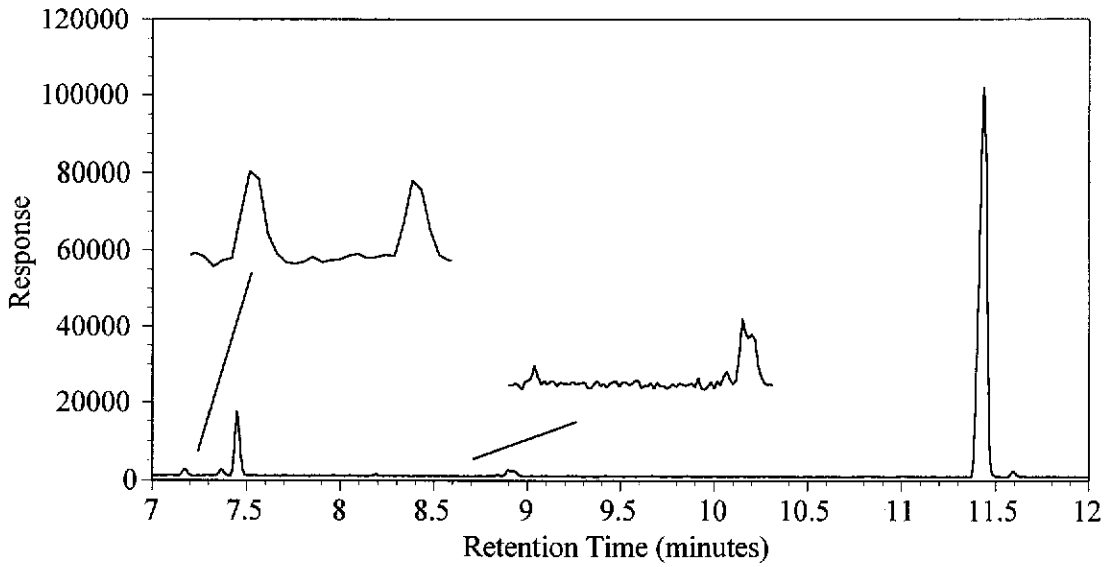

Figure 4.5: TD-py-GC-MS total ion chromatogram of α-terpineol heated at 25°C min^{-1} in an inert atmosphere.

The main gas evolved was α-terpineol along with some limonene (the dehydration product of α-terpineol). Other gases of similar structure to α-terpineol also evolved in minor quantities.

RT	Relative Peak Area (%)	Gas Evolved
7.17	1.84	α-terpinene
7.36	1.75	σ-isopropyltoluene
7.45	9.37	limonene
8.19	0.98	3-carene
8.90	3.37	isoterpinolene
11.44	80.8	α-terpineol
11.59	1.91	α-terpinyl acetate

Table 4.1: Pyrolysis gases of α-terpineol heated from 150 to 500 °C at 25°C min^{-1} in an inert atmosphere.

The total ion chromatogram of the MiBC TD-py-GC-MS analysis displayed only one peak due to the evolution of MiBC. Thus MiBC simply boils off and no chromatogram is presented here.

Hence of the four frothing agents examined, three boiled off apparently unchanged. Pine oil was the only compound that showed any thermal degradation on heating, consisting of 10 % degradation due to dehydration of the parent compound, and another 10 % from some other minor decomposition compounds.

4.2 Thermogravimetry - Evolved Gas Analysis of Frothing Agents

The thermal decomposition the four frothing agents were each studied by TG-EGA, at a heating rate of 10°C min^{-1} under an argon atmosphere. The evolved gases were analysed by MS and FTIR spectroscopy. The TG curve of each frothing agent consisted of one broad mass loss. The mass losses and their corresponding extrapolated onset/offset temperatures are presented in Table 4.2.

	Frothing Agent			
	PPG	PPGME	α-terpineol	MiBC
Mass Loss (%)	94.6	94.9	96.7	36.6
Temperature (°C)	249-338	144-292	171-198	85-112

Table 4.2: Mass losses and their corresponding temperatures of PPG, PPGME, α-terpineol, and MiBC heated at 10°C min^{-1} in argon atmospheres.

The maximum rate of mass loss for PPG, PPGME, and α-terpineol occurred at 315, 226, and 171°C respectively. All the frothing agents left no residue in the sample crucible after analysis, indicating all had boiled off. The low percentage of MiBC and the actual TG curve showed that it started evaporating before the analysis had started. The TG curves of the PPG, PPGME, α-terpineol, and MiBC along with the MS and FTIR GS curves are presented in Figures 4.6 to 4.9 respectively.

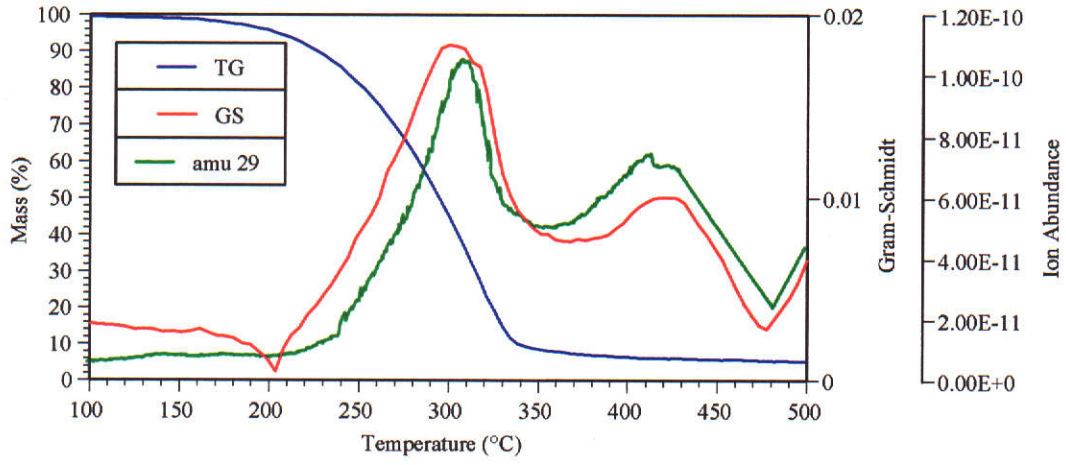

Figure 4.6: TG-GS-MS curves for PPG heated from ambient to 500°C at 10°C min^{-1} in an argon atmosphere.

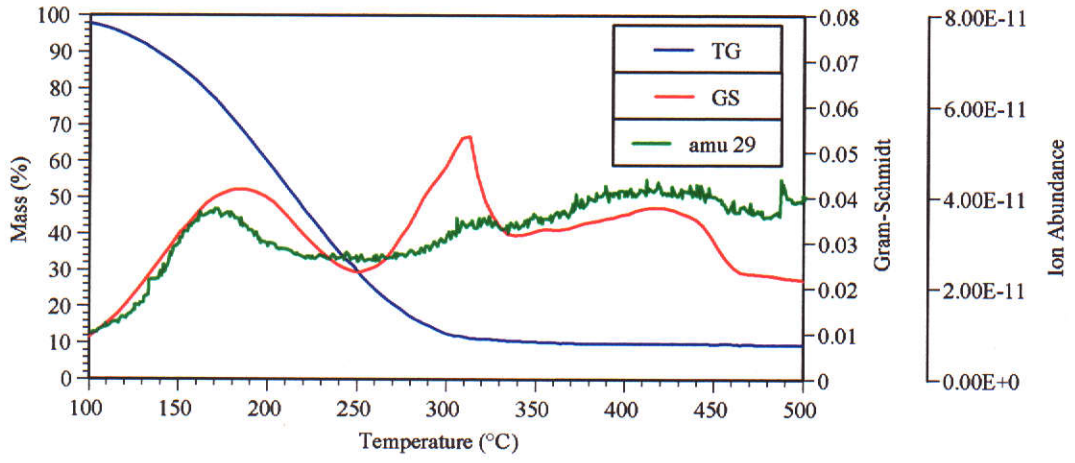

Figure 4.7: TG-GS-MS curves for PPGME heated from ambient to 500°C at 10°C min^{-1} in an argon atmosphere.

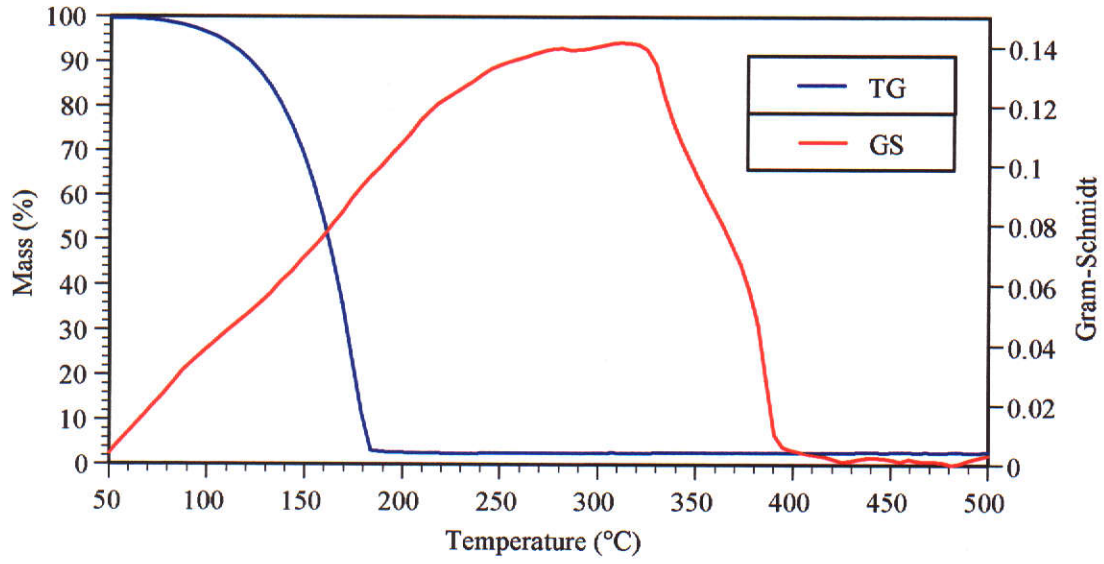

Figure 4.8: TG-GS curves for α-terpineol heated from ambient to 500°C at 10°C min^{-1} in an argon atmosphere.

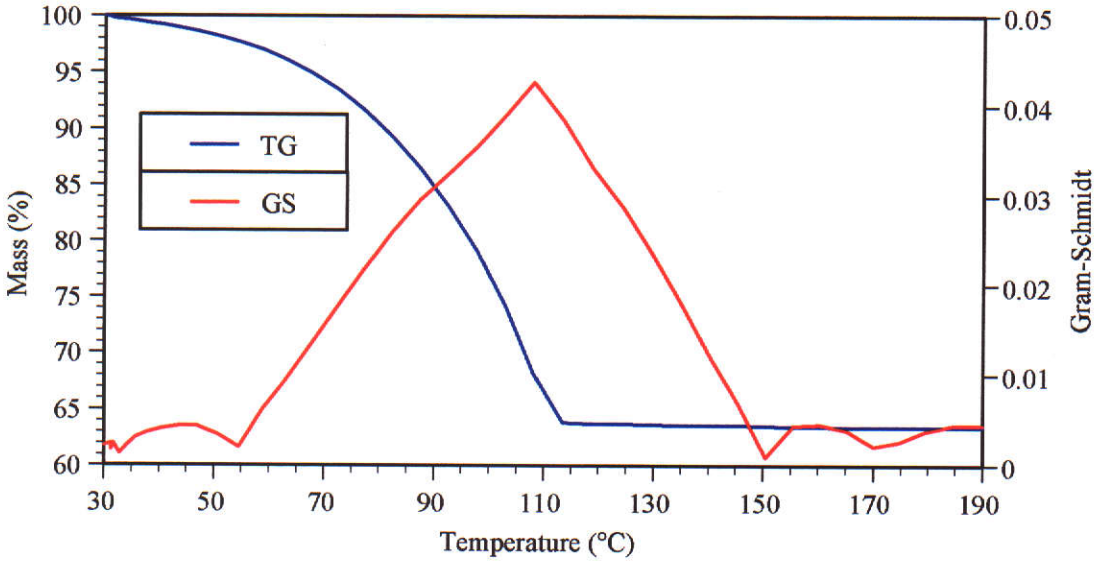

Figure 4.9: TG-GS curves for MiBC heated from ambient to 200°C at 10°C min^{-1} in an argon atmosphere.

All of the four GS profiles extended beyond the temperature range of the mass losses, and for PPG and PPGME appeared as more than one peak in the GS curve. The ion chromatograms of amu 29 from the SIM analysis of PPG and PPGME are presented in Figures 4.6 and 4.7, and these peaks also extend beyond the end of the mass loss. All of the other ions monitored in this manner displayed similar curves to

amu 29 and are not shown here. These observations could be explained by the volatile material condensing in the MS transfer line, where they would evolve as a function of time, not temperature. This could not be avoided, as the transfer line was operated at the maximum temperature of 200°C, which was clearly insufficient to volatilise the higher molecular weight components.

4.2.1 MS Analysis of the Evolved Gases

The scan mode (SM) mass spectra of the PPG and PPGME volatiles displayed very few peaks, and the highest amu detected was 59 and 73. However, the thermal desorption data indicated a lot more peaks should have been present in the mass spectra. That is, there should have been peaks due to molecular ions at 134, 192, and 250 amu for the PPG decomposition and peaks due to molecular ions at 148, 206, and 264 amu for the PPGME decomposition. There should also have been numerous fragment peaks above 59 and 73 amu respectively. Again this effect was due to the lack of higher molecular weight gases present due to the condensation that took place in the transfer line.

The SM mass spectra of α-terpineol and MiBC were simple and they matched their respective reference spectra. Thus SIM analyses were not required and no ion chromatograms are displayed in Figures 4.8 and 4.9.

4.2.2 FTIR Spectroscopy Analysis of the Evolved Gases

The GS chromatogram of PPG and PPGME shown in Figures 4.6 and 4.7 are very similar to their MS ion chromatograms displayed in the same figures. Thus the PPG and PPGME volatiles also condensed in the FTIR transfer line. To confirm this the background spectrum of the FTIR cell was recorded over several hours. Each background spectrum displayed characteristic PPG or PPGME peaks. Also upon dismantling the FTIR transfer line and inspecting the inner tubing, liquid drops were seen which could only be PPG or PPGME volatiles.

The infrared spectrum of the gases evolved from the PPG mass loss is shown in Figure 4.10. The infrared spectrum displayed all the characteristic peaks of the PPG

in the liquid state. The only difference was the O-H stretch, which exists as a broad peak in the liquid state (around 3600-3200 cm^{-1}) and as a small sharp peak in the gaseous state (around 3600 cm^{-1}).

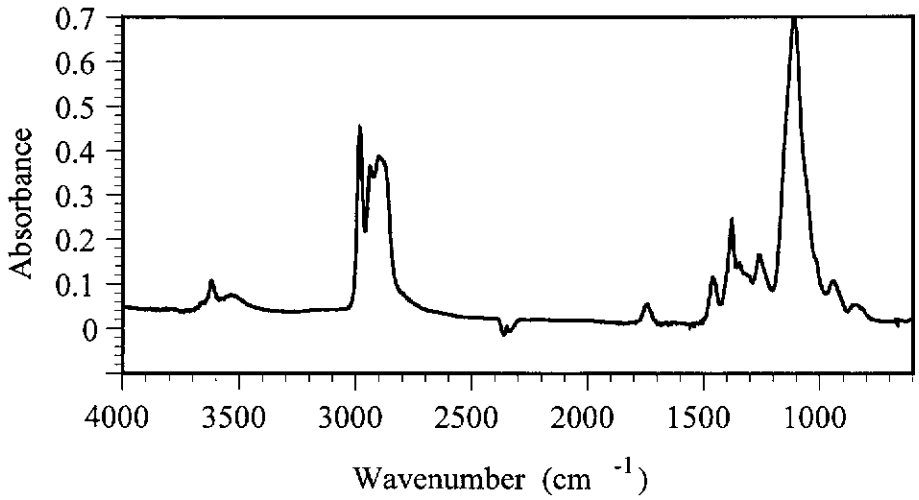

Figure 4.10: Infrared spectrum of the gases evolved from the PPG mass loss at 315°C.

The infrared spectrum from the PPGME mass loss is shown in Figure 4.11. The infrared spectrum displayed all the characteristic peaks of the PPGME in the liquid state, except that the O-H stretch was a small sharp peak.

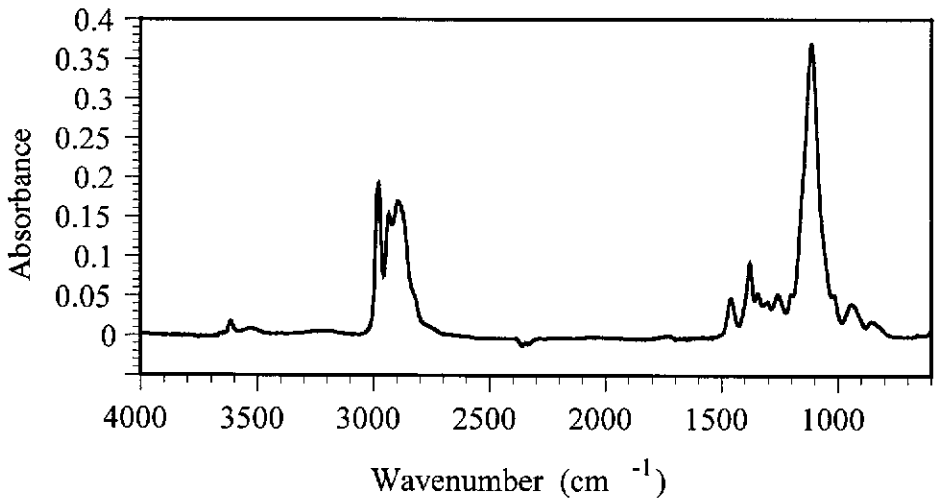

Figure 4.11: Infrared spectrum of the gases evolved from the PPGME mass loss at 226°C.

The GS chromatogram of α-terpineol shown in Figure 4.8 has a large broad peak coinciding with the TG curve, as expected. The infrared spectrum of the gases evolved from the mass loss is shown in Figure 4.12 and it displays all the characteristic peaks of the reference α-terpineol spectrum. Peaks due to limonene (as identified by the TD-py-GC-MS analysis), such as alkene C-H stretching, were not found in the infrared spectrum.

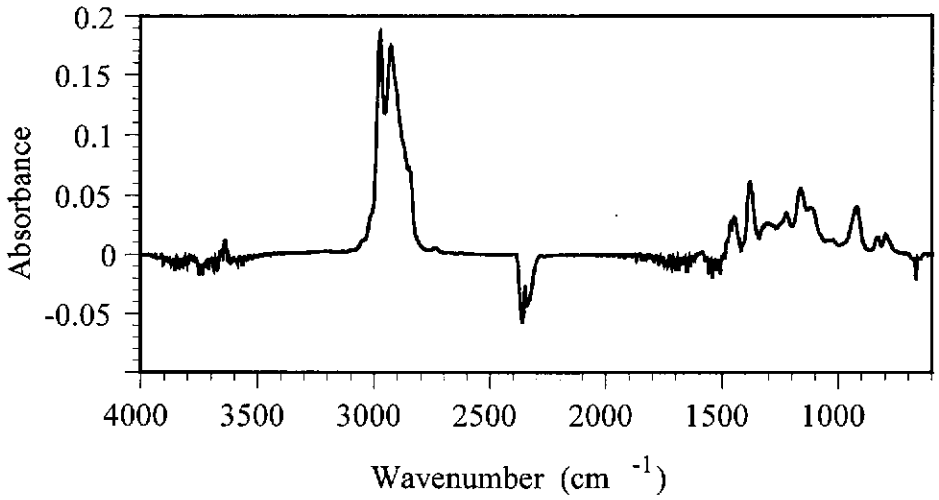

Figure 4.12: Infrared spectrum of the gases evolved from the α-terpineol mass loss at 171°C.

The GS chromatogram of MiBC shown in Figure 4.9 has a large broad peak slightly offset with the TG curve. The infrared spectrum of the gases evolved from the mass loss is shown in Figure 4.13 and it displays all the characteristic peaks of the reference MiBC spectrum.

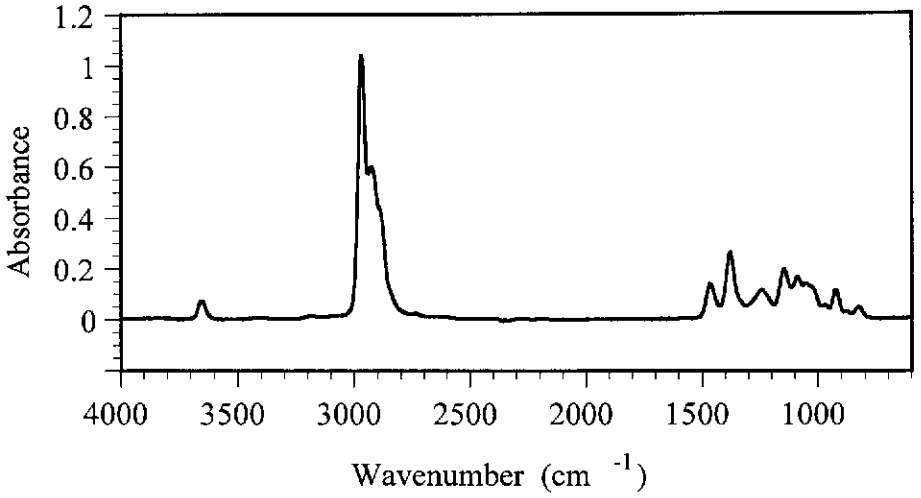

Figure 4.13: Infrared spectrum of the gases evolved from the MiBC mass loss.

4.3 TD-py-GC-MS Analysis of the Frothing Agents Adsorbed on Activated Carbon

The amounts of PPG, PPGME, α-terpineol, and MiBC individually adsorbed onto the Haycarb (-45 μm) were 29.8, 30.9, 16.9, and 14.1 % w/w respectively.

TD-py-GC-MS was used to identify the gases evolved from each frothing agent adsorbed on activated carbon when heated in an inert atmosphere from ambient to 1000°C. Each pyrolysis produced numerous gases. The total ion chromatograms of the frothing agents are presented in Figures 4.14, 4.15, 4.16, and 4.17.

For simplicity, gases with a peak area less than 10 % of the largest peak were excluded from the study, as well as those gases identified from the blank experiment (see section 3.3). The remaining gases were identified using a mass spectra database and manual interpretation. The gases produced for each pyrolysis, along with their retention time and relative peak area (%), are presented in Table 4.3.

	Peak	RT (min)	Relative Peak Area (%)	Gas Evolved
PPG-AC	1	1.07	18.3	propanal
	2	2.67	12.2	2-ethyl-4-methyl-1,3-dioxolane
	3	3.23	6.18	2,5-dimethyl-1,4-dioxane
	4	3.82	2.77	di-isopropyl ether
	5	7.24 - 9.05	11.9	3,3-oxybis-2-butanol
	6	13.8 - 14.9	6.94	PPG (n = 2)
	7	19.7 – 21.0	6.31	PPG (n = 3)
	8	24.0 – 26.3	9.00	PPG (n = 4)
	9	29.5 – 30.7	6.13	PPG (n = 5)
	10	33.4 – 34.8	8.61	PPG (n = 6)
	11	37.0 – 38.3	8.85	PPG (n = 7)
	12	40.3 – 41.4	2.78	PPG (n = 8)
PPGME-AC	1	1.04	8.87	propanal
	2	2.75	5.95	2-ethyl-4-methyl-1,3-dioxolane
	3	2.87	4.74	dimethyl-1,4-dioxane
	4	3.03	4.58	2,5-dimethyl-1,4-dioxane
	5	3.26	3.78	2,5 and 2,6 dimethyl dioxene
	6	3.56	8.59	2-methyl-2-pentenal
	7	4.05	2.75	2-isopropoxy-1-propanol
	8	4.84	1.80	2-methyl-2-cyclopenten-1-one
	9	7.52 - 9.50	22.6	3,3-oxybis-2-butanol
	10	13.84 - 14.24	2.99	PPGME (n = 3)
	11	14.40 - 15.25	14.52	dipropylene glycol
	12	19.92 - 21.04	12.9	PPGME (n = 4)
	13	24.99 - 26.02	5.93	PPGME (n = 5)
α-terpineol –AC	1	0.94	2.10	propene
	2	1.23	15.0	propanal
	3	1.40	3.56	propanol
	4	2.62	3.77	toluene
	5	2.87	9.46	2-ethyl-4-methyl-1,3-dioxolane
	6	3.00	7.61	isomer of above peak
	7	3.14	6.61	2,5-dimethyl-1,4-dioxane
	8	3.37	5.13	2,5 and 2,6-dimethyl dioxane
	9	3.53	3.46	trans-2,6-dimethyl-P-dioxane
	10	3.61	5.60	2-methyl-2-pentanal
	11	4.07	2.84	di-isopropyl ether
	12	4.89	2.50	2-methyl-2-cyclopenten-1-one
	13	7.67 - 8.93	27.8	3,3-oxybis-2-butanol
	14	14.45-14.96	4.84	dipropylene glycol
MiBC-AC	1	1.23	2.48	4-methyl-1-pentene
	2	1.28	3.37	2,3-dimethyl-1-butene
	3	2.37	5.09	4-methyl-2-pentanone
	4	3.11	87.6	MiBC
	5	3.51	1.42	2-hexanol

Table 4.3: Gases evolved from the pyrolysis of PPG, PPGME, α-terpineol, and MiBC adsorbed on activated carbon.

The typical total ion chromatogram of PPG adsorbed on activated carbon is shown in Figure 4.14. After excluding gases as indicated above, twelve significant peaks were identified. Propanal had the largest relative peak area, followed by 2-ethyl-4-methyl-1,3-dioxolane, 3,3-oxybis-2-butanol, and PPG (n = 2 - 8). The PPG volatiles were identified by comparison to the non-adsorbed PPG TIC. Aldehydes, dioxolanes, dioxanes, and ethers have been previously reported for the pyrolysis of high molecular weight PEG (Voorhees, Baugh and Stevenson 1994).

The typical total ion chromatogram of PPGME adsorbed on activated carbon is shown in Figure 4.15. After excluding gases as indicated above, thirteen significant peaks were identified. 3,3-oxybis-2-butanol had the largest relative peak area, followed by dipropylene glycol, PPGME (n = 4), propanal, and 2-methyl-2-pentenal. The PPGME volatiles were identified by comparison to the non-adsorbed PPGME TIC. The dipropylene glycol was identified by comparison to the adsorbed PPG TIC.

The typical total ion chromatogram of α-terpineol adsorbed on activated carbon is shown in Figure 4.16. After excluding gases as indicated above, fourteen significant peaks were identified. 3,3-oxybis-2-butanol had the largest relative peak area, followed by propanal, and 2-ethyl-4-methyl-1,3-dioxolane. Five significant peaks were identified from the decomposition of MiBC adsorbed on activated carbon as shown in Figure 4.17. MiBC was the most abundant gas evolved and all other gases were minor in comparison.

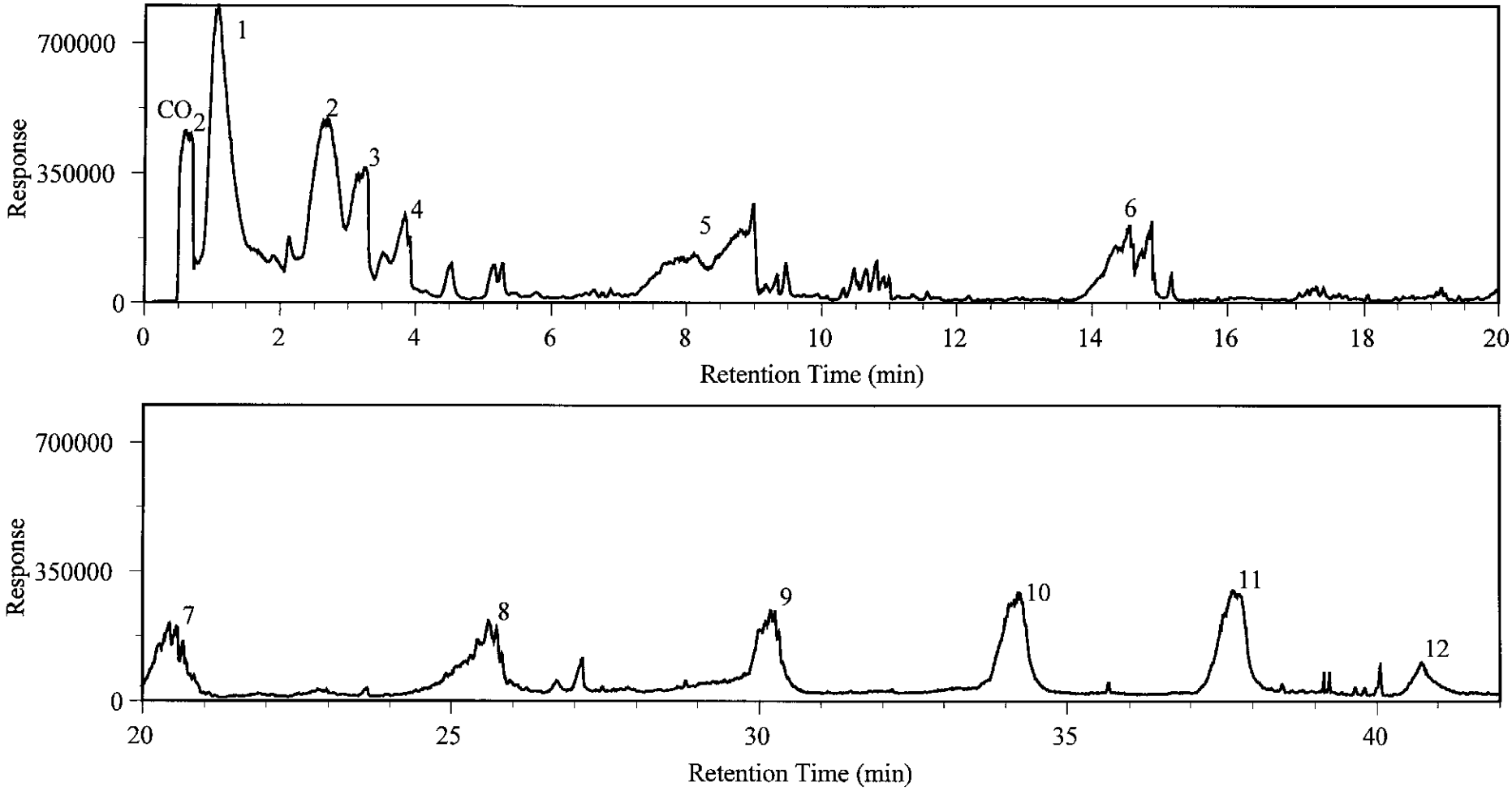

Figure 4.14: TD-py-GC-MS total ion chromatogram of PPG adsorbed on Haycarb, heated at 25°C min^{-1} in an inert atmosphere.

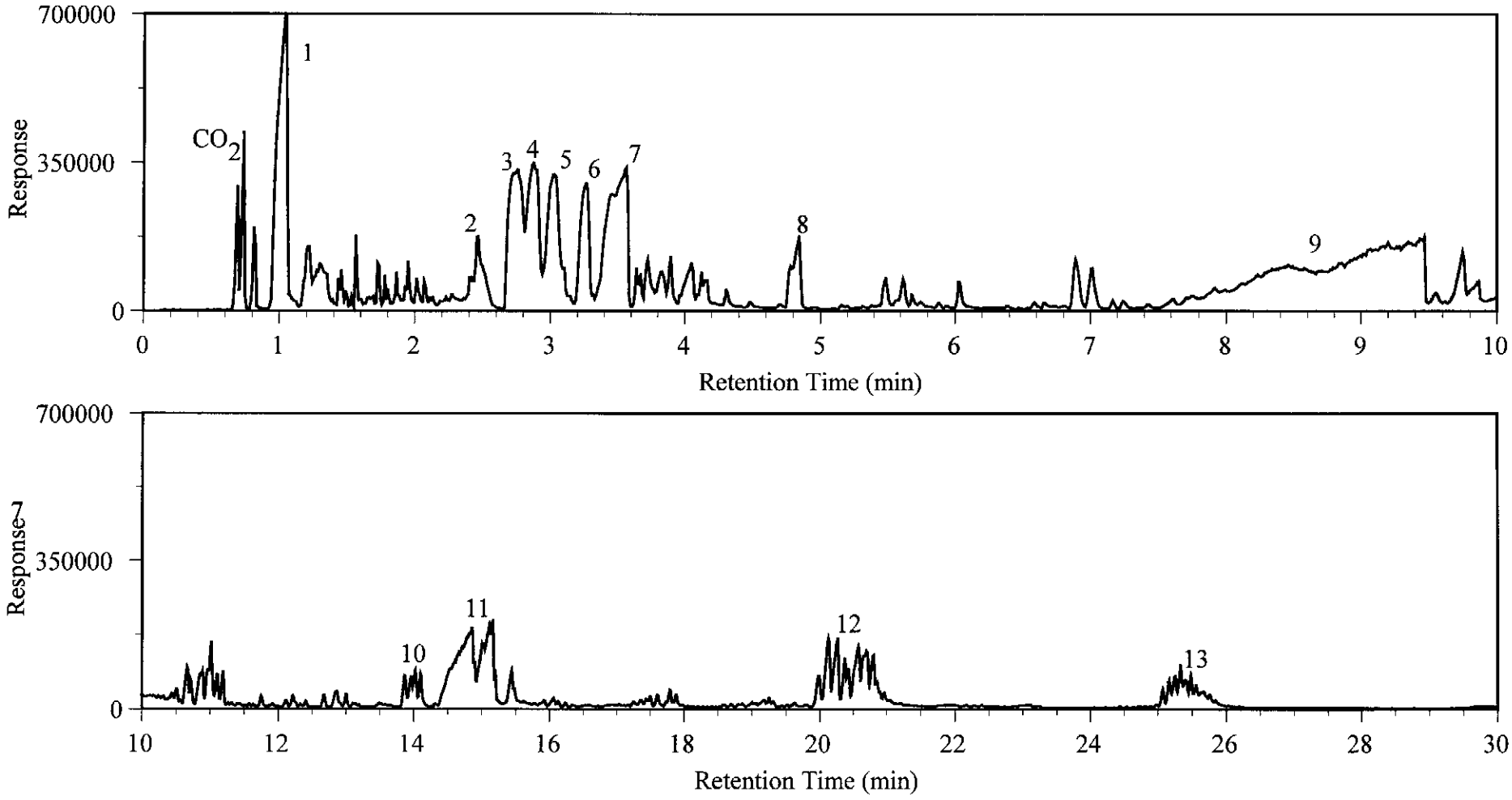

Figure 4.15: TD-py-GC-MS total ion chromatogram of PPGME adsorbed on Haycarb, heated at 25°C min^{-1} in an inert atmosphere.

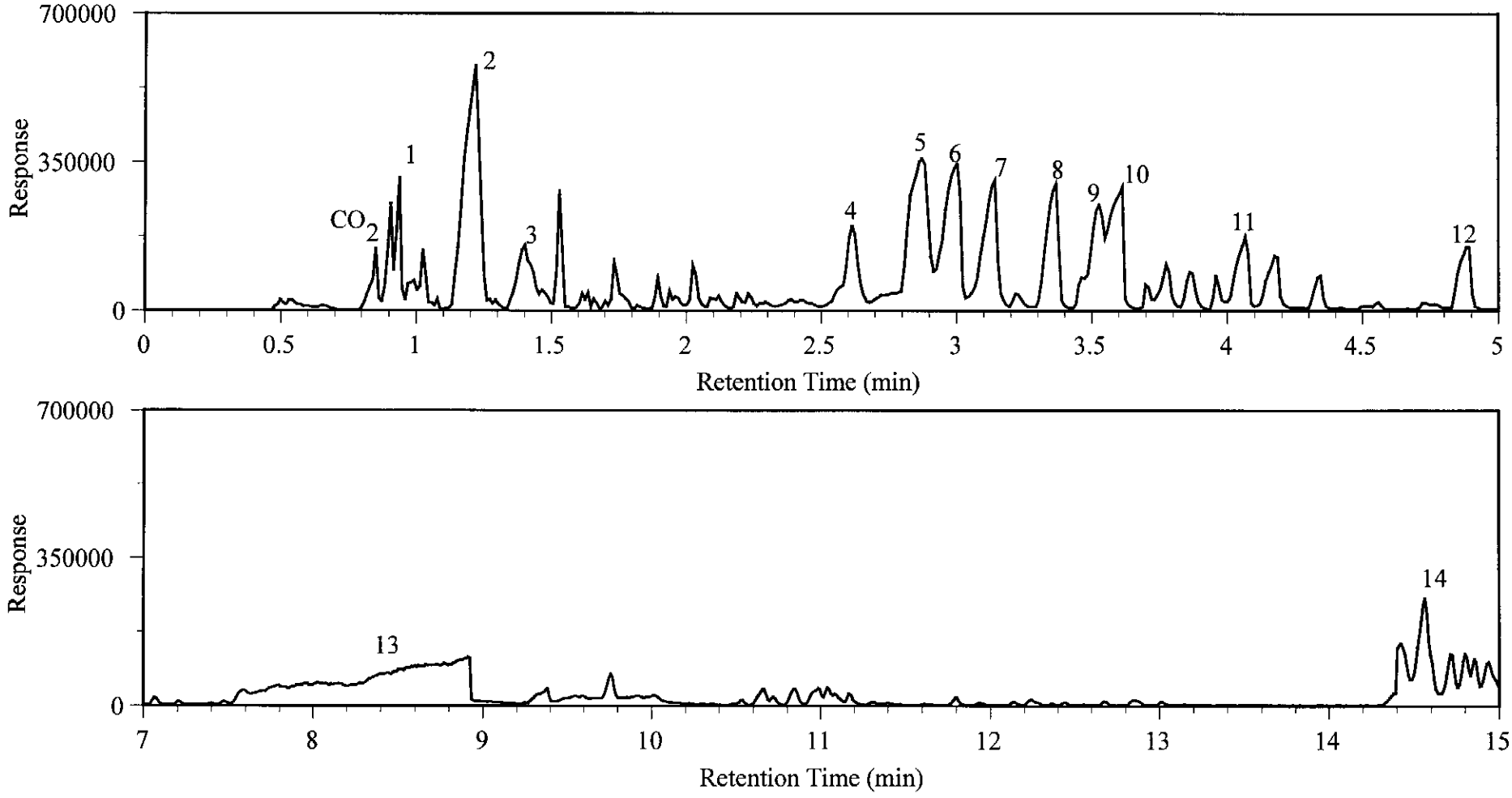

Figure 4.16: TD-py-GC-MS total ion chromatogram of α-terpineol adsorbed on Haycarb, heated at 25°C min^{-1} in an inert atmosphere.

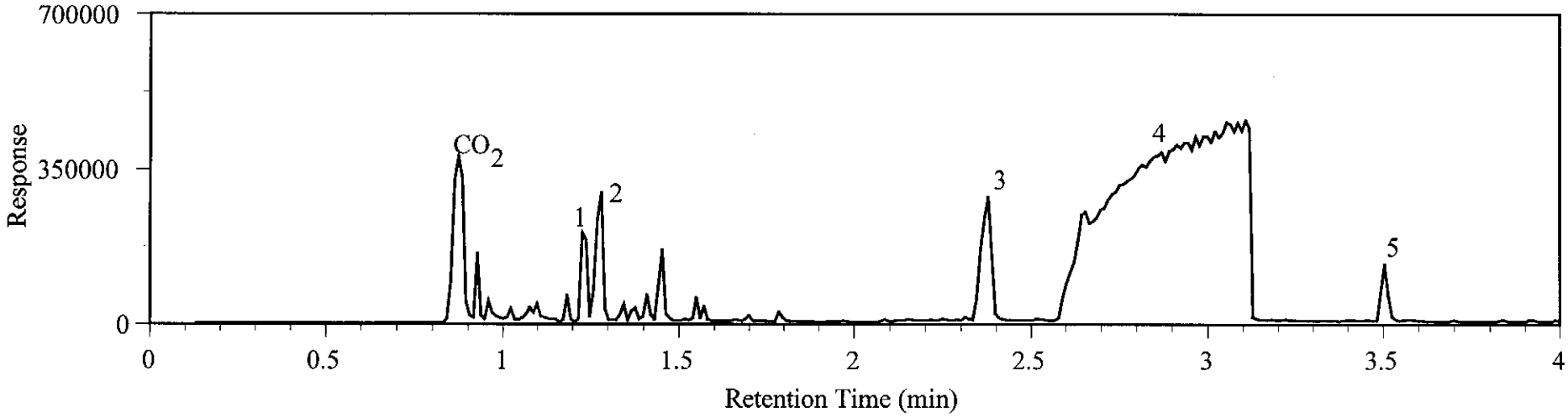

Figure 4.17: TD-py-GC-MS total ion chromatogram of MiBC adsorbed on Haycarb, heated at 25°C min^{-1} in an inert atmosphere.

4.4 Thermogravimetry - Evolved Gas Analysis of the Frothing Agents Adsorbed on Activated Carbon

The thermogravimetric curve of each frothing agent adsorbed on Haycarb (-45 μm) displayed only one mass loss due to the adsorbed frothing agent. The two other mass losses that were observed for each sample were due to water evolution from ambient to 180°C, and from activated carbon breakdown from 441 to 1000°C. The mass losses and their extrapolated onset/offset temperatures for each sample are presented in Table 4.4.

	Frothing Agent			
	PPG	**PPGME**	**α-terpineol**	**MiBC**
Mass Loss (%)	25.9	24.4	18.6	14.8
Temperature (°C)	258-351	255-363	275-357	186-311

Table 4.4: Mass losses and their corresponding temperatures for PPG, PPGME, α-terpineol, and MiBC adsorbed on Haycarb.

The maximum rate of mass loss for PPG, PPGME, α-terpineol, and MiBC occurred at 308, 316, 312, and 254°C respectively. Presented in Figures 4.18, 4.19, 4.20, and 4.21 are the TG curves along with their GS and MS curves for PPG, PPGME, α-terpineol, and MiBC adsorbed on activated carbon respectively.

For each frothing agent adsorbed onto the activated carbon it was possible to calculate a theoretical mass loss. To do this it was assumed 100 % of each frothing agent decomposed, that is the theoretical mass loss should be the same figure as the amount adsorbed. To correct for the mass loss due to the decomposition of activated carbon, 1.4 % was subtracted from each experimental mass loss. This number was obtained from the activated carbon TG curve with no other compounds adsorbed. The theoretical and experimental mass losses for each xanthate are presented in Table 4.5.

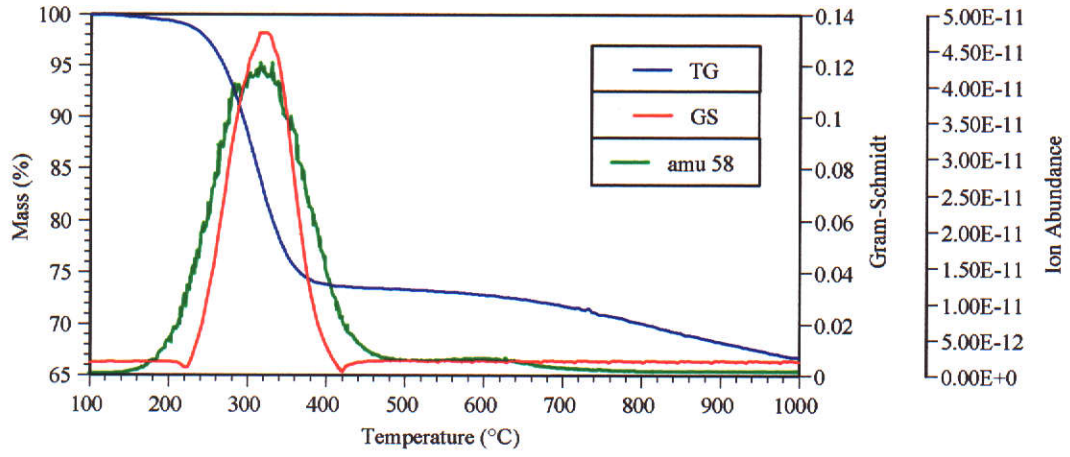

Figure 4.18: TG-GS-MS curves for PPG adsorbed on Haycarb, heated from ambient to 1000°C at 10°C min^{-1} in an argon atmosphere.

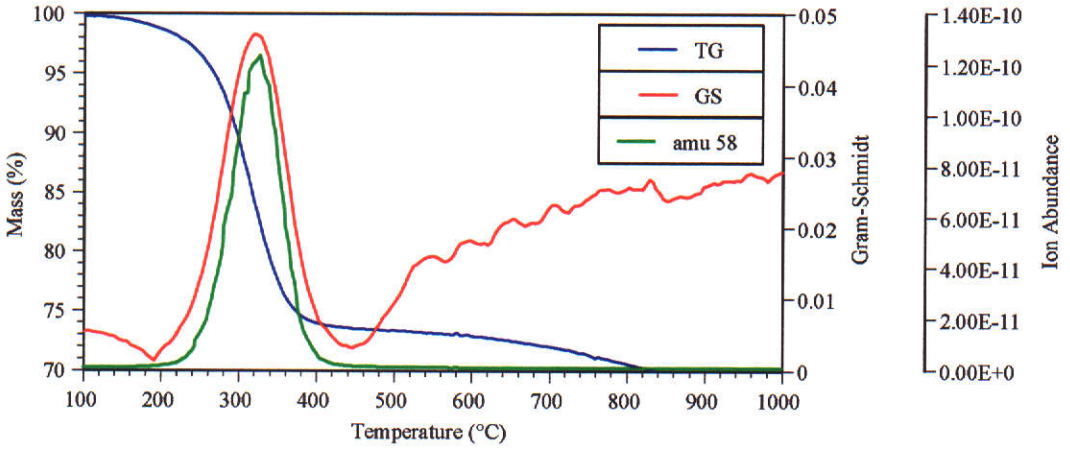

Figure 4.19: TG-GS-MS curves for PPGME adsorbed on Haycarb, heated from ambient to 1000°C at 10°C min^{-1} in an argon atmosphere.

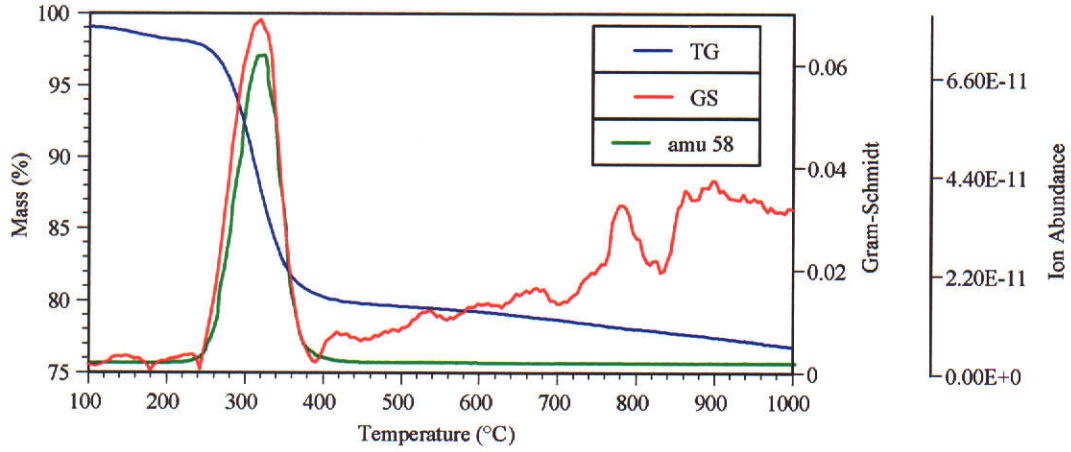

Figure 4.20: TG-GS-MS curves for α-terpineol adsorbed on Haycarb, heated from ambient to 1000°C at 10°C min^{-1} in an argon atmosphere.

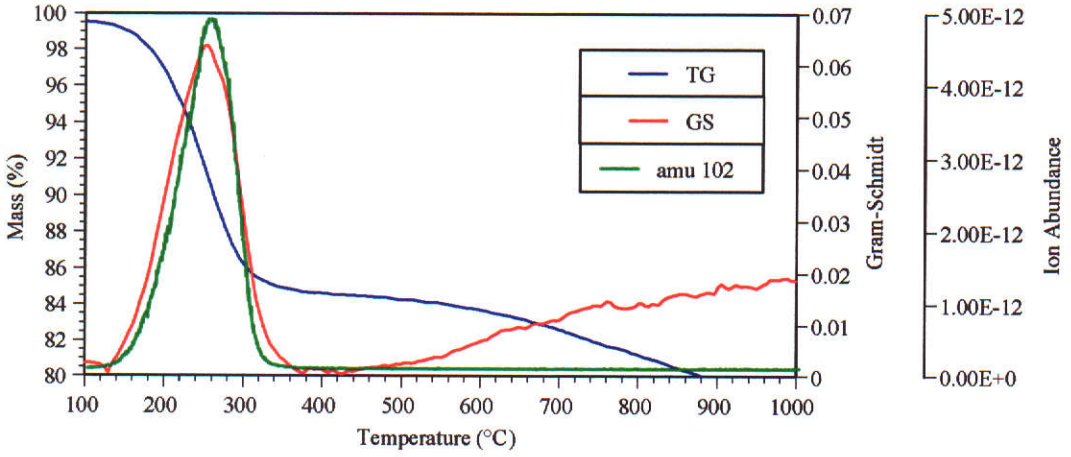

Figure 4.21: TG-GS-MS curves for MiBC adsorbed on Haycarb, heated from ambient to 1000°C at 10°C min^{-1} in an argon atmosphere.

	PPG	PPGME	α-terpineol	MiBC
Experimental	24.5	23.0	17.2	13.4
Theoretical	29.8	30.9	16.9	14.1

Table 4.5: Experimental versus theoretical mass losses for PPG, PPGME, α-terpineol, and MiBC adsorbed onto Haycarb.

The experimental mass loss for PPG, PPGME, and MiBC were lower than the theoretical mass losses. This could mean that some of each frothing agent was retained on the activated carbon. However, the experimental and theoretical mass losses for α-terpineol were similar indicating that all the α-terpineol had volatilised.

4.4.1 MS Analysis of the Evolved Gases

The gases evolved from each frothing agent adsorbed on activated carbon were studied by SIM from ambient to 1000°C in argon atmospheres. The gases evolved were identified from the TD-py-GC-MS analyses and were monitored via their molecular ions.

All the ions monitored in the SIM analyses of PPG, PPGME, and α-terpineol displayed the same curve, that is one broad peak, coinciding with the TG curve. Displayed in Figures 4.18, 4.19 and 4.20 are the chromatograms for amu 58, which also is the molecular ion for propanal. In the SIM analysis of MiBC, all the ions monitored displayed one broad peak, which coincided with the TG curve. Displayed in Figure 4.21 is the chromatogram for amu 102, which also is the molecular ion for MiBC.

Presented in Table 4.6 is the relative peak area of the gases evolved from each SIM analysis. The relative peak area of each gas evolved has been expressed as a percentage, which enables a semi-quantitative comparison of the abundance of each gas to be made.

	amu	Relative Peak Area (%)	Gas
PPG	58	94.7	propanal
	102	0.91	di-isopropyl ether
	116	2.14	2-ethyl-4-methyl-1,3-dioxolane 2,5-dimethyl-1,4-dioxane
	134	0.79	PPG (n = 2)
	162	0.72	3,3-oxybis-2-butanol
	192	0.78	PPG (n = 3)
PPGME	58	93.7	propanal
	96	1.80	2-methyl-2-cyclopenten-1-one
	98	1.22	2-methyl-2-pentenal
	114	1.34	2,5 and 2,6 dimethyl dioxene
	116	1.91	2-ethyl-4-methyl-1,3-dioxolane dimethyl-1,4-dioxane 2,5-dimethyl-1,4-dioxane
α-terpineol	42	46.3	propene
	58	43.1	propanal
	60	6.32	propanol
	92	2.13	toluene
	96	0.70	2-methyl-2-cyclopenten-1-one
	114	0.51	2,5 and 2,6-dimethyl dioxane
	116	0.87	2-ethyl-4-methyl-1,3-dioxolane 2,5-dimethyl-1,4-dioxane trans-2,6-dimethyl-P-dioxane
MiBC	84	78.4	4-methyl-1-pentene 2,3-dimethyl-1-butene
	100	12.6	4-methyl-2-pentanone
	102	9.06	MiBC 2-hexanol

Table 4.6: Relative peak area of the evolved gases from PPG, PPGME, α-terpineol, and MiBC adsorbed on Haycarb and heated at 10°C min^{-1} in an argon atmosphere.

A number of gases detected in the TD-py-GC-MS analyses were not detected in the TG-MS analyses. For the PPG analysis these were the PPG gases (n = 4 to 8); for PPGME these were 2-isopropoxy-1-propanol, 3,3-oxybis-2-butanol, PPGME (n = 3 to 5), and dipropylene glycol; and for α-terpineol these were 2-methyl-2-pentanal, di-isopropyl ether, 3,3-oxybis-2-butanol, and dipropylene glycol.

As shown in Table 4.6, propanal had the largest relative peak area for the PPG and PPGME analyses. All other gases were minor compared to propanal. There is a

possibility that the high ion abundance of amu 58 may also be due to the detection of fragment ions from the breakdown of higher molecular weight gases. However it is more likely due to condensation of the higher molecular weight gases before entering the MS as the technique suffers from this problem (Raemaekers and Bart 1997).

The gases with the largest relative peak areas for the decomposition of α-terpineol were propene and propanal. All other detected gases were minor when compared to propene and propanal.

In the MiBC SIM analysis, 4-methyl-1-pentene and 2,3-dimethyl-1-butene had the largest relative peak area (these gases have the same molecular weight and thus do not have separate ion signals).

4.4.2 FTIR Analysis of the Evolved Gases

For each frothing agent, the GS chromatograms of the gases evolved from thermal decomposition are shown in Figures 4.18 to 4.21, and are very similar to their MS ion chromatograms displayed in the same figure, coinciding with the TG curve.

The infrared spectrum of the gases evolved from the PPG mass loss is presented in Figure 4.22. The spectrum shows all the characteristic peaks of PPG plus significant peaks at 2816, 2721 and around 1750 cm^{-1}. The peaks at 2816 and 2721 cm^{-1} are very characteristic stretching vibrations of the aldehydic C-H contained in aldehydes. The large peak around 1750 cm^{-1} is very characteristic of carbonyl stretching (Socrates 1994).

The infrared spectra of the gases evolved from the thermal decomposition of PPGME and α-terpineol are not presented as they were almost identical to the PPG mass loss spectrum. Also the infrared spectrum from the MiBC mass loss is not shown as it was almost identical to Figure 4.13, indicating that the MiBC had simply boiled off.

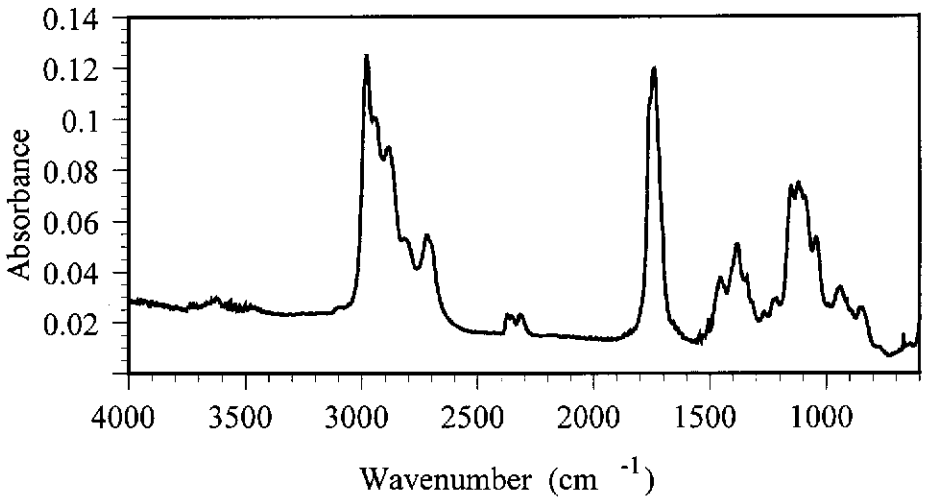

Figure 4.22: Infrared spectrum of the gases evolved from the mass loss of PPG adsorbed on Haycarb, at 308°C.

4.5 Surface Analysis of Frothing Agents Adsorbed on Activated Carbon

A surface examination of the frothing agents adsorbed on activated carbon was attempted in order to aid in the explanation of mass losses and the gases evolved. DRIFT spectroscopy was used to study the activated carbon surface. Spectra were obtained for ground and unground samples. Unfortunately the high absorption of infrared radiation interfered with the analyses. Therefore interpretation of the results was not possible.

4.6 Summary

Comparisons of the thermal decomposition results of the frothing agents versus the frothing agents adsorbed on activated carbon showed that, with the exception of MiBC, there was a major difference in the gases evolved. When analysed alone, the frothing agents essentially boiled off unchanged. However, when absorbed on activated carbon, the analyses showed that a variety of different gases were evolved.

The TG (see Tables 4.2 and 4.4), MS (see Table 4.6) and FTIR results showed that the pure frothing agents simply boiled off. When adsorbed on activated carbon, the PPG, PPGME, and α-terpineol decomposed producing one mass loss at

approximately 260-360°C. The most significant gas evolved during the decomposition of these three reagents was propanal. MiBC again just boiled off. Hence for the first three frothing agents the evolution of propanal from industrial plant samples in this temperature range would indicate the presence of frothing agent fouling due to polyglycol ethers and α-terpineol found in pine oil.

Identifying the reactions responsible for the gases evolved when the frothing agents are adsorbed on activated carbon is difficult. However a possible mechanism for the formation of propanal from the PPG decomposition is presented in Figure 4.23. Cleavage would most likely occur via the C-O bonds, as these are the generally the weakest. The cleavage would also be influenced by the adsorption of the PPG on the carbon surface, as this would weaken the surrounding PPG bonds. After cleavage, hydrogen abstraction may occur, followed by dehydration, and finally tautomerism of the enol to a keto form (equilibrium generally lies in favour of the keto form) (Morrison and Boyd 1992). Similarly, formation of propanal from the PPGME decomposition could occur in the same manner.

Finally, identification of the formation of propanal from α-terpineol is not obvious according to common organic reactions. Thus no attempt at proposing a mechanism will be presented here.

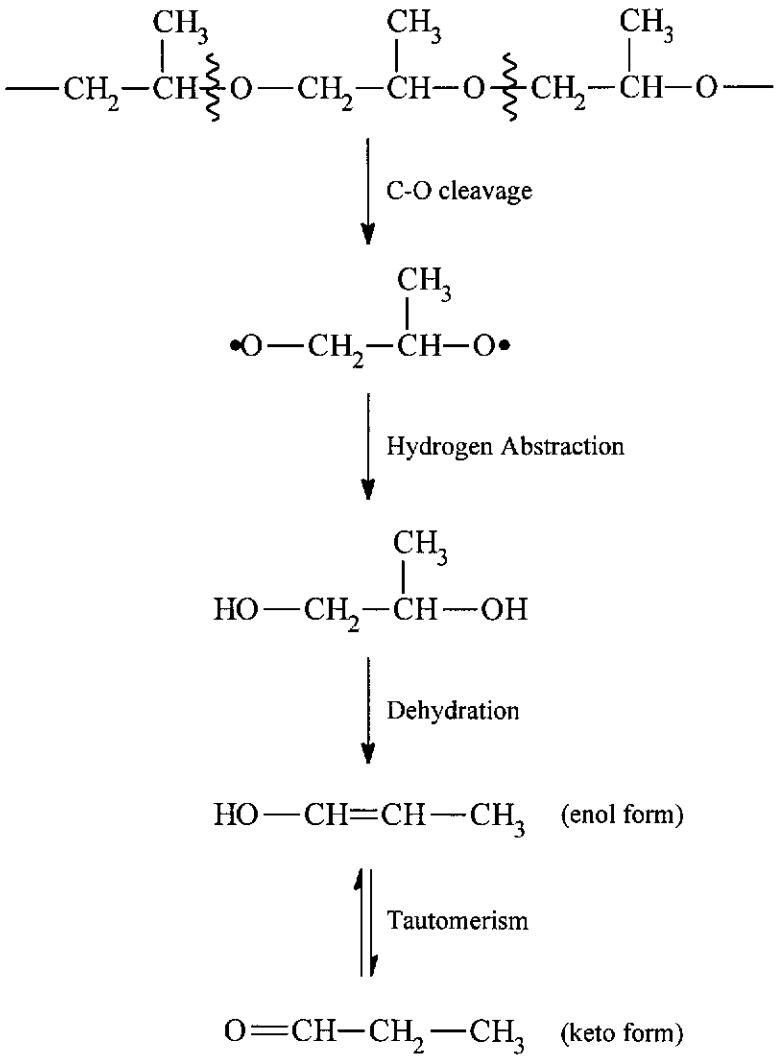

Figure 4.23: Possible formation of propanal from the thermal decomposition of PPG adsorbed on activated carbon.

Analysis of the frothing agents adsorbed on activated carbon by the various techniques reveal some differences between the type and amount of decomposition products for the same sample.

Presented in Table 4.7 is a comparison of the relative peak areas (%) for the TD-py-GC-MS and TG-MS analysis of the gases evolved from the thermal decomposition of the frothing agents adsorbed on Haycarb. Unfortunately it was not possible to determine if different gases evolved due to the different techniques, as the TG-MS data collection was dependent on the results of the TD-py-GC-MS analyses. Also it

is not possible to compare the data from TD-py-GC-MS and TG-MS to the TG-FTIR data, as only qualitative information was available.

	Relative Peak Areas (%)		Gas
	TD-py-GC-MS	TG-MS	
PPG	18.3	94.7	propanal
	12.2	2.14	2-ethyl-4-methyl-1,3-dioxolane
	6.18		2,5-dimethyl-1,4-dioxane
	2.77	0.91	di-isopropyl ether
	11.9	0.72	3,3-oxybis-2-butanol
	6.94	0.79	PPG (n = 2)
	6.31	0.78	PPG (n = 3)
	9.00	ND	PPG (n = 4)
	6.13	ND	PPG (n = 5)
	8.61	ND	PPG (n = 6)
	8.85	ND	PPG (n = 7)
	2.78	ND	PPG (n = 8)
PPGME	8.87	93.7	propanal
	5.95	1.91	2-ethyl-4-methyl-1,3-dioxolane
	4.74		dimethyl-1,4-dioxane
	4.58		2,5-dimethyl-1,4-dioxane
	3.78	1.34	2,5 and 2,6 dimethyl dioxene
	8.59	1.22	2-methyl-2-pentenal
	2.75	ND	2-isopropoxy-1-propanol
	1.80	1.80	2-methyl-2-cyclopenten-1-one
	22.6	ND	3,3-oxybis-2-butanol
	2.99	ND	PPGME (n = 3)
	14.52	ND	dipropylene glycol
	12.9	ND	PPGME (n = 4)
	5.93	ND	PPGME (n = 5)
α-terpineol	2.10	46.3	propene
	15.0	43.1	propanal
	3.56	6.32	propanol
	3.77	2.13	toluene
	9.46	0.87	2-ethyl-4-methyl-1,3-dioxolane
	7.61		isomer of above peak
	6.61		2,5-dimethyl-1,4-dioxane
	3.46		trans-2,6-dimethyl-P-dioxane
	5.13	0.51	2,5 and 2,6-dimethyl dioxane
	5.60	ND	2-methyl-2-pentanal
	2.84	ND	di-isopropyl ether
	2.50	0.70	2-methyl-2-cyclopenten-1-one
	27.8	ND	3,3-oxybis-2-butanol
	4.84	ND	dipropylene glycol
MiBC	2.48	78.4	4-methyl-1-pentene
	3.37		2,3-dimethyl-1-butene
	5.09	12.6	4-methyl-2-pentanone
	87.6	9.06	MiBC
	1.42		2-hexanol

Table 4.7: Comparison of the relative peak area (%) of gases evolved from the thermal decomposition of the frothing agents adsorbed on Haycarb by TD-py-GC-MS and TG-MS (ND = not detected).

The main difference between the relative peak areas of the gases is that for three of the frothing agents, a greater amount of higher molecular weight gases was observed in the TD-py-GC-MS analyses relative to the TG-MS analyses. The exception is in the analyses of MiBC adsorbed on Haycarb where the molecular weights of the evolved gases were fairly similar.

For example in the TD-py-GC-MS analysis of PPG, the higher molecular weight gases (PPG, n = 2-8) contribute 48.6 % of all the gases evolved; while in the TG-MS analysis these gases only contributed 1.57 %. Also in the TD-py-GC-MS analysis of PPG the lower molecular weight gas, propanal, constitutes 18.3 % of all gases evolved, while in the TG-MS analysis propanal constitutes 94.7 %. The most likely explanation for this behaviour is the condensation of higher molecular weight gases in the connecting line between the TG apparatus and either the MS or FTIR detectors. This condensation effect was pointed out in section 4.4.1.

The TD-py-GC-MS and TG-MS analyses of MiBC adsorbed on Haycarb show they are different compared to the other frothing agent analyses. It was expected in the TG-MS analysis evolution of MiBC would display the largest relative peak area, but 4-methyl-1-pentene (the dehydration product of MiBC) and 2,3-dimethyl-1-butene displayed the largest relative peak areas. This effect could not be due to dehydration of the MiBC in the TG-MS transfer line, as this did not occur in the analysis of pure MiBC. However it is more likely this effect was due to overlapping fragment ion signals from MiBC ionisation.

CHAPTER 5

THERMAL DECOMPOSITION OF INDUSTRIAL SAMPLES

5.0 Introduction

In this chapter the thermal decomposition of material adsorbed on activated carbon samples from two gold processing plants is reported. The activated carbon samples came from the Three Mile Hill plant located in Coolgardie, Western Australia, and the Salsigne plant in France.

Three Mile Hill processes its sulfidic ores by crushing, grinding, flotation, fine grinding, CIL, stripping, and then gold recovery by electrowinning. The flotation circuit uses PAX (30-50 g/t of ore) as the collector, and Interfroth 50 (10-20 g/t) as the frothing agent. After flotation the tailings are disposed of into the tailings dam. The activated carbon used in the CIL circuit is Haycarb YAO. The activated carbon is regenerated by acid washing followed by thermal reactivation at 650°C (Bax and Bax 1993).

No information could be found on the processing route of gold at Salsigne.

5.1 Three Mile Hill Samples

Activated carbon samples were taken from several points in the Three Mile Hill circuit, namely after gold adsorption (loaded), after gold stripping (barren), after acid washing, and after thermal regeneration. The samples received were ground to -45 μm so that the effects of gaseous diffusion through the pore system of the activated carbon were minimised, thus improving resolution in gas evolution as well as in mass losses observed in the TG curves.

5.1.1 TD-py-GC-MS

TD-py-GC-MS was used to identify the gases evolved from each sample when heated at 25°C min^{-1} in an inert atmosphere from ambient to 800°C. Typical total ion chromatograms for the samples are presented in Figures 5.1 and 5.2, and the identity of the peaks for each sample, along with their retention time (RT), and relative peak area (%), are given in Table 5.1. Products resulting from gases evolved from decomposition reactions of the activated carbon alone have been omitted from

Table 5.1 (see section 3.3. Also, for simplicity, gases with a peak area less than 10 % of the largest peak were excluded from the study.

	Peak	RT (min)	Relative Peak Area (%)	Gas Evolved
Loaded	1	0.89	14.5	butene
	2	1.00	10.0	ethylcyclopropane
	3	1.03	9.20	2-methyl-1-butene
	4	1.31	2.78	1-chloro-2-methyl-propane
	5	1.43	8.99	isobutanol
	6	1.48	17.8	1-chlorobutane
	7	1.66	27.7	butanol
	8	1.87	5.22	1-chloro-3-methyl butane
	9	2.13	3.69	3-methyl-1-butanol
Barren	1	0.90	12.9	butene
	2	1.01	9.59	2-methyl-1-butene
	3	1.03	3.95	1,4-pentadiene
	4	1.06	3.81	cis-1,2-dimethyl-cyclopropane
	5	1.27	3.19	butanal
	6	1.47	7.92	isobutanol
	7	1.50	3.39	1-chlorobutane
	8	1.72	32.2	butanol
	9	2.19	9.48	3-methyl-1-butanol
	10	2.49	3.79	3-methyl-thiophene
	11	2.94	5.24	butyl acetate
	12	3.89	4.43	isoamyl acetate
Acid Washed	1	0.90	21.7	butene
	2	0.94	8.25	2-methyl-1-propene
	3	0.97	11.9	2-methyl-1-butene
	4	1.02	11.5	ethylcyclopropane
	5	1.05	13.3	2-methyl-1,3-butadiene
	6	1.08	4.08	cis-1,2-dimethyl-cyclopropane
	7	1.50	10.2	1-chlorobutane
	8	1.60	3.51	thiophene
	9	1.63	5.32	butanol
	10	1.90	7.13	1-chloro-3-methylbutane
	11	2.93	3.07	butyl acetate
Regenerated	1	0.87	23.7	butene
	2	0.94	8.33	2-methyl-1-butene
	3	0.98	10.8	ethylcyclopropane
	4	1.01	9.11	cis-1,2-dimethyl-cyclopropane
	5	1.23	7.70	hexane
	6	1.58	10.0	butanol
	7	1.71	5.04	unidentified
	8	2.05	4.88	3-methyl-1-butanol
	9	2.44	5.54	3-methyl thiophene
	10	2.79	5.47	tetrachloroethene
	11	2.89	5.21	butyl acetate
	12	3.31	4.24	chlorobenzene

Table 5.1: Gases evolved from the pyrolysis of Three Mile Hill samples.

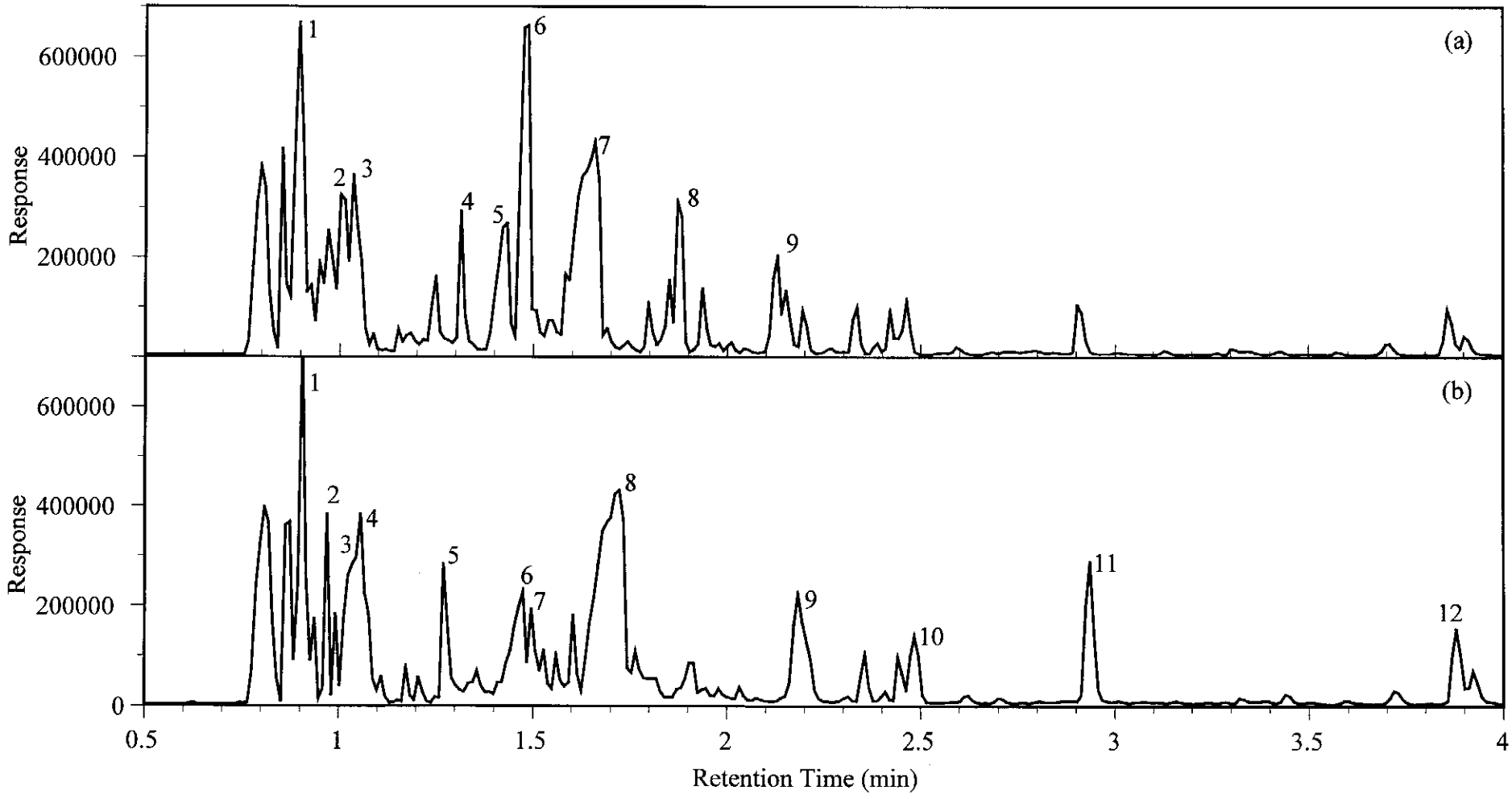

Figure 5.1: TD-py-GC-MS total ion chromatogram of (a) loaded, and (b) barren samples from Three Mile Hill heated at 25°C min^{-1} in an inert atmosphere.

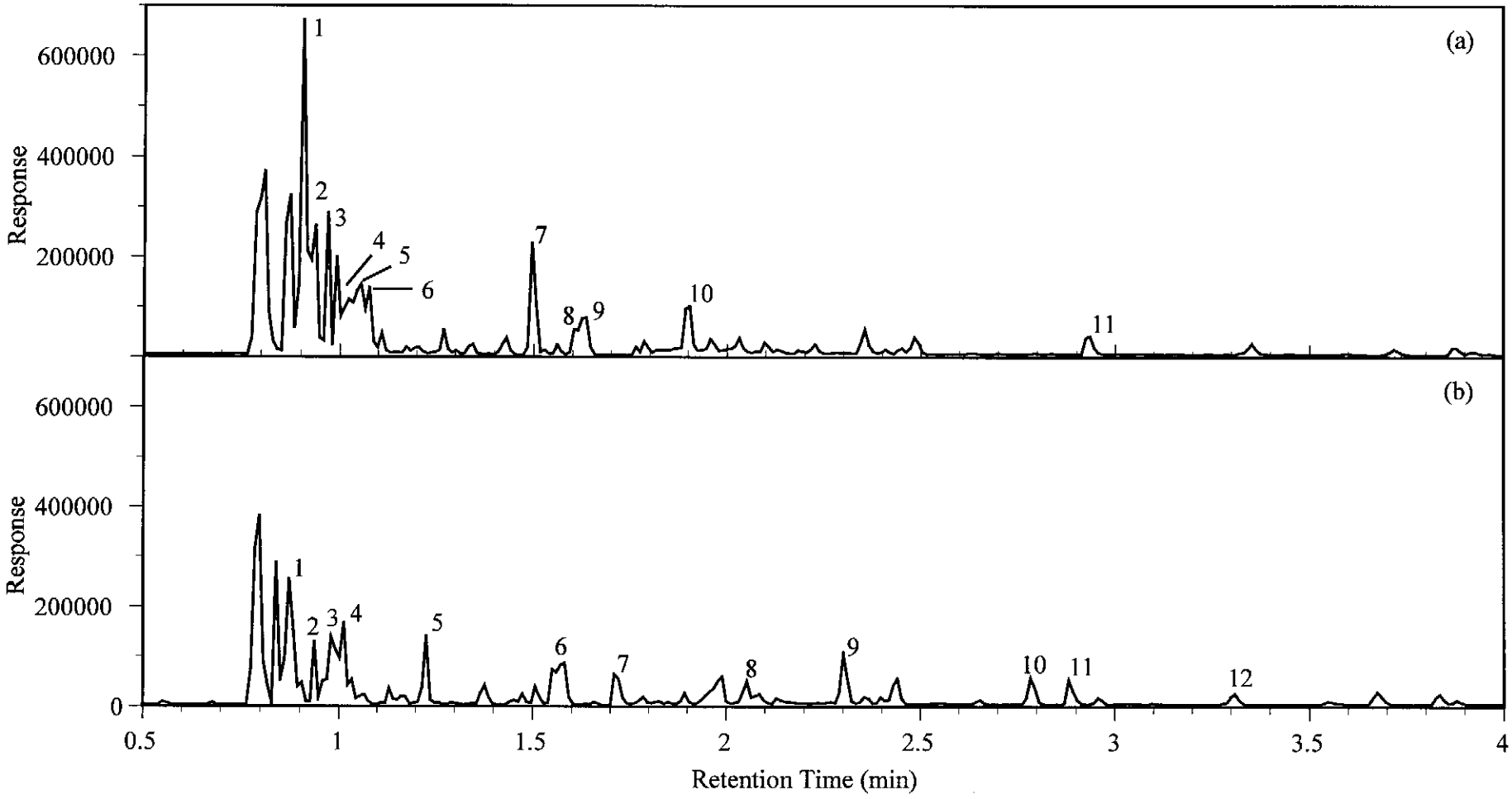

Figure 5.2: TD-py-GC-MS total ion chromatogram of (a) acid washed, and (b) regenerated samples from Three Mile Hill heated at 25°C min^{-1} in an inert atmosphere.

A typical TIC of the loaded sample (Figure 5.1a) displays at least 44 peaks. The first two peaks in each TIC are CO_2/SO_2, which are breakdown products of the carbon. After excluding peaks with areas less than 10 % of the largest peak, nine significant peaks were identified. The largest peak in the chromatogram was due to the presence of butanol, followed by 1-chlorobutane, and butene. The TIC of the barren sample (Figure 5.1b) displays at least 39 peaks, which after eliminating peaks on the same basis as before leaves twelve significant peaks. The largest peak in the chromatogram was due to the presence of butanol, followed by butene, and 2-methyl-1-butene. Similarly, the acid washed sample (Figure 5.2a) showed eleven significant peaks. The largest peak in the chromatogram was due to the presence of butene, followed by 2-methyl-1,3-butadiene, and 2-methyl-1-butane. Finally the regenerated sample (Figure 5.2b) displayed twelve significant peaks. The largest peak in the chromatogram was due to the presence of butene, followed by ethylcyclopropane, and butanol. Only one peak could not be identified.

Comparison of the TICs in Figures 5.1 and 5.2 show they are similar and the gases evolved elute very close together. For each sample the evolution of butene, 2-methyl-1-butene and butanol was common. There were also many other evolved gases that were common for at least 3 analyses. In some cases certain gases may not have been observed due to the very close retention times of the gases.

The largest peak in the loaded and barren TICs was due to the evolution of butanol. However, in the acid washed and regenerated samples the largest peak was due to butene evolution.

5.1.2 TG-MS and TG-FTIR

The thermal decomposition of the four samples was studied by TG-EGA, at a heating rate of 10°C min^{-1} under an argon atmosphere. The evolved gases were analysed by MS and FTIR spectroscopy. The TG curve of each sample exhibited three mass losses. The mass losses and their corresponding temperature ranges are presented in Table 5.2.

Mass Loss	Sample (%)			
	Loaded	Barren	Acid washed	Regenerated
First (amb.-223°C)	11.0	6.42	14.1	11.2
Second (223-514°C)	4.37	2.28	3.90	2.57
Third (514-1000°C)	2.76	1.93	2.58	2.75
Total	18.1	10.6	20.6	16.5

Table 5.2: Mass losses and their corresponding temperature ranges for loaded, barren, acid washed, and regenerated activated carbon samples from Three Mile Hill.

As seen in Table 5.2 there was no trend between the sample analysed and any of the mass losses observed.

The molecular ions of the gases identified in the TD-py-GC-MS analyses were monitored using the SIM mode of the MS from ambient to 1000°C. An ion chromatogram was produced for each evolved gas. Typical ion chromatograms for the decomposition gases of the loaded sample are presented in Figure 5.3, along with its mass loss curve. Ion chromatograms are not presented for the barren, acid washed, and regenerated samples as they were very similar to Figure 5.3.

A comparison of the relative percent peak area of each gas evolved for each sample is presented in Table 5.3. That is the ion abundance (in amps per degree Celsius) of each gas was divided by the sum of the ion abundances. Only a semi-quantitative comparison between each gas and sample was possible due to the differences in efficiency of formation of the molecular ions, and overlapping of fragment/isotope ion signals with the molecular ions.

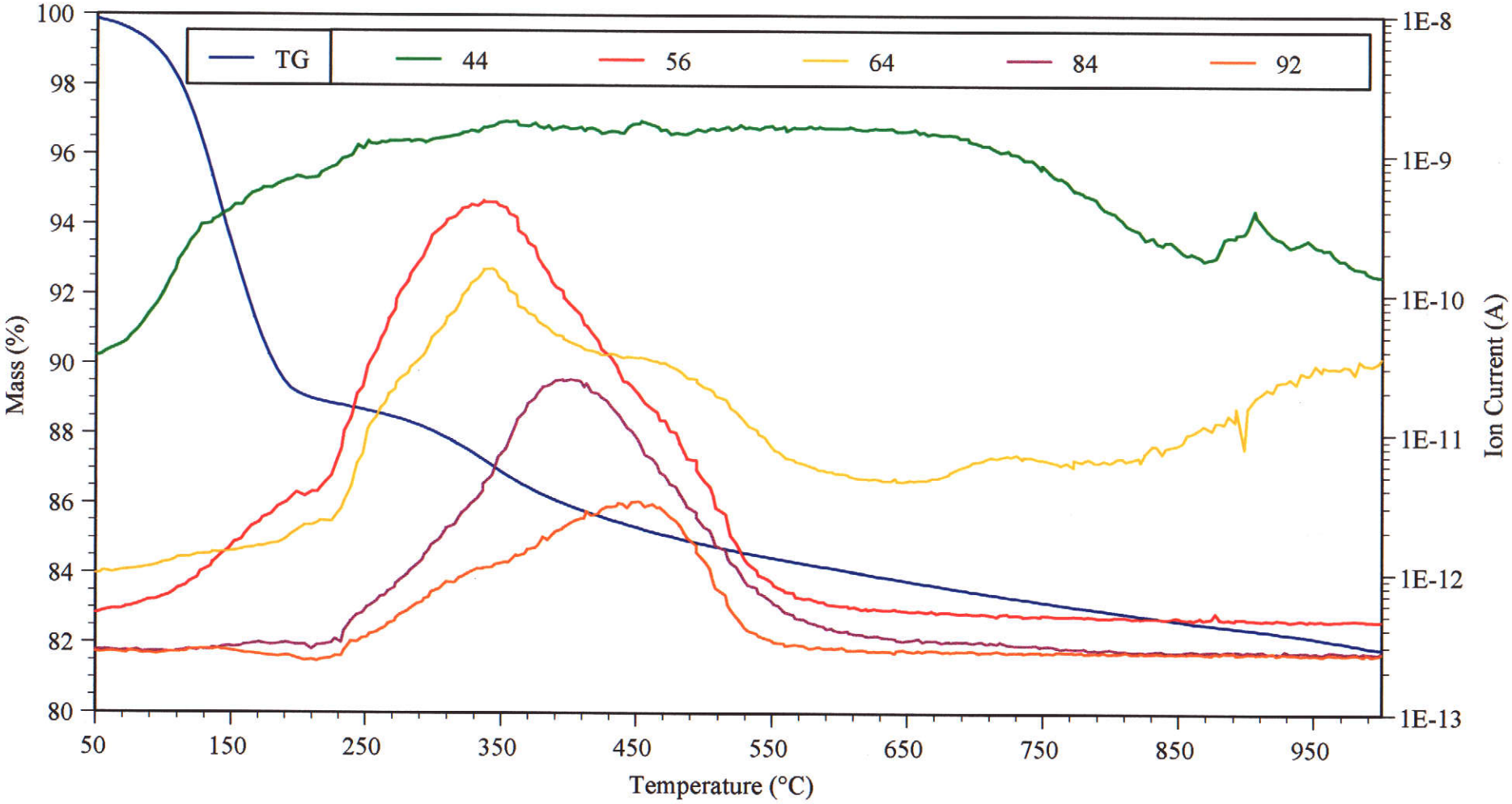

Figure 5.3: Ion chromatograms of the gases evolved from the decomposition of the Three Mile Hill loaded sample heated at 10°C min^{-1} in an argon atmosphere.

amu	Gas	Relative Peak Area (%)			
		Loaded	Barren	Acid washed	Regen-erated
56	butene	80.8	75.9	89.6	69.7
68	2-methyl-1,3-butadiene	2.10	3.14	1.84	3.68
70	ethylcyclopropane 2-methyl-1-butene cis-1,2-dimethyl cyclopropane	8.96	9.22	6.28	9.15
72	butenal	1.24	1.96	0.42	2.43
74	butanol	0.28	0.22	0.02	0.17
84	thiophene	4.43	7.07	1.16	11.3
86	hexane	0.33	0.47	0.12	0.71
90	3-methyl-1-butanol	0.12	0.08	0.04	0.05
92	1-chloro-2-methyl-propane 2-methyl-1-propanol 1-chlorobutane	0.74	0.77	0.18	1.01
98	3-methyl-thiophene	0.90	1.08	0.32	1.69
106	1-chloro-3-methyl butane	0.09	0.06	0.04	0.09
116	butyl acetate	ND	ND	ND	ND
130	isoamyl acetate	ND	ND	ND	ND
164	chlorobenzene	ND	ND	ND	ND

Table 5.3: Relative peak areas of the evolved gases from the Three Mile Hill samples heated at 10°C min^{-1} in argon atmospheres.

Although the ion chromatograms displayed in Figure 5.3 occur over the same temperature range (during the second mass loss), the temperature at which the evolved gas reached a maximum in evolution varies. The ion chromatogram of butene (amu 56) shows a maximum in evolution at 340°C, and the same type of evolution profile was observed for amu 68, 70, 72, and 74 (thus they are not displayed in Figure 5.3). Thiophene evolution (amu 84) peaked at 400°C (along with amu 86, 90, and 98). The ion chromatogram of amu 92 (attributed to three gases) peaked at 450°C (along with amu 106). Ions of amu 116, 130, and 164 were not detected.

Assuming that the ion signal contribution of fragment ions is very small, butene has the largest relative peak area for all samples. All other gases had small peak areas in comparison. It is difficult to compare the other gases monitored for each sample due to the low relative peak areas. However it appears there are not any large differences between the samples.

The TG-GS curves for the FTIR analysis of evolved gases from the samples are presented in Figure 5.4.

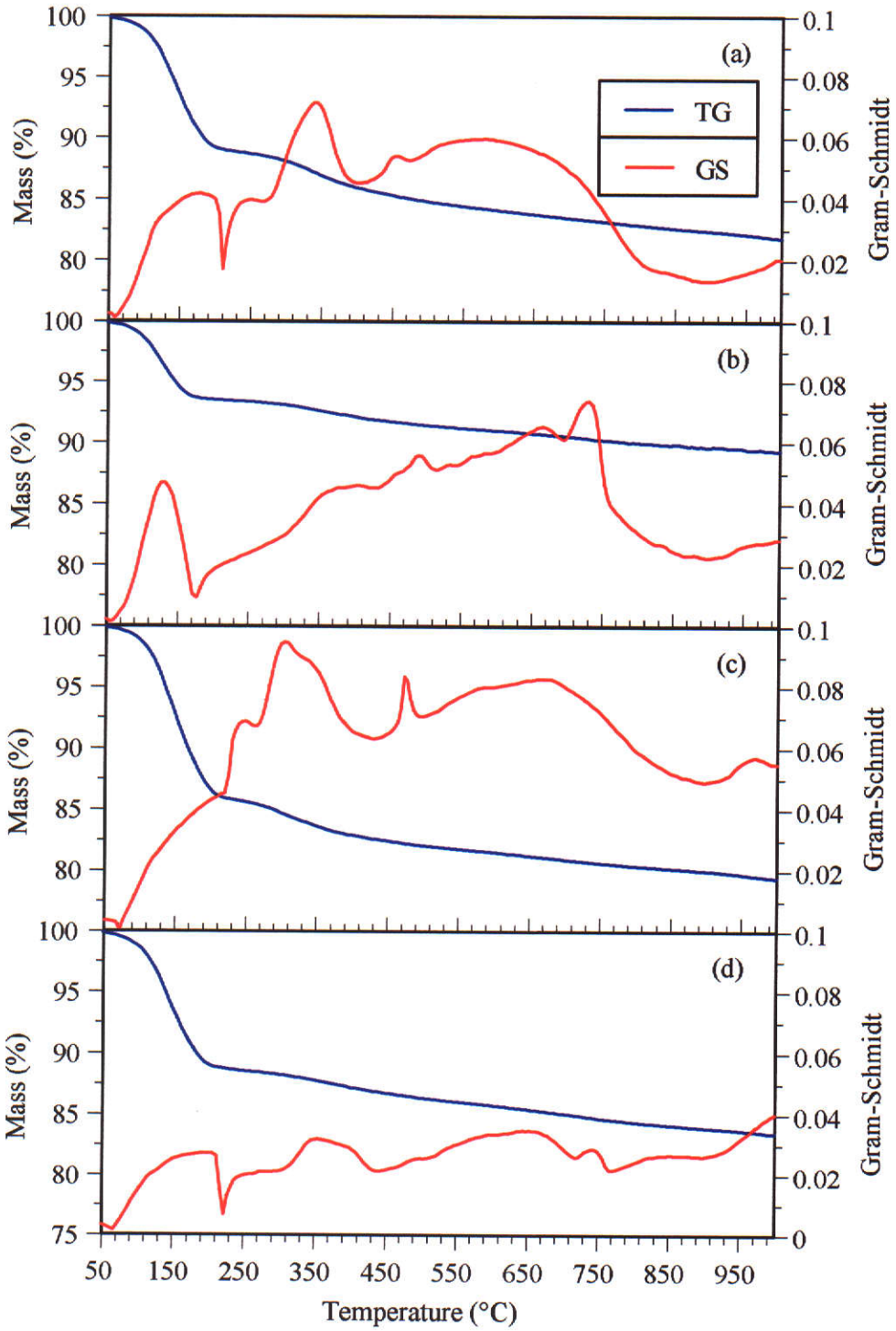

Figure 5.4: TG-GS curves of Three Mile Hill samples heated from ambient to 1000°C at 10°C min^{-1} in an argon atmosphere; (a) loaded, (b) barren, (c) acid washed, and (d) regenerated.

The infrared spectra from the first mass loss of each sample were similar and an example is shown in Figure 5.5. Figure 5.5 shows that the first mass losses were due to the evolution of water and carbon dioxide. Therefore the mass loss would depend on the water content of each sample. The source of carbon dioxide is not known, as comparison to a blank activated carbon shows no carbon dioxide evolving in this temperature range.

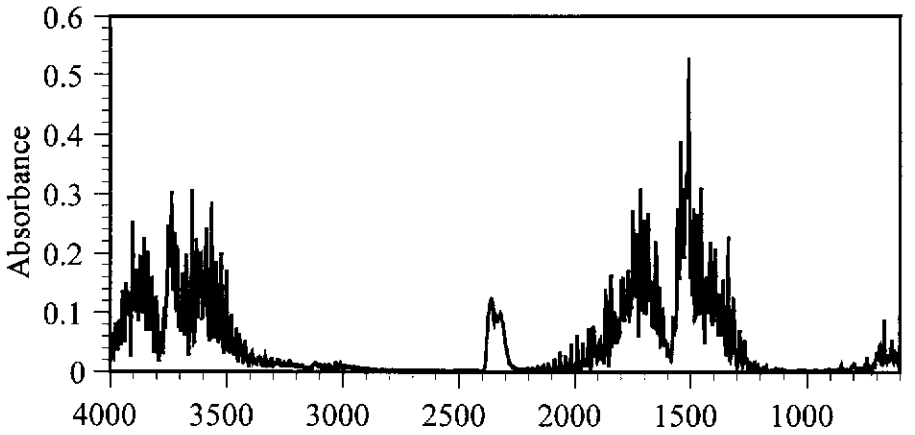

Figure 5.5: Typical infrared spectrum of the gases evolved from the first mass loss of a Three Mile Hill sample.

The infrared spectra of the second mass loss of each sample are presented in Figure 5.6. These spectra were taken from where the GS curve reached a peak during the second mass losses.

Figure 5.6 shows that the infrared spectra from the second mass loss of each sample were similar. Each displayed two small peaks at 3300-3400 cm^{-1}, these are probably due to N-H symmetric and asymmetric stretching (although C-H stretching of alkynes cannot be ruled out) (Socrates 1994). The small peaks at 3000-3100 cm^{-1} are due to C-H stretching of alkenes and the large peaks at 3000-2800 cm^{-1} are due to C-H stretching of alkanes (Morrison and Boyd 1992). The large peaks at 2400-2250 cm^{-1} are due to carbon dioxide evolution (Herzberg 1945) and the small peaks beside them at 2250-2150 cm^{-1} are most likely to the stretching of C≡N of inorganic cyanides (Socrates 1994). At 2100-2000 cm^{-1} are two peaks which are highly

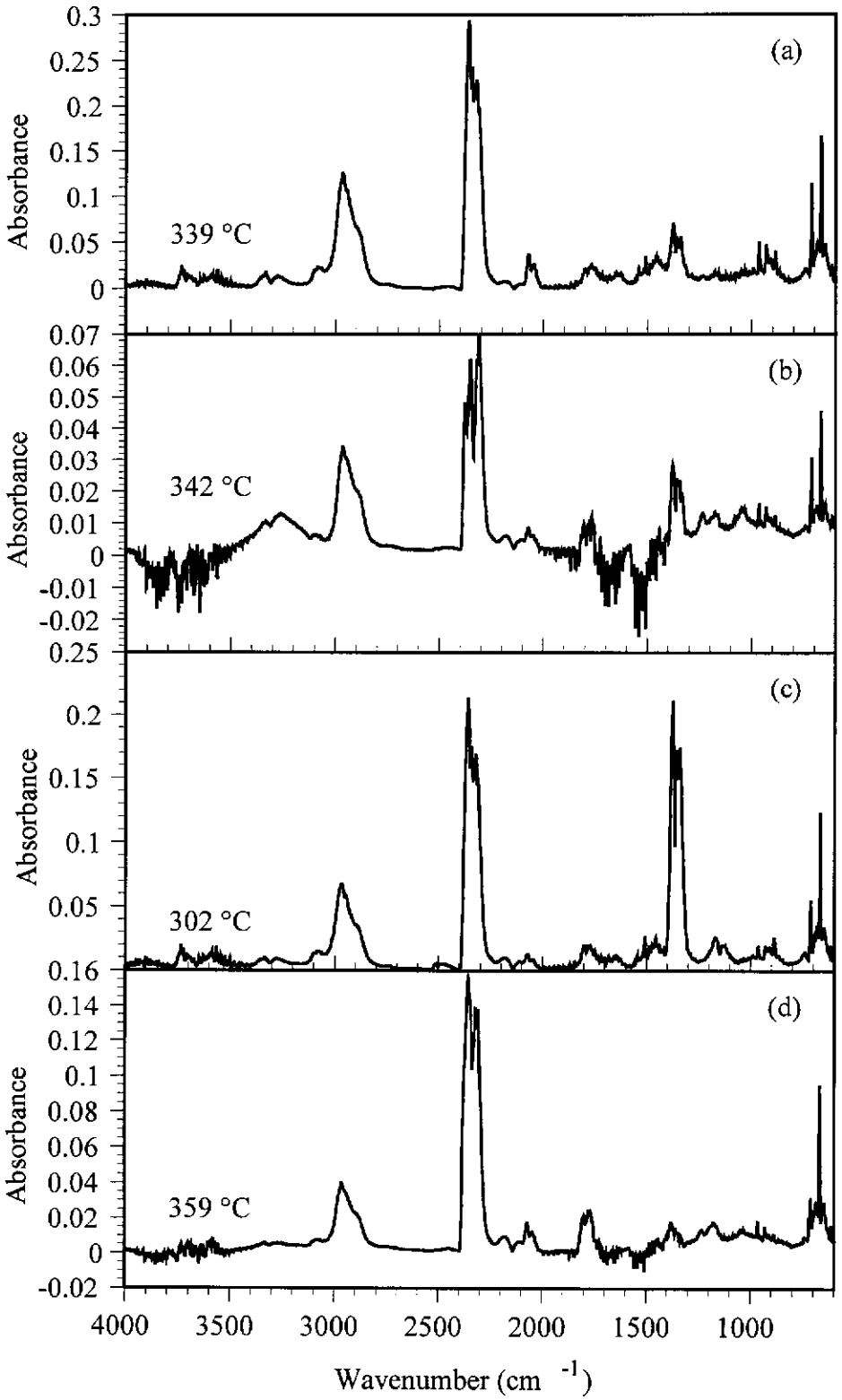

Figure 5.6: Infrared spectra of the second mass loss gases of the Three Mile Hill industrial samples; (a) loaded, (b) barren, (c) acid washed, and (d) regenerated.

characteristic of symmetric and asymmetric stretching of C=O in carbonyl sulfide (Kagann 1982; Herzberg 1945; Locker, Burkholder and Bair 1983). At 1750 cm^{-1} there is a small peak which is most prominent in the spectrum of the regenerated sample, and this is due to the stretching of a C=O (carbonyl) group. Below 1500 cm^{-1} it is difficult to identify most peaks in an infrared spectrum, especially when it is comprised of many different compounds. Besides the carbon dioxide peaks at 700-600 cm^{-1}, there is only one set of peaks that are prominent in this region at 1300-1400 cm^{-1}. These peaks are quite large in the spectrum of the acid washed sample, and their identity is unknown.

The evolution of carbonyl sulfide did not peak at the same temperature as the majority of the other gases, during the second mass loss of each sample. Instead carbonyl sulfide evolution peaked at 363, 393, 376, and 396°C for the loaded, barren, acid washed, and regenerated samples respectively. Inspection of the infrared spectra at the peak in evolution of carbonyl sulfide for each sample shows they were similar.

The infrared spectra of the third mass loss of each sample were similar and an example is shown in Figure 5.7. Figure 5.7 shows that the third mass losses were due to the evolution of carbon dioxide. Although calcium carbonate (a known inorganic foulant) adsorbed on activated carbon does decompose at 700-750°C to produce carbon dioxide (Jones et al 1988) there is no difference between the samples before and after acid washing. Also in this temperature range the blank activated carbon infrared spectra showed carbon dioxide evolution. This is due to the breakdown of the activated carbon as indicated in section 3.4.

Methane was also evolved for each sample during the third mass losses. This is also shown in Figure 5.7, where the very characteristic methane peak at 3015 cm^{-1} due to C-H stretching has been enlarged. The source of this peak is not known and does not appear in the blank activated carbon spectra. However it is suspected the methane may be a decomposition product of humates which decompose in this temperature range.

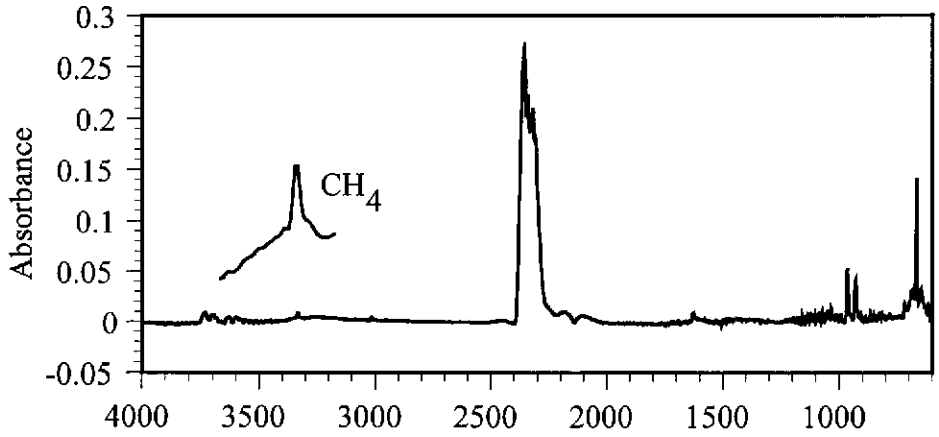

Figure 5.7: Typical infrared spectrum of the third mass loss gases of Three Mile Hill industrial samples.

Although only three mass losses are reported in Table 5.3, there may be in fact be four mass losses. This is because infrared spectra (above 810 °C) as shown in Figure 5.8 were observed for each sample. The infrared spectra of Figure 5.8 show that carbon dioxide is no longer the dominant gas evolved but now it is carbon monoxide (peaks at 2250-2000 cm^{-1}. The reason why it is not clear there is a fourth mass loss in Figure 5.4 is due to the weight loss being very small.

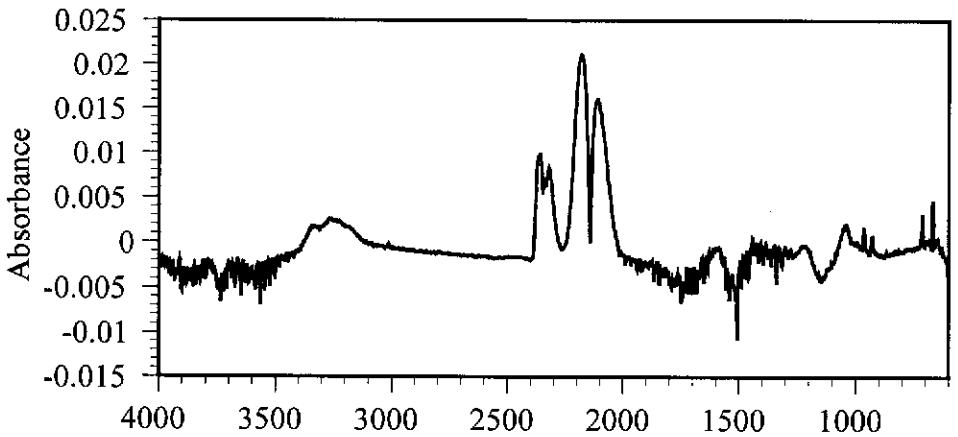

Figure 5.8: Typical infrared spectrum of the suspected fourth mass loss gases of Three Mile Hill industrial samples.

5.2 Salsigne

The samples taken from Salsigne in France were from the concentrate and tailings CIL circuits (after gold adsorption and after gold stripping for both circuits), and after thermal regeneration. These samples will be referred to as cloaded, cbarren (c = concentrate), tloaded, tbarren (t = tailings), and regenerated. The samples were treated in the same manner as the Three Mile Hill samples.

5.2.1 TD-py-GC-MS

The same conditions and treatment of data used for the Three Mile Hill samples were applied to the Salsigne samples. Typical total ion chromatograms for the samples are presented in Figures 5.9, 5.10, and 5.11. Presented in Table 5.4 is the identity of the peaks for each sample, along with their retention time (RT), and relative peak area.

A typical TIC of the cloaded sample (Figure 5.9a) displays at least 35 peaks (including CO_2/SO_2). After excluding peaks with areas less than 10 % of the largest peak, nine significant peaks were identified. The largest peak in the chromatogram was due to the presence of propanal, followed by butene, and 3-methyl-thiophene. A typical TIC of the cbarren sample (Figure 5.9b) displays at least 40 peaks (including CO_2/SO_2). After excluding minor peaks (with areas less than 10 % of the largest peak), thirteen significant peaks were identified. The largest peak in the chromatogram was due to the presence of propanal, followed by pentanol, and isoamyl alcohol. A typical TIC of the tloaded sample (Figure 5.10a) displays at least 41 peaks (including CO_2/SO_2). After excluding minor peaks, fourteen significant peaks were identified. The largest peak in the chromatogram was due to the presence of propanal, followed by pentanol, and isoamyl alcohol. A typical TIC of the tbarren sample (Figure 5.10b) displays at least 41 peaks (including CO_2/SO_2). After excluding minor peaks, nine significant peaks were identified. The largest peak in the chromatogram was due to the presence of propanal, followed by pentanol, and isoamyl alcohol. A typical TIC of the regenerated sample (Figure 5.11) displays at least 40 peaks (including CO_2/SO_2). After excluding minor peaks, eleven significant peaks were identified. The largest peak in the chromatogram was due to the presence of 2-pentene, followed by cyclopropane, and butene.

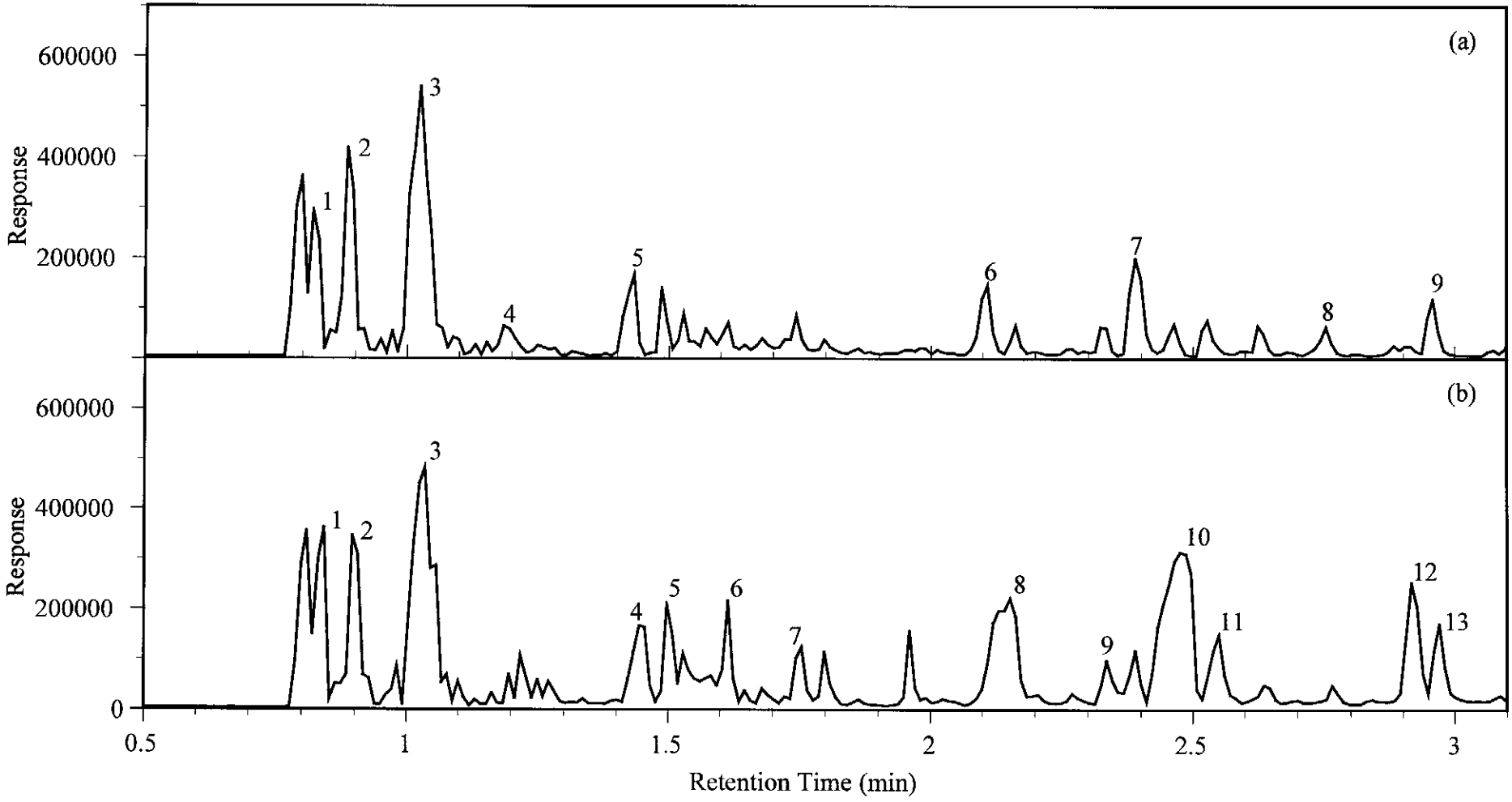

Figure 5.9: TD-py-GC-MS total ion chromatogram of (a) cloaded, and (b) cbarren samples from Salsigne heated at 25°C min^{-1} in an inert atmosphere.

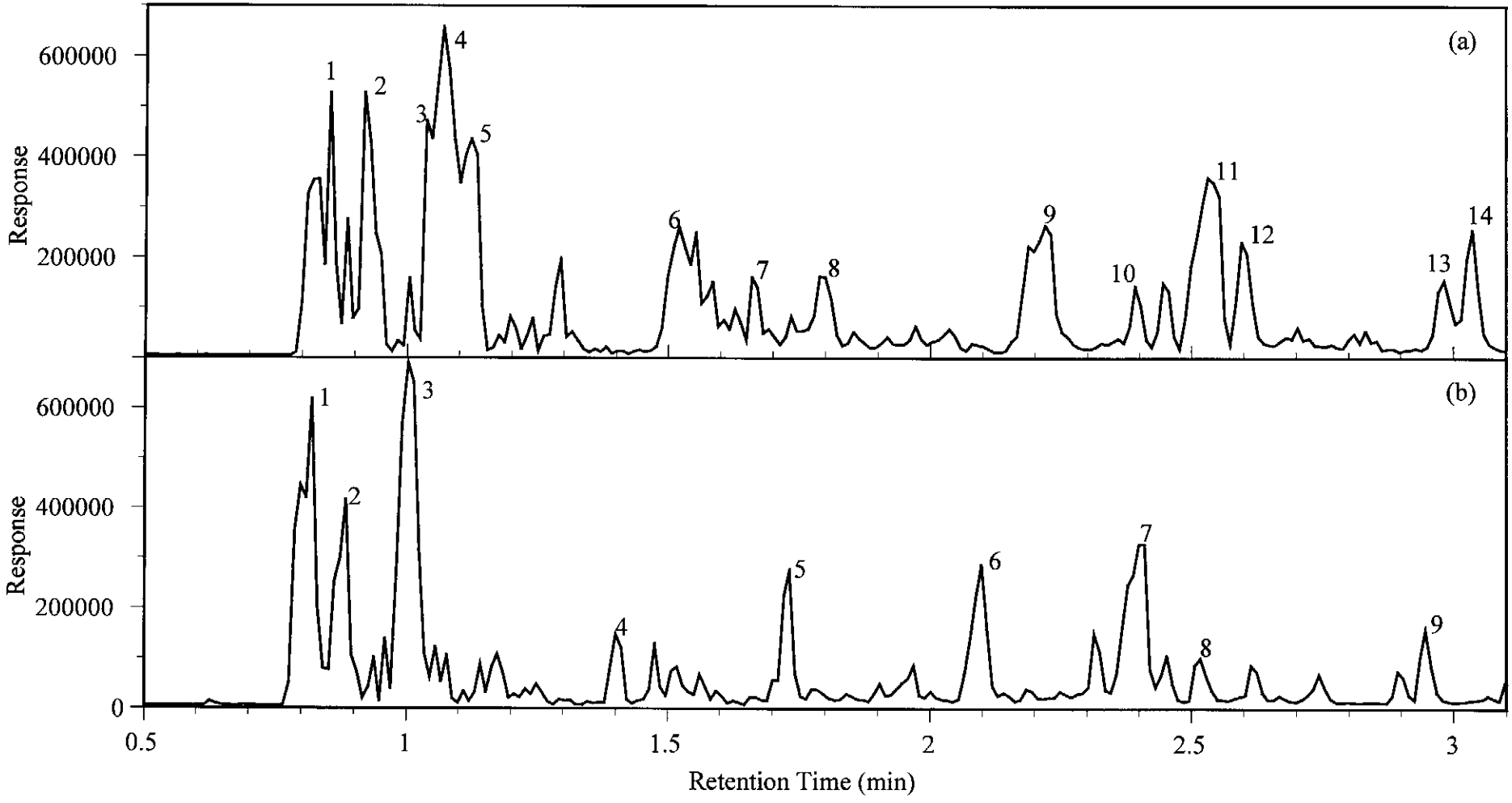

Figure 5.10: TD-py-GC-MS total ion chromatogram of (a) tloaded, and(b) tbarren samples from Salsigne heated at 25°C min^{-1} in an inert atmosphere.

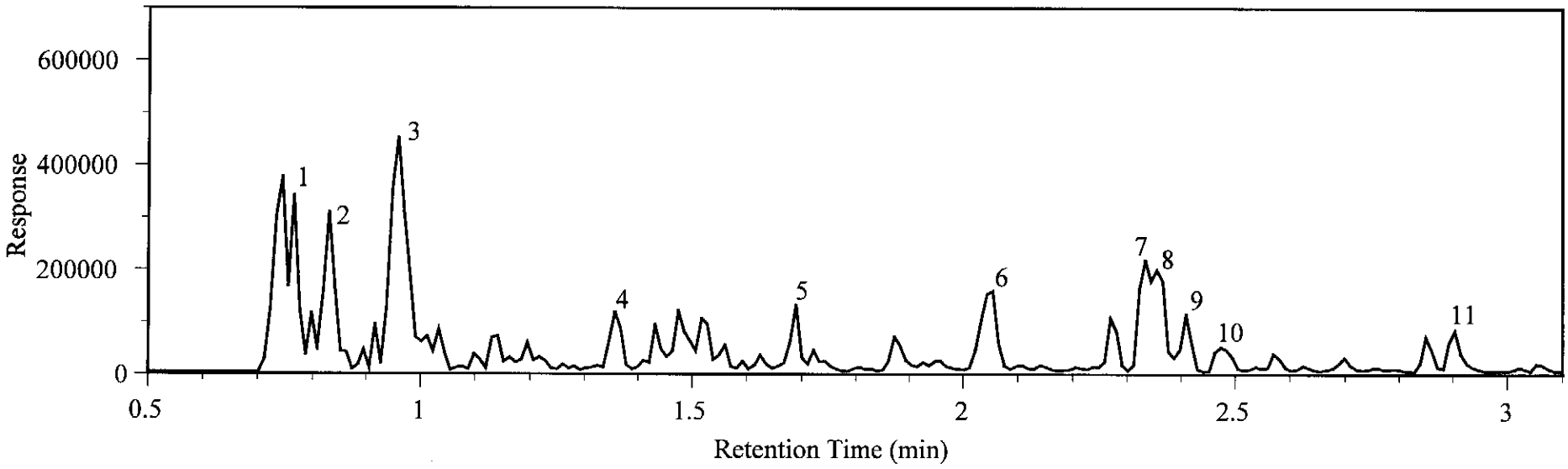

Figure 5.11: TD-py-GC-MS total ion chromatogram of the regenerated sample from Salsigne heated at 25°C min^{-1} in an inert atmosphere.

	Peak	RT (min)	Relative Peak Area (%)	Gas Evolved
Cloaded	1	0.82	8.91	cyclopropane
	2	0.89	16.8	butene
	3	1.02	36.2	propanal
	4	1.19	4.12	2-methyl-2-propanal
	5	1.43	7.73	isobutanol
	6	2.11	7.19	isoamyl alcohol
	7	2.39	10.5	3-methyl-thiophene
	8	2.53	3.74	2-ethyl-4-methyl-1,3-dioxolane
	9	2.96	4.87	2,5 and 2,6-dimethyl dioxene
Cbarren	1	0.84	6.64	cyclopropane
	2	0.90	8.07	butene
	3	1.03	20.4	propanal
	4	1.45	5.67	isobutanol
	5	1.50	4.09	2-butenal
	6	1.61	2.63	2-methyl-1-propanethiol
	7	1.75	2.32	pentenal
	8	2.15	12.1	isoamyl alcohol
	9	2.39	2.36	3-methyl-thiophene
	10	2.48	19.7	pentanol
	11	2.55	4.63	2-methyl-butanethiol
	12	2.92	7.45	pentanethiol
	13	2.97	4.00	2,5 and 2,6-dimethyl dioxene
Tloaded	1	0.85	4.37	cyclopropane
	2	0.92	8.74	butene
	3	1.04	8.40	ethylcyclopropane
	4	1.07	15.6	propanal
	5	1.12	10.6	ethanol
	6	1.52	6.05	isobutanol
	7	1.66	2.81	2-methyl-1-propanethiol
	8	1.79	4.11	pentenal
	9	2.22	10.1	isoamyl alcohol
	10	2.45	2.73	3-methyl thiophene
	11	2.54	13.6	pentanol
	12	2.60	5.37	2-ethyl-4-methyl-1,3-dioxolane
	13	2.98	3.05	pentanethiol
	14	3.04	4.36	2,5 and 2,6-dimethyl dioxene
Tbarren	1	0.82	10.3	cyclopropane
	2	0.88	12.3	butene
	3	1.00	32.4	propanal
	4	1.40	4.02	isobutanol
	5	1.73	5.93	pentenal
	6	2.10	10.5	isoamyl alcohol
	7	2.41	16.7	pentanol
	8	2.52	3.35	2-ethyl-4-methyl-1,3-dioxolane
	9	2.95	4.55	2,5 and 2,6-dimethyl dioxene
Regenerated	1	0.76	12.4	cyclopropane
	2	0.83	12.2	butene
	3	0.96	29.9	2-pentene
	4	1.36	5.64	isobutanol
	5	1.69	3.30	pentenal
	6	2.05	10.2	isoamyl alcohol
	7	2.34	4.60	2-methyl thiophene
	8	2.36	10.2	pentanol
	9	2.41	4.31	3-methyl thiophene
	10	2.48	3.74	2-ethyl-4-methyl-1,3-dioxolane
	11	2.91	3.50	2,5 and 2,6-dimethyl dioxene

Table 5.4: Gases evolved from the pyrolysis of the Salsigne samples.

Comparison of the TICs in Figures 5.9a, 5.9b, 5.10a, 5.10b, and 5.11 show they are very similar and the gases evolved elute very close together. For each analysis evolution of cyclopropane, butene, isobutanol, isoamyl alcohol, 2,5 and 2,6-dimethyl dioxene were common for each sample. There were also were many other evolved gases that were common for at least 3 analyses. In some cases certain gases may not have been observed due to the close retention time of the gases.

The largest peak in the all the chromatograms except the regenerated sample was due to the evolution of propanal.

5.2.2 TG-MS and TG-FTIR

The thermal decomposition of the five samples was studied by TG-EGA using the same conditions as applied to the Three Mile Hill samples. The TG curve of each sample exhibited four mass losses. The mass losses and their corresponding temperature ranges are presented in Table 5.5.

	Sample (%)				
Mass Loss	**Cloaded**	**Cbarren**	**Tloaded**	**Tbarren**	**Regenerated**
First (amb.-215°C)	1.31	4.61	8.21	6.63	11.2
Second (215-542°C)	4.59	4.57	6.37	4.00	2.44
Third (542-774°C)	2.11	1.31	1.98	1.31	1.67
Fourth (774-1000°C)	0.56	0.54	0.58	0.67	0.56
Total	8.57	11.0	17.1	12.6	15.9

Table 5.5: Mass losses and their corresponding temperature ranges for cloaded, cbarren, tloaded, tbarren, and regenerated activated carbon samples from Salsigne.

As seen in Table 5.5 there was no trend observed between the samples for the first, third and fourth mass losses. However the second mass loss of the concentrate and

tailings samples were similar; while the regenerated sample mass loss was approximately half that of the other samples.

The SIM mode of the MS was used to monitor molecular ions of the gases identified in the TD-py-GC-MS from ambient to 1000°C. An ion chromatogram was produced for each evolved gas. Typical ion chromatograms for the decomposition of the cloaded sample are presented in Figures 5.12a and 5.12b, along with its mass loss curve. Ion chromatograms are not presented for the other samples as they were very similar to Figures 5.12a and 5.12b.

A comparison of the relative percent peak area of each gas evolved for each sample is presented in Table 5.6 (same treatment of data as for Table 5.3).

amu	Gas	Relative Peak Area (%)				
		A	B	C	D	E
42	cyclopropane	50.4	62.0	61.0	52.8	61.3
46	ethanol	8.70	3.90	7.79	4.29	2.65
56	butene	16.2	11.4	11.0	13.8	11.1
58	propanal	14.9	13.0	10.5	16.0	15.0
70	2-methyl-2-propanal 2-butenal ethylcyclopropane 2-pentene	6.44	7.35	7.36	9.29	6.52
74	isobutanol	0.56	0.48	0.50	0.57	0.42
86	pentenal	0.27	0.24	0.21	029	0.25
88	isoamyl alcohol pentanol	0.08	0.06	0.07	0.08	0.06
90	2-methyl-1-propanethiol	0.15	0.16	0.19	0.26	0.16
98	3-methyl thiophene	1.89	1.21	1.08	2.19	2.27
104	2-methyl-butanethiol pentanethiol	0.08	0.09	0.09	0.14	0.10
114	2,5 and 2,6-dimethyl dioxene	0.19	0.10	0.10	0.17	0.06
116	2-ethyl-4-methyl-1,3-dioxolane	0.12	0.05	0.10	0.10	0.05

Table 5.6: Relative peak areas of the evolved gases from the Salsigne samples heated at 10°C min^{-1} in argon atmospheres (A = cloaded, B = cbarren, C = tloaded, D = tbarren, E = regenerated).

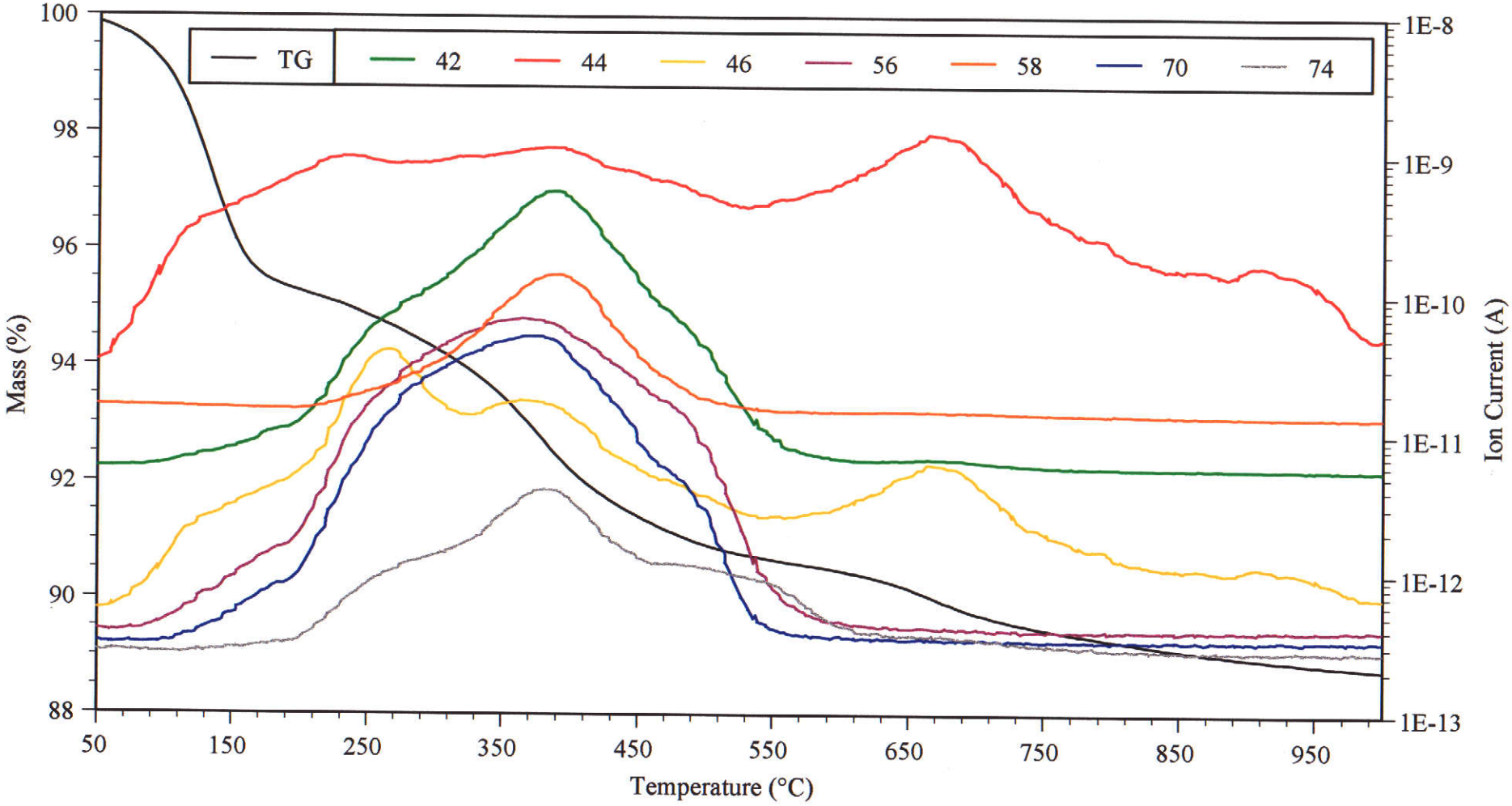

Figure 5.12a: Ion chromatograms of the evolved gases for the decomposition of the cloaded sample from Salsigne heated at 10°C min^{-1} in an argon atmosphere.

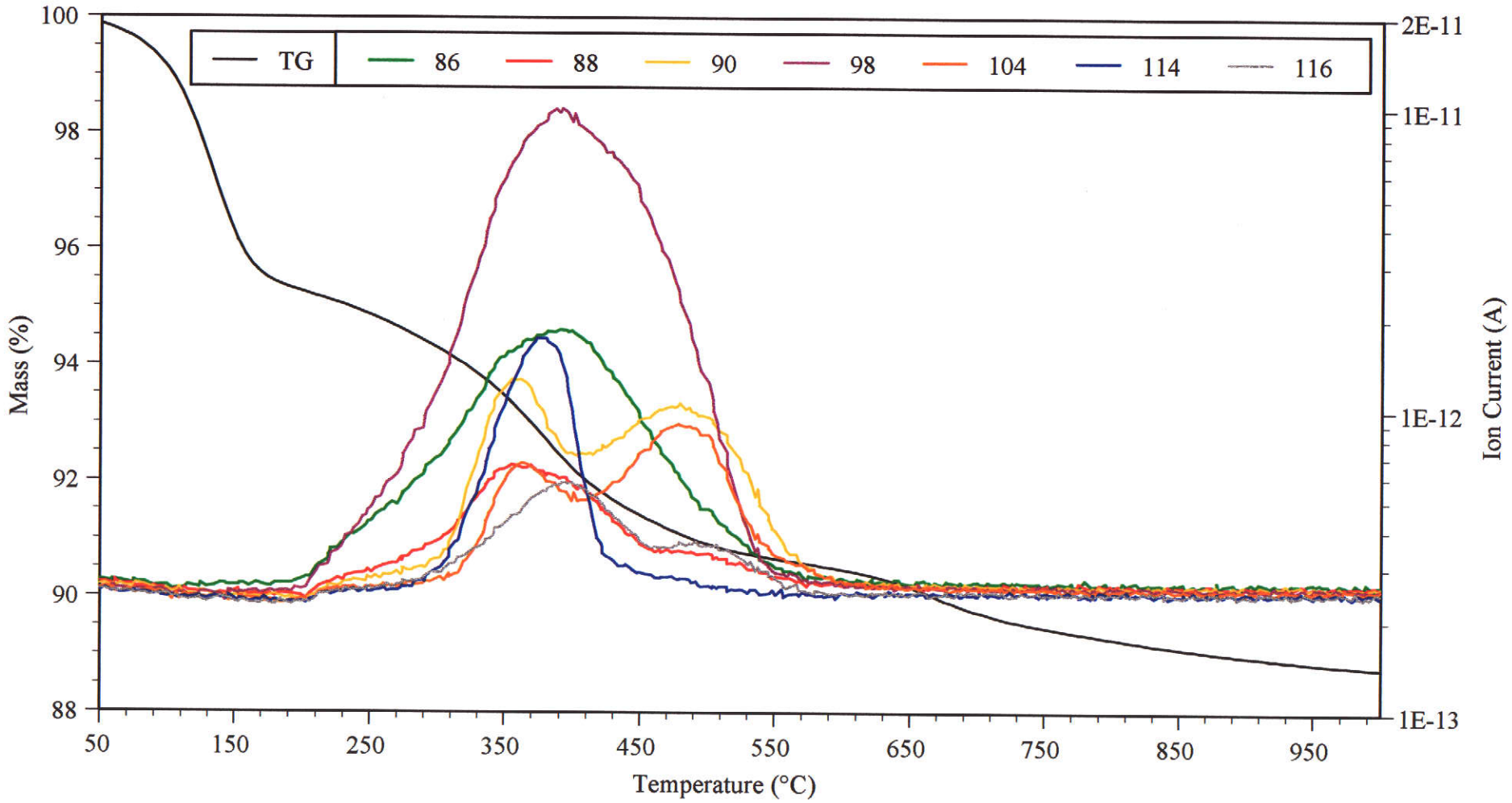

Figure 5.12b: Ion chromatograms of the evolved gases for the decomposition of the cloaded sample from Salsigne heated at 10°C min^{-1} in an argon atmosphere.

Although the ion chromatograms displayed in Figures 5.12a and 5.12b occur over the same temperature range (during the second mass loss), the peak in evolution of the chromatograms varies. The ion chromatograms of amu 42, 58, 86, 98, and 116 showed a peak at 390°C; amu 56, 70, and 114 at 360°C; amu 74 at 380°C, amu 88 at 350°C. Ion chromatograms of amu 90 and 104 displayed two peaks at 350°C and 480°C. The ion chromatogram of amu 46 displayed 3 peaks at 260, 370, and 670°C, although this last peak is probably due to evolution of some gas other than ethanol.

Assuming that the ion signal contribution of fragment ions to the amu is very small, cyclopropane has the largest relative peak area for all samples. Propanal and then butene showed the next largest relative peak areas. All other gases monitored above amu 74 had small peak areas in comparison.

The TG-GS curves for the FTIR analysis of evolved gases from the activated carbon samples are presented in Figure 5.13a and 5.13b.

The infrared spectra from the first mass loss for each sample were all similar and displayed peaks due to water and carbon dioxide (similar to Figure 5.5). The source of the carbon dioxide is not known.

The infrared spectra from the second mass loss for each sample were also similar and they show this is the region where most organic fouling agents decompose. The infrared spectra of gases evolved for the concentrate and tailings samples are presented in Figure 5.14a, and for the regenerated sample in Figure 5.14b (spectra were taken at the peak in the GS curve during the second mass loss).

Figures 5.14a and 5.14b show that the second mass loss infrared spectra were all similar. These are also similar to those observed in the TG-FTIR analysis of the Three Mile Hill samples. Thus assignment of the peaks will not be repeated here as they are the same as for the Three Mile Hill decomposition sample spectra. The only significant difference to the Three Mile Hill spectra are the higher absorbances observed in the 3000-3100 cm^{-1} region and the carbonyl peak at 1750 cm^{-1}.

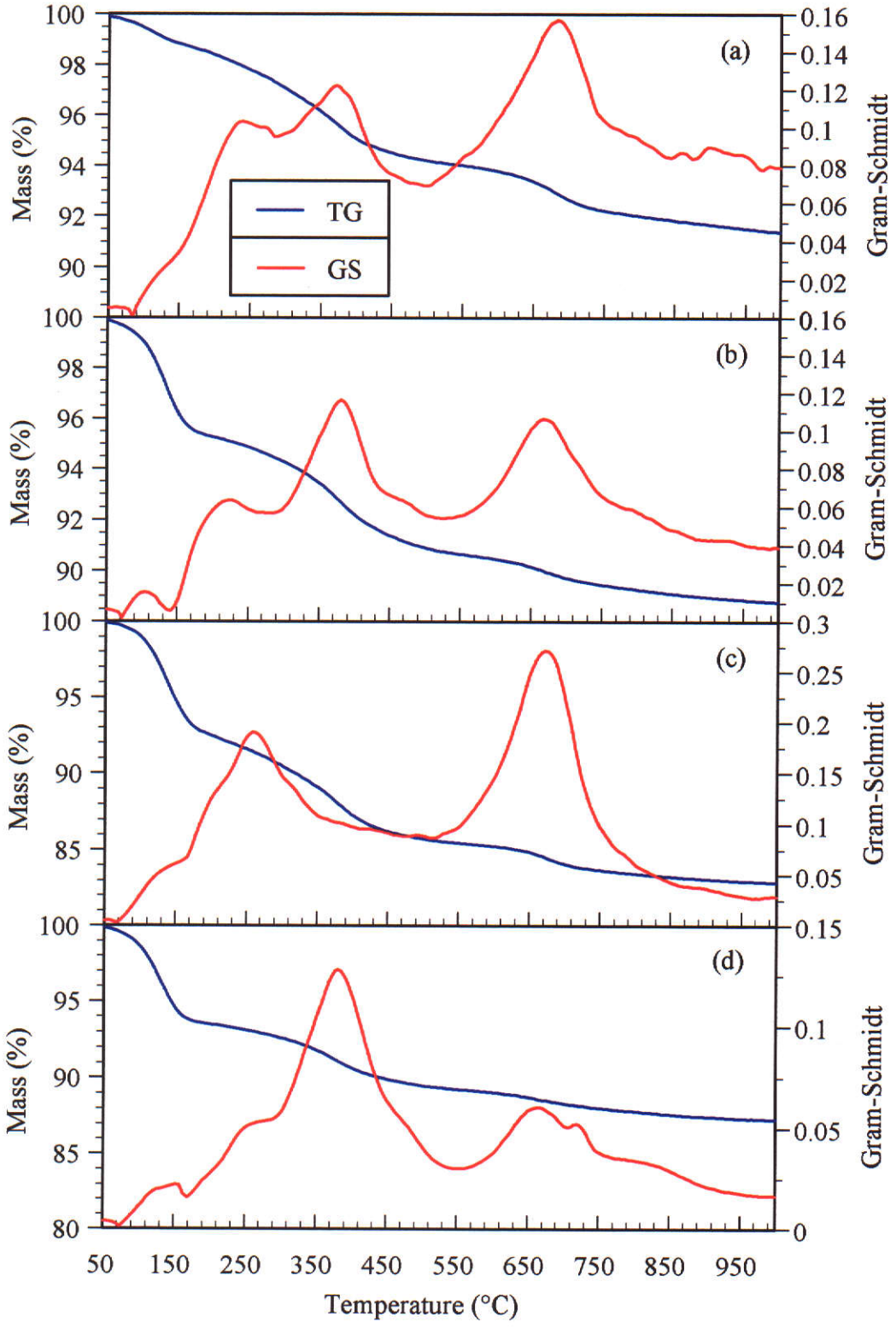

Figure 5.13a: TG-GS curves of Salsigne samples heated from ambient to 1000°C at 10°C min^{-1} argon atmospheres; (a) cloaded, (b) cbarren, (c) tloaded, and (d) tbarren.

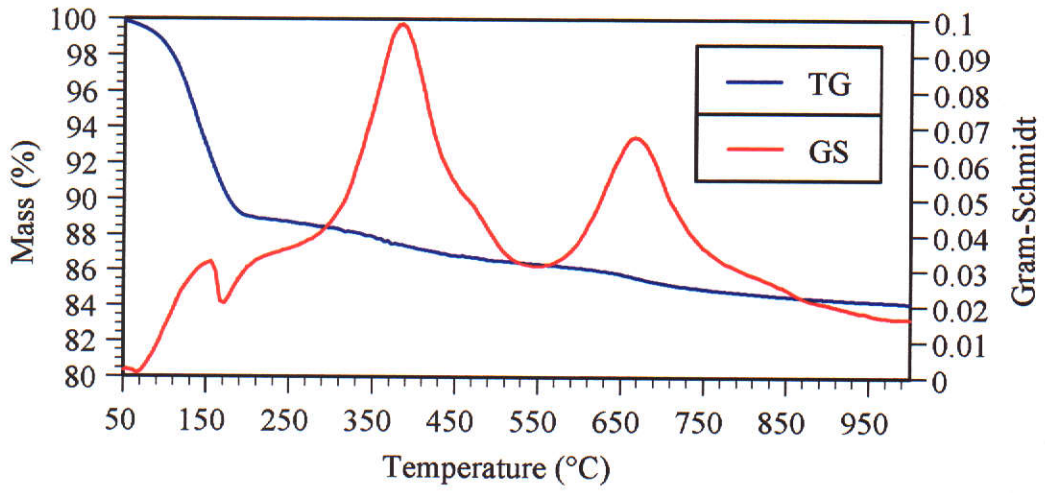

Figure 5.13b: TG-GS curves of Salsigne regenerated sample heated from ambient to 1000°C at 10°C min^{-1} in an argon atmosphere.

During the second mass loss the evolution of carbonyl sulfide did not peak at the same time as the other gases. Table 5.7 shows the temperatures where carbonyl sulfide evolution peaked and the temperature between these two peaks when it was at its lowest abundance. The regenerated sample displayed only one peak at 358°C.

	Temperature (°C)		
	First Maxima	**Minima**	**Second Maxima**
cloaded	245	296	375
cbarren	261	307	344
tloaded	249	306	331
tbarren	263	309	347

Table 5.7: Maximum and minimum temperatures of carbonyl sulfide evolution during the second mass loss of each Salsigne activated carbon sample.

The infrared spectra of the third mass loss of each sample were similar to that of Figure 5.7 showing evolution of carbon dioxide. Again this could be due to carbonate decomposition and/or activated carbon decomposition. Typical infrared spectra are not displayed for the fourth mass loss as only carbon monoxide was evolved for each sample (similar spectra seen in Figure 5.8).

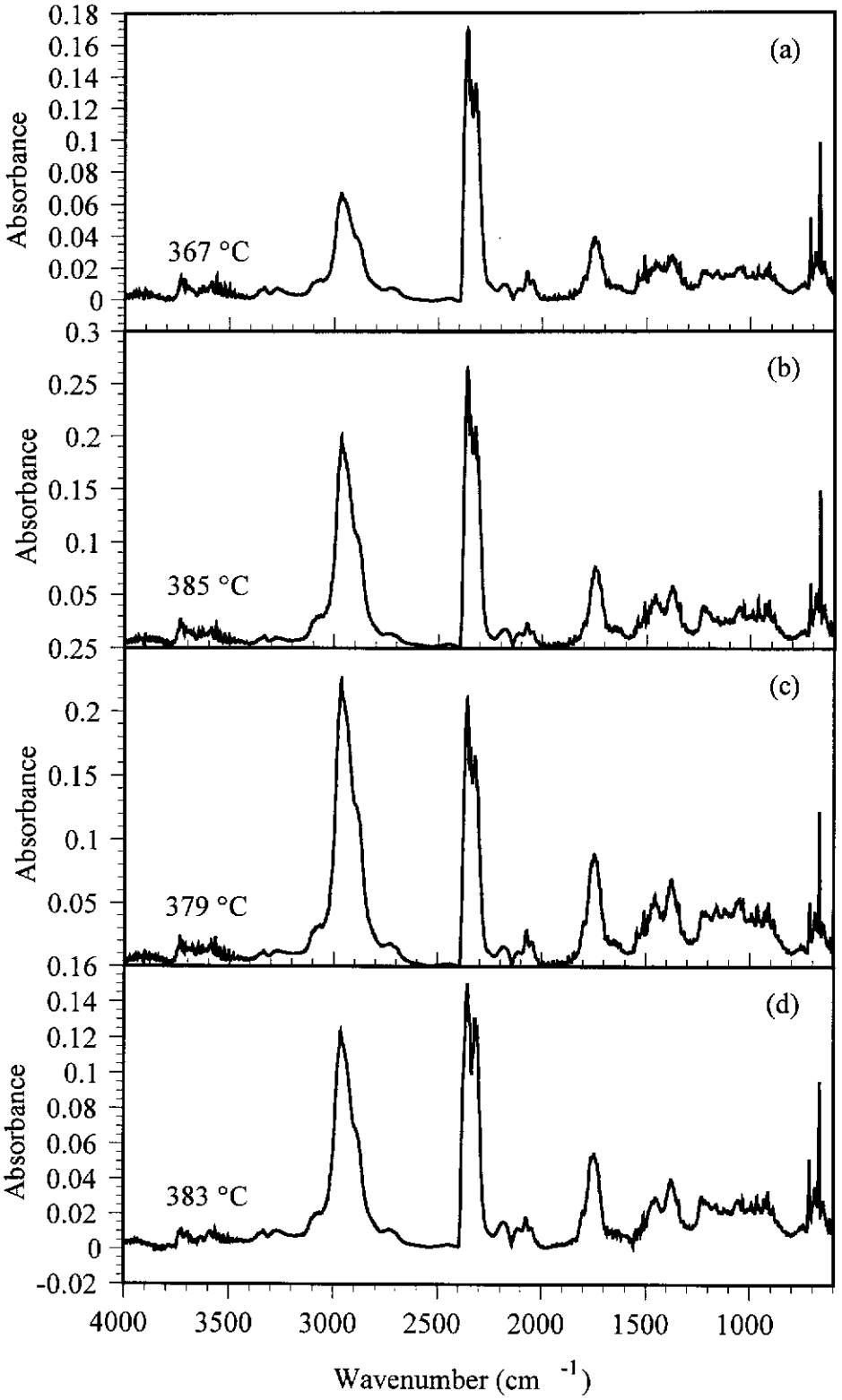

Figure 5.14a: Infrared spectra of the second mass loss evolved gases from the Salsigne concentrate and tailing samples (a) cloaded, (b) cbarren, (c) tloaded, and (d) tbarren.

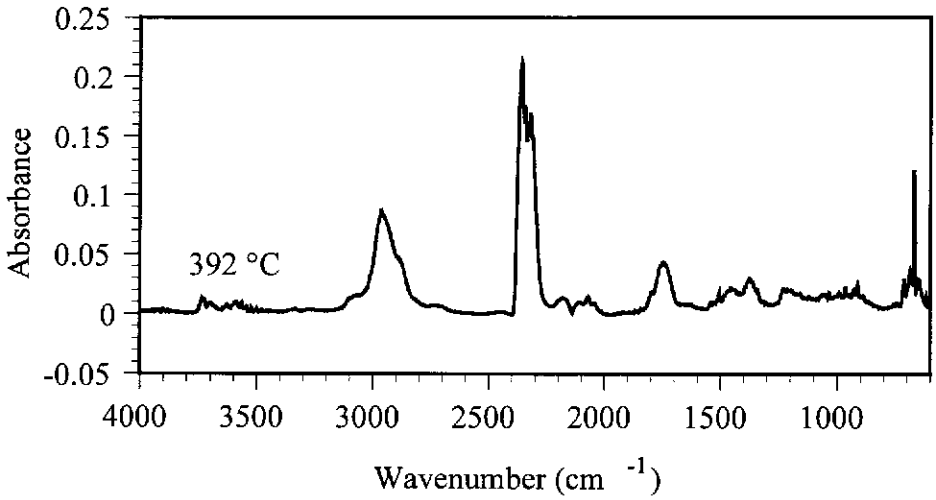

Figure 5.14b: Infrared spectra of the second mass loss evolved gases from the Salsigne regenerated sample.

5.3 Summary

Two sets of samples from industrial gold processing plants were subjected to the same analysis methods used in Chapters 3 and 4, and their evolved gas profiles determined as a function of temperature. Comparisons of the evolved gases from the industrial samples were made with the pure systems, in order to identify any residual fouling agents on the industrial samples.

Comparison of the relative peak areas (%) of the Three Mile Hill samples shows for the TD-py-GC-MS analyses butanol was evolved in the greatest amount (except for the regenerated sample where butene had the largest relative peak area). In the TG-MS analyses butene (amu 56) had the largest relative peak area for all samples. One decomposition gas that was not identified in the TD-py-GC-MS or TG-MS analyses was carbonyl sulfide. Carbonyl sulfide was only identified by the TG-FTIR analyses.

The evolution of butanol and butene from a specific foulant could not be related back to the information obtained in Chapters 3 and 4. Thus the source of these gases cannot be determined from the current study, except to state that they are probably not derived from either flotation or frothing reagents. However, in Chapter 3 it was

established that between approximately 150-400°C the detection of carbonyl sulfide and carbon disulfide indicates the presence of xanthate fouling. Thus the detection of carbonyl sulfide at approximately 360-400°C for the decomposition of the Three Mile Hill samples probably indicates xanthate fouling. Although this temperature region is higher than for the synthetic samples, it may be due to other adsorbed fouling agents blocking the activated carbon pore system until they are decomposed, which then releases the COS, or due to differences in the type of activated carbon used. Some increase in temperature would be due to the size of the sample used for the industrial samples (approximately 1000 mg) compared to the 10 mg samples used for the samples prepared in the laboratory. That is, TG curves will shift to higher temperatures with the use of higher masses.

The decomposition of xanthates produces carbon disulfide and carbonyl sulfide. Because no carbon disulfide was detected for the industrial samples, samples were prepared of activated carbon containing approximately 1 and 0.1 % w/w of sodium ethyl xanthate. When 1000 mg samples of these were analysed by TG-FTIR, only carbonyl sulfide was detected in the evolved gas and no carbon disulfide. Thus for the Three Mile Hill samples the amount of xanthate fouling must be very low. These samples also showed that the analysis of 1000 mg samples shifted the maximum temperature of evolution for COS up to 330°C. Thus larger, more dilute samples shift the temperature by approximately 130°C compared to the saturated samples studied in Chapter 3. Also only one maxima for carbonyl sulfide evolution is observed in samples with less xanthate adsorbed compared to three for the saturated samples.

By comparing the data for the acid washed and regenerated samples, comments can be made on the efficiency of the thermal regeneration step on the Three Mile Hill plant. In the TD-py-GC-MS analysis there were no significant differences between the gases evolved for the acid washed and regenerated samples. In the TG analysis, the second mass loss (where the thermal decomposition of organic fouling agents mainly occurs) for the regenerated sample was only 1.33 % lower than for the acid washed sample mass loss. The MS data of the acid washed and regenerated samples are also similar; the main difference is thiophene, with a relative peak area ten times

greater for the regenerated sample decomposition. The FTIR data are only different where the unassigned peaks in the 1300-1400 cm^{-1} region in the acid washed decomposition spectra are barely visible in the regenerated decomposition spectra. Thus these comparisons indicate the thermal regeneration process on the plant has not oxidised or volatised the amount of organic fouling agents adsorbed on the carbon to any significant extent.

Comparison of the relative peak areas (%) of the Salsigne samples shows for the TD-py-GC-MS analyses propanal was evolved in the greatest amount (except for the regenerated sample where 2-pentene had the largest relative peak area). In the TG-MS analyses cyclopropane (amu 42) had the largest relative peak area for all samples (however this is most likely due to ion signal overlapping of fragment ions since it is at such a low amu). Also carbonyl sulfide was evolved, which was only detected by TG-FTIR.

In Chapter 4 it was established that between approximately 250-350°C the detection of propanal indicated frothing agent fouling. Thus detection of propanal at approximately 370°C for the decomposition of the Salsigne samples indicates fouling by a frothing agent. Again the higher temperature observed for propanal evolution could be due to any of the reasons outlined previously for the Three Mile Hill samples. As with the Three Mile Hill samples detection of carbonyl sulfide for the Salsigne samples indicating xanthate fouling.

Comments on the efficiency of the thermal regeneration step on the Salsigne plant is slightly more difficult as no acid washed sample was obtained (if in fact an acid washing step is employed on the plant). Comparisons then have to be made between the cbarren and tbarren samples with the regenerated sample. In the TD-py-GC-MS analyses of the cbarren and tbarren samples, propanal and pentanol had the largest relative peak areas; while in the analysis of the regenerated sample 2-pentene had the largest relative peak area. This could be due to an acid washing step, as dehydration of an alcohol to an alkene is achieved by the application of heat and an acid (although in general organic chemistry sulfuric or phosphoric acid is used) (Morrison and Boyd 1992).

Comparison of the second mass losses in the TG curves reveals that the regenerated sample mass loss is approximately half that of the cbarren and tbarren samples. The MS data was similar for all the samples analysed, therefore no comparison can be made. The FTIR spectra showed that after regeneration the alkane/alkene stretching peaks and the carbonyl peak decrease (when compared to the CO_2 peak, assuming this must stay relatively the same). Also the evolution of carbonyl sulfide no longer produces 2 peaks after thermal regeneration as the first peak around 250°C no longer appears. This indicates the source of carbonyl sulfide has been oxidised or volatised to some degree. In general these analyses have shown the thermal regeneration process on the plant has only slightly oxidised or volatised the amount of organic fouling agents adsorbed on the carbon. Thus the regeneration circuit on the Salsigne plant is not very efficient in destroying unwanted organic fouling agents.

CHAPTER 6

CONCLUSION

6.0 Conclusion

The main aim of this work was to develop thermal methods of analysis that could be used to identify the fouling agents adsorbed on activated carbon samples from gold processing plants. The techniques used were TD-py-GC-MS, TG-MS, and TG-FTIR. When the adsorbed agents were decomposed, a complex gas mixture was evolved, and hence TD-py-GC-MS was the only method that could be used to unambiguously identify the individual gases. The information from this technique could then be used to identify the gases evolved from experiments carried out with TG-MS and TG-FTIR techniques. These last two techniques provided information on the temperature ranges over which the fouling agents decomposed, as well as quantitative mass loss data. Consequently the three different methods provided different kinds of complementary and interdependent information.

The organic fouling agents studied by the three techniques were xanthates and frothing agents used as flotation reagents in gold plants.

The thermal decomposition of the xanthates, SEX, SiBX, PEX, and PAX adsorbed on activated carbon each produced two major, slightly overlapping mass losses at approximately 140-230°C and 210-290°C. The most significant gases evolved during the first and second mass losses were carbon disulfide and carbonyl sulfide respectively. Compared to the pure xanthates the activated carbon appeared to have little effect on the their thermal decomposition. The main difference was the abundance of carbon disulfide resulting from hydrolysis of the xanthates by water trapped in the pores of the activated carbon.

The thermal decomposition of the frothing agents PPG, PPGME, α-terpineol and MiBC adsorbed on activated carbon each produced one mass loss. The temperature range for the decomposition of PPG, PPGME and α-terpineol all occurred in the same region at approximately 260-360°C. The most significant gas evolved during the decomposition of these three reagents was propanal. Compared to the pure frothing agents, which all essentially boiled off unchanged, the activated carbon had a significant effect on their thermal decomposition, altering the gases evolved and

thus the type of reactions occurring. On the other hand, MiBC boiled off unchanged in both the pure and adsorbed states.

The thermal decomposition of activated carbon samples from the Three Mile Hill plant showed organic fouling agents decomposed at approximately 220-510°C. Compared to the pure xanthates adsorbed on activated carbon, only a minor quantity of carbonyl sulfide evolved, reaching a maximum at 380°C. This was approximately 100°C higher than that observed for the pure xanthates adsorbed on activated carbon. However, further experiments showed a 130°C increase in the maximum temperature of carbonyl sulfide evolution for activated carbon samples with a very small amount of xanthate adsorbed. Thus for the Three Mile Hill samples it was concluded that xanthate fouling was very low. In addition, there was no evidence of contamination by frothing agents.

Similar to the Three Mile Hill samples, organic fouling agents adsorbed on activated carbon from Salsigne decomposed at approximately 215-540°C. In this region maximum carbonyl sulfide evolution was observed at approximately 250 and 350°C, while maximum propanal evolution was observed at approximately 380°C. The evolution of carbonyl sulfide at 250°C compared well to that observed for the pure xanthate xanthates adsorbed on activated carbon. The evolution of carbonyl sulfide at 350°C was similar to that observed in the Three Mile Hill samples. Also propanal evolved at 370°C in the same temperature region (250-350°C) where the frothing agents adsorbed on activated carbon (except MiBC) decomposed to produce propanal. Therefore for the Salsigne activated carbon samples it can be concluded a xanthate and a frothing agent have fouled the carbon.

Thus the comparison of synthetically fouled activated carbon and industrial samples has proved that the thermal methods employed in this study can be used to identify individual organic fouling agents. Additionally, it can be seen that the methods also allow additional assessment as to the efficiency of plant regeneration. Thus the plant operator should be able to use this information to determine what fouling agents are of significant importance on the plant and take steps to minimise their migration to the CIP or CIL circuit.

A comparison of the thermal analysis techniques in terms of gas identification, mass loss information, gas evolution temperature, and gas quantification is presented in Table 6.1.

	TD-py-GC-MS	TG-MS	TG-FTIR
Gas identification	YES	NO	YES/NO
Mass loss	NO	YES	YES
Gas evolution temperature	NO	YES	YES
Gas quantification	NO	NO	NO

Table 6.1: Advantages and limitations of TD-py-GC-MS, TG-MS, and TG-FTIR techniques for thermal analysis of organic fouling agents on activated carbon.

Only the TD-py-GC-MS technique was able to unambiguously identify the gases evolved. However, the technique did not give any mass loss data, temperatures of gas evolution or gas quantification. Also it appears the type gases evolved are affected by their cold trapping after pyrolysis and before subsequent heating of the GC column. That is, during this part of the analysis, gases in the liquid state have sufficient time and possibility of reacting with one another. Thus this technique cannot be used for the quantitative determination of products evolved directly from the decomposing reagents.

It was not possible to identify any new gases using the TG-MS technique, as the only information obtained from the mass spectrometer were ion signals from molecular, fragment, and isotope ions of the gases evolved. It was possible to monitor the ion signals of the molecular ions from evolved gases as a function of temperature. However, the molecular ion signals were affected by overlapping fragment and/or isotope ion signals. Thus quantification was not possible. Finally, the use of the technique relied on previous identification of the gases by TD-py-GC-MS. Although this TG-MS did not permit organic foulant identification, in the future, software may be developed which can unravel the mass spectra of coevolving gases (Raemaekers and Bart 1997).

The TG-FTIR technique allowed identification of gases with characteristic infrared absorption frequencies such as carbonyl sulfide and carbon disulfide, and in fact was found to be the most sensitive technique in this work for the identification of these gases. Also it allowed identification of groups of gases containing functional groups with characteristic infrared absorption frequencies such as propanal. Thus it was possible to monitor the temperature of evolution of these gases using their characteristic absorption frequencies. Although quantification has been reported in the literature for TG-FTIR it was not investigated.

Although Table 6.1 suggests that the best technique to identify organic fouling agents on activated carbon is TG-FTIR, the TD-py-GC-MS technique must be used as well. For example, although the TG-FTIR Salsigne analysis of the samples produced characteristic absorption frequencies for propanal (indicating frothing agent fouling), propanal was only unambiguously identified by TD-py-GC-MS analysis. Therefore further research in this area should be the insertion of a GC between the TG and MS, so that the TD-py-GC-MS (which introduces other variables) does not have to be used. Hence all three methods have their strengths and weaknesses, and no one technique alone can provide all the necessary information. However, in combination, the methods provide a wealth of information concerning the status of activated carbon in gold processing plants.

REFERENCES

REFERENCES

A.C.T.E.D. Pty Ltd 'Activated Carbon for Gold Processing in Australia', [Online]. Available: http://www.acted.au/ [1998, Feburary 19].

Amicarelli, V., Baldassarre, G. and Liberti, L. (1979) 'Thermoanalytical Study of Activated Carbon Regeneration I. Desorption of Phenol and Aniline', Thermochimica Acta, 30:247-253.

Bansel, R.C., Donnet, JB., and Stoeckli, F. (1988) Active Carbon, Marcel Dekker, Inc., New York.

Bax, A.R. and Bax, A.C. (1993) 'Gold Ore Treatment by Goldfan Ltd at Three Mile Hill, Coolgardie, WA', The Sir Maurice Mawby Memorial Volume, (2nd ed) 2 (19):958-966.

Bellamy, L.J. (1975) The Infrared Spectra of Complex Molecules, Chapman and Hall, London.

Bodsworth, C. (1994) The Extraction and Refining of Metals, CRC Press, London.

Boehm, H.P. (1994) 'Some Aspects of the Surface Chemistry of Carbon Blacks and Other Carbons', Carbon, 32 (5) 759-769.

Cavell, K.J., Sceney, C.G., Hill, J.O. and Magee, R.J. (1973) 'Thermal Studies on Nickel Alkyl Xanthate Complexes', Thermochimica Acta, 5:319-328

Chartoff, R.P. (1997) 'Thermoplastic Polymers' in *Thermal Characterization of Polymeric Materials, (2nd ed) vol. 1*, eds E.A. Turi, Academic Press, San Diego.

Cookson, J.T. (1978) 'Adsorption Mechanisms: The Chemistry of Organic Adsorption On Activated Carbon' in *Carbon Adsorption Handbook*, eds P.N. Cheremisinoff and F. Ellerbusch, Ann Arbor Science, Michigan.

Crowson, P. (1994) Minerals Handbook 1994-95 Statistics and Analyses of the World's Minerals Industry, Antony Rowe Ltd., Chippenham, Wiltshire.

Crozier, R.D. (1992) Flotation Theory, Reagents, and Ore Testing, Pergamon Press, Oxford.

Cutifani, M. (1993) 'Gold Ore Treatment at Kalgoorlie Consolidated Gold Mines Pty Ltd, Kalgoorlie, WA', The Sir Maurice Mawby Memorial Volume, (2nd ed) 2 (19): 966-976.

Dahya, A.S. and King D.J. (1983) 'Developments in Carbon-in-Pulp Technology for Gold Recovery', CIM Bulletin, 76 (857): 55-61.

Dunn, A.D. and Rudorf, W.D. (1989) Carbon Disulphide in Organic Chemistry, Ellis Horwood Limited, Chichester, England.

Dunn, J.G. and Sharp, J.H. (1993) 'Thermogravimetry' in *Treatise on Analytical Chemistry: Thermal Methods, Part 1, Vol. 13 (2^{nd} edn)*, eds J.D. Winefordner, John Wiley and Sons, Inc., Chichester, England.

Fanning, P.E. and Vennice, M.A. (1993) 'A DRIFTS Study of the Formation of Surface Groups on Carbon by Oxidation', Carbon, 31 (5) 721-730.

Finar, I.L. (1973) Organic Chemistry The Fundamental Principles Volume 1, (6th ed) Longman, London.

Friedel, R.A. and Hofer, L.J.E. (1970) 'Spectral Characterization of Activated Carbon', The Journal of Physical Chemistry, 74 (15) 2921-2922.

Haines, P.J. (1995) Thermal Methods of Analysis: Principles, Applications and Problems, Blackie Academic and Professional, London.

Harris, P.J. (1984) 'Influence of the Substituent Group on the Decomposition of Xanthates in Aqueous Solutions' South African Journal of Chemistry, 37:91-95.

Hassler, J.W. (1974) Purification with Activated Carbon, Chemical Publishing Co., Inc., New York.

Hatakeyama, T. and Quinn, F.X. (1994) Thermal Analysis: Fundamentals and Applications to Polymer Science, Wiley, New York.

Herzberg, G. (1945) Molecular Spectra and Molecular Structure, (vol. 2) van Nostrand Reinhold Co., Melbourne.

Hill, J.O. and Magee, R.J. (1981) 'The Thermochemistry of Metal Dithiocarbamate Complexes and Related Compounds', Reviews in Inorganic Chemistry, 3:141-197.

Hoechst, 'Determination of the Active Substance Content of Technical Xanthates' in *Notes from the Technical Service and Development Department*, Special Fields No. 25.

Ibrado, A.S. and Fuerstenau, D.W. (1995) 'Infrared and X-ray Photoelectron Spectroscopy Studies on the Adsorption of Gold Cyanide on Activated Carbon', Minerals Engineering, 8 (4/5) 441-458.

Jones, M.H, Macrae, C.M., Sparrow, G.J. and Woodcock, J.T. (1988) 'Distribution of Inorganics and Gold on the External and Internal Surfaces of Activated Carbons from CIP Plants', The AusIMM Bulletin and Processings, 293 (6) 121-126.

Kagann, R.H. (1982) 'Infrared Absorption Intensities for OCS', Journal of Molecular Spectroscopy, 94:192-198.

Kelly, D. (1992) 'Gold and Base Metals Industry of WA', Extractive Metallurgy of Gold and Base Metals, October, Kalgoorlie, 9-13.

Khwaja, M.A., Cardwell, T.J. and Magee, R.T. (1973) 'Thermal Studies on Arsenic, Antimony and Bismuth Alkylxanthate Complexes', Analytica Chimica Acta, 64:9-17.

Kolthoff, I.M., Sandell, E.B., Meehan, E.J. and Buckenstein, S. (1969) Quantitative Chemical Analysis, (4th ed) the Macmillan Company, London.

La Brooy, S.R. (1988) 'Properties of Activated Carbon for Gold Recovery', 1st International Conference on Hydrometallurgy, October, Beijeng.

La Brooy, S.R. and Bax, A.R. (1985) 'The Fouling of Activated Carbon by Organic Reagents', CHEMECA 85.

La Brooy, S.R., Bax, A.R., Muir, D.M., Hosking, J.W., Hughes, H.C. and Parentich, A. (1986) 'Fouling of Activated Carbon by Circuit Organics', Gold 100 MINTEK.

La Brooy, S.R., Hosking, J.W., Muir, D.M., Ruane, M., Smith, I. and Hinchliffe, W.D. (1984) 'Studies on the Fouling and Regeneration of C.I.P. Carbon', The Aus.I.M.M. Perth and Kalgoorlie Branches, Regional Conference on "Gold-Mining, Metallurgy and Geology", 1-13.

LaBrooy, S.R., Linge, H.G. and Walker, G.S. (1994) "Review of Gold Extraction from Ores', Minerals Engineering, 7 (10) 1213-1241.

Locker, J.R., Burkholder, J.B. and Bair, E.J. (1983) 'Thermally Excited Vibrational Components of the $A \leftarrow X^1\Sigma^+$ System of OCS', Journal of Physical Chemistry, 87:1864-1868.

March, J. (1992) Advanced Organic Chemistry Reactions, Mechanisms, and Structure, (4th ed) John Wiley & Sons, New York.

Mattson, J.S., Mark, H.B. and Weber, W.J. (1969) 'Identification of Surface Groups on Active Carbon by Infrared Internal Reflection Spectrometer', Analytical Chemistry, 41 (2) 355-358.

McDougall, G.J. (1991) 'The Physical Nature and Manufacture of Activated Carbon', Journal of the South African Institute of Mining and Metallurgy, 91 (4): 109-120.

McLafferty, F.W. (1980) Interpretation of Mass Spectra, (3rd ed) University Science Books, California.

Myers, J.S. and Hickman, A.H. (1990) 'Pilbara and Yilgarn Cratons-Regional Geology and Mineralisation', Geology of the Mineral Deposits of Australia and Papua New Guinea, 1 (14) 129-133.

Morgan, H.M. (1993) 'Overview of the Australasian Gold Industry', The Sir Maurice Mawby Memorial Volume, (2nd ed) 2 (19):801-804.

Morrison, R.T. and Boyd, R.N. (1992) Organic Chemistry (6th ed) Prentice Hall International, Inc., London.

Nakanishi, K. and Solomon, P.H. (1977) Infrared Absorption Spectroscopy, (2nd ed) Holden-Day, U.S.A.

Nishikida, K., Nishio, E. and Hannah, R.W. (1995) Selected Applications of Modern FT-IR Techniques, Kodansha Ltd., Tokyo.

Odd, P.A.R. and Hardy, H.J. (1993) 'Gold Mining and Ore Treatment Operations of Asarco Australia Limited at Wiluna, WA', The Sir Maurice Mawby Memorial Volume, (2nd ed) 2 (19):804-808.

Pandey, O.P. (1988) 'Chemistry and Mechanism of Thermal Degradation Reactions of Zirconium(IV) Alkyl Xanthate Complexes', Thermochimica Acta, 127:193-199.

Pandey, O.P., Sengupta, S.K. and Tripathi, S.C. (1985) 'Thermochemistry of Metal Xanthato Complexes. A Review', Thermochimica Acta, 96:155-167.

Park, S.H., McClain, S., Tian, Z.R., Suib, S.L. and Karwacki, C. (1997) 'Surface and Bulk Measurements of Metals Deposited on Activated Carbon', Chemistry of Materials, 9:176-183.

Raemaekers, K.G.H. and Bart, J.C.J. (1997) 'Applications of Simultaneous Thermogravimetry-Mass Spectrometry in Polymer Analysis', Thermochimica Acta, 295:1-58.

Rao, S.R. (1971) Xanthates and Related Compounds, Marcel Dekker Inc., New York.

Reggers, G., Ruysen, M., Carleer, R. and Mullens, J. (1997) 'TG-GC-MS, TG-MS and TG-FTIR Applications on Polymers and Waste Products', Thermochimica Acta, 295:107-117.

Robards, .K, Haddad, P.R. and Jackson, P.E. (1994) Principles and Practice of Modern Chromatographic Methods, Academic Press Ltd., London.

Ruane, M., Hinchliffe, W., Hosking, J.W. and Muir, D.M. (1983) 'Carbon-in-Pulp Gold Processing Techonology (Project No. 10)', Western Australian Mining and Petroleum Research Institute Report No. 2 .

Sceney, C.G., Hill, J.O. and Magee, R.J. (1973) 'Thermal Studies on Palladium Alkyl Xanthates', Thermochimica Acta, 6:111-117.

Snell, F.D. and Ettre, L.S. (eds) (1971) Encyclopedia of Industrial Chemical Analysis, Interscience Publishers, New York.

Socrates, G. (1994) Infrared Characteristic Group Frequencies: Tables and Charts, (2nd ed) John Wiley and Sons, Chichester, England.

Suzuki, M., Misic, D.M., Koyama, O. and Kawazoe, K. (1978) 'Study of Thermal Regeneration of Spent Activated Carbons: Thermogravimetric Measurement of Various Single Component Organics Loaded on Activated Carbons', Chemical Engineering Science, 33:271-279.

Tyden, I. (1966) 'Gas Chromatographic Study of the Pyrolysis of Potassium salts of Xanthic Acids', Talanta, 13:1353-1360.

Vaughan, J.P. and Dunne, R.C. (1987) 'Mineralogy and Processing Characteristics of Archaean Gold Ores from Western Australia', Gold Mining 87, 241-259.

Voorhees, K.J., Baugh, S.F. and Stevenson, N. (1994) 'An Investigation of the Thermal Degradation of Poly(ethylene glycol)', Journal of Analytical and Applied Pyrolysis, 30:47-57.

Vo Van, K., Malhotra, S.L. and Blanchard, L.P. (1974a) 'Kinetic Study of the Thermal Decomposition of Poly(oxypropylene) Glycols by Differential Scanning Calorimetry', Journal of Applied Polymer Science, 18:2671-2691.

Vo Van, K., Malhotra, S.L. and Blanchard, L.P. (1974b) 'Kinetics of the Decomposition of Polyoxypropylene Glycols by Differential Scanning Calorimetry and Thermogravimetric Analysis', Journal of Macromolecular Science-Chemistry, A8 (5) 843-860.

Vreugdenhil, A,J., Brienne, S.H.R., Markwell, R.D., Butler, I.S. and Finch, J.A. (1997) 'Headspace Analysis Gas-Phase Infrared Spectroscopy: A Study of Xanthate Decomposition on Mineral Surfaces', Journal of Molecular Structure, 405:67-77.

Wang, X. and Eric Forssberg, K.S. (1990) 'The Chemistry of Cyanide-Metal Complexes in Relation to Hydrometallurgical Processes of Precious Metals', Mineral Processing and Extractive Metallurgy Review, 6:81-125.

Wills, B.A. (1997) Mineral Processing Technology, (6th ed) Butterworth-Heinemann, Oxford.

Woodall, R. (1990) 'Gold in Australia', Geology of the Mineral Deposits of Australia and Papua New Guinea, 1 (14) 45- 67.

Yapu, W., Segarra, M., Fernandez, M. and Espiell, F. (1994) 'Adsorption Kinetics of Dicyanoaurate and Dicyanoargentate Ions in Activated Carbon', Metallurgical and Materials Transactions B, 25B:185-191.